NPS ARCHIVE
1967
EFFRON, H.

CORRELATION OF ARGON-COPPER SPUTTERING MECHANISMS WITH EXPERIMENTAL DATA USING A DIGITAL COMPUTER SIMULATION TECHNIQUE

HERBERT M. EFFRON

CORRELATION OF ARGON-COPPER SPUTTERING MECHANISMS WITH EXPERIMENTAL DATA USING A DIGITAL COMPUTER SIMULATION TECHNIQUE

by

Herbert M. Effron
Lieutenant, United States Navy
B.A., San Jose State College, 1958

Submitted in partial fulfillment of the
requirements for the degree of

MASTER OF SCIENCE IN PHYSICS

from the

NAVAL POSTGRADUATE SCHOOL
JUNE 1967

NPS ARCHIVE
1967
EFFRON, H.

Thesis
E258
c.1

ABSTRACT

The sputtering process has been investigated by simulating the sputtering of single-crystal copper with 1-7 keV argon. A digital computer was used to build the crystal, bombard it, and move crystal atoms. Four mechanisms were observed which cause surface atoms to sputter. An atom is sputtered when (1) it is squeezed out of the surface, (2) it is scooped out when another atom strikes its inner hemisphere, (3) it is ejected when an atom passes behind it, and (4) it is knocked out by a second layer atom which is moving outward. Nearly all sputtered atoms were surface atoms. Second and third layer atoms were sputtered only for ion energies greater than 5 keV. They were sputtered by mechanisms similar to the surface atom mechanisms. "Silsbee chains" were observed to be directed <u>into</u> the crystal, and momentum focusing was observed to cause sputtering only when it occurred in close packed, <u>surface rows</u>. Outward directed chains were not observed. Sputtering deposit patterns, sputtering ratios, and sputtered atom energy distributions were obtained for (100), (110), and (111) surfaces. All data

LIBRARY
NAVAL POSTGRADUATE SCHOOL
MONTEREY, CALIF. 93940

TABLE OF CONTENTS

	PAGE
Title and Approval	1
Abstract	2
Table of Contents	3
List of Figures	5
Acknowledgements	11
Chapter 1 - Introduction	13
Chapter 2 - Purpose of the Investigation	19
Chapter 3 - Model	20
Chapter 4 - Dynamics	23
Chapter 5 - Results	31
Chapter 6 - Conclusions	59
Bibliography	64
Appendix A - The Beam Model	67
Appendix B - Positioning the Ion	72
Appendix C - Production and Analysis of Sputtering Deposit Patterns	74
Appendix D - The sputtering program, FCCSPUT	77
Appendix E - Glossary for FCCSPUT	107
Appendix F - Pattern Production and Analysis Programs (DATASORT, DATAPLOT, and DATA-GRID)	115
Initial Distribution List	136
Figures	137

LIST OF FIGURES

1. Force function error for atoms further apart than $2r_o$.

2. (111) surface crystal.

3. (100) surface crystal.

4. (110) surface crystal.

5. Atoms involved in sputtering mechanisms.

6. Argon-copper Deposit Pattern, (111) surface, 1 keV Ion Energy, 3.00 ev Binding Energy.

7. Argon-copper Deposit Pattern, (111) surface, 2 keV Ion Energy, 3.00 ev Binding Energy.

8. Argon-copper Deposit Pattern, (111) surface, 3 keV Ion Energy, 1.50 ev Binding Energy.

9. Argon-copper Deposit Pattern, (111) surface, 3 keV Ion Energy, 2.00 ev Binding Energy.

10. Argon-copper Deposit Pattern, (111) surface, 3keV Ion Energy, 2.50 ev Binding Energy.

11. Argon-copper Deposit Pattern, (111) surface, 3 keV Ion Energy, 3.00 ev Binding Energy.

12. Argon-copper Deposit Pattern, (111) surface, 3 keV Ion Energy, 4.00 ev Binding Energy.

13. Argon-copper Deposit Pattern, (111) surface, 3 keV Ion Energy, 4.50 ev Binding Energy.

14. Argon-copper Deposit Pattern, (111) surface, 3 keV Ion Energy, 5.50 ev Binding Energy.

15. Argon-copper Deposit Pattern, (111) surface, 4 keV

Ion Energy, 3.00 ev Binding Energy.

16. Argon-copper Deposit Pattern, (111) surface, 5 keV Ion Energy, 3.00 ev Binding Energy.

17. Argon-copper Deposit Pattern, (111) surface, 5 keV Ion Energy, 3.50 ev Binding Energy.

18. Argon-copper Deposit Pattern, (111) surface, 7 keV Ion Energy, 3.00 ev Binding Energy.

19. Argon-copper Deposit Pattern, (111) surface, 10 keV Ion Energy, 3.50 ev Binding Energy.

20. Argon-copper Deposit Pattern, (111) surface, 20 keV Ion Energy, 3.50 ev Binding Energy.

21. Argon-copper Deposit Pattern, (111) surface, 40 keV Ion Energy, 3.50 ev Binding Energy.

22. Sputtering Frequency-Location, (111) surface, 1 keV Ion Energy.

23. Sputtering Frequency-Location, (111) surface, 2 keV Ion Energy.

24. Sputtering Frequency-Location, (111) surface, 3 keV Ion Energy.

25. Sputtering Frequency-Location, (111) surface, 4 keV Ion Energy.

26. Sputtering Frequency-Location, (111) surface, 5 keV Ion Energy.

27. Sputtering Frequency-Location, (111) surface, 7 keV Ion Energy.

28. Sputtering Frequency-Location, (111) surface, 10 keV Ion Energy.

29. Sputtering Frequency-Location, (111) surface, 20 keV Ion Energy.

30. Sputtering Frequency-Location, (111) surface, 40 keV Ion Energy.

31. Sputtering Profiles, Atoms Sputtered by Surface Mechanisms, (111) surface.

32. Sputtering Profiles, Atoms Sputtered by Deep Mechanism, (111) surface.

33a. Sputtering Ratio, (111) surface, Regular Surface Condition.

33b. Sputtering Ratio, (111) surface, Vacancy Surface Condition.

33c. Sputtering Ratio, (111) surface, Stub Surface Condition.

34. Energy Distribution of Sputtered Atoms, (111) surface, 1-4 keV Ion Energy.

35. Energy Distribution of Sputtered Atoms, (111) surface, 5 keV Ion Energy.

36. Energy Distribution of Sputtered Atoms, (111) surface, 7 keV Ion Energy.

37. Energy Distribution of Sputtered Atoms, (111) surface, 10 keV Ion Energy.

38. Energy Distribution of Sputtered Atoms, (111) surface, 20 keV Ion Energy.

39. Energy Distribution of Sputtered Atoms, (111) surface, 40 keV Ion Energy.
40. Argon-copper Deposit Pattern, (100) surface, 1 keV Ion Energy, 3.50 ev Binding Energy.
41. Argon-copper Deposit Pattern, (100) surface, 3 keV Ion Energy, 3.00 ev Binding Energy.
42. Argon-copper Deposit Pattern, (100) surface, 5 keV Ion Energy, 2.00 ev Binding Energy.
43. Argon-copper Deposit Pattern, (100) surface, 5 keV Ion Energy, 3.00 ev Binding Energy.
44. Argon-copper Deposit Pattern, (100) surface, 7 keV Ion Energy, 1.50 ev Binding Energy.
45. Argon-copper Deposit Pattern, (100) surface, 7 keV Ion Energy, 3.00 ev Binding Energy.
46. Sputtering Frequency-Location, (100) surface, 1 keV Ion Energy.
47. Sputtering Frequency-Location, (100) surface, 3 keV Ion Energy.
48. Sputtering Frequency-Location, (100) surface, 5 keV Ion Energy.
49. Sputtering Frequency-Location, (100) surface, 7 keV Ion Energy.
50. Sputtering Profiles, Atoms from (100) surface.
51a. Sputtering Ratios, (100) surface, Regular Surface Condition.

51b. Sputtering Ratios, (100) surface, Vacancy Surface Condition.

51c. Sputtering Ratios, (100) surface, Stub Surface Condition.

52. Energy Distribution of Sputtered Atoms, (100) surface, 1 keV Ion Energy.

53. Energy Distribution of Sputtered Atoms, (100) surface, 3 keV Ion Energy.

54. Energy Distribution of Sputtered Atoms, (100) surface, 5 keV Ion Energy.

55. Energy Distribution of Sputtered Atoms, (100) surface, 7 keV Ion Energy.

56. Sputtering Frequency-Location, (110) surface, 1 keV Ion Energy.

57. Sputtering Frequency-Location, (110) surface, 3 keV Ion Energy.

58. Sputtering Frequency-Location, (110) surface, 5 keV Ion Energy.

59. Sputtering Frequency-Location, (110) surface, 7 keV Ion Energy.

60. Sputtering Profiles, Atoms Sputtered from (110) surface.

61. Argon-copper Deposit Pattern, (110) surface, 1 keV Ion Energy, 3.50 ev Binding Energy.

62. Argon-copper Deposit Pattern, (110) surface, 3 keV Ion Energy, 3.50 ev Binding Energy.

63. Argon-copper Deposit Pattern, (110) surface, 5 keV

Ion Energy, 3.50 ev Binding Energy.

64. Argon-copper Deposit Pattern, (110) surface, 7 keV Ion energy, 3.50 ev Binding Energy.

65. Sputtering Ratio, (110) surface.

66. Energy Distribution of Sputtered Atoms, (110) surface, 1 keV Ion Energy.

67. Energy Distribution of Sputtered Atoms, (110) surface, 3 keV Ion Energy.

68. Energy Distribution of Sputtered Atoms, (110) surface, 5 keV Ion Energy.

69. Energy Distribution of Sputtered Atoms, (110) surface, 7 keV Ion Energy.

70. Sputtering Ratio, (110) surface, Channel Shots.

71. Sputtering Frequency-Location, (100) surface, 100 ev.

72. Crystal Instrinsic Volumes.

73. Impact Areas.

74. Sputtering Ratio Variation with Impact Point Sets.

75. Scattering from a fixed force center.

76. Ion deflection as a function of the product of energy and impact parameter.

77. Ion positioning process.

ACKNOWLEDGEMENTS

A digital computer simulation of the sputtering process requires the cooperation of many personnel not directly concerned with the project. I am indebted to Mr. Edward Ward and to Mr. Maxwell J. Feuerman of the Computer Facility, Naval Postgraduate School (NPGS) for the nearly 1000 hours of computer time required to gather and analyze the data. The photography process for converting point plots to sputtering patterns was developed by Messrs. Richard A. DuBrau and Howard Bensch of the Photography Laboratory, NPGS. The reproduction of these patterns was made possible by the efforts of Mr. Wayne Shipton and Jackie A. Skinner, Specialist Fifth Class, U.S. Army of the Defense Language Institute, West Coast.

I am especially grateful to Dr. Don E. Harrison, Jr. of the Naval Postgraduate School for his supervision and assistance in this project. The many hours of stimulating discussion of the phenomenon of sputtering intensified the efforts directed towards this work. To my wife, Carolee, I express my sincere appreciation for her patience, understanding, and assistance in both the project and preparation of the manuscript.

1. INTRODUCTION.

Material is lost from a substance undergoing ionic bombardment. This is sputtering. Many authors have tried to define sputtering using terms such as "(atoms)...ejected or knocked out", "emission", "ionic erosion", "disintegration", and "breakdown." A reader who blithely accepts one of these definitions in the course of his reading may conclude: This definition describes the mechanism of sputtering. This is an illogical, if not erroneous, conclusion; the definition of sputtering must be derived from the mechanism, not the mechanism from the definition. The sputtering process has been investigated utilizing one of two general mechanisms, ejection or emission. Ejection implies an immediate or direct reaction release of an atom from a crystal; emission, a delayed or indirect reaction process which results in the release of an atom.

In 1923, Kingdon and Langmuir [1] bombarded thoriated tungsten with various ions in a glow discharge tube. This was a special case of sputtering since the thin surface film of thorium on a tungsten substrate was sputtered rather than the tungsten itself. The results of this experiment, that the sputtering ratio, atoms removed per incident ion, increased with increased ion mass and increased ion energy, qualitatively suggested an ejection mechanism. A few years later, Von Hippel and Blechschmidt [2] proposed a theory which described sputtering as an evaporation of surface atoms, an emission

mechanism. Earlier, Von Hippel[3] had found by spectroscopic means that at least some sputtered atoms were in an excited state. The sputtering theory showed that atoms in the region of impact could rapidly acquire thermal energy if the kinetic energy of incident ions was converted to thermal energy at the target surface. If an atom acquired a sufficient amount of thermal energy, it would then evaporate from the surface, some atoms evaporating while in an excited state. This theory was improved by Townes[4] in 1944, who calculated a sputtering flux and the number of atoms evaporated per incident ion. Keywell[5] in 1954, used neutron diffusion theory to approximate atomic interactions within the crystal, a new approach to the theoretical investigation of sputtering. Direct application of statistical methods to sputtering was made by Harrison[6] who envisioned the interaction of two distribution functions (the crystal lattice and the ion beam). These models, based on statistical methods, implicitly accept ejection type mechanisms.

One of the most important contributions to the study of sputtering was made by Wehner[7] in 1953. In the first sentence of his paper, Wehner stated, "The most widely accepted sputtering theory is the evaporation theory...", but the deposit patterns of <u>single crystal</u> sputtering which he obtained showed pronounced, high density areas or "spots". There was now strong evidence for a momentum transfer process, and further development of the evaporation theory

ceased. Shortly after Wehner's findings were reported, Henschke[8] proposed a theory of sputtering based solely on classical collision theory, treating normal and oblique incidence sputtering separately. Oblique incidence sputtering could be explained by two body collision processes. The incident ion penetrated the surface layer with little or no interaction, was relected outward by second layer atoms, and ejected a surface atom by striking it on its inside hemisphere. His concept of normal incidence sputtering required many-body collisions in which the ion was eventually reflected outward to sputter surface atoms. This theory was plausible for oblique incidence sputtering, however, the case for normal incidence sputtering required that the ion be reflected inside the crystal. (For an ion more massive than the target this requirement cannot be met.)

Silsbee [9] noted that in any discussion of momentum transfer effects in sputtering, the geometry of the crystal should be considered; successive collisions in a crystalline structure might be influenced by the structure itself. His calculations showed: in a two-body collision, an atom has a departure angle β_i with respect to an axis specified by a close packed direction. In subsequent collisions, the departure angle β_{i+1} will decrease if the energy is low enough, and the collision sequence occurs along a close packed row of atoms. This concept of "momentum focusing", "Silsbee chains", or "focusons" was considered by

many investigators, excepting Wehner[10], to be a fully satisfactory explanation of the spots in deposit patterns. But the deposit pattern is only one of many observable features of single crystal sputtering.

The sputtering ratio is another important characteristic of the sputtering process. If a theory or model is to explain sputtering, both patterns and sputtering ratios must be explained qualitatively and quantitatively. Almén and Bruce (AB) [11] measured sputtering ratios of a variety of metals using N, Ne, Ar, Kr, and Xe ions over a 5-65 keV range of bombardment energies. (Although polycrystalline specimens were sputtered, the qualitative results are the same as those obtained for single crystal sputtering.) They noted that the sputtering ratio was an increasing function of bombardment energy provided the ion mass was greater than the target mass. Sputtering ratios showing a maximum, or of a slowly varying nature, were observed in all cases in which the ion was lighter. Evidence such as this coincides with any gross conception of an ejection mechanism.

Single crystal copper was sputtered by argon at intermediate energies by Magnuson and Carlson (MC)[12] and Southern, Willis, and Robinson (SWR)[13]. MC measured sputtering ratios (using 1-10 keV argon) for the (111), (100) and (110) surfaces and found that sputtering ratios decreased in this order of surfaces. SWR sputtered single crystal copper with

1-5 keV argon and measured sputtering ratios, but of greater significance was the quality of their deposit patterns which clearly showed the presence of only certain spots:

(111) surface 3-(110), 1-(111) but not seen due to beam aperture.

(110) surface 1-(110), 2-(100)

(100) surface 4-(110), 1-(100)

The work of AB, MC, and SWR indicated that the sputtering ratio is at least a function of bombardment energy (or momentum) and of mass ratios. However, consideration of spot patterns indicates that the sputtering process itself is also highly dependent on the gross and/or surface geometry of the crystal and on ion penetration depth.

Ion penetration of solids has been investigated experimentally and by computer simulation. Piercy, McCargo, Brown, and Davies(14) investigating channeling of various heavy ions in monocrystalline aluminum, found that the ion penetration distance increased in the order (111), (100), and (110) beam orientations. This is the same order as the sputtering ratio decrease found by MC. A number of studies of ion penetration have also been made using computer simulations (Oen, Holmes, and Robinson(15), Robinson and Oen(16), Harrison, Leeds, and Gay(17)).

The most apparent correlation between the results of ion penetration and sputtering studies is the concept of <u>transparency</u>, defined by Fluit, Rok and Kistemaker(18). Both

experimental and simulation investigations of ion penetration indicate that channels exist in certain crystallographic directions of a crystal. Results of normal incidence sputtering experiments indicates that sputtering ratios are lower for surfaces in which these channels are parallel to the beam. One might initially suspect that sputtering ratios will be low if ions and target atoms are confined to these channels; momentum is directed into the crystal rather than laterally, reversal of momentum to produce sputtering not occuring. Accordingly, some incident ions should see a transparent surface rather than a wall of atoms.

The obvious complexities of the sputtering process may be investigated separately by digital computer simulation. This of course involves the selection of a gross mechanism (ejection or emission) and a model (hardsphere or otherwise). If factors such as the interatomic potential function and its parameters are known, then the use of the right model in the computer may be expected to simulate the actual sputtering process. Explanation of deposit pattern characteristics and sputtering ratios will necessarily follow from an exact simulation.

2. PURPOSE OF THE INVESTIGATION.

The belief that the formation of spots in sputtering deposit patterns is solely a consequence of momentum focusing was widely accepted for a number of years. The importance of momentum focusing, not only in spot formation, but in the entire sputtering process is now believed to be much less than originally thought [18-25]. This investigation was undertaken to explore the single crystal sputtering process using a digital computer to simulate a copper crystal which is being bombarded with a beam of argon ions. Primary effort was directed towards:

a. Finding the mechanisms which result in atoms being deposited in the spots or high density regions of the deposit pattern.

b. Determining the correlation between crystal structure and sputtering ratios and patterns.

c. Investigating the surface binding energy and its effect on deposit patterns.

3. MODEL.

A. A space lattice is established whose sites represent the equilibrium positions of copper atoms in a face centered cubic crystal. Atomic spacing is that determined by x-ray crystallographic studies (for copper, a = 3.615 Å). The potential function, with parameters for copper-copper interaction, is the Born-Mayer type Gibson Number Two[26]. The interaction between argon and copper is similarly described using a Born-Mayer potential, $V(r) = e^{A+Br}$, but the numerical values of the parameters A and B, for this function are those determined by Harrison, Carlston, and Magnuson (HCM)[27] from a study of secondary electron emission. The range of both potential functions is eroded at r_o, one half the nearest neighbor distance such that the potential and force go to zero for atoms whose centers are farther apart than $2r_o$. Use of this eroded form of the potential functions permits establishment of the crystal in a stable, static state without use of an attractive potential. This equilibrium state is destroyed only when an atom moves from its lattice site.

The lattice as a whole is restricted by the current computer program to perfect form. Defects such as interstitial atoms cannot be used, however, irregularities in the surface layer are introduced by using two types of variation from a perfect surface: vacancy and stub conditions. The perfect or regular surface is identical to a full lattice plane. In the vacancy

configuration the atom which would normally be hit first by the ion is removed from the perfect surface. The stub surface has an atom added on the perfect surface in a stable position and adjacent to the target atom. Additional atoms can also be added on the surface or removed from the perfect surface to provide a variety of random irregularities.

B. Each ion of the beam is approximated by a single, neutral argon atom whose velocity vector intersects the plane of surface atoms at an impact point. (The term ion is used throughout this thesis for the incident particle to avoid confusion with target atoms.)

Successive runs are made using different impact points to simulate use of the entire beam area. The use of this simple model for the ion beam is subject to four conditions:

1. The results obtained using one random set of impact points are essentially the same as those obtained using any other random set of impact points.
2. The majority of beam ions are neutralized before reaching some arbitrary boundary which defines the surface.
3. Prior to neutralization, the path of a beam ion is not appreciably affected by the surface potential.
4. A crystal region is in an equilibrium state each time a neutralized ion impacts in that region.

Each of these conditions has been satisfied either in the model itself or by calculation. A full discussion is contained in Appendix A.

4. DYNAMICS.

The force functions for copper-copper and argon-copper interactions are derived from the respective potential functions. Atom position and velocity are then determined using Newton's Second Law of Motion. Normally, one would determine these values by numerical integration methods over small time intervals, however, this process uses too much computer time. Special methods approximating integration have been developed which are used to minimize computer run time yet maintain a good approximation to the integration.

A. Gay[28] developed an iterative method of solution which is similar to that used by Gibson, Goland, Milgram, and Vineyard[26]. Both Gay's and Gibson's methods use the technique of replacing differential quantities with finite differences to approximate the equation of motion, $F/m = dv/dt$ by $F/m = \Delta v/\Delta t$. Using this equation and the relationships $\Delta x = v\Delta t$ and $\bar{v} = (v + v_o)/2$, equations (3-1) and (3-2) are obtained.

$$\Delta v = v - v_o = \left[F\,(x_o)/m\right]\Delta t \tag{3-1}$$

$$\Delta x = x - x_o = \left\{\left[F\,(x_o)/m\right]\Delta t/2 + v_o\right\}\Delta t \tag{3-2}$$

The known values $\underline{F(x_o)}$, $\underline{v_o}$, $\underline{x_o}$, and $\underline{\Delta t}$ in these equations are usually associated with a time $t = t_o$; $\underline{x}$ and $\underline{v}$, the unknown values, are to be evaluated using these equations at time $t = T(t_o, \Delta t)$.

Gibson's technique associates the value of $\underline{x_o}$ with a time

$t_{ox} = t_o$, but v_o is associated with a time $t_{ov} = t_o - \Delta t/2$. Current values of $\underline{x}$ and $\underline{v}$ are alternately computed at intervals Δt using equations (3-1) and (3-2).

$$v(t_o + \Delta t/2) = v_o(t_o - \Delta t/2) + \left[F(x_o)/m\right]\Delta t$$

$$x(t_o + \Delta t) = x(t_o) + \left\{\left[F(x_o)/m\right]\Delta t/2 + v(t_o + \Delta t/2)\right\}\Delta t$$

The advantage of this technique over that of evaluating both variables at time $t = t_o + \Delta t$ is that a continuous smoothing of the values of $\underline{x}$ and $\underline{v}$ occurs with each successive computation.

Gay recognized the need for some sort of smoothing procedure but considered that an averaging process for equation parameters rather than computed results would result in a better approximation. His method replaces the evaluated force function $\underline{F(x_o)}$ in these two equations with an arbitrary force function $\underline{f(x)}$ which is linear in some interval to be determined. Consider the following two step cycle:

Move an atom from x_o to x_1 using computed values of $F(x_o)$ and v_o to solve equations (3-1) and (3-2). Compute $F(x_1)$ and average this value with $F(x_o)$. Now, move the atom from x_1 to x_2 using the averaged force, $\overline{F}(x_o, x_1)$ and v_o to solve the equations using the same constant value of Δt. Let $\underline{f}$ now be defined in the interval (x_o, x_2), such that $f(x_o) = \overline{F}(x_o, x_1)$. Equations (3-1) and (3-2) may now be written:

$$v(t + \Delta t) = v(t) + \left[f(x_o)/m\right]\Delta t$$

$$x(t + \Delta t) = x(t) + \left\{ \left[f(x_o)/m \right] \Delta t/2 + v(t) \right\} \Delta t$$

The values of $\underline{v}$ and $\underline{x}$ are determinable in any interval in which $\underline{f}$ approximates $\underline{F}$ to some arbitrary degree, therefore, in every complete cycle or timestep a new interval and new function $\underline{f}$ are defined.

A determination of which of these two methods is better must be based on some standard or condition. In many cases the accuracy of numerical solutions such as these may be compared to the exact value one obtains by integration. But, there are no truly exact results in a simulation since a physical model is in the computer rather than the computer being used as a means of solving equations. However, if the model is physical, physical laws must be satisfied, and the energy gain or loss due to the mathematical approximations must be small. This condition of energy balance has been used by Harrison[31] who found that, in simulations involving atomic interactions such as channeling or sputtering, use of Gay's method resulted in a better energy balance.

B. The value of these approximation techniques may be substantially reduced by injudicious selection of a numerical value for Δt. Too large a value invalidates the approximation, but too small a value increases computer running time. The program used in this simulation of sputtering incorporates not only Gay's approximation method but also a procedure which he developed for automatic adjustment of Δt. Its value is

calculated using the relationship $\delta t = \delta r/v$ where Δt is replaced here by δt to indicate that its value varies with each timestep. The velocity, v is the magnitude of the velocity of the most energetic atom in that timestep, and δr is used here as an input parameter, the timestep multiplier. This parameter is assigned the computer variable name DTI and is defined: the maximum displacement of any atom in any timestep shall be the numerical value of DTI in appropriate units of length. Gay considered the value of Δt, consequently that of DTI, to be a function of ion energy, impact point, and start point, but he was unable to find the relationship. Trial and error methods were used to find optimum values, and reasonably good results were obtained using these values. Johnson(29) reported that the energy balance was maintained to within 3% for all his runs.

The difficulties in choosing a value for DTI have been largely eliminated in this study. Some problem areas such as start point and impact point dependence were avoided by always positioning the ion tangent to the first atom it would hit. This, at worst, will result in a constant error for which adjustments may be made (this has not been necessary). The positioning procedure is described in Appendix B. The dependence on ion energy is inherent to the DTI computation process and is easily explained once the clutter of impact point and start point dependence has been cleared away. Use of the DTI process excludes all variable dependence except the inverse

proportionality to velocity, but the interval in which the force function is considered linear is exactly the same width as the numerical value of DTI. Accordingly, a straightforward analysis is made to show the interdependence.

The force function, F(r), is expanded about an arbitrary point r* using a Taylor's series for a function of one variable:

$$F(r)=F(r^*) + \left.\frac{\partial F}{\partial r}\right|_{r^*} (r-r^*) + \frac{1}{2!}\left.\frac{\partial^2 F}{\partial r^2}\right|_{r^*} (r-r^*)^2 + \ldots \frac{1}{k!}\left.\frac{\partial^k F}{\partial r^k}\right|_{r^*} (r-r^*)^k$$

Since F(r) is derived from the potential function $V(r) = {}_eA+Br$, e^{A+Br}, F(r) is necessarily of exponential form and $\frac{\partial^k F}{\partial r^k} = B^k F$

$B F$, and the series is rewritten in the following form:

$$F(r)= \left\{F(r^*) \left[1 + B(r-r^*)\right]\right\} + \left\{F(r^*) \left[\sum_{n=2}^{\infty} \frac{B^n}{n!} (r-r^*)^n\right]\right\} \quad (3\text{-}3)$$

The quantity (r-r*) is now defined as a variable displacement δr, and equation (3-3) may be written: $F(r) = f(\delta r) + g(\delta r)$ where $f(\delta r)$ and $g(\delta r)$ are the terms in braces in the force function expansion. The function $f(\delta r)$ is assumed to be the linear function used in Gay's approximation method; the function $f(\delta r)$ is to approximate F(r). Thus, it is required that the ratio $g(\delta r)/f(\delta r)$ be some fraction less than one.

Let an assumption be made that the ratio is much less than one, but that the actual value is the fractional deviation from linearity, a variable whose value is to be specified. Then, since B is a negative constant (from the potential function), the truncation error for the series is easily found, and the

[illegible]

quantity $\underline{B\delta r}$ is known for every specified value of fractional deviation. But $\underline{B}$ is constant, and once the fractional deviation is specified, $\underline{\delta r}$ is fixed. Consequently, specified to the fractional deviation from linearity, there is a function f(r) which is a valid approximation to the function F(r) in every interval (r, r+δr) where $\underline{\delta r}$ is fixed. The quantity $\underline{\delta r}$ is thus the value to be used for DTI, and $\delta t = \delta r/v = DTI/v$.

It is now assurred that Δt will always be the maximum possible value which minimizes computer running time without introducing errors due to the non-linearity of the true force function. One would expect therefore, that the energy balance would be maintained to the same order as the linearity of the force function. Further consideration will show that the energy balance is maintained to a considerably better degree than that anticipated. First, since DTI is the maximum displacement of the <u>most energetic atom</u>, essentially all other atoms will be displaced a distance less than DTI. Thus, the interval in which the force function f(r) is used is smaller, and $\underline{f}$ is an even better approximation to $\underline{F}$. Second, for a given fractional deviation from linearity, the value of $\underline{\delta r}$ is total displacement, not $\underline{x}$, $\underline{y}$, or $\underline{z}$ component displacement; and the velocity used in the determination $\Delta t = DTI/v$ for each timestep is the total velocity $\underline{v}$, not the component velocity v_i. The result of these considerations may be summarized by a calculation for the maximum displacement of

an atom along the $\underline{i}$ component of its displacement vector: $\Delta x_i = v_i \Delta t$, but $v_i \leq v \leq v_{max}$ and $\Delta t = DTI/v_{max}$. It follows that $\Delta x_i = v_i \ (DTI/v_{max}) \leq DTI$.

These analyses appear to provide a tidy solution to the time optimization and energy balance problem. This would be true except for the complications introduced by the eroded form of the potential function. Consider a situation in which one atom is separated from another by a distance $(2r_o + d)$ where $\underline{d}$ is some distance less than the total distance $\underline{D}$ that the atom will move in the next timestep. When the atom is moved the distance $\underline{D}$, as shown in figure 1, the force on the atom at its new position is the same force it would have if it had moved only (D-d) units. Since the force is zero for $r > 2r_o$, the model assumes that the atom had a velocity $v = (D-d)/\Delta t$ (which is smaller than its actual velocity $v = D/\Delta t$, and a smaller kinetic energy is computed using this smaller velocity. This difficulty was originally foreseen by Gay who included corrections to the force calculations for such situations. Both Levy[30] and Johnson[29] improved the methods of corrections, and recent improvements in the force calculations have been made by Harrison[31].

The continuous improvement of the dynamics section of the program has resulted in a model in which not only has the computer running time been minimized, but of greatest significance, for nearly all of the 700-800 combinations of surfaces,

ion energies, and impact points used in this study, the energy balance was maintained to within 1%.

5. RESULTS.

Reports of sputtering studies often include ad hoc formulations of mechanisms which are used to explain deposit patterns, sputtering ratios, and sputtered atom energy distributions. The sputtering process is discussed in this thesis in terms of mechanisms which have been observed in the simulation to sputter atoms. The observance of these mechanisms is an advantage peculiar to a simulation. Each crystal atom (and the ion) must be identified by number, at least for purposes of computer calculations. Since every atom is identified, its complete track can be plotted and labeled. The tracks of selected atoms can then be superimposed to show a complete set of interactions. The mechanisms which were observed to cause an atom to sputter are considered the prime observable quantity of the simulation.

The results of the simulation are discussed for each crystal surface. The determination that an atom having energy E is sputtered, was made using a probability-of-sputtering function, $P(E) = 1 - e^{-E/E_b}$ where E_b is the assumed binding energy. The value of P is compared with a random number R having a value between 0 and 1. If $P > R$, the atom is considered sputtered. (This method of selection has been compared with one using a step function in which all atoms with $E > E_b$ are assumed sputtered. A selection method using another probability-of-sputtering function, $P(E) = 1 - e^{-(E-E_b)}$ has also been

tested. No differences were observed in the sputtering patterns based on the atom selection method.)

Mechanisms observed to cause sputtering are discussed first for each surface. Deposit patterns, sputtering ratios, and sputtered atom energy distributions are then discussed. The deposit patterns shown are superpositions of those obtained by sputtering the crystal separately with regular, vacancy, and stub surface conditions. This practice follows that used by Johnson[29] who found that pattern features were difficult to recognize when viewing separate patterns from each surface condition. The energy distributions are also superpositions of the three surface conditions. The use of superposition is considered to most realistically simulate the condition of the crystal surface at various times during sputtering. There are strong arguments however, for using only the regular surface condition. Sputtering ratios are not averaged (which would correspond to the superposition of other data) since a probability factor for the existence of each surface condition would need to be determined. Instead, the simulation sputtering ratios for vacancy and stub surface conditions are included and discussed briefly only for completeness. (The (110) surface was sputtered only at 1 and 3 keV using all three surface conditions.)

Crystallographic nomenclature is used generically in the discussion of spots. Reference to an (hkl) spot does not

imply $\langle hkl \rangle$ ejection. The $\langle hkl \rangle$ directions are with respect to a right handed coordinate system in which the crystal is described. The (hkl) surface is contained in the *x-z* plane; the *y* direction is into the drystal. The three crystals used in the simulation are shown in figures 2-4; all contain 150 atoms. This crystal size has been found sufficient to contain nearly all energetic collisions for ion energies up to 7 keV.

A. The (111) surface.

The (111) surface was sputtered normally with argon at 1-5, 7, 10, 20, and 40 keV. (Although the potential function is considered valid only for ion energies less than about 7 keV, the higher energy runs were used to search for additional mechanisms.) Four mechanisms were found. These were especially evident at the lower (1-5 keV) ion energies. Three of these are classified *surface mechanisms* since only surface atoms were found to participate in the sputtering event. The fourth mechanisms is a *deep* mechanism in which an inward moving *atom* is reflected and then initiates a sputtering event. In all cases, the dominant mechanisms were found to be *surface mechanisms.*

Except for head-on collisions, the ion is scattered by the target (atom 2) with a component of momentum parallel to the surface as well as a much larger perpendicular component into the crystal. The effect of this combination of momenta is to drive a nearest neighbor (n. n.), for example atom 6 in

figure 5, into an apparent ⟨112⟩ channel formed by atoms 7, 8, and 9. The channel is apparent since it terminates abruptly thus causing atom 6 to drive atoms 7 and 8 into the crystal and atom 9 outward. Since atom 6 passes nearly directly behind atom 9, the impulse is more normal to the surface than parallel to it. This is termed a mole mechanism since one atom burrows between two layers parallel to the surface to sputter an atom in the outermost layer. Atoms sputtered by this mechanism are almost always a next nearest neighbor (n.n.n.) to the target and located in or near the sextant defined by the impact area. They usually sputter with greater than 10 ev. The target always receives the majority of energy transferred by the ion, but it is normally driven into the (111) trigonal array of atoms directly behind it. These three atoms act as buffers and dissipate the target's energy and momentum into the crystal. The target is reflected, but it does not retain sufficient energy to sputter a surface atom nor sputter itself.

The second and third surface mechanisms occur when the impact parameter is about one third of an atom radius or less. In both mechanisms a n.n., atom 6, is struck by the ion such that the parallel and perpendicular momentum component magnitudes which it acquires are of the same order. If the perpendicular component is greater, atom 8 scoops a n.n.n., atom 9, relatively high up in the surface plane of atoms and

into their outer hemispheres. These atoms are densely packed in the surface and act as a rigid reflector for atom 9. It is found that atoms sputtered by the scoop mechanism have ejection angles nearer the normal than would be found in the absence of reflection in the surface. If the perpendicular momentum component of atom 6 is nearly the same or less than the parallel component, it squeezes atom 9 against its surface neighbors. The squeezing causes the surface plane to warp and atom 9, 10, or 11 is sputtered. Atoms sputtered by either the scoop or squeeze mechanism usually sputter with less than 10 ev. Atoms sputtered by combinations of the three surface mechanisms are found to sputter with higher energies than when sputtered by a single mechanism.

The fourth mechanism requires that an atom be reflected. The atom which is most often apt to be reflected is the target. If the impact parameter is greater than one half the atom radius, the target is driven towards an edge of the trigonal array behind it rather than into it. It will penetrate this edge if it has sufficient energy, but it will lose most of the energy during the penetration. The reflection occurs from third layer atoms and the target atom's reversed momentum is transferred to a second layer atom. The second layer atom will then sputter one or two surface atoms at energies upwards of 5 ev. At lower ion energies the target atom cannot penetrate the array edge and is reflected from the second

layer; it may or may not sputter a surface atom, but it rarely sputters itself.

When the crystal was sputtered at 7 keV, the ion was found to penetrate well into the second layer. This is a significant increase in ion penetration depth since 5 keV ions are found to penetrate only to the order of half an atom radius. The effect of deeper ion penetration is to cause a lateral compression of the second layer with accompanying warping. Second layer atoms which are squeezed outward will sputter a surface atom but are rarely found to sputter themselves. At the higher bombardment energies tested (10, 20, 40 keV), the number of second layer atoms which sputtered increased nearly proportionally to the increase in ion energy. The sputtering process at these higher energies appears to be predominantly by the three surface mechanisms described for lower energy sputtering. Mechanisms peculiar to high energy sputtering have not been observed although this may be due to the limited energy range for model validity.

All (111) simulation deposit patters showed the characteristic features of three (110) spots and a central (111) spot. The 2 keV pattern definitely showed the presence of three additional spots which were found in the regions in which streaking occurred at other energies. These patterns are shown in figures 6-21. The appearance of a hexagonal pattern at 2 keV was a surprising result, but it is not a unique

occurrence in sputtering studies. Anderson and Wehner[10] found a hexagonal pattern for (111) copper sputtered by mercury. The expected trigonal pattern was found for energies up to 400 ev, a hexagonal pattern appeared at 400 ev, and it disappeared as the ion energy increased. Very recently, Robinson and Southern[32] have found additional spots near ⟨114⟩ positions for (111) gold sputtered with 4 keV argon.

The pattern features vary slowly with binding energy provided its value is restricted to the range 2.50-3.50 ev. The upper limit is the sublimation energy for copper (33); above it the patterns appear to deteriorate. This was most evident at a 3 keV bombardment energy. A set of patterns at this bombardment energy is shown in figures 8-14 for a binding energy range of 1.50-5.50 ev. The pattern deterioration is most evident in the region of the (111) central spot. Figures 11 and 12 show the transition from a well defined central spot at 3.00 ev to complete deterioration of the central spot at 4.00 ev.

The half-intensity width of the (110) spots is estimated from pattern data and from numerical data to be about 11 degrees. The width of the central spot is an unreliable datum and was not determined.

Sputtered atoms were always found to be surface layer atoms for sputtering at 5 keV or less. The atoms which

were sputtered most frequently appeared to naturally group by energies into two categories; atoms with perpendicular energy greater than 3 but less than 10 ev and atoms with perpendicular energy greater than 10 ev. The higher energy atoms were found to be equally distributed between the three (110) spots and the central spot. They were also found in the narrow sectors defining the streaks and at distances from pattern center corresponding to the distances of the (110) spots. This distance was found to be 0.7 units, the distance measured for the spots in the patterns of SWR. The lower energy atoms were usually found in the central spot which explained its sensitivity to binding energy.

The correlation of sputtering frequency and crystal location of sputtered atoms was found using <u>frequency-location</u> diagrams. These are shown in figures 22-29 for regular surface sputtering. Similar diagrams have been made for sputtering the vacancy and stub surfaces. It was found that a 1 keV ion does not cause frequent sputtering of n.n.n.'s or n.n.'s in the sextant defined by the impact area. However, at 2 and 3 keV, n.n.n.'s are found to be sputtered most frequently, and at higher energies, both n.n.n.'s and n.n.'s are frequently sputtered. The three-fold relationship between the frequency of sputtering, location of the atom with respect to the target, and the ion energy may be clarified by considering the sputtering mechanisms.

At 1 keV and an impact parameter of about three fourths an atom radius, the ion is found to penetrate less than half an atom radius. At energies up to 5 keV the penetration is only slightly greater. It was found that, although the target is always driven into the crystal, the n.n. which initiates the majority of sputtering may not be driven far enough into the crystal to provide the scoop mechanism. If it is not driven inward a sufficient distance to scoop the n.n.n., its energy will be propagated in the surface along close packed rows which originate at the n.n.n. This is not a "focuson." At an early point in the propagation the surface will have warped sufficiently to cause an atom to sputter. The sputtering is a result of a squeeze mechanism but not one directly involving the n.n. As the ion energy is increased the scoop and mole mechanisms are more apt to occur although the squeeze mechanism is found to occur at all ion energies. The transitions from dominance of one mechanism to another with increasing ion energies may be inferred from the profiles shown in figure 31 for atoms which sputter most frequently.

A relatively constant sputtering frequency is observed for atoms 102 and 132, but the percentage of high and low energy sputs varies for atom 102 which is a n.n.n. The percentage does not vary for atom 132 which is neither a n.n.n. nor a n.n. Atom 102 sputters most frequently at low ion energies by the squeeze mechanisms, at higher ion energies by the scoop

and mole mechanisms. These relationships have been confirmed by the atom track displays. They also have shown that atom 132 is sputtered by atom 102 through a squeeze mechanism alone at low ion energies but in conjunction with the mole mechanism at higher ion energies. The profile shown for atom 86 is the result of simple reflection from second layer atoms. Atoms 87 and 101, which are not in the impact sextant but are sputtered frequently, are sputtered by the squeeze mechanism.

Figure 32 shows profiles of atoms sputtered by the deep mechanism. At low ion energies the target reflects at an oblique angle from second layer atoms rather than penetrating the layer, and it enters one of the apparent ⟨112⟩ channels. Atoms 25 and/or 55 are then sputtered directly by the target. (Although this is similar to a mole mechanism it is a distinct mechanism since the target must be reflected in this case but not in the former case.) At higher ion energies the target will penetrate the second layer and is reflected from third layer atoms. It does not channel, but it causes a second layer atom to sputter surface atoms. Accordingly, atom 55 is sputtered by the deep mechanism more often than atom 25 is sputtered by a channeled target. Atom 40 or 70 is sputtered by a squeeze mechanism, usually in conjunction with the sputtering of atoms 25 and 55.

These results for the sputtering of a regular surface

have been found to be generally applicable to sputtering vacancy and stub surfaces. Equal numbers of atoms from the three surfaces are found in the spots and in the streak regions. It is also found that these atoms are usually the same from all three surface conditions. They differ only in energy since it is the ion penetration distance which indirectly determines the magnitude and direction of momentum transferred to surface atoms. The vacancy surface sees an ion which penetrates deeper; this is analogous to an ion of greater energy. In the stub condition, the ion does not penetrate the surface; it transfers energy to the stub atom. The stub then assumes the role of the ion impinging on the surface, but the stub appears as an ion with less energy.

Figure 33 shows the sputtering ratios for each surface condition as a function of ion energy; assumed binding energy is a parameter. A statistical variation of $\pm$ 20% of the sputtering ratio has been assumed. This would normally be an unreasonably large deviation for laboratory results, but it is considered conservative for the numerical results from a simulation in which many parameters are unknown. The actual value of sputtering ratios obtained for the regular surface is generally low by 2-3 atoms/ion for a binding energy of 3.5 ev. Further investigation showed that, in a few cases, surface atoms 3 planes below the impact point would be sputtered with about 4-5 ev. The average increase in the (111) sputtering

ratio over the 1-7 keV range is estimated to be no greater than 2.0 atoms/ion for a binding energy range of 1.5 to 3.5 ev. This range is shown by the dotted lines in figure 32a. Vacancy and stub sputtering ratios show erratic behavior over the energy range studied.

Energy distributions of sputtered atoms are shown in figures 35-39. The preponderance of atoms with energies less than 5 ev is caused by the lack of an intrinsic surface binding energy. The sputtering selection process considers <u>all</u> atoms having <u>E</u> greater than 1 ev. Thus the P(0.50) energy, using an assumed binding energy of 3.5 ev, is 2.42 ev. This is especially evident for the 1 and 5 keV distributions. If this region is disregarded, the peaks which occur at 5-8 ev for all ion energies are assumed to be the maximum for each distribution. Secondary maxima appear at 16 ev for 1 keV sputtering, 16 ev for 2 keV, and at 14 ev for 3 keV sputtering. At higher ion energies, a secondary maximum may be present at 47 ev for 5 keV sputtering. The number of atoms sputtered in the simulation is too small to make a definite statement regarding maxima. Differences are usually measured by one, at most, two atoms.

B. The (100) Surface.

The (100) surface was sputtered normally with 1, 3, 5, and 7 keV argon. Mechanisms observed to cause sputtering were found to be nearly identical to the <u>surface mechanisms</u>

discussed for (111) sputtering. A mechanism directly comparable to the <u>deep</u> mechanism was not observed. Instead, it was found that the <u>scoop</u> and <u>mole</u> mechanisms are enhanced by the presence of the (110) channels parallel to the surface. Surface atoms which are driven into these channels do not have to burrow between the first and second layer in order to sputter nearby surface atoms. Additionally, it was found that these atoms will frequently sputter themselves by reflection from second layer atoms. The <u>squeeze</u> mechanism was observed to be the most effective sputtering mechanism at 3 and 5 keV. At 1 and 7 keV ion energies, variations of the <u>scoop</u> and <u>mole</u> mechanisms were dominant. The low-high and middle ion energy dependence observed for the dominant mechanism is directly related to the shape of the impulse by which the tion transfers energy to a n.n.

At low ion energies, the impulse is sufficiently broad that the n.n. is directed into the edge of the square of atoms behind it. The n.n. will enter the (110) channel without immediately sputtering a surface atom. When the impulse is narrow, the peak force is not necessarily greater. The target has received most of the energy given up by the ion, and the ion-n.n. impact parameter is larger. The n.n. will then <u>scoop</u> or <u>squeeze</u> a surface atom causing it to sputter. At high ion energies (7 keV) the ion was found to penetrate at least into the second layer where it was deflected towards but not into

a (110) channel. This was observed to cause second layer atoms to be scooped up and sputter surface atoms. Second layer atoms are also squeezed by their neighbors and may sputter through the vacancy left by a sputtered surface atom.

Sputtering at 3 and 5 keV was found to be caused by the scattering of surface atoms along the surface as the ion was being reflected from second layer atoms. The squeeze mechanism was observed to sequentially sputter atoms along a close packed surface row. The occurrence of a mole mechanism was conspicuously rare; even at 5 keV the energy propagation was clearly restricted to propagation parallel to the surface layer of atoms and to propagation into the crystal. The only definite momentum reversals observed were for the target atom and the ion.

The characteristic features of (100) sputtering deposit patterns are four (110) spots and a central (100) spot. The patterns are usually outlined by a hypocycloid-shaped haze; the (110) spots form the cusps of the hypocycloid. Simulation patterns were found to show these characteristic features quite well for 3 and 5 keV sputtering. The 3 keV pattern (figure 41) is a very good likeness to one at 2.5 keV reported by SWR. The (110) spot distances from pattern center were found to be 1.0 TC unit which corresponds to the distances in the 2.5 keV experimental pattern. It was further determined from numerical data that the (110) spots

were actually elliptical rather than circular. This latter characteristic is undoubtedly the result of distortion inherent in flat plate collection of sputtered atoms [13]. The 3 keV pattern was found to remain essentially unchanged as the binding energy was varied from 2.50 to 3.50 ev. The 5 keV pattern (figure 42) was almost identical to the one at 3 keV only when a binding energy near 2.00 ev was used. As the binding energy was increased, the (110) spots became less well defined (figure 43) and spots corresponding to $\langle 210 \rangle$ became the most prominent feature. The intensification of $\langle 210 \rangle$ regions was accompanied by a loss in definition of the hypocycloid outline. Similar results were obtained when sputtering at 7 keV. The hypocycloid outline in the pattern could only be observed for a binding energy near 1.50 ev.

The deposit pattern for 1 keV sputtering (figure 40) showed very little similarity to those obtained from higher energy sputtering. Four spots corresponding to $\langle 211 \rangle$ were observed; four (110) spots may also be defined but they are extremely diffuse. (The (110) spots are best seen in the point plot in figure 40a.) The finding of (211) spots at 1 keV, and the appearance of (210) spots for 5 and 7 keV ion energies suggested that the pattern might be rotated 45 degrees for low ion energy sputtering. The possibility that a rotation occurs has been investigated [35], but one has never been experimentally observed.

The different (100) pattern features which appeared with varying ion energies and binding energies were a marked contrast to the relative constancy observed for (111) patterns. (The use of a binding energy of 3.00 ev resulted in comparable (111) patterns for all ion energies.) The lack of constancy for the pattern simulations may be explained as a result of the subtraction of a binding energy from the perpendicular component of a sputtered atom's energy. (This is done to simulate the energy lost in overcoming the surface potential.) An atom sputtered with small perpendicular energy, less than 15 ev for example, may suffer an apparently small change in its perpendicular velocity, but the direction of its velocity may be considerably altered. The average <u>perpendicular</u> energy of atoms found in spot regions is about 15-20 ev from sputtering the (100) face. It is about 20-25 ev for (111) sputtering for which variations of up to 1 ev binding energy have had little effect on pattern features. This explanation does not, however, explain why the pattern at 3 keV is valid for a range of binding energies. A consideration of the atoms sputtered may clarify but not completely explain this situation. The dissimilarities seen in the (100) patterns may be directly inferred from the frequency-location diagrams for (100) sputtering (figures 46-49).

When the energy propagation is restricted to the surface, as it is for 1 keV sputtering, the (111) surface can dissipate energy through four atoms in the momentum forward semi-

circle. The (100) has only three atoms comparably located to dissipate the energy. Track displays have shown that for 1 keV sputtering, atoms 26, 116, and 132 are sputtered by a combination of <u>mole</u> and <u>squeeze</u> mechanisms. The <u>mole</u> is predominant in sputtering the atoms nearest the target, the <u>squeeze</u> mechanism becoming predominant for surface atoms which are located further from the target. Atom 26 sputters less frequently than atom 116 since it is on the opposite side of the of the crystal with respect to the impact area. Both of these atoms are found in (211) spots, but atom 116 is also found in (110) regions of the pattern. Atom 132 is found in (211) spots and the (100) spot; it is sputtered only by the <u>squeeze</u> mechanisms. When the bombardment energy is 3 keV, the deposit pattern has its expected characteristics. Correlation of high atom density regions with frequency-location data showed that the (110) spots are the result of sputtering of n.n.n.'s. Concurrently, the hypocycloid outline was found to be formed by: (1) the sputtering of the same atoms which formed (211) spots at 1 keV, and (2) the sputtering of the n.n.n.'s in the surface. These atoms were not densely deposited in the (211) regions but formed diffuse ellipses whose semi-minor axes were along quadrant bisectors. The appearance of well defined (110) spots at 3 keV is strongly suggested by the 3 keV frequency-location diagram, figure 47. Atoms 70 and 72 were observed to be sputtered with about the same

frequency as atoms 55, 56 and 86. Since atoms 70 and 72 are along a (100) axis, one might expect that they would be found in (110) spots, and this has been observed. Atoms 55 and 56 are in positions relative to the target such that they would sputter within adjacent 45 degree sectors in quadrants II and III. These atoms are found in the hypocycloid outline.

The absence of the hypocycloid at 1 keV and its presence at 3, 5 and 7 keV is readily apparent when one considers the sputtering profiles in figure 50. At 1 keV ion energy, n.n.'s are never sputtered, however, they are sputtered with increasing frequency as the ion energy increases. Atom 86, the n.n. in the quadrant containing the impact area, exhibits this behavior of increasing sputtering frequency. Atom 72 shows a sputtering profile which indicates the (110) spot formation at ion energies of 3 keV or greater. The constant nature of the profile for atom 102 at 3 keV and higher ion energies is indicative of the hypocycloid outline rather than ⟨211⟩ spot formation. Atoms 26, 116 and 132 show a generally decreasing frequency of sputtering with high ion energy. This is consistent with the loss of (211) spots at higher ion energies.

The track patterns observed for 5 and 7 keV (100) sputtering showed that atoms ejected by a squeeze mechanism are often ejected in directions opposite to those one would expect solely on the basis of the location of the atom with respect to the impact point. These occurrences were caused

by two factors: (1) the atom was squeezed against its neighbor and reflected outward and with its parallel component of momentum reversed rather than being strictly ejected outward. (2) Sputtering by near simultaneous squeeze and mole mechanisms results in ejection of an atom where the ejection direction is dependent only on the impulse delivered by the channeling atom in the mole mechanism.

Sputtering ratios for the (100) surface are shown in figure 51. The correspondence between simulation values and experimental values is quite good for the regular surface for a binding energy of 3.50 ev. The ratios for vacancy and stub surfaces show a closer correlation to the regular surface for (100) sputtering then for (111) sputtering.

The energy distributions of sputtered atoms are shown in figures 52-55. No specific maxima other than that near 5-7 ev appeared to be present.

C. The (110) Surface.

This was the last of the three face centered cubic crystal surfaces to be sputtered in this simulation. It is purposely the last to be discussed. First, experimental deposit patterns from (110) sputtering show only a large central oval area for bombardment energies greater than a few hundred ev (10). Second, a unique feature of this surface is the (110) channel; no other (hkl) surface in a face centered cubic crystal shows $\langle hkl \rangle$ channels. The sputtering mechanisms occurring for 1, 3,

5 and 7 keV ion energies were most readily observed for sputtering of this surface, and they are interrelated with the presence of (110) channels. The mechanisms are, again, identical in concept to those previously discussed for (111) and (100) sputtering. Before discussing these mechanisms separately in terms of individual crystal atoms, the features of the frequency-location diagrams (figures 56-59) are summarized.

Sputtering of the (110) surface differs significantly from the sputtering of (100) and (111) surfaces: (1) the target atom was the atom sputtered most frequently at all ion energies. (This is in agreement with results obtained by Levy [30].) (2) the number of sputtered atoms with high energies were generally those in the close packed row containing the target atom, but with the target atom located at the <u>center</u> of the row rather than at the <u>origin</u> of the row. These findings are wholly consistent with expected results when one considers the sputtering mechanisms with respect to this particular surface.

The frequent sputtering of the target is made possible by the nature of the <u>squeeze</u> mechanism but the mechanism does not itself cause the sputtering. When the target is driven into the crystal it squeezes the n.n. (in its row) and ejects it. Once the n.n. position is vacant, the target will travel through a large, potential-free area before striking a second

layer atom. The target strikes this second layer atom and is free to reflect outward without finding a surface atom directly in its path. The target then transfers most of its parallel momentum to a n.n.n. in the row. The parallel impulse is then propagated down the surface row. Warping of this one row causes additional atoms to sputter. This sputtering sequence is also observed as a result of the ion striking the n.n. which is in the quadrant defined by the impact area. A rather surprising continuation of this sputtering mechanism was observed to occur in atom rows located both above and below the horizontal row containing the target. Second layer atoms which receive energy from the target or ion are driven into (111) apparent channels. They pass behind another second layer atom causing it to be ejected outward and strike two adjacent surface atoms. Sputtering is, again, initiated in a surface row. Sputtering profiles for the target (atom 72) and atoms 42, 71, 73 and 102 are shown in figure 60. Atoms 42 and 102 are the n.n.'s to the target; atoms 71 and 73 are those which initiate sputtering in the horizontal rows containing them. Second layer atoms are sputtered more frequently as the ion energy is increased.

Simulation deposit patterns from (110) sputtering (figures 61-64) tend to show more of an oval outline than a uniformly dense central oval region. The central region can be made more dense by including atoms sputtered with less than 1 ev

perpendicular energy in the probability-of-sputtering selection process. This did not seem justifiable for (110) pattern production since these small energy atoms were excluded from (100) and (111) patterns. The 1 keV point plot (figure 61a) showed indications of (100) spots but these cannot be clearly seen in the deposit pattern (figure 61b). Their presence was substantiated by numerical data. The average energy deposit data showed that the average energy of atoms in ⟨100⟩ regions was nearly double that of atoms found in the central oval. This is a constant characteristic of <u>non-central</u> spot regions. At higher ion energies there was no direct indication of the presence of these spots either by numerical data or energy deposit data. A few atoms having high energy were found in these regions but the area density was too small to form a spot in the pattern. The set of atoms found to form the central oval for sputtering at all ion energies was not a well defined group such as has been found for (100) and (111) sputtering. The atoms forming the (100) spots from 1 keV sputtering are those which are either n.n.'s to the target or n.n.'s to the atom which initiates sputtering in each horizontal row.

The sputtering ratio for (110) sputtering is shown in figure 65. Agreement with experimental data from the numerical and curve shape aspect was poorer for this surface than the other two surfaces. This is apparently caused by

(110) sensitivity of the sputtering ratio to the A parameter in the argon-copper potential function. Levy [30] obtained better curve shapes using A = 11.435 whereas A = 12.56 has been used in this study. This sensitivity has not been observed for (100) and (111) sputtering.

Energy distributions are shown in figures 66-69. The notable feature of (110) sputtering is that the energy of sputtered atoms is generally higher for (110) sputtering than (100) or (111) sputtering.

D. Results of Ancillary Studies.

During the course of the simulation, it became apparent that certain extensions of this study should be made. It was particularly desirable to probe five areas:

(1) Sputtering mechanisms peculiar to high bombardment energies (up to 40 keV).

(2) Sputtering of the (110) surface by high energy ions which are directed towards (110) channels.

(3) Sputtering mechanisms for an ion heavier than the target.

(4) Sputtering of the (0001) basal surface of a hexagonal close packed crystal.

(5) Sputtering the (100) surface at ev ion energies.

Investigation of the first two of these five areas were limited somewhat by the restrictions for the copper-copper and argon-copper potential function. They are usually assumed

valid up to about 10 keV, however, if small impact parameters are assumed to rarely occur, valid results may be expected. Areas (3) and (4) involve the use of unknown parameters. Accordingly, the validity of results from investigating these two areas cannot be assured.

The search for mechanisms peculiar to high energy sputtering was made using the (111) surface. This surface was considered the one most likely to show additional mechanisms since it is the most densely packed surface. The failure to find mechanisms (part A of this section) peculiar to high energy sputtering was not too surprising.

The sputtering of the (110) surface by ions directed into (110) channels was investigated by determining the sputtering ratio for ions impacting at the two impact points located nearest the channels. The sputtering ratio curve for channel shots is shown in figure 70. The discontinuity between the low and high ion energy curves is assumed to be the result of breakdown of the potential functions. The important result is that sputtering always occurred for channel shots, even when 40 keV ions were used.

The third area was examined using xenon to sputter the (111) surface. Argon-copper potential parameters were used since those for xenon-copper were not available. Runs were made at 3 and 5 keV. At both energies, the ion penetrated at least to the fourth layer of atoms; no indication of momentum

reversal of the ion was observed. The ion was found to be channeled, just before penetrating the third layer, into (110) channels. It initiated cascades which propagated into the crystal.

The fourth area was investigated to see if the effect of surface geometry on the sputtering deposit patterns could be determined by a comparison of (111) sputtering of a face centered cubic crystal with sputtering the (0001) surface of a hexagonal close-packed crystal. Hasiguti, Hanada, and Yamaguchi[36] have sputtered zinc with 8 keV argon; the deposit pattern showed an outlined, equilateral hexagon with a central haze. An attempt was made to reproduce this pattern with the simulation model modified for zine-zinc interactions. The potential parameter was adjusted for a Born-Mayer type potential $V(r) = Ae^{-r/b}$ where $A = 52 (Z_1Z_2)^{3/4}$ keV. This relationship was determined by Andersen and Sigmund[37]. The argon-zinc potential parameters (assuming a Born-Mayer type potential) were approximated by using those for argon-copper interactions. Neither the sputtering ratio nor deposit pattern matched the reported results. This was not unexpected since the zinc atoms in the crystal must be represented as ellipsiods (with the minor axis in the basal plane) rather than represented as spheres.

The (100) surface was sputtered at 100 ev to investigate the possibility of a 45 degree pattern rotation for low ion

energy sputtering. The number of atoms which were sputtered was extremely small. All sputtered atoms had energies less than 10 ev. It was found that the atoms sputtered most frequently from the regular surface were n.n.n.'s (figure 71). Bombarding vacancy and stub surface conditions also resulted in a predominance of n.n.n.'s being sputtered rather than sputtering of the atoms forming the square about the target atom.

E. Results Common to All Surfaces.

Momentum focusing was observed to occur only <u>into</u> the crystal for the three copper surfaces studied. This was particularly evident from atom track displays of (111) surface sputtering. If an atom underwent momentum reversal, it was always by reflection from atoms located no deeper in the crystal than the third layer. Even for 7 keV ion energies, crystal atoms located deep in the crystal were always driven inward. A surprisingly large number of atoms with large energies were found to move between second and third layers with their motion nearly parallel to the surface and with a small, inward-directed momentum component. The energy which appeared to be delivered in impulses to atoms still at lattice sites, dissipated through the crystal. These atoms rarely acquired more than 20 ev through the energy impulse process. Their motion was restricted since they were surrounded by other atoms.

The target atom in the (100) and the (110) surfaces, when struck at near zero impact parameter by the ion, always transmitted the majority of its energy billiard-ball fashion in close packed rows perpendicular to the surface. (Atoms to which this energy was transferred escaped through the back face of the crystal.) There were a few cases in which one of these atoms would initiate another chain. The chain was never more than 2-3 atoms in length before the energy was either wholly dissipated or the chain stopped by divergence of the momentum to form numerous small cascades directed into the crystal interior.

The unique arrangement of atoms in the first layer was observed to be a dominant factor in determining ejection directions for all surfaces. Atoms which were ejected other than nearly normal to the surface were always influenced by their neighbors. Atoms which were ejected at angles near 45 degrees to the normal would reflect from their neighbors, often ending up as normally ejected atoms. This effect was most pronounced for (111) sputtering since the six atoms acted as a lens, but it was also seen for (110) sputtering in which a lens is formed by second layer atoms. The (100) surface showed a strong lens effect although one would not necessarily assume that it occurs. Sputtered atoms, originally adjacent in the (100) surface, were often observed to be ejected almost simultaneously. In these situations they

were ejected nearly normal to the surface. This may be the genesis of dimers recently observed by Woodyard[35].

The spot regions of the deposit patterns from (100) and (111) sputtering always contained more high energy (> 10 ev) than low energy atoms. But the energy distribution was more uniform than increasing with the ion energy. It was not peaked at any one or group of energies. Atoms with low ion energies were predominantly found in the central region of the pattern.

6. Conclusions.

The observable quantities of sputtering appear to be interdependent on only the sputtering mechanisms. There is no evidence that these quantities are interrelated. The qualitative and quantitative data from the simulation indicate that the deposit pattern, sputtering ratio, and energy distribution of sputtered atoms cannot be correlated with each other; one cannot predict a sputtering ratio from an energy distribution. But, each of these quantities can be cross-correlated between surfaces.

The main features of deposit patterns appear to be determined only by the surface geometry of the crystal. The formation of (111) pattern spots is attributed primarily to assisted focusing by the hexagonal lens. The predominance of trigonal rather than hexagonal symmetry is considered a natural result of the brief (112) channeling observed in the mole mechanism. The appearance of streaks between the spot pairs and the appearance of a hexagonal spot pattern at 2 keV suggests that use of a hemispherical collector in the simulation will show the three (114) spots which were observed by Southern and Robinson[33]. However, no distinction can be made between the (110) and (114) spots on the basis of pattern location. If the mole mechanism is predominant at certain energies the (110) spots should be more intense than the (114) spots. If the squeeze mechanism is predominant,

the (110) and (114) spots should have more equal intensities.

The nearly exact simulation of a (100) pattern at 3 keV is considered one of the best arguments that sputtering is mostly a surface phenomenon. Neither the potential form nor its parameters for copper-copper and argon-copper interactions are known with certainty. If sputtering was a deep phenomenon, one might accept an argument that spots in the pattern could be produced without exact knowledge of the potential. However, the hypocycloid outline, definitely present in the simulation pattern, is considered the feature of the pattern which would be most sensitive to small variations in the potential if sputtering involved more than the first few layers. This conclusion is consistent with the apparent rotation of the 1 keV pattern. Atoms found in ⟨211⟩ regions were sputtered when the energy transferred by the ion to the target was as small as 40 ev. This compares favorably with a calculated transfer value of 75 ev for a 0.5 Å impact parameter [21]. A sputtering threshold energy of 50 ev has been reported [32].

The inability to produce consistent (100) patterns at a given binding energy for 5 and 7 keV sputtering is undoubtedly due to the unknown condition of the surface. It would be unreasonable to assume that the binding energy is a decreasing function of ion energy only for the (100) surface. The disruption of the surface by the first group of incident ions

is a factor which cannot be ignored. The sputtering ratios determined for the (100) surface as well as for the (110) and (111) surfaces, were within reasonable limits when the assumed binding energy is in the range 1.50 to 3.50 ev. No definite value of binding energy can be determined from the patterns and sputtering ratios unless a weighting factor is used for the surface condition at the time of ion impact. The assignment of weighting factors would be, at best, a guess.

Three surprising features were observed in simulation deposit patterns. The first, the apparent rotation of the (100) pattern at 1 keV, will be further discussed. The rotation of the (100) pattern for low energy sputtering has not been observed. The results of the simulation indicate that such a rotation is possible. This conclusion is based on empirical rather than theoretical considerations. The hypocycloid outline found at 3 keV in the simulation appears to be formed by the same atoms which form (211) spots at 1 keV. Furthermore, no explanations have been previously proposed as to why the outline is a hypocycloid in experimental patterns. One would expect that a circular or perhaps a non-distinct outline would be observed when the (100) surface is sputtered. Accordingly, it is proposed that the hypocycloid outline is a result of the inability of the (100) surface to completely focus atoms sputtered by a squeeze mechanism for bombardment

energies at which the energy propagation is not confined in the surface.

The second feature was the unique form of the bonds which connected the spots in the simulation pattern for (111) copper sputtered at 5 keV. The appearance of the similar outline, a spherical triangle, was observed in a pattern of (111) copper sputtered with 1.5 keV krypton by Yurasova and Bukhanov[34]. The third feature was the hexagon spot pattern at 2 keV, a pattern seen by Anderson and Wehner[10] for (111) copper sputtered with 400 ev mercury. The similarities observed in the simulation patterns with these anomalous features of the experimental patterns suggested that common factor other than the (111) copper surface might be present. The momentum ratios of 400 ev mercury-2 keV argon and 1.5 keV krypton-5 keV argon are 1.0 and 0.8 respectively. This is not considered to definitely establish a sputtering correlation based only on ion momentum. The momentum ratios for 1.5 keV krypton and 4 and 3 keV argon are 0.9 and 1.0 respectively. Ideally, the spherical triangle would be observed in the 3 keV (111) simulation pattern. Additionally, when (111) copper is sputtered at high temperatures, the triangular outline has been observed to become more pronounced [34]. The absence of such a momentum scaling effect could be easily shown by experimentally sputtering (111) copper with ion momentum comparable to that of 400 ev mercury.

The general consistency of the numerical values of sputtering ratios, and energy distributions of sputtered atoms and likeness of the patterns with experimental data is a strong argument for the validity of a computer simulation of sputtering. It is remarkable that the consistency is as good as it is. The model uses only a repulsive potential, the crystal size used in the simulation is an infinitesimal portion of the smallest laboratory specimens, and the potential form and parameters are comparatively crude. It is concluded that the results obtained substantiate the concept of transparency and the occurrence of momentum focusing only within the surface layer.

BIBLIOGRAPHY

1. K.H. Kingdon and I. Langmuir, Physical Review 22, 148 (1923).

2. E. Blechschmidt and A. von Hippel, Annalen der Physik 86, 1006 (1928).

3. A. von Hippel, Annalen der Physik 80, 672 (1926).

4. C. H. Townes, Physical Review 65, 319 (1944).

5. F. Keywell, Physical Review 97, 1611 (1955).

6. D. E. Harrison Jr., Physical Review 102, 1473 (1956).

7. G. K. Wehner, Journal of Applied Physics 25, 270 (1953).

8. E. B. Henschke, Physical Review 106, 737 (1957).

9. R. H. Silsbee, Journal of Applied Physics 28, 1246 (1957).

10. G. S. Anderson and G. K. Wehner, Journal of Applied Physics 31, 2305 (1960).

11. O. Almén and G. Bruce, Nuclear Instruments and Methods 11, 257 (1961).

12. G. D. Magnuson and C. E. Carlston, Journal of Applied Physics 34, 3267 (1963).

13. A. L. Southern, W. R. Willis, and M. T. Robinson, Journal of Applied Physics 34, 153 (1963).

14. C. R. Piercy, M. McCargo, F. Brown, and J. A. Davies, Canadian Journal of Physics 42, 1116 (1964).

15. O. S. Oen, D. K. Holmes, and M. T. Robinson, Journal of Applied Physics 34, 302 (1963).

16. M. T. Robinson and O. S. Oen, Physical Review 132, 2385 (1963).

17. D. E. Harrison Jr., R. W. Leeds, and W. L. Gay, Journal of Applied Physics 36, 3154 (1965).

18. J. M. Fluit, P. K. Rol and J. Kistemaker, Journal of Applied Physics 34, 690 (1963).

19. J. M. Fluit and P.K. Rol, Physica 30, 857 (1964).

20. C. Lehman and P. Sigmund, Physica Status Solidi 16, 507 (1966).

21. D. Onderdelinden, F. W. Saris, and P. K. Rol, Proceedings of the Seventh Internation Conference on Phenomena in Ionized Gas I (Beograd 1966).

22. D. Onderdelinden, F. W. Saris, and P.K. Rol, Nuclear Instruments and Methods 38, 269 (1965)

23. J. B. Sanders and J. M. Fluit, Physica 30, 129 (1964)

24. J. B. Sanders and D. Onderdelinden, Proceedings of the Seventh International Conference on Phenomena in Ionized Gases I, (Beograd 1966).

25. J. B. Sanders, Physica 32, 2197 (1966).

26. J. B. Gibson, A. N. Goland, M. Milgram, and G. H. Vineyard, Physical Review 120, 1229 (1960)

27. D. E. Harrison Jr., C. E. Carlston, and G. D. Magnuson, Physical Review 139, A737 (1965).

28. W. L. Gay, Machine Calculation of Energy Transfer Phenomena in a Bombarded Lattice, Master of Science Thesis (Unpublished), Naval Postgraduate School.

29. J. P. Johnson III, Calculation of Surface Binding Energies by Computer Simulation of the Sputtering Process, Master of Science Thesis (Unpublished), Naval Postgraduate School.

30. N. S. Levy (Deceased), Computer Simulation of the Sputtering Process, Master of Science Thesis (Unpublished), Naval Postgraduate School.

31. D. E. Harrison Jr., private communication.

32. D. E. Harrison Jr., and G. D. Magnuson, Physical Review 122, 1421 (1961)

33. M. T. Robinson and A. L. Southern, Sputtering Experiments with 1- to 5- keV Ar^+ Ions II. Monocrystalline Targets of Al, Cu, and Au, (To be published).

34. V. E. Yurasova and V. M. Bukhanov, Soviet Physics - Crystallography 7, 199 (1962).

35. J. H. Woodyard, private communication.

36. R. R. Hasiguti, R. Hanada, and S. Yamaguchi, Journal of the Physical Society of Japan 18, Supplement III, 164 (1963).

37. H. H. Andersen and P. Sigmund, On the Determination of Interatomic Potentials in Metals by Electronic Irradiation Experiments, Danish Atomic Energy Commission, Risö Report No. 103, May 1965.

38. H. D. Hagstrum, Physical Review 96, 336 (1954).

APPENDIX A

The Beam Model

A. Impact areas and Impact points.

Each crystal surface contains an intrinsic, plane geometric shape; hexagon for (111) surface, square for (100) surface, and rectangle for (110) surface. A volume element of the (hkl) surface is defined by the area of this intrinsic shape and a depth of some number of (hkl) planes. This volume is chosen so that by translation along axes of a Cartesian coordinate system the entire crystal may be generated. The smallest intrinsic area which can be chosen for each surface and still satisfy the translation requirement is shown in figure 72. A finite number of points is symmetrically distributed within each of these areas to represent the infinite set of possible points of impact for an incident ion. These smallest areas are further divided into representative <u>impact areas</u> which are seen from figure 73 to be degenerate under appropriate rotations and/or inversions of the coordinate axes. Since the sectors are degenerate, the set of <u>impact points</u> in each sector is also degenerate; only the points contained in one impact area need be used to represent bombardment of the entire area. The coordinate axes rotation and inversion schemes are discussed in Appendix C (Deposit Pattern Production).

The independence of the impact point set used, with

respect to number and kinetic energy of atoms sputtered, was tested using two sets of points. No dependence was found. Results for the (111) surface using a 3 keV ion are shown in figure 74 as an example. Set 1 points are those shown in figure 73, set 2 (not shown) is a set of eleven points which are located between the points of set 1.

B. Neutralization of Beam ions.

The assumption that argon ions are neutralized prior to impact on copper may be inferred from results of a theoretical study of secondary electron emission by Harrison et. al.[27]. Consideration of atom-atom rather than ion-atom interactions gave results in reasonable agreement with experimental data.

A supporting argument for neutralization is based on Hagstrum's theory of Auger ejection of electrons[38]. The probability of an ion being neutralized in dx at x is:

$$P_t(x,v) = a \exp\left\{ - \exp\left[-a(x-x_m)\right] \quad -a(x-x_m)\right\}$$

where $x_m = (1/a)\ \ln\ (A/av)$ is the value of x where P_t is a maximum. The parameters A and a occur in the transition rate function, and v is the velocity of an ion starting at $x = \infty$. Hagstrum used tungsten as an example and obtained the value of A by empirical means, the value of a from published data. Rather than attempt an exact proof of neutralization for argon on copper, Hagstrum's results for argon on tungsten have been used to give an order of magnitude, at worst, approximation. Accordingly, $1.63 < x_m < 2.18$ Å for 1 to 10 keV argon ions on

copper; this is a reasonable distance from the crystal surface and one may assume that neutralization occurs.

C. Ion Deflection by Surface Potential.

As a first approximation, it is assumed that a singly positive-charged argon ion sees the crystal as a single, fixed scattering center having Z-1 positive charge. The well known equation for a central force-induced hyperbolic orbit is used in conjunction with figure 75 to determine the deflection.

$$r(\theta) = (L^2/mk) \Big/ \left[-1 + (1 + 2EL^2/mK^2)^{1/2} \cos(\theta - \theta_0) \right]$$

L = ion angular momentum m = ion mass

E = ion energy $K = Q_1 Q_2 / 4\pi\epsilon_0$

θ_0 = angle of closest approach

The angular momentum L is determined at $r \to \infty, \theta \to \pi$ to be $L = mvb$ where $mv^2/2 = E$ and b is the impact parameter. The equation for $r(\theta)$ is put in a more convenient form by making the substitution $L^2 = (mvb)^2 = 2mEb^2$ to give

$$r(\theta) = b\,(2Eb/k) \Big/ \left\{ -1 + \left[1 + (2Eb/k)^2 \right]^{1/2} \cos(\theta - \theta_0) \right.$$

The angle of closest approach θ_0, is determined as a function of the product Eb by requiring the denominator to vanish for $\theta = \pi$. Once θ_0 (as a function of Eb) is known, the deflection ratio r/b is calculated at the crystal surface. The deflection calculated is for an unneutralized ion, thus greater than that for an ion which is neutralized at some distance in front of the surface. Plots of r/b at the surface and θ_0 as functions of the ion kinetic energy-impact parameter

product are contained in figure 76. The numerical values are for an $Ar^+ - Cu^+$ system.

A more sophisticated approximation, scattering from a fixed dipole of same charge sign, requires a messy integration. Rather than follow this line, one may expect from the nature of the problem that the path of the approaching ion will undergo some oscillatory motion or perhaps corkscrew motion as the ion is influenced by the surface potential. In either case one would expect that the net acceleration of the ion parallel to the crystal surface would be no greater than that due to a single fixed scattering center. With these considerations, figure 76 is used to determine the percentage of ions which will be appreciably deflected. As an example of an appreciable ion deflection, consider r/b = 2.0; from figure 76, Eb = 3.5×10^{-2} keV-Å. An energy range of 1-10 keV for argon ions, that used in this study, corresponds to a range of impact parameters of 0.035 - 0.0035 Å. The fraction of surface area, and therefore fraction of ions which will be appreciably deflected is $(0.035)^2/(1.26)^2 = 7.7 \times 10^{-4}$ for 1 keV ions and 7.7×10^{-6} for 10 keV ions (1.26 Å is the copper atom effective radius in the crystal). This negligibly small fraction of ions cannot influence the macro aspects of the sputtering model.

D. Equilibrium State During Impact.

The use of a single atom approximation to the beam with

the crystal model described in the main text requires that the crystal region be in an equilibrium state at the time of an ion impact. It is not necessary that this equilibrium state be identical to previous equilibrium states since the variety of surface configurations available in the model provides for random surface conditions. It is necessary that the time required for the crystal region to return to an equilibrium state be small with respect to the arrival-time intervals of the ions. Satisfaction of this condition is determined by comparing an experimental beam flux over the area of the crystal face of the model used to the time required for completion of all energetic collisions in the model.

Beam intensities of the order of 100 μamps/cm^2 were used by Magnuson and Carlston[12]. If a beam of this intensity is incident on a crystal surface area of less than $10^3 \mathring{A}^2$ such as in the model, the ion flux over this area is less than 100 ions/sec, an ion arrival-time interval of 10^{-2} seconds; all energetic collisions in the model are completed within about 10^{-12} seconds. The relaxation time of the region is thus much smaller than the ion arrival-time intervals and the condition, that the crystal region be in an equilibrium state at the time of impact, is satisfied.

APPENDIX B

Positioning the Ion

The ion is positioned tangent to the first target atom it will strike. Since this is a dynamic rather than static process it is not necessary that this be a stable position on the crystal surface. Figure 77 shows the ion at its arbitrary initial position and calculated final position, both with respect to the impact point and target atom. The initial position is a small distance in front of the surface, beyond the eroded potential range of the crystal atoms. This position is described by a vector $\underline{r_1}$ originating at the impact point and having direction parallel but opposite to the ion's velocity vector. The vector $\underline{r_2}$, from the impact point to the target atom, is known since the target atom's coordinates are known; the vector $\underline{r_1}$ is known, and it is desired that vector $\underline{r_{12}}$ have a magnitude equal to the distance between centers of two tangent atoms, $\underline{2r_o}$. The law of cosines is used to compute the magnitude of $\underline{r_3}$ which lies along $\underline{r_1}$. Accordingly, the following calculations are made:

$$\cos\alpha = \frac{\vec{r}_1 \cdot \vec{r}_2}{|r_1|\;|r_2|}$$

$$(r_3)^2 - (2r_2\cos\alpha)\,(r_3) + (r_2^2 - (2r_o)^2) = 0$$

$$(r_3) = r_2\cos\alpha + \left[r_2^2\cos^2\alpha - (r_2^2 - (2r_o)^2)\right]^{1/2}$$

The positive square root solution is chosen to give the tangent on the outside hemisphere of the target atom.

The ion positioning is accomplished automatically for each run by subroutine START, which is contained in the computer program for the sputtering simulation.

APPENDIX C

Production and Analysis of Sputtering Deposit Patterns

A. Production.

A sputtering deposit pattern represents the intersection points of atoms' velocity vectors with the surface of a collector plate. The sputtered atoms from the simulation are collected on a flat plate by determining these points of intersection. Each atom which exits through the crystal surface is initially assumed to have been sputtered and a data card has been prepared for each one. Data of particular interest are each velocity component magnitude and the kinetic energy perpendicular to the surface; data of secondary interest are atom number, impact point used and ion kinetic energy. (The use of these last data will be discussed shortly.)

It is recognized that each sputtered atom has lost some energy to overcome the surface binding energy. An assumed value of binding energy is subtracted from the perpendicular kinetic energy and a new perpendicular velocity component is calculated. Parallel velocity components are normalized to the new perpendicular component to give a two dimensional coordinate point. This point is the intersection of the atom's velocity vector with an imaginary collector plate placed at unit distance from the target surface. Each point is then rotated and/or mirrored about the coordinate axes to give the intersection of a velocity vector which would have resulted for an

ion impacting at the corresponding impact point in each of the other impact areas. The impact areas are shown in figure 73 and the coordinate point rotation and mirroring values are listed in program DATASORT which is used to generate the points. Each point is plotted using program DATAPLOT with a CDC160A computer and a CalComp plotter to give a point plot. The dimensions of the plots are in target-to-collector or T-C units since these points have been normalized to unit target-to-collector distance. The scale which has been used permits plotting deposit points of atoms which have been sputtered within an escape cone of about 63 degrees (57 degree cone shown in figures). This has been found satisfactory to contain all pattern features of interest.

The point plots show only point patterns and therefore do not accurately simulate experimental patterns which are area density patterns. The conversion of a point plot to a smooth area density pattern is made by photographing the point plot with the camera defocused such that no single point is distinguishable but high and low density areas are prominent. Developing and printing is controlled to bring out the high density areas while maintaining the haze background. Loss of intensity in some spot regions cannot be avoided such as seen in figures 6b and 12b. The process must be adjusted for each pattern; the sequence of photography, developing, and the printing of the positive image is highly dependent on the

ability of the photographer. Concurrently, the quality of reproduction of these patterns in printed form depends on the plate preparation, the printing press, and the paper used.

B. Analysis.

A 30 x 30 square grid is placed over the central 3.0 x 3.0 unit square of the raw pattern by program DATAGRID. The identification number of an atom and the impact point and impact area of the run in which that atom was sputtered are recorded for each atom in the grid square. The total number of atoms, the total energy, and the average energy per atom for each grid square are printed in separate square arrays. The individual grid square data provides for correlation between an atom's crystal location and its deposit point in the pattern; the square arrays of the number of atoms and the total and average energy densities may be compared directly with the point plot or smooth pattern for analysis of pattern features.

APPENDIX D

1. The sputtering program.

```
      PROGRAM FCCSPUT
C
C     THIS IS A REDO OF TWOPOT 3 FOR F63
C THIS PROGRAM CONSTRUCTS THE MICROCRYSTALLITE AND INTEGRATES THE
C FORCE LAWS FOR ALL ORIENTATIONS. DT IS RECALULATED EACH TIMESTEP,
C AND THE IMPROVED ROEM METHOD AT THE SURFACE IS INCLUDED
C

                              SECTION 1

      DIMENSION VX(500),VY(500),VZ(500)
      DIMENSION RXI(500),RYI(500),RZI(500)
      DIMENSION RXK(500),RYK(500),RZK(500)
      DIMENSION DX(500),DY(500),DZ(500)
      DIMENSION PKE(500),PTE(500),KCUT(500),PKEY(500)
      DIMENSION IH1(10),IHS(5),IHT(3),IHB(3),TARGET(2),BULLET(2)
      COMMON/COM1/RX(500),RY(500),RZ(500),LCUT(500),LL
      COMMON/COM2/ROE,ROE2,ROEM,AC,PAC,PPTC,PTC,PFPTC,FPTC,FM,PFIV,TPOT
      COMMON/COM3/EXA,EXB,FXA,PEXA,PEXB,PFXA
      COMMON/COM4/IX,IY,IZ,IXP,IYP,IZP,SCX,SCY,SCZ
      COMMON/COM5/FX(500),FY(500),FZ(500),PPE(500)
      COMMON/COM6/COXI,COYI,COZI,RXS,RYS,RZS,FAC
      COMMON/COM7/R1,LSS,SPX,SPZ,COY
      EQUIVALENCE(RXK,DX),(RYK,DY),(RZK,DZ)
      FORF(X)=EXPF(FXA+EXB*X)
      PFORF(X)=EXPF(PFXA+PEXB*X)
      FPTF(X)=EXPF(AC+EXB*X)
      PFPTF(X)=EXPF(PAC+PEXB*X)
      POTF(X)=EXPF(EXA+EXB*X)
      PPOTF(X)=EXPF(PEXA+PEXB*X)
      DO 2 I=1,2000
      FX(I)=0.0
      PKE(I)=0.0
    2 RX(I)=0.0
```

```
      DO 3 I=1,4500
    3 VX(I)=0.0
 9010 FORMAT(10A8)
 9020 FORMAT(5A8,1X,A7,5I2,2F5.2,2F6.2)
 9030 FORMAT(2A8,3F8.5,3A8,F6.2)
 9040 FORMAT(2A2,1X,A4,1X,F6.2,4F8.5,1X,F5.3,1X,I5,2I4,1X,A4)
 9601 FORMAT(1H1)
 9610 FORMAT(40X,5A8,/,20X,10A8,/)
 9620 FORMAT(3(I5,3F8.5,10X))
 9630 FORMAT(105X,4HPAGE,I3,/,1H1)
 9640 FORMAT(1H(,A4,8H) PLANE ,1X,A7,8H SURFACE,18H, PRIMARY ENERGY =,
     2 F6.2,21H KEV, CRYSTAL SIZE ( ,I2,3H X ,I2,3H X ,I2,18H ),  IMPACT
     3 POINT ,A4/)
 9645 FORMAT(9HTARGET - ,2A8,10HPRIMARY   ,2A8,1X,14HLATTICE UNIT =,F7.4
     2,9H ANG,    ,18HCUTOFF ENERGY    =,F6.2,5H   EV)
 9650 FORMAT(4X,6HMASS =,F7.2,13X,6HMASS =,F7.2,9X,14HLATTICE TEMP =F7.4
     2,7H DEG K,,20H  THERMAL CUTOFF   =,F6.2,5H   EV/)
 9655 FORMAT(12HPOTENTIAL   ,3A8,3X,5HPEXA=,F9.5,2X,5HPEXB=,F9.5,2X,5HFX
     1A =,F9.5)
 9660 FORMAT(12X,3A8,3X,5HEXA =,F9.5,2X,5HEXB =,F9.5,2X,5HPFXA=,F9.5/)
 9665 FORMAT(30HTARGET POINT ON CRYSTAL    X =,F8.5,5H, Z =,F8.5,4H,   ,
     2 7X,12H  COS TO X =,F7.4,12H  COS TO Y =,F7.4,12H  COS TO Z =,F7.4
     3,)
 9670 FORMAT(30HPRIMARY START POINT (LU)   X =,F8.5,5H, Y =,F8.5,5H, Z =
     2,F8.5/)
 9675 FORMAT(10H TIMESTEP ,I4,40X,22H  ELAPSED TIME (SEC) =,E10.4,21H, L
     2AST TIMESTEP WAS =, E10.4/)
 9680 FORMAT(107H     ATOM     DX          DY          DZ          VX          VY
     1          VZ          KE          PE          TE        KE(Y)      /)
 9685 FORMAT(1I8,3F10.5,3E10.2,4F10.4 )
 9690 FORMAT(/4X,F10.3,24H EV,TOTAL KINETIC ENERGY,,F10.3,27H EV,TOTAL P
     1OTENTIAL ENERGY,F10.3,17H EV,TOTAL ENERGY   )
 9695 FORMAT(47X,16HSUMMARY OF ATOMS//)
 9700 FORMAT(119H ATOM      RX              RY           RZ               VX
     1           VY                VZ           PKE          PPE LCUT KCUT /)
 9705 FORMAT(I4,3F12.8,3E16.9,2F10.4,I2,I5)
```

```
9710 FORMAT(111H ATOM   RX       RY       RZ       DX       DY       DZ       VX
    1   VY        VZ       DCOSXDCOSYDCOSZ   PKEY LCUT KCUT        /)
9715 FORMAT(I4,3F7.2,3F7.2,3E9.2,3F5.2,1F8.2,2I4)
9720 FORMAT(2A2,1X,A4,1X,F6.2,1X,A4,1X,I4,3E10.2,1X,I1,1X,F8.2,1X,F8.5)
     ZE= .0
     ECUT=0.1
     ICUT=15
     FM=1.0E-8
     QM= .01
     PFIV=0.5
     QUIT=0.5
     SLOW=0.5E-12
     EI=25.0
      READ (50,9010) IH1
      READ (50,9020) IHS,SUR,IX,IY,IZ,LS,LSS,SPX,SPZ,CVR,CVS
      READ (50,9030) BULLET,GMAS,PEXA,PEXB,IHB,THERM
      READ (50,9030) TARGET,TMAS,EXA,EXB,IHT,TEMP
     CELS=-CVS*1.0E-13
     CVE=1.60E-19
     GVM=1.672E-27
     CVD=CVR*1.0E-10
     FXA=LOGF(-EXB*CVE/CVD)+EXA
     PFXA=LOGF(-PEXB*CVE/CVD)+PEXA
     AC=LOGF(CVE/CVD)+EXA
     PAC=LOGF(CVE/CVD)+PEXA
     ROE2=2.0
     ROE=SQRTF(ROE2)
     PTC=POTF(ROE)
     FRC=FORF(ROE)
     FPTC=FPTF(ROE)
     PFPTC=PFPTF(ROE)
     PFRC=PFORF(ROE)
     PPTC=PPOTF(ROE)
     BENGY=2.0
     CVB=0.774E-9
```

SECTION 2

```
 4 READ (50,9040) TAR,PRI,PLA,EVR,RBX,RBZ,COX,COY,DTI,NTT,NS,ND,PNUM
   IF(EVR) 9999,9999,5
 5 ROEM=ROE-DTI
   PLANE=PLA
   BX=RBX+SPX
   BZ=RBZ+SPZ
   EV=EVR*1.0E+3
   PGMAS=GMAS*CVM
   PTMAS=TMAS*CVM
   HGMAS=0.5*PGMAS/CVE
   HTMAS=0.5*PTMAS/CVE
   IXP=(IX+1)/2
   IYP=(IY+1)/2
   IZP=(IZ+1)/2
   RX(1)=0.0
   RY(1)=0.0
   RZ(1)=0.0
   DO 8 I=1,500
   KCUT(I)=0
 8 LCUT(I)=0
   GO TO ( 10,15,20),LS
10 CALL L100
   GO TO 30
15 CALL L110
   GO TO 30
20 CALL L111
30 AIX=IX
   WRITE (51,9601)
   AIY=IY
   AIZ=IZ
   RXBND=AIX*SCX
   RYBND=AIY*SCY
   RZBND=AIZ*SCZ
```

```
      RXS=BX*SCX
      RYS=0.0
      RZS=BZ*SCZ
      FAC=ABSF(0.05*COY)
      R1=R1+FAC
      VOL=SQRTF(EV/HGMAS)
      VX(1)=VOL*COX
      VY(1)=VOL*COY
      COZ=1.0-COX*COX-COY*COY
      COZ=ABSF(COZ)
      COZ=SQRTF(COZ)
      VZ(1)=VOL*COZ
      COXI=-COX
      COYI=-COY
      COZI=-COZ
      DO 55 I=2,LL
      VX(I) = 0.0
      VY(I) = 0.0
   55 VZ(I) = 0.0
      CALL START
      DO 60 I=1,LL
      RXI(I)=RX(I)
      RYI(I)=RY(I)
   60 RZI(I)=RZ(I)
      DT=DTI*CVD/VOL
      TIME=0.0
      NT=
      NSHUT=0
      ISHUT=0
      JSHUT=0
      INDEX=0
      WRITE (51,9695)
      DO 65 I=1,LL,3
      K=I+1
      J=I+2
   65 WRITE(51,9620)  I,RX(I),RY(I),RZ(I),K,RX(K),RY(K),RZ(K),J,RX(J),
```

```
2  RY(J),RZ(J)
  NPAGE=1
  WRITE (51,9630) NPAGE
  NPAGE=NPAGE+1
```

```
 68 DTOD=DT/CVD
    HDTOD=0.5*DTOD
    DTOMB=DT/PGMAS
    HDTOMB=0.5*DTOMB
    DTOM=DT/PTMAS
    HDTOM=0.5*DTOM
    EMAX=0.0
100 CALL STEP
    IF(INDEX) 9999,210,260
210 INDEX=1
    I=1
    RXK(I)=RX(I)
    RYK(I)=RY(I)
    RZK(I)=RZ(I)
    RX(I)=RX(I)+DTOD*(HDTOMB*FX(I)+VX(I))
    RY(I)=RY(I)+DTOD*(HDTOMB*FY(I)+VY(I))
    RZ(I)=RZ(I)+DTOD*(HDTOMB*FZ(I)+VZ(I))
    DO 250 I=2,LL
    RXK(I)=RX(I)
    RYK(I)=RY(I)
    RZK(I)=RZ(I)
    RX(I)=RX(I)+DTOD*(HDTOM*FX(I)+VX(I))
    RY(I)=RY(I)+DTOD*(HDTOM*FY(I)+VY(I))
    RZ(I)=RZ(I)+DTOD*(HDTOM*FZ(I)+VZ(I))
250 CONTINUE
    GO TO 100
260 INDEX=0
    TIME=TIME+DT
262 NT=NT+1
    I=1
    VSS=VX(I)
    VX(I)=VSS+HDTOMB*FX(I)
    RX(I)=RXK(I)+(VX(I)+VSS)*HDTOD
```

```
      VSS=VY(I)
      VY(I)=VSS+HDTOMB*FY(I)
      RY(I)=RYK(I)+(VY(I)+VSS)*HDTOD
      VSS=VZ(I)
      VZ(I)=VSS+HDTOMB*FZ(I)
      RZ(I)=RZK(I)+(VZ(I)+VSS)*HDTOD
      FX(I)=0.0
      FY(I)=0.0
      FZ(I)=0.0
      PKE(I)=VX(I)*VX(I)+VY(I)*VY(I)+VZ(I)*VZ(I)
      IF(LCUT(I)) 270,265,270
  265 EMAX=PKE(I)
  270 DO 290 I=2,LL
      VSS=VX(I)
      VX(I)=VSS+HDTOM*FX(I)
      RX(I)=RXK(I)+(VX(I)+VSS)*HDTOD
      VSS=VY(I)
      VY(I)=VSS+HDTOM*FY(I)
      RY(I)=RYK(I)+(VY(I)+VSS)*HDTOD
      VSS=VZ(I)
      VZ(I)=VSS+HDTOM*FZ(I)
      RZ(I)=RZK(I)+(VZ(I)+VSS)*HDTOD
      FX(I)=0.0
      FY(I)=0.0
      FZ(I)=0.0
      PKE(I)=VX(I)*VX(I)+VY(I)*VY(I)+VZ(I)*VZ(I)
      IF(LCUT(I)) 290,275,290
  275 IF(PKE(I)-EMAX) 290,290,280
  280 EMAX=PKE(I)
  290 CONTINUE
```

```
      TI=TIMEF(IDUM)
      INOW=TI
      ISHUT=INOW-ICUT
      IF(ISHUT) 410,410,305
  305 DT=DTI*CVD/SQRTF(EMAX)
      IF(DT-SLOW) 310,308,308
  308 NSHUT=1
      GO TO 410
  310 IF(NS-NT)400,400,68
  400 WRITE (51,9610) IHS,IH1
      WRITE (51,9640) PLANE,SUR,EVR,IXP,IYP,IZP,PNUM
      WRITE (51,9645) TARGET,BULLET,CVR,EI
      WRITE (51,9650) TMAS,GMAS,TEMP,THERM
      WRITE (51,9655) IHB,PEXA,PEXB,PFXA
      WRITE (51,9660) IHT,EXA,EXB,FXA
      WRITE (51,9665) BX,BZ,COX,COY,COZ
      WRITE (51,9670) RXI(1),RYI(1),RZI(1)
      WRITE (51,9675) NT,TIME,DT
      WRITE (51,9680)
  410 TPOT=0.0
      DO 450 I=1,LL
      PPE(I)=0.0
  450 PTE(I)=0.0
      CALL ENERGY
      I=1
      PKE(I)=PKE(I)*HGMAS
      TPKE=PKE(I)
      PTE(I)=PKE(I)+PPE(I)
      PKEY(I)=HGMAS*VY(I)*VY(I)
      DO 620 I=2,LL
      PKE(I)=HTMAS*PKE(I)
      TPKE=TPKE+PKE(I)
      PTE(I)=PKE(I)+PPE(I)
```

```
620 PKEY(I)=HTMAS*(VY(I)*VY(I))
    TE=TPOT+TPKE
    IF(NSHUT) 700,700,950
700 IF(ISHUT) 950,950,705
705  IF(NT-30) 710,708,708
708 IF(TPOT-QUIT) 709,710,710
709 JSHUT=1
710 DO 750 I=1,LL
    DX(I)=RX(I)-RXI(I)
    DY(I)=RY(I)-RYI(I)
    DZ(I)=RZ(I)-RZI(I)
    IF(PTE(I)-THERM) 750,720,720
720 WRITE (51,9685) I,DX(I),DY(I),DZ(I),VX(I),VY(I),VZ(I),
   1 PKE(I),PPE(I),PTE(I),PKEY(I)
750 CONTINUE
    WRITE (51,9690) TPKE,TPOT,TE
    WRITE (51,9630) NPAGE
    NPAGE=NPAGE+1
```

```
753 IF(NT-NTT) 754,950,950
754 EMAX=0.0
760 DO 780 I=1,LL
    IF(LCUT(I))780,761,780
761 IF(PKE(I)-QM) 780,780,762
762 IF(PPE(I)-FM)766,766,764
764 IF(EMAX-PPE(I))765,765,780
765 EMAX=PPE(I)
    ISS=I
    GO TO 780
766 LCUT(I)=1
    IF(RY(I))767,767,768
767 KCUT(I)=1
    GO TO 780
768 IF(RY(I)-RYBND)770,769,769
769 KCUT(I)=2
    GO TO 780
770 IF(RX(I))771,771,772
771 KCUT(I)=3
    GO TO 780
772 IF(RX(I)-RXBND)774,774,773
773 KCUT(I)=4
    GO TO 780
774 IF(RZ(I))775,775,776
775 KCUT(I)=5
    GO TO 780
776 IF(RZ(I)-RZBND)780,780,777
777 KCUT(I)=6
780 CONTINUE
    IF(JSHUT) 950,790,950
790 NS=NS+ND
    IF(EMAX-ECUT) 950,950,68
```

```
950 CONTINUE
    WRITE (51,9610) IHS,IH1
    WRITE (51,9695)
    WRITE (51,9640) PLANE,SUR,EVR,IXP,IYP,IZP,PNUM
    WRITE (51,9645) TARGET,BULLET,CVR,EI
    WRITE (51,9650) TMAS,GMAS,TEMP,THERM
    WRITE (51,9655) IHB,PEXA,PEXB,PFXA
    WRITE (51,9660) IHT,EXA,EXB,FXA
    WRITE (51,9665) BX,BZ,COX,COY,COZ
    WRITE (51,9670) RXI(1),RYI(1),RZI(1)
    WRITE (51,9675) NT,TIME,DT
    WRITE (51,9700)
    WRITE (51,9705) (I,RX(I),RY(I),RZ(I),VX(I),VY(I),VZ(I),PKE(I),
   1 PPE(I),LCUT(I),KCUT(I),I=1,LL)
    WRITE (51,9630) NPAGE
    NPAGE=NPAGE+1
    WRITE (51,9610) IHS,IH1
    WRITE (51,9640) PLANE,SUR,EVR,IXP,IYP,IZP,PNUM
    WRITE (51,9645) TARGET,BULLET,CVR,EI
    WRITE (51,9650) TMAS,GMAS,TEMP,THERM
    WRITE (51,9655) IHB,PEXA,PEXB,PFXA
    WRITE (51,9660) IHT,EXA,EXB,FXA
    WRITE (51,9665) BX,BZ,COX,COY,COZ
    WRITE (51,9670) RXI(1),RYI(1),RZI(1)
    WRITE (51,9675) NT,TIME,DT
    WRITE (51,9710)
    DO 965 I=1,LL
952 IF(VY(I))955,965,965
955 IF(RY(I)) 958,956,956
956 IF(PKEY(I)-BENGY)965,958,958
958 IF(I-1)960,959,960
959 B=1.0/SQRTF(PKE(1)/HGMAS)
    GO TO 961
```

```
 960 B=1.0/SQRTF(PKE(I)/HTMAS)
 961 DCOX=VX(I)*B
     DCOY=VY(I)*B
     DCOZ=VZ(I)*B
     WRITE (51,9715) (I,RX(I),RY(I),RZ(I),DX(I),DY(I),DZ(I),
    1 VX(I),VY(I),VZ(I),DCOX,DCOY,DCOZ,PKEY(I),LCUT(I),KCUT(I))
     WRITE (52,9720) TAR.PRI,PLANE,EVR,PNUM,I,VX(I),VY(I),VZ(I),KCUT(I)
    1, PKEY(I),COY
 965 CONTINUE
     WRITE (51,9630) NPAGE
     IF(ISHUT) 9999,9999,970
 970 IF(SENSE SWITCH 3) 9999,4
9999 STOP
     END
```

```
      SUBROUTINE L111
C
C        THIS IS A LATTICE GENERATOR FOR THE (111) ORIENTATION.
C        THE CRYSTAL IS DEVELOPED IN THE ORDER, Z FOLLOWED BY Y, FOLLOWED BY X
C
      COMMON/COM1/RX(500),RY(500),RZ(500),LCUT(500),LL
      COMMON/COM2/ROE,ROE2,ROEM,AC,PAC,PPTC,PTC,PFPTC,FPTC,FM,PFIV,TPOT
      COMMON/COM4/IX,IY,IZ,IXP,IYP,IZP,SCX,SCY,SCZ
      COMMON/COM7/R1,LSS,SPX,SPZ,COY
      SCX=1.0/SQRTF(2.0)
      SCY=2.0/SQRTF(3.0)
      SCZ=SQRTF(1.5)
      SSCZ=SCZ/3.0
      M=1
      IT=0
      X=-SCX
      DO 60 I=1,IX
      X=X SCX
      JT=0
      Y=-SCY
      DO 59 J=1,IY
      Y=Y SCY
      Z=-SCZ
      KT=0
      JTS=JT+JT/3
      DO 58 K=1,IZ
      Z=Z SCZ
      IN=IT+JTS+KT
      IF(IN-(IN/2)*2) 57,30,57
   30 RX(M)=X
      RY(M)=Y
      IF(JT-3*(JT/3)) 41,45,41
   41 JTT=JT
   42 JTT=JTT-3
      IF(JTT) 43,45,42
   43 JTT=JTT+3
```

```
      ZP=JTT
      RZ(M)=Z+ZP*SSCZ
      GO TO 50
   45 RZ(M)=Z
   50 M=M+1
   57 KT=KT+1
   58 CONTINUE
      JT=JT+1
   59 CONTINUE
      IT=IT+1
   60 CONTINUE
      LL=M-1
      GO TO ( 70,80,90),LSS
   70 R1=ROE/ABSF(COY)
      M=2
      GO TO 100
   80 ISPX=SPX
      ISPZ=SPZ
      N=71
      LCUT(N)=1
      R1=ROE/ABSF(COY)
      M=2
      GO TO 100
   90 M=2
      RX(M)=SPX*SCX
      RY(M)=-SCY
      RZ(M)=(SPZ+1.0)*SCZ
      R1=(ROE+SCY)/ABSF(COY)
      M=3
  100 DO 110 I=M,9
  110 LCUT(I)=-1
      END
```

```
      SUBROUTINE L110
C
C        THIS IS A LATTICE GENERATOR FOR THE (110) ORIENTATION.
C        THE CRYSTAL IS DEVELOPED IN THE ORDER, Z FOLLOWED BY Y, FOLLOWED BY X
C
      COMMON/COM1/RX(500),RY(500),RZ(500),LCUT(500),LL
      COMMON/COM2/ROE,ROE2,ROEM,AC,PAC,PPTC,PTC,PFPTC,FPTC,FM,PFIV,TPOT
      COMMON/COM4/IX,IY,IZ,IXP,IYP,IZP,SCX,SCY,SCZ
      COMMON/COM7/R1,LSS,SPX,SPZ,COY
      RO=1.0/SQRTF(2.0)
      SCX=RO
      SCY=RO
      SCZ=1.0
      M=1
      IT=0
      X=-SCX
      DO 60 I=1,IX
      X=X SCX
      JT=0
      Y=-SCY
      DO 59 J=1,IY
      Y=Y SCY
      KT=0
      Z=-SCZ
      DO 58 K=1,IZ
      Z=Z SCZ
      IF(IT-(IT/2)*2) 21,11,21
   11 IF(JT-(JT/2)*2) 57,12,57
   12 IF(KT-(KT/2)*2) 57,30,57
   21 IF(JT-(JT/2)*2) 22,57,22
   22 IF(KT-(KT/2)*2) 30,57,30
   30 RX(M)=X
      RY(M)=Y
      RZ(M)=Z
      M=M 1
   57 KT=KT+1
```

```
 58 CONTINUE
    JT = JT + 1
 59 CONTINUE
    IT =IT+1
 60 CONTINUE
    LL=M-1
    GO TO ( 70,80,90),LSC
 70 R1=ROE/ABSF(COY)
    M=2
    GO TO 100
 80 ISPX=SPX
    ISPZ=SPZ
    N=72
    LCUT(N)=1
    R1=ROE/ABSF(COY)
    M=2
    GO TO 100
 90 M=2
    RX(M)=(SPX+1.0)*SCX
    RY(M)=-SCY
    RZ(M)=(SPZ+1.0)*SCZ
    R1=(ROE+SCY)/ABSF(COY)
    M=3
100 DO 110 I=M,9
110 LCUT(I)=-1
    END
```

```
      SUBROUTINE L100
C
C        THIS IS A LATTICE GENERATOR FOR THE (100) ORIENTATION.
C        THE CRYSTAL IS DEVELOPED IN THE ORDER, Z FOLLOWED BY Y, FOLLOWED BY X
C
      COMMON/COM1/RX(500),RY(500),RZ(500),LCUT(500),LL
      COMMON/COM2/ROE,ROE2,ROEM,AC,PAC,PPTC,PTC,PFPTC,FPTC,FM,PFIV,TPOT
      COMMON/COM4/IX,IY,IZ,IXP,IYP,IZP,SCX,SCY,SCZ
      COMMON/COM7/R1,LSS,SPX,SPZ,COY
      SCX=1.0
      SCY=1.0
      SCZ=1.0
      M=1
      IT=O
      X=-SCX
      DO 60 I=1,IX
      X=X SCX
      JT=
      Y=-SCY
      DO 59 J=1,IY
      Y=Y SCY
      KT=O
      Z=-SCZ
      DO 58 K=1,IZ
      Z=Z+SCZ
      ITT=IT+JT+KT
      IF(ITT-(ITT/2)*2) 57,30,57
   30 RX(M)=X
      RY(M)=Y
      RZ(M)=Z
      M=M+1
   57 KT=KT+1
   58 CONTINUE
      JT = JT + 1
   59 CONTINUE
      IT =IT+1
```

```
 60 CONTINUE
    LL=M-1
    GO TO ( 70,80,90),LL
 70 R1=ROE/ABSF(COY)
    M=2
    GO TO 100
 80 ISPX=SPX
    ISPZ=SPZ
    N=72
    LCUT(N)=1
    R1=ROE/ABSF(COY)
    M=2
    GO TO 100
 90 M=2
    RX(M)=SPX*SCX
    RY(M)=-SCY
    RZ(M)=(SPZ+1.0)*SCZ
    R1=(ROE+SCY)/ABSF(COY)
    M=3
100 DO 110 I=M,9
110 LCUT(I)=-1
    END
```

```
      SUBROUTINE START
C
C        THIS SUBROUTINE FINDS THE START POINT FOR EACH INPACT POINT
C
      COMMON/COM1/RX(500),RY(500),RZ(500),LCUT(500),LL
      COMMON/COM2/ROE,ROE2,ROEM,AC,PAC,PPTC,PTC,PFPTC,FPTC,FM,PFIV,TPOT
      COMMON/COM6/COXI,COYI,COZI,RXS,RYS,RZS,FAC
      COMMON/COM7/R1,LSS,SPX,SPZ,COY
  100 R1=R1-FAC
      R1X=R1*COXI+RXS
      R1Y=R1*COYI+RYS
      R1Z=R1*COZI+RZS
      IF(R1) 300,105,105
  105 DO 195 J=2,LL
      IF(LCUT(J)) 195,110,195
  110 DRX=RX(J)-R1X
      IF(DRX) 113,117,117
  113 IF(DRX+ROE) 195,195,120
  117 IF(DRX-ROE) 120,195,195
  120 DRY=RY(J)-R1Y
      IF(DRY) 123,127,127
  123 IF(DRY+ROE) 195,195,130
  127 IF(DRY-ROE) 130,195,195
  130 DRZ=RZ(J)-R1Z
      IF(DRZ) 133,137,137
  133 IF(DRZ+ROE) 195,195,140
  137 IF(DRZ-ROE) 140,195,195
  140 DIST=DRX*DRX+DRY*DRY+DRZ*DRZ
      IF(DIST-ROE2) 200,195,195
  195 CONTINUE
      GO TO 100
  200 I=J
      R2SQ=(RX(I)-RXS)*(RX(I)-RXS)+(RY(I)-RYS)*(RY(I)-RYS)+(RZ(I)-RZS)*
     1 (RZ(I)-RZS)
      R2=SQRTF(R2SQ)
      R1R2=(R1X-RXS)*(RX(I)-RXS)+(R1Y-RYS)*(RY(I)-RYS)+(R1Z-RZS)*
```

```
    1 (RZ(I)-RZS)
     ALFA=R1R2/(R1*R2)
     ALFA2=ALFA*ALFA
     R3=R2*ALFA+SQRTF(R2SQ*ALFA2-R2SQ+ROE2)
     RX(1)=R3*COXI+RXS
     RY(1)=R3*COYI+RYS
     RZ(1)=R3*COZI+RZS
     RETURN
 300 RX(1)=RXS
     RY(1)=RYS
     RZ(1)=RZS
9700 FORMAT(41H THIS DID NOT LOCATE A PROPER START POINT)
      WRITE (51,9700)
     RETURN
     END
```

```
      SUBROUTINE STEP
C
C        THIS SUBROUTINE DOES THE DYNAMICS FOR ONE TIMESTEP
C
      COMMON/COM1/RX(500),RY(500),RZ(500),LCUT(500),LL
      COMMON/COM2/ROE,ROE2,ROEM,AC,PAC,PPTC,PTC,PFPTC,FPTC,FM,PFIV,TPOT
      COMMON/COM3/EXA,EXB,FXA,PEXA,PEXB,PFXA
      COMMON/COM5/FX(500),FY(500),FZ(500),PPE(500)
      FORF(X)=EXPF(FXA+EXB*X)
      PFORF(X)=EXPF(PFXA+PEXB*X)
      FPTF(X)=EXPF(AC+EXB*X)
      PFPTF(X)=EXPF(PAC+PEXB*X)
  100 DO 200 I=1,LL
      IF(LCUT(I)) 200,105,200
  105 IP=I+1
      DO 195 J=IP,LL
      IF(LCUT(J)) 195,110,195
  110 DRX=RX(J)-RX(I)
      IF(DRX) 113,117,117
  113 IF(DRX+ROE) 195,195,120
  117 IF(DRX-ROE) 120,195,195
  120 DRY=RY(J)-RY(I)
      IF(DRY) 123,127,127
  123 IF(DRY+ROE) 195,195,130
  127 IF(DRY-ROE) 130,195,195
  130 DRZ=RZ(J)-RZ(I)
      IF(DRZ) 133,137,137
  133 IF(DRZ+ROE) 195,195,140
  137 IF(DRZ-ROE) 140,195,195
  140 DIST=DRX*DRX+DRY*DRY+DRZ*DRZ
      IF(DIST-ROE2) 150,195,195
  150 DIST=SQRTF(DIST)
      IF(1-I) 170,160,170
  160 IF(DIST-ROEM) 162,162,165
  162 FORCE=PFORF(DIST)
      GO TO 180
```

```
      SUBROUTINE ENERGY
C
C        THIS SUBROUTINE CALCULATES THE MUTUAL POTENTIAL ENERGIES
C
      COMMON/COM1/RX(500),RY(500),RZ(500),LCUT(500),LL
      COMMON/COM2/ROE,ROE2,ROEM,AC,PAC,PPTC,PTC,PFPTC,FPTC,FM,PFIV,TPOT
      COMMON/COM3/EXA,EXB,FXA,PEXA,PEXB,PFXA
      COMMON/COM5/FX(500),FY(500),FZ(500),PPE(500)
      POTF(X)=EXPF(EXA+EXB*X)
      PPOTF(X)=EXPF(PEXA+PEXB*X)
      PFIV=0.5
      DO 600 I=1,LL
      IF(LCUT(I)) 600,505,600
  505 IP=I+1
      DO 595 J=IP,LL
      IF(LCUT(J)) 595,510,595
  510 DRX=RX(J)-RX(I)
      IF(DRX) 513,517,517
  513 IF(DRX+ROE) 595,595,520
  517 IF(DRX-ROE) 520,595,595
  520 DRY=RY(J)-RY(I)
      IF(DRY) 523,527,527
  523 IF(DRY+ROE) 595,595,530
  527 IF(DRY-ROE) 530,595,595
  530 DRZ=RZ(J)-RZ(I)
      IF(DRZ) 533,537,537
  533 IF(DRZ+ROE) 595,595,540
  537 IF(DRZ-ROE) 540,595,595
  540 DIST=DRX*DRX+DRY*DRY+DRZ*DRZ
      IF(DIST-ROE2) 550,595,595
  550 DIST=SQRTF(DIST)
      IF(1-I) 570,560,570
  560 POT=PPOTF(DIST)-PPTC
      GO TO 580
  570 POT=POTF(DIST)-PTC
  580 TPOT=TPOT+POT
```

```
      SAVE=PFIV*FCT
      PPE(I)=PPE(I)+SAVE
      PPE(J)=PPE(J)+SAVE
  595 CONTINUE
  600 CONTINUE
      END
```

```
         IDENT        TIMEF                                  00000
         EXT          TIMO                                   00001
ARG      BSS          1                                      00002
         ENTRY        TIMEF                                  00003
TIMEF    SLJ          **                                     00004
         LDA          TIMEF                                  00005
         ARS          24                                     00006
         INA          +1                                     00007
         SAU          TIMEF                                  00008
         ENQ          0                                      00009
         LAC     7    =00                                    00010
         SCL          =0400000000000000                      00011
+        STA          ARG                                    00012
-        RTJ          TIMO                                   00013
         ZRO          ARG                                    00014
+        SLJ          TIMEF                                  00015
         END                                                 00016
```

```
      FUNCTION TIMO(IT)
      XIT=IT                                                            00017
      TIMO=XIT/60.                                                      00018
      RETURN                                                            00019
      END                                                               00020
                                                                           21
```

APPENDIX D

2. Section 1: Memory block allocations and functions are established. All storage cells are zeroed. Input and output formats are specified. Constants are set, and the target material, ion species, and crystal face to be sputtered are read in.

Section 2: The ion energy, impact area, and impact point are read in. Constants peculiar to the run are established. The appropriate subroutine is called to build the crystal, and crystal boundaries are calculated. Subroutine START is called to position the ion. The initial value of Δt is calculated. Initial coordinates of all atoms are assigned, and their velocity components are zeroed (except for the ion). The initial coordinates of the crystal atoms are printed.

Section 3: Forces are calculated by calling subroutine STEP. Atoms are moved to their intermediate positions in the two step cycle. Subroutine STEP is called again, and atoms are moved to their final positions. Final velocities are then computed. Force components are zeroed in preparation for the next timestep.

The maximum kinetic energy is determined for the calculation of Δt.

Section 4: The time remaining until cutoff is determined. If there is insufficient time to complete another timestep, terminal data is printed. Potential energy is calculated and summed with kinetic energy to give the total energy for energy balance check (manual check). The data for atoms having potential energy greater than the thermal energy are printed.

Section 5: Atoms which have kinetic energy but not potential energy are assumed to be free of the crystal. They are assigned LCUT=1. The surface through which an atom exited is determined and a code assigned. A maximum potential energy is found (for Δt calculation) among atoms which do not have LCUT=1. If the maximum potential energy is less than a minimum value the terminating process begins. If this energy is greater than the minimum value, another timestep begins.

Section 6: Pertinent data for all atoms is printed. Atoms which have exited through the front of the crystal or will exit through the front are assumed to be sputtered. Data for these

atoms areprinted and a data card punched for each atom. A new data card is then read into initiate another run.

APPENDIX E

Glossary for FCCSPUT

AC	Parameter for target force function correction.
AIX AIY AIZ	Floating point form of IX, IY, IZ.
ALFA	Cosine of the angle between vectors R1, R2.
ALFA2	ALFA squared.
B	Reciprocal of magnitude of atom velocity.
BENGY	Energy which an atom within the crystal at shut-down must have to be considered sputtered.
BULLET	Variable representing primary material.
BX BZ	Unscaled x, z coordinates of the impact point
CELS	Frictional force multiplier. (See CVS)
COX COY COZ	Direction cosines of primary velocity vector.
COXI COYI COZI	Negative values of COX, COY, COZ.
CVB	A constant.
CVD	Converts meters to angstrom units.
CVE	Converts electron volts to joules.
CVM	Converts atomic mass units to kilograms.
CVR	Converts lattice units to angstrom units.
DCOX DCOY DCOZ	Direction cosines of sputtered atom velocity vector.
DFF	Distance difference between nearest neighbor distance and actual atom differences.
DIST	Distance between any two atoms.

DRX DRY DRZ	x, y, z components of DIST.
DT	Length of timestep in seconds.
DTI	Number of lattice units most energetic atom may move in one timestep.
DTOD	DT/CVD - a ratio used to avoid repeated division.
DTOM	DT/PTMAS - a ratio used to avoid repeated division.
DTOMB	DT/PGMAS - a ratio used to avoid repeated division.
DX DY DZ	x, y, z distances atom has moved from initial position.
ECUT	A lower limit on an atom's potential energy. If energy is less than or equal to ECUT the program shuts down.
EI	A cutoff energy.
EMAX	The maximum energy encountered in any cycle.
EV	Primary energy in electron volts.
EVR	Primary energy in kilo-electron volts.
EXA EXB	Potential function parameters.
FA	The component force increment on an atom.
FAC	The minimum distance the primary is positioned in front of the first xz plane at start time.
FM	A small number used in checking potential energy zero point.
FOD	FORCE/DIST - a ratio used to avoid repeated division.
FORCE	Numerical value of the force function with a variable parameter.

FORF	Target atom force function.
FPTC	The corrective force value at ROE.
FPTF	The corrective force function.
FRC	Numerical value of the target force function at ROE.
FX FY FZ	x, y, z components of total force on an atom.
FXA	Force function parameter.
GMAS	Target atom mass (in a.m.u.)
HDTOD	1/2 DTOD - a ratio used to avoid repeated division.
HDTOM	1/2 DTOM - a ratio used to avoid repeated division.
HDTOMB	1/2 DTOMB - a ratio used to avoid repeated division.
HGMAS	1/2 GMAS - a ratio used to avoid repeated division.
HTMAS	1/2 TMAS - a ratio used to avoid repeated division.
ICUT	Used to provide output prior to time limit shutdown.
IDUM	Dummy variable.
IHB IHS IHT IH1	Alpha-numeric arrays for titling.
IN	Odd-even integer used to determine atom site establishment.
INDEX	Integer (0 or 1) used in determining dynamics cycle step.
INOW	Time program has been running in seconds.

IP	Subscript value of atom. Used in subroutine STEP.
ISHUT	Time left prior to time limit.
ISPX ISPZ	Fixed point values of SPX, SPZ.
ISS	Subscript value of most energetic atom.
IT	Unscaled fixed point x coordinate used in lattice generation. Also a dummy variable in function TIMEF.
ITT	Odd-even integer used to determine atom site establishment.
IX IY IZ	Number of x, y, z planes of crystal.
IXP IYP IZP	Crystal dimensions in x, y, z.
JSHUT	Cutoff variable based on total potential energy of crystal.
JT	Unscaled y coordinate used in crystal generation.
JTS JTT	Variables used to establish atom sites.
KCUT	Identifies exit point of atom.
KT	Unscaled z coordinate used to establish atom site.
LCUT	Used to identify atoms which are not included in calculations.
LL	The highest numbered atom in the crystal.
LS	Sum of the Miller index integers.
LSS	Used to identify type of surface, i.e., regular, stub, vacancy.
M	An integer used to begin atom numbering.

N	Subscript of the atom to be removed for vacancy surface.
ND	Data output increment.
NPAGE	Page numbering variable.
NS	Initial print statement cycle .
NSHUT	Cutoff variable based on too long a timestep.
NT	Timestep.
NTT	Timestep limit before shutdown.
PAC	Same as AC except applicable to primary.
PEXA PEXB	Primary force function parameters.
PFIV	A constant = 0.5.
PFORF	Primary force function.
PFPTC	PFPTF evaluated at ROE.
PFPTF	Primary corrective force function.
PFRC	PFORF evaluated at ROE.
PFXA	Primary force function parameter.
PGMAS	Primary mass in kilograms.
PKE	Kinetic energy of an atom.
PKEY	Y component of kinetic energy of an atom.
PLA	Crystal plane (alphanumeric variable).
PLANE	Same as PLA.
PNUM	Impact point (alphanumeric variable).
POT	Potential energy between two atoms.
POTF	Target potential function.
PPE	Potential energy of an atom.

PPOTF	Primary potential function.
PPTC	PPOTF evaluated at ROE.
PRI	Chemical symbol for primary material.
PTC	POTF evaluated at ROE.
PTE	Total energy of an atom (potential + kinetic).
PTMAS	Target mass in kilograms.
QM	A small number used in checking kinetic energy zero point.
QUIT	Cutoff variable checked against total potential energy.
RBX RBZ	Unscaled x, z coordinates of impact area reference point
ROE	Nearest neighbor distance.
ROEM	ROE - DTI (one timestep distance less than n.n. distance).
ROE2	ROE squared.
RX RY RZ	x, y, z coordinates of atom at any time.
RXBND RYBND RZBND	x, y, z coordinates of crystal boundaries other than zero.
RXI RYI RZI	x, y, z coordinates of atom's initial position.
RXK RYK RZK	x, y, z coordinates of temporary position of atom during force cycle.
RXS RYS RZS	x, y, z coordinates of impact point.
R1	Vector from impact point to initial primary position.

R1X R1Y R1Z	x, y, z coordinates of initial primary position.
R1R2	Scalar product of vectors R1, R2.
R2	Magnitude of vector from impact point to first atom hit by primary.
R2SQ	R2 squared.
R3	Magnitude of vector from impact point of primary start position.
SAVE	1/2 POT.
SCX SCY SCZ	x, y, z coordinate scale factors.
SLOW	Cutoff variable checked against a long DT.
SPX SPZ	x, z distance from impact area reference point to impact point.
SSCZ	A z scale factor used for (111) plane lattice generation.
SUR	Plane (alphanumeric variable).
TAR	Chemical symbol for target material.
TARGET	Target material (alphanumeric variable).
TE	Total energy of crystal atoms (kinetic + potential).
TEMP	Temperature of lattice in degrees Kelvin.
THERM	Thermal energy of atom.
TI	Computer time program has been running.
TIME	Elapsed problem time.
TIMO	A function to convert seconds to minutes.
TMAS	Target atom mass in kilograms.

TPKE	Total kinetic energy of crystal atoms.
TPOT	Total potential energy of crystal atoms.
VOL	Magnitude of primary velocity vector.
VSS	Storage variable for velocity components.
VX VY VZ	x, y, z components of atom velocity.
X	Unscaled x coordinate used in crystal generation.
XIT	Floating point form of IT used in function TIMO.
Y	Unscaled y coordinate used in crystal generation.
Z	Unscaled z coordinate used in crystal generation.
ZE	A constant = 0.0
ZP	Floating point form of JTT.

Pattern Production and Analysis Programs (DATASORT, DATAPLOT, DATAGRID)

```
      PROGRAM DATASORT
C
C
C     DATA CARD ORDER
C      1. THRESHOLD ENERGY
C      2. INPUT DATA
C      3. PLANE, NUMBER OF IMPACT POINTS, NUMBER OF ROTATIONS
C      4. TITLE FOR HISTOGRAM OF SPUTTERED ATOMS
C      5. TITLE FOR HISTOGRAM OF NON-SPUTTERED ATOMS
C
C
    2 FORMAT(3I1,8X,F2.0,16X,F1.0)
    3 FORMAT(17X,F5.2)
    4 FORMAT(5X,A4,1X,F6.2,1X,A4,1X,I4,3E10.2,3X,F8.2,1X,F8.5)
    5 FORMAT(17X,A4,1X,I4,3E10.2,3X,F8.2)
    6 FORMAT(I4)
  165 FORMAT(///5X,I5,18H ATOMS CONSIDERED,,I5,18H ATOMS SPUTTERED, ,I5,
     115H ATOMS REJECTED)
  166 FORMAT(5X,I3,19H PER CENT SPUTTERED)
      DIMENSION KEYES(500),KENO(500)
      REWIND 2
      REWIND 3
      REWIND 4
      READ 3,EGYCUT
      READ 4,PLANE,EVK,PNUM,NR,VX,VY,VZ,PKEY,COY
      WRITE TAPE 2,PLANE,EVK,COY,EGYCUT
      WRITE TAPE 2,PNUM,NR,VX,VY,VZ,PKEY
      WRITE TAPE 3,PLANE,EVK,COY,EGYCUT
      WRITE TAPE 4,PLANE,EVK,COY,EGYCUT
      DO 110 I=2,3000
      READ 5,PNUM,NR,VX,VY,VZ,PKEY
      IF(NR)100,120,100
  100 WRITE TAPE 2,PNUM,NR,VX,VY,VZ,PKEY
  110 CONTINUE
  111 STOP 111
  120 NATOMS=I-1
```

```
      END FILE 2
      REWIND 2
      READ 2,IPLA,JPLA,KPLA,SHOTS,ROT
      SAME=ROT*SHOTS
      IPLANE=IPLA+JPLA+KPLA
      GO TO(200,210,220),IPLANE
  200 CALL ROT100(NATOMS,KEYES,KENO,NPTS,LPTS)
      GO TO 230
  210 CALL ROT110(NATOMS,KEYES,KENO,NPTS,LPTS)
      GO TO 230
  220 CALL ROT111(NATOMS,KEYES,KENO,NPTS,LPTS)
  230 CONTINUE
      PRINT 6,IPLANE
      IROT=ROT
      LATOMS=NATOMS*IROT
      PRINT 165,LATOMS,NPTS,LPTS
      IRATIO=(NPTS*100)/LATOMS
      PRINT 166,IRATIO
      CALL HIST1(KEYES,SAME)
      CALL HIST1(KENO,SAME)
      END
```

```
      SUBROUTINE ROT100(KATOMS,KEYES,KENO,L,M)
      DIMENSION KEYES(500),KENO(500)
   10 FORMAT(13HIMPACT POINT ,A4,6H ATOM ,I4,16H KINETIC ENERGY ,F8.2,3H
     1 EV)
      READ TAPE 2,PLANE,EVK,COY,EGYCUT
      AA=1.0/EGYCUT
      HTMAS=3.32E-07
      RHTMAS=1.0/HTMAS
      L=0
      M=0
      DO 3000 J=1,500
      KEYES(J)=0
 3000 KENO(J)=0
      DO 3900 I=1,KATOMS
      READ TAPE 2,PNUM,NR,VX,VY,VZ,PKEY
      IF(PKEY)3004,3003,3004
 3003 PKEY=VY*VY*HTMAS
 3004 FACTOR=PKEY-EGYCUT
      IF(FACTOR)3005,3005,3010
 3005 VY= VY*PKEY*AA
      GO TO 3011
 3010 VY=SQRTF(FACTOR*RHTMAS)
 3011 CONTINUE
      A=VX/VY
      B=VZ/VY
      ETEST=1.0-EXPF(-AA*PKEY)
C
C
C  PKEY ADJUSTED FOR ENERGY LOSS IN OVERCOMING SURFACE BINDING ENERGY
C
C
      PKE=(VX*VX + VY*VY + VZ*VZ)*HTMAS
      II=PKE + 0.49
      IF(II-500)3060,3050,3050
 3050 II=500
      PRINT 10,PNUM,NR,PKEY
```

```
3060 CONTINUE
3100 R=RANF(-1)
     IOCT=1
     IF(R.LT.ETEST)3125,3150
3125 XP=A
     ZP=B
     KEYES(II)=KEYES(II)+1
     L=L 1
     WRITE TAPE 3,XP,ZP,PNUM,NR,IOCT,PKE
     GO TO 3200
3150 M=M 1
     KENO(II)=KENO(II)+1
     WRITE TAPE 4,PNUM,IOCT,NR
3200 R=RANF(-1)
     IOCT=2
     IF(R.LT.ETEST)3225,3250
3225 XP= A
     ZP=B
     KEYES(II)=KEYES(II)+1
     L=L 1
     WRITE TAPE 3,XP,ZP,PNUM,NR,IOCT,PKE
     GO TO 3300
3250 M=M 1
     KENO(II)=KENO(II)+1
     WRITE TAPE 4,PNUM,IOCT,NR
3300 R=RANF(-1)
     IOCT=3
     IF(R.LT.ETEST)3325,3350
3325 XP= B
     ZP=A
     KEYES(II)=KEYES(II)+1
     L=L 1
     WRITE TAPE 3,XP,ZP,PNUM,NR,IOCT,PKE
     GO TO 3400
3350 M=M 1
     KENO(II)=KENO(II)+1
```

```
      WRITE TAPE 4,PNUM,IOCT,NR
3400 R=RANF(-1)
      IOCT=4
      IF(R.LT.ETEST)3425,3450
3425 XP= B
      ZP= A
      KEYES(II)=KEYES(II)+1
      L=L 1
      WRITE TAPE 3,XP,ZP,PNUM,NR,IOCT,PKE
      GO TO 3500
3450 M=M 1
      KENO(II)=KENO(II)+1
      WRITE TAPE 4,PNUM,IOCT,NR
3500 R=RANF(-1)
      IOCT=5
      IF(R.LT.ETEST)3525,3550
3525 XP= A
      ZP= B
      KEYES(II)=KEYES(II)+1
      L=L 1
      WRITE TAPE 3,XP,ZP,PNUM,NR,IOCT,PKE
      GO TO 3600
3550 M=M 1
      KENO(II)=KENO(II)+1
      WRITE TAPE 4,PNUM,IOCT,NR
3600 R=RANF(-1)
      IOCT=6
      IF(R.LT.ETEST)3625,3650
3625 XP=A
      ZP= B
      KEYES(II)=KEYES(II)+1
      L=L 1
      WRITE TAPE 3,XP,ZP,PNUM,NR,IOCT,PKE
      GO TO 3700
3650 M=M 1
      KENO(II)=KENO(II)+1
```

```
      WRITE TAPE 4,PNUM,IOCT,NR
 3700 R=RANF(-1)
      IOCT=7
      IF(R.LT.ETEST)3725,3750
 3725 XP=B
      ZP= A
      KEYES(II)=KEYES(II)+1
      L=L 1
      WRITE TAPE 3,XP,ZP,PNUM,NR,IOCT,PKE
      GO TO 3800
 3750 M=M 1
      KENO(II)=KENO(II)+1
      WRITE TAPE 4,PNUM,IOCT,NR
 3800 R=RANF(-1)
      IOCT=8
      IF(R.LT.ETEST)3825,3850
 3825 XP=B
      ZP=A
      KEYES(II)=KEYES(II)+1
      L=L 1
      WRITE TAPE 3,XP,ZP,PNUM,NR,IOCT,PKE
      GO TO 3900
 3850 M=M 1
      KENO(II)=KENO(II)+1
      WRITE TAPE 4,PNUM,IOCT,NR
 3900 CONTINUE
      END FILE 3
      END FILE 4
      REWIND 2
      REWIND 3
      REWIND 4
      RETURN
      END
```

```
      SUBROUTINE ROT110(KATOMS,KEYES,KENO,L,M)
      DIMENSION KEYES(500),KENO(500)
   10 FORMAT(13HIMPACT POINT ,A4,6H ATOM ,I4,16H KINETIC ENERGY ,F8.2,3H
     1 EV)
      READ TAPE 2,PLANE,EVK,COY,EGYCUT
      AA=1.0/EGYCUT
      HTMAS=3.32E-07
      RHTMAS=1.0/HTMAS
      L=0
      M=0
      DO 3000 J=1,500
      KEYES(J)=0
 3000 KENO(J)=0
      DO 3900 I=1,KATOMS
      READ TAPE 2,PNUM,NR,VX,VY,VZ,PKEY
      IF(PKEY)3004,3003,3004
 3003 PKEY=VY*VY*HTMAS
 3004 FACTOR=PKEY-EGYCUT
      IF(FACTOR)3005,3005,3010
 3005 VY= VY*PKEY*AA
      GO TO 3011
 3010 VY=SQRTF(FACTOR*RHTMAS)
 3011 CONTINUE
      A=VX/VY
      B=VZ/VY
      ETEST=1.0-EXPF(-AA*PKEY)
C
C
C  PKEY ADJUSTED FOR ENERGY LOSS IN OVERCOMING SURFACE BINDING ENERGY
C
C
      PKE=(VX*VX + VY*VY + VZ*VZ)*HTMAS
      II=PKE + 0.49
      IF(II-500)3060,3050,3050
 3050 II=500
      PRINT 10,PNUM,NR,PKEY
```

```
3060 CONTINUE
3100 R=RANF(-1)
     IQUAD=1
     IF(R.LT.ETEST)3125,3150
3125 XP=A
     ZP=B
     KEYES(II)=KEYES(II)+1
     L=L 1
     WRITE TAPE 3,XP,ZP,PNUM,NR,IQUAD,PKE
     GO TO 3200
3150 M=M 1
     KENO(II)=KENO(II)+1
     WRITE TAPE 4,PNUM,IQUAD,PKEY
3200 R=RANF(-1)
     IQUAD=2
     IF(R.LT.ETEST)3225,3250
3225 XP= A
     ZP=B
     KEYES(II)=KEYES(II)+1
     L=L 1
     WRITE TAPE 3,XP,ZP,PNUM,NR,IQUAD,PKE
     GO TO 3300
3250 M=M 1
     KENO(II)=KENO(II)+1
     WRITE TAPE 4,PNUM,IQUAD,PKEY
3300 R=RANF(-1)
     IQUAD=3
     IF(R.LT.ETEST)3325,3350
3325 XP= A
     ZP= B
     KEYES(II)=KEYES(II)+1
     L=L 1
     WRITE TAPE 3,XP,ZP,PNUM,NR,IQUAD,PKE
     GO TO 3400
3350 M=M 1
     KENO(II)=KENO(II)+1
```

```
      WRITE TAPE 4,PNUM,IQUAD,PKEY
3400  R=RANF(-1)
      IQUAD=4
      IF(R.LT.ETEST)3425,3450
3425  XP=A
      ZP= B
      KEYES(II)=KEYES(II)+1
      L=L 1
      WRITE TAPE 3,XP,ZP,PNUM,NR,IQUAD,PKE
      GO TO 3900
3450  M=M 1
      KENO(II)=KENO(II)+1
      WRITE TAPE 4,PNUM,IQUAD,PKEY
3900  CONTINUE
      END FILE 3
      END FILE 4
      REWIND 2
      REWIND 3
      REWIND 4
      RETURN
      END
```

```
      SUBROUTINE ROT111(KATOMS,KEYES,KENO,L,M)
      DIMENSION KEYES(500),KENO(500)
   10 FORMAT(13HIMPACT POINT ,A4,6H ATOM ,I4,16H KINETIC ENERGY ,F8.2,3H
     1 EV)
      READ TAPE 2,PLANE,EVK,COY,EGYCUT
      AA=1.0/EGYCUT
      HTMAS=3.32E-07
      RHTMAS=1.0/HTMAS
      L=0
      M=0
      DO 3000 J=1,500
      KEYES(J)=0
 3000 KENO(J)=0
C
C MIRROR/ROTATION SCHEME
C     1. MIRROR POINT ABOUT Z AXIS TO PROVIDE IMPACT AREA 2.
C     2. ROTATE POINT 120 DEGREES CLOCKWISE FOR IMPACT AREA 5
C     3. MIRROR POINT FROM IMPACT AREA 5 ABOUT Z AXIS FOR IMPACT AREA 4
C     4. ROTATE POINT 120 DEGREES COUNTERCLOCKWISE FOR IMPACT AREA 3.
C     5. MIRROR POINT FROM IMPACT AREA 3 ABOUT Z AXIS FOR IMPACT AREA 6.
C
      DO 3900 I=1,KATOMS
      READ TAPE 2,PNUM,NR,VX,VY,VZ,PKEY
      IF(PKEY)3004,3003,3004
 3003 PKEY=VY*VY*HTMAS
 3004 FACTOR=PKEY-EGYCUT
      IF(FACTOR)3005,3005,3010
 3005 VY= VY*PKEY*AA
      GO TO 3011
 3010 VY=SQRTF(FACTOR*RHTMAS)
 3011 CONTINUE
      A=VX/VY
      B=VZ/VY
      TEMP1=0.866*B - 0.5*A
      TEMP2=0.866*A + 0.5*B
      TEMP3=0.866*B + 0.5*A
```

```
      TEMP4=0.866*A - 0.5*B
      ETEST=1.0-EXPF(-AA*PKEY)
C
C
C  PKEY ADJUSTED FOR ENERGY LOSS IN OVERCOMING SURFACE BINDING ENERGY
C
C
      PKE=(VX*VX + VY*VY + VZ*VZ)*HTMAS
      II=PKE + 0.49
      IF(II-500)3060,3050,3050
 3050 II=500
      PRINT 10,PNUM,NR,PKEY
 3060 CONTINUE
 3100 R=RANF(-1)
      ISEX=1
      IF(R.LT.ETEST)3125,3150
 3125 XP=A
      ZP=B
      KEYES(II)=KEYES(II)+1
      L=L 1
      WRITE TAPE 3,XP,ZP,PNUM,NR,ISEX,PKE
      GO TO 3200
 3150 M=M 1
      KENO(II)=KENO(II)+1
      WRITE TAPE 4,PNUM,ISEX,NR
 3200 R=RANF(-1)
      ISEX=2
      IF(R.LT.ETEST)3225,3250
 3225 XP= A
      ZP=B
      KEYES(II)=KEYES(II)+1
      L=L 1
      WRITE TAPE 3,XP,ZP,PNUM,NR,ISEX,PKE
      GO TO 3300
 3250 M=M 1
      KENO(II)=KENO(II)+1
```

```
      WRITE TAPE 4,PNUM,ISEX,NR
 3300 R=RANF(-1)
      ISEX=3
      IF(R.LT.ETEST)3325,3350
 3325 XP=TEMP1
      ZP= TEMP2
      KEYES(II)=KEYES(II)+1
      L=L 1
      WRITE TAPE 3,XP,ZP,PNUM,NR,ISEX,PKE
      GO TO 3400
 3350 M=M 1
      KENO(II)=KENO(II)+1
      WRITE TAPE 4,PNUM,ISEX,NR
 3400 R=RANF(-1)
      ISEX=4
      IF(R.LT.ETEST)3425,3450
 3425 XP= TEMP1
      ZP= TEMP2
      KEYES(II)=KEYES(II)+1
      L=L 1
      WRITE TAPE 3,XP,ZP,PNUM,NR,ISEX,PKE
      GO TO 3500
 3450 M=M 1
      KENO(II)=KENO(II)+1
      WRITE TAPE 4,PNUM,ISEX,NR
 3500 R=RANF(-1)
      ISEX=5
      IF(R.LT.ETEST)3525,3550
 3525 XP= TEMP3
      ZP=TEMP4
      KEYES(II)=KEYES(II)+1
      L=L 1
      WRITE TAPE 3,XP,ZP,PNUM,NR,ISEX,PKE
      GO TO 3600
 3550 M=M 1
      KENO(II)=KENO(II)+1
```

```
      WRITE TAPE 4,PNUM,ISEX,NR
3600  R=RANF(-1)
      ISEX=6
      IF(R.LT.ETEST)3625,3650
3625  XP=TEMP3
      ZP=TEMP4
      KEYES(II)=KEYES(II)+1
      L=L 1
      WRITE TAPE 3,XP,ZP,PNUM,NR,ISEX,PKE
      GO TO 3900
3650  M=M 1
      KENO(II)=KENO(II)+1
      WRITE TAPE 4,PNUM,ISEX,NR
3900  CONTINUE
      END FILE 3
      END FILE 4
      REWIND 2
      REWIND 3
      REWIND 4
      RETURN
      END
```

```
      SUBROUTINE HIST1(KEYES,SHOTS)
      DIMENSION X(4),Y(4)
      DIMENSION ITITLE(12)
      DIMENSION KEYES(500)
   11 FORMAT(5X,I4,29H ATOM(S) WITH KINETIC ENERGY ,I4,3H EV)
   12 FORMAT(5X,I5,28H ATOMS PLOTTED WITH ENERGY  ,I3,3H EV,18H SPUTTERI
     1NG RATIO ,F7.3)
   13 FORMAT(38HENERGY DISTRIBUTION OF SPUTTERED ATOMS///)
   14 FORMAT(//55X,5HTOTAL,F7.3,41H NOT ADJUSTED FOR NUMBER OF SURFACES
    1 FORMAT(1H1)
     1USED)
   15 FORMAT(68X,42HSEE IMPACT POINT CODING IN DATAGRID OUTPUT///)
   16 FORMAT(10A8/2A8)
      READ 16,(ITITLE(I),I=1,12)
      SUM=0.0
      PRINT 1
      PRINT 13
      LABEL=8H
      MOD=1
      DO 200 I=1,140
      IF(KEYES(I).GT.0)100,200
  100 A=141-I
      X(1)=0.0
      BB=KEYES(I)
      X(2)=BB/SHOTS
      X(3)=X(2)
      X(4)=X(1)
      Y(1)=A
      Y(2)=Y(1)
      Y(3)=A-1.0
      Y(4)=Y(3)
      CALL DRAW(4,X,Y,MOD,0,LABEL,ITITLE,0.5,10.0,0,0,2,2,9,15,1,LAST)
      PRINT 12,KEYES(I),I,X(2)
      SUM=SUM+X(2)
      MOD=2
  200 CONTINUE
```

```
      MOD=3
      X(1)=0.0
      Y(1)=0.0
      X(2)=0.1
      Y(2)=0.0
      CALL DRAW(2,X,Y,MOD,0,LABEL,ITITLE,0.5,10.0,0,0,2,2,9,15,1,LAST)
      PRINT 14,SUM
      PRINT 15
      DO 300 I=141,500
      IF(KEYES(I).GT.0)250,300
  250 PRINT 11,KEYES(I),I
  300 CONTINUE
      RETURN
      END
```

```
      PROGRAM DATAPLOT
C
C     DATA CARDS
C     TITLE FOR GRAPH OF SPUTTERING DEPOSIT/SYMBOL FOR MODE OF PLOT
C
      DIMENSION XP(4000),ZP(4000)
C
C     TAPE NR. 234 FOR SELECTED ATOMS. PUT ON LOGICAL UNIT NR. 3
C     TAPE NR. 235 FOR REJECTED ATOMS. PUT ON LOGICAL UNIT NR. 4
C
      CALL SPUTDRAW(NPTS,XP,ZP)
      END



      SUBROUTINE SPUTDRAW(NPTS,XP,ZP)
      DIMENSION PXP(30),PZP(30)
      DIMENSION ITITLE(12)
      DIMENSION XP(4000),ZP(4000)
   15 FORMAT(10A8/2A8,14X,I1)
      LABEL=8H
      READ 15,((ITITLE(I),I=1,12),ITYPE)
      IF(ITYPE)199,198,199
  198 ITYPE=3
  199 CONTINUE
      REWIND 3
      READ TAPE 3,PLANE,EVK,COY,EGYCUT
      DO 2001 J=1,4000
      IF(EOF,3)2004,2000
 2000 READ TAPE 3,XP(J),ZP(J),QNUM,NUM,KSEX,QKE
 2001 CONTINUE
      STOP 1
 2004 NPTS=J
      REWIND 3
      MOD=1
```

```
      XINC=0.25
      ZINC=0.25
      XSTART=-2.5
      XSTOP=XSTART+XINC
      ZSTART=2.5
      ZSTOP=2.5-ZINC
      J=0
 2005 ISTART=1
 2010 DO 2100 I=ISTART,NPTS
      IF(XP(I)-XSTART)2100,2020,2020
 2020 IF(XP(I)-XSTOP)2030,2030,2100
 2030 IF(ZP(I)-ZSTART)2035,2035,2100
 2035 IF(ZP(I)-ZSTOP)2100,2040,2040
 2040 J=J 1
      ISTOP=I
      PXP(J)=XP(I)
      PZP(J)=ZP(I)
      IF(J-30)2100,2300,2300
 2100 CONTINUE
 2120 XSTART=XSTOP
      XSTOP=XSTART+XINC
      IF(XSTART-2.5)2005,2005,2140
 2140 XSTART=-2.5
      XSTOP=XSTART+XINC
      ZSTART=ZSTOP
      ZSTOP=ZSTART-ZINC
      IF(ZSTART+2.5)2400,2005,2005
 2300 CALL DRAW(J,PXP,PZP,MOD,ITYPE,LABEL,ITITLE,0.5,0.5,4,4,2,2,8,8,0,L
     1AST)
      MOD=2
      J=0
      ISTART=ISTOP+1
      IF(NPTS-ISTART)2005,2005,2010
 2400 MOD=3
      IF(J-2)2410,2430,2430
 2410 IF(J-1)2420,2425,2430
```

```
2420 ITYPE=0
     PXP(1)=-3.0
     PZP(1)=0.0
2425 PXP(2)=3.0
     PZP(2)=0.0
     J=2
2430 CALL DRAW(J,PXP,PZP,MOD,ITYPE,LABEL,ITITLE,0.5,0.5,4,4,2,2,8,8,0,L
    1AST)
     RETURN
     END
     END
```

```
      PROGRAM DATAGRID
      CALL GRID(NPTS)
      END


      SUBROUTINE GRID(NPTS)
      COMMON XP(4000),ZP(4000)
      COMMON PNUM(4000),NUM(4000)
      COMMON ISEX(4000),PKE(4000)
      COMMON KEGRID(30,30),IGRID(30,30)
      COMMON KTGRID(30,30)
   20 FORMAT(5X,13HIMPACT POINT ,A4,11H, ROTATION ,I1,14H, ATOM NUMBER ,
     1I4,42H, KINETIC ENERGY (ADJUSTED FOR THRESHOLD) ,F8.2,3H EV)
   30 FORMAT(/14HGRID SQUARE - ,I2,1H,,I2,5X,I4,7H ATOMS,,F8.2,18H EV, T
     1OTAL ENERGY,,F8.2,19H EV, AVERAGE ENERGY//////////)
   40 FORMAT(1H1)
   41 FORMAT(38X,28HSPUTTERING DEPOSIT OF ATOMS ,1X,2H( ,A4,8H ) PLANE/)
   420FORMAT(35X,F5.2,13H KEV PRIMARY,,1X,F4.2,20H EV THRESHOLD ENERGY/)
   43 FORMAT(30X,30I2)
   44 FORMAT(40X,25HENERGY DEPOSIT PER ATOM, ,1X,2H( ,A4,8H ) PLANE/)
   45 FORMAT(15X,30I3/)
   46 FORMAT(//////)
   47 FORMAT(42X,22HTOTAL ENERGY DEPOSIT, ,2H( ,A4,8H ) PLANE/)
   90 FORMAT(52X,16HNORMAL INCIDENCE///)
   91 FORMAT(46X,I2,26H DEGREE INCIDENCE ANGLE///)
      REWIND 3
      READ TAPE 3,PLANE,EVK,COY,EGYCUT
      DO 300 I=1,4000
      IF(EOF,3)310,240
  240 READ TAPE 3,XP(I),ZP(I),PNUM(I),NUM(I),ISEX(I),PKE(I)
  300 CONTINUE
  310 NPTS=I
      PRINT 40
```

```
      PRINT 41,PLANE
      PRINT 46
      YSTART=1.6
      XINC=0.1
      YINC=0.1
      DO 600 M=1,30
      YSTART=YSTART-YINC
      YSTOP=YSTART-YINC
      XSTART=-1.5
      DO 500 I=1,30
      N=0
      TKE=0.0
      XSTOP=XSTART+XINC
      DO 480 J=1,NPTS
      IF(ZP(J)-YSTART)210,210,480
  210 IF(ZP(J)-YSTOP)480,215,215
  215 IF(XP(J)-XSTART)480,220,220
  220 IF(XP(J)-XSTOP)230,230,480
  230 N=N 1
      PRINT 20,PNUM(J),ISEX(J),NUM(J),PKE(J)
      TKE=TKE+PKE(J)
  480 CONTINUE
      IF(N)485,490,485
  485 EN=N
      AVGKEY=TKE/EN
      GO TO 495
  490 AVGKEY=0.0
  495 KEGRID(M,I)=AVGKEY+0.49
      KTGRID(M,I)=TKE+0.49
      IGRID(M,I)=N
      IF(N)498,499,498
  498 PRINT 30,M,I,N,TKE,AVGKEY
  499 XSTART=XSTOP
  500 CONTINUE
  600 CONTINUE
      PRINT 40
```

```
      PRINT 41,PLANE
      PRINT 42,EVK,EGYCUT
      IF(COY.EQ.1.0)211,212
  211 PRINT 90
      GO TO 213
  212 RADIAN=ACOSF(COY)
      LAMBDA=RADIAN*57.29577866
      PRINT 91,LAMBDA
  213 CONTINUE
      DO 249 I=1,30
  249 PRINT 45,(IGRID(I,J),J=1,30)
      PRINT 40
      PRINT 44,PLANE
      PRINT 42,EVK,EGYCUT
      IF(COY.EQ.1.0)250,260
  250 PRINT 90
      GO TO 265
  260 PRINT 91,LAMBDA
  265 CONTINUE
      DO 266 I=1,30
  266 PRINT 45,(KEGRID(I,J),J=1,30)
      PRINT 40
      PRINT 47,PLANE
      PRINT 42,EVK,EGYCUT
      IF(COY.EQ.1.0)270,280
  270 PRINT 90
      GO TO 285
  280 PRINT 91,LAMBDA
  285 CONTINUE
      DO 287 I=1,30
  287 PRINT 45,(KTGRID(I,J),J=1,30)
      REWIND 3
      RETURN
      END
      END
```

INITIAL DISTRIBUTION LIST

		No. Copies
1.	Defense Documentation Center Cameron Station Alexandria, Virginia 22314	20
2.	Library Naval Postgraduate School Monterey, California 93940	2
3.	Professor Don E. Harrison Department of Physics Naval Postgraduate School Monterey, California 93940	20
4.	LT Herbert M. Effron, USN USS WILLIAM H. STANDLEY (DLG-32) FPO New York 09501	2
5.	CAPT John P. Johnson, III United States Military Academy West Point, New York 10996	1
6.	Commander, Ordnance Systems Command Department of the Navy Washington, D. C. 20360	1

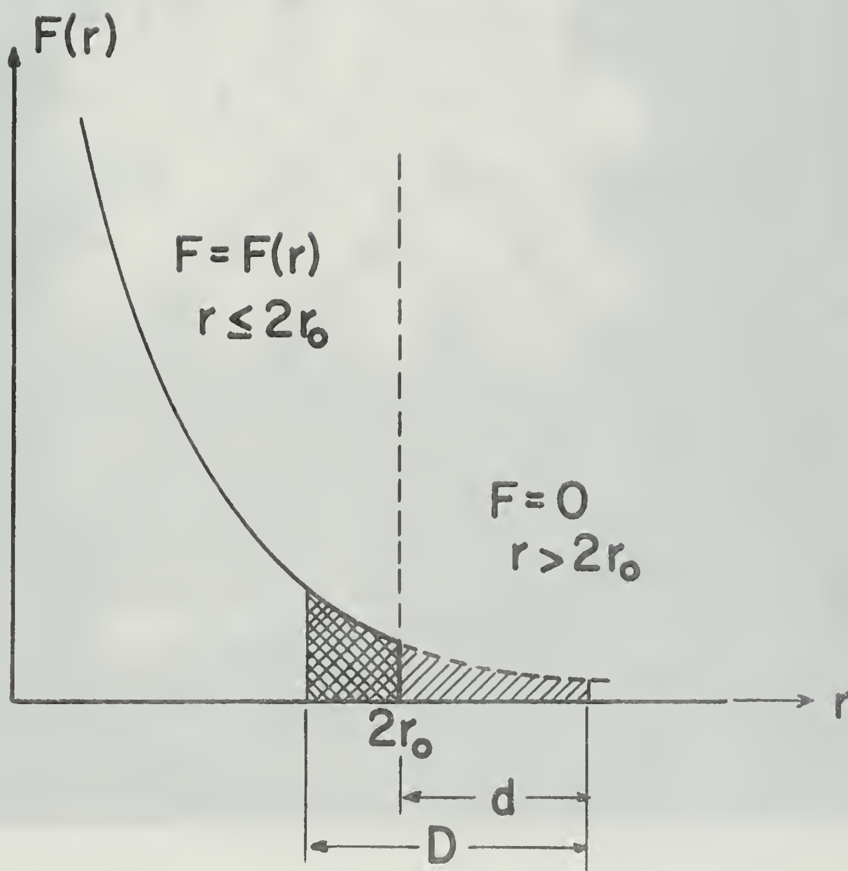

Erosion of the force function at $r = 2r_o$ results in a loss of energy in the model. This is corrected in the STEP subroutine.

Figure 1

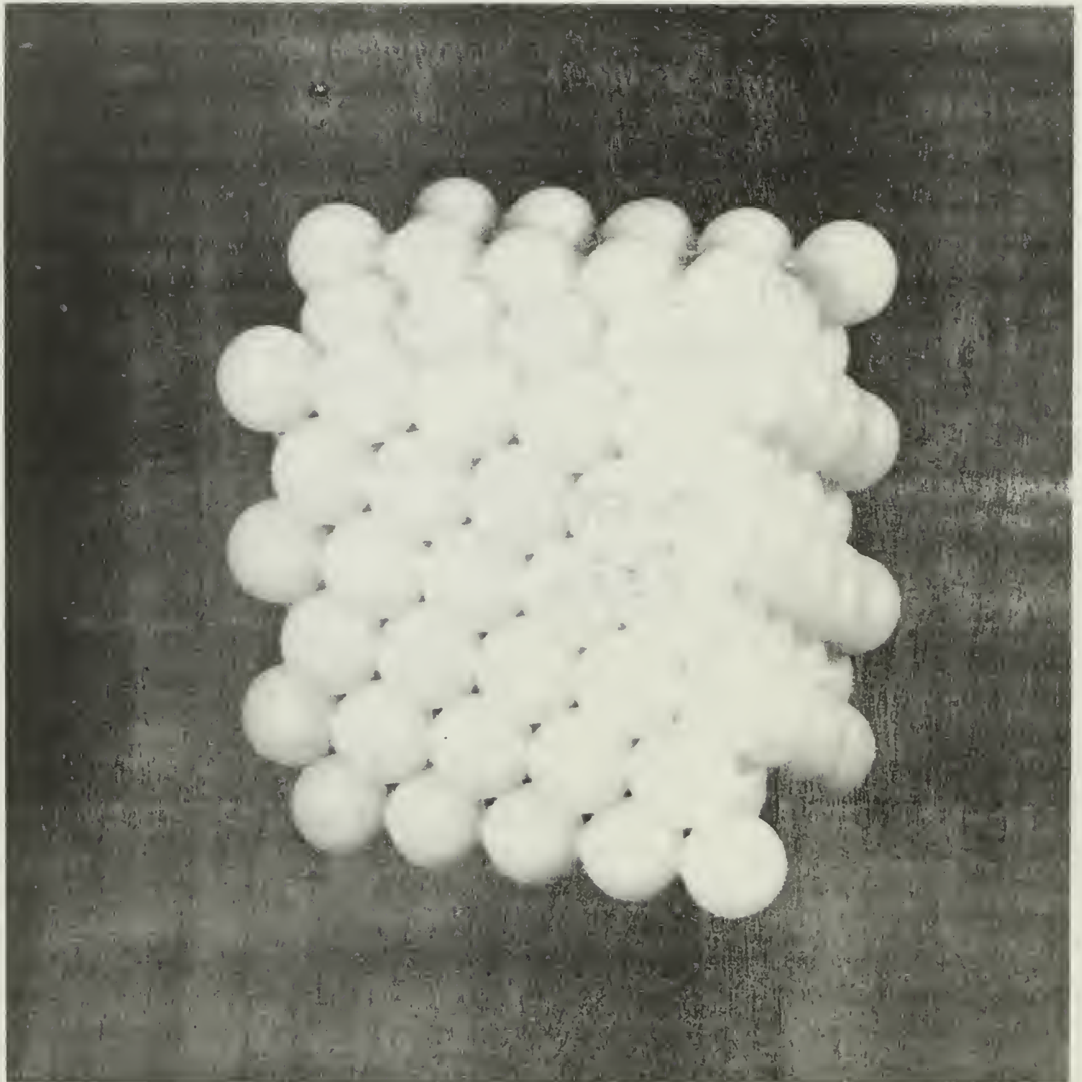

The (111) surface crystal

Figure 2

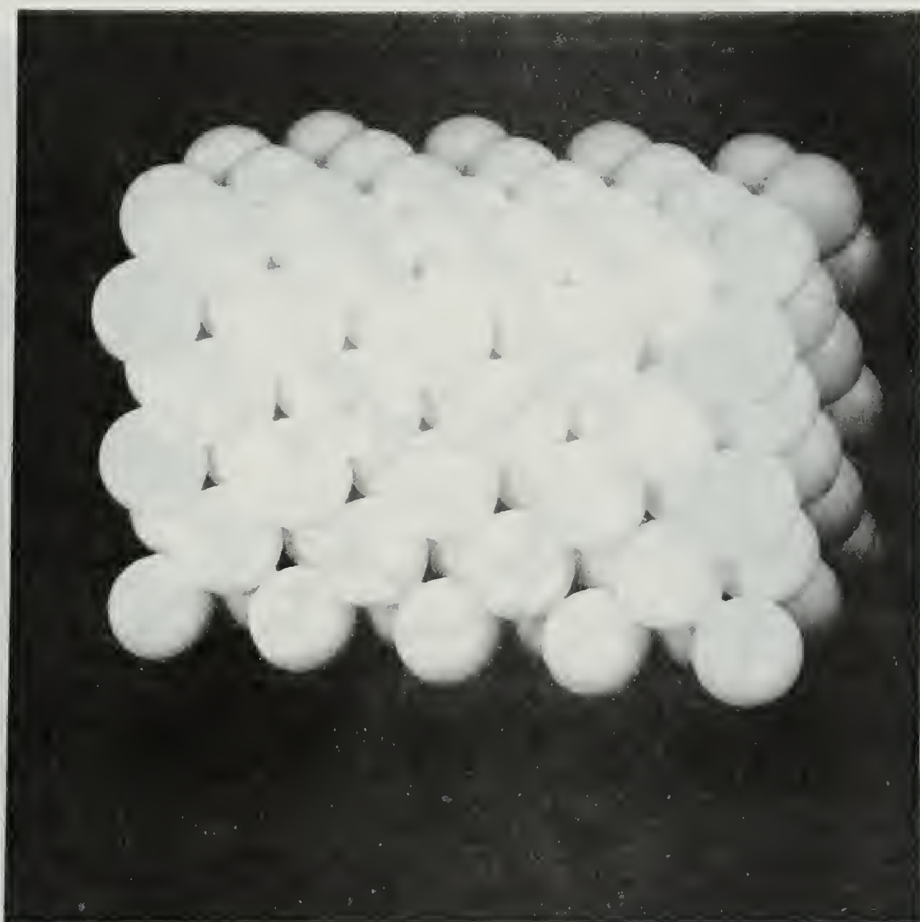

The (100) surface crystal

Figure 3

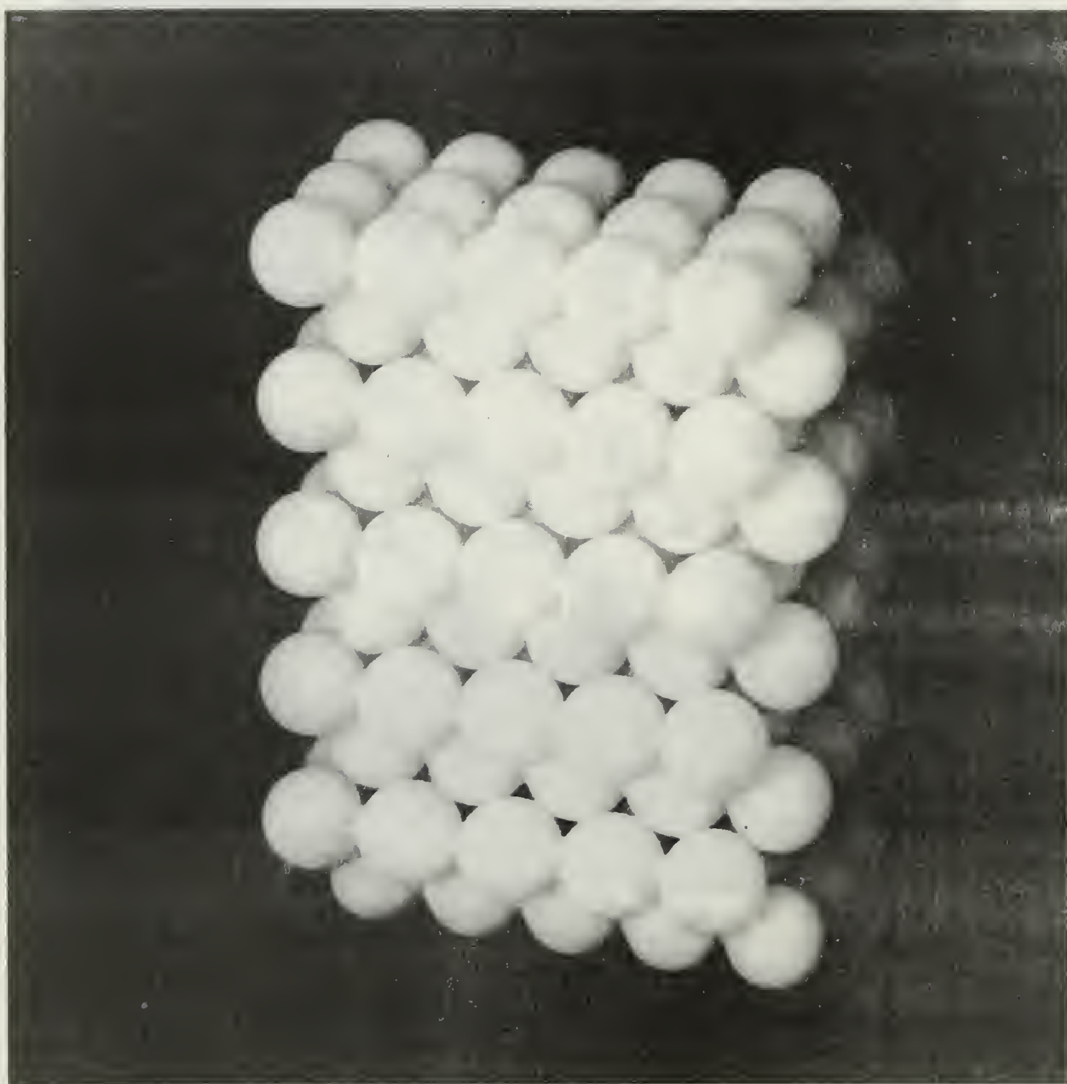

The (110) surface crystal

Figure 4

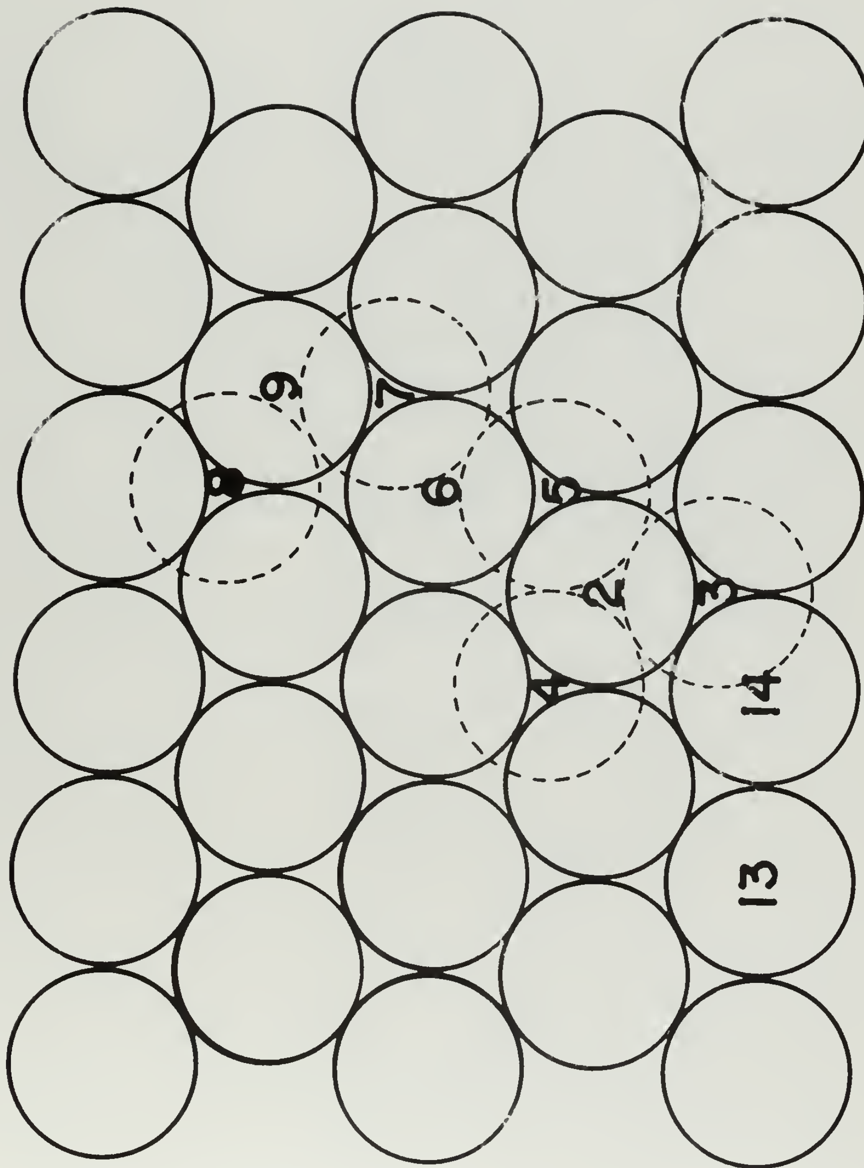

Atoms involved in the sputtering mechanisms.

Figure 5

Argon Copper Sputtering
(III) Surface

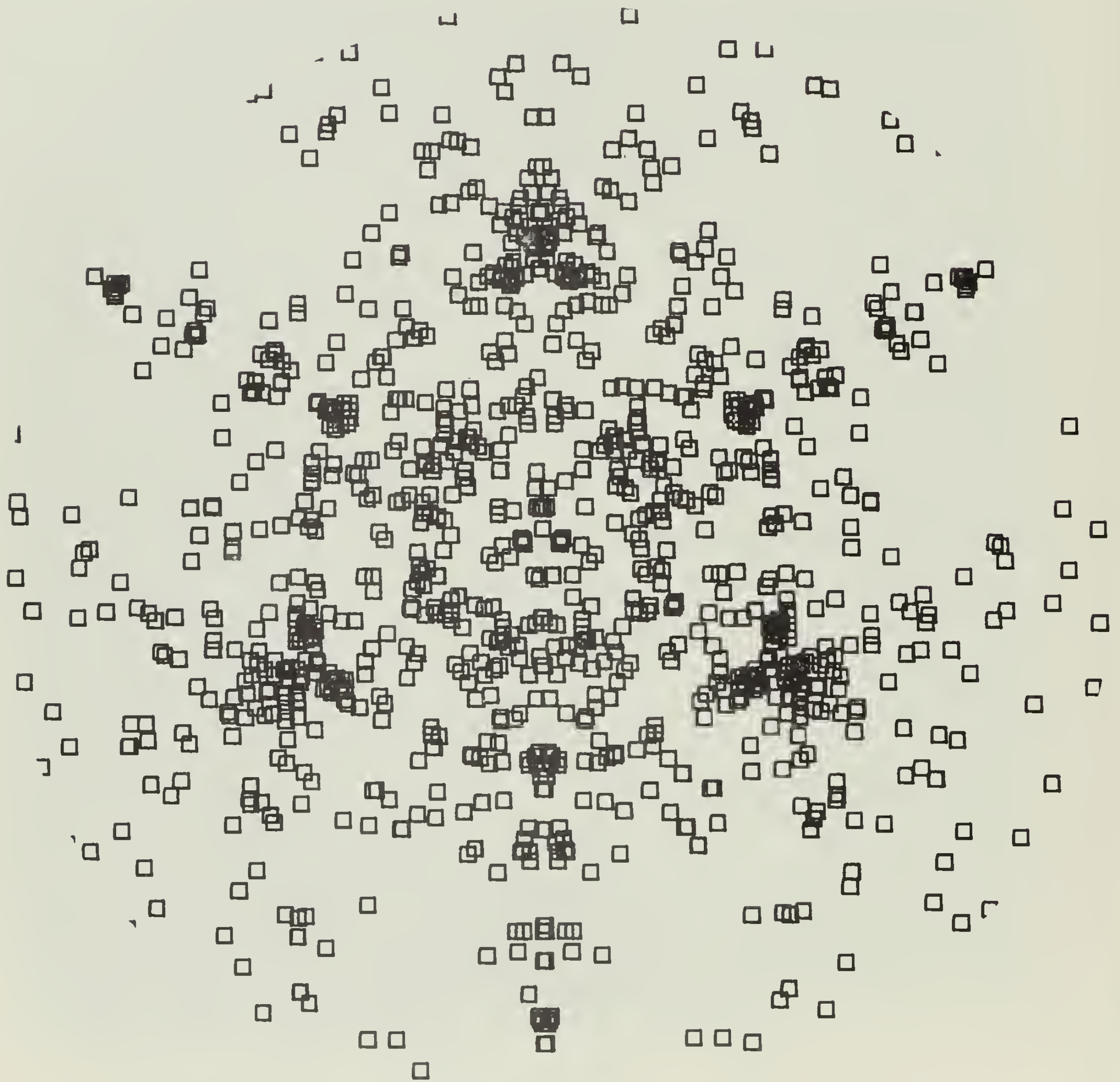

1.0 Kev Bombardment Energy
3.00 ev Binding Energy

Figure 6a

Argon Copper Sputtering
(111) Surface

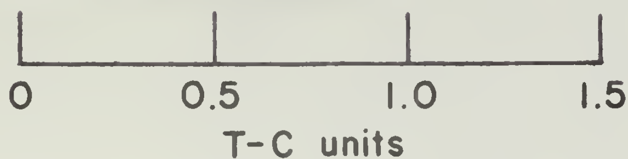

1.0 Kev Bombardment Energy
3.00 ev Binding Energy

Figure 6b

Argon Copper Sputtering

(111) Surface

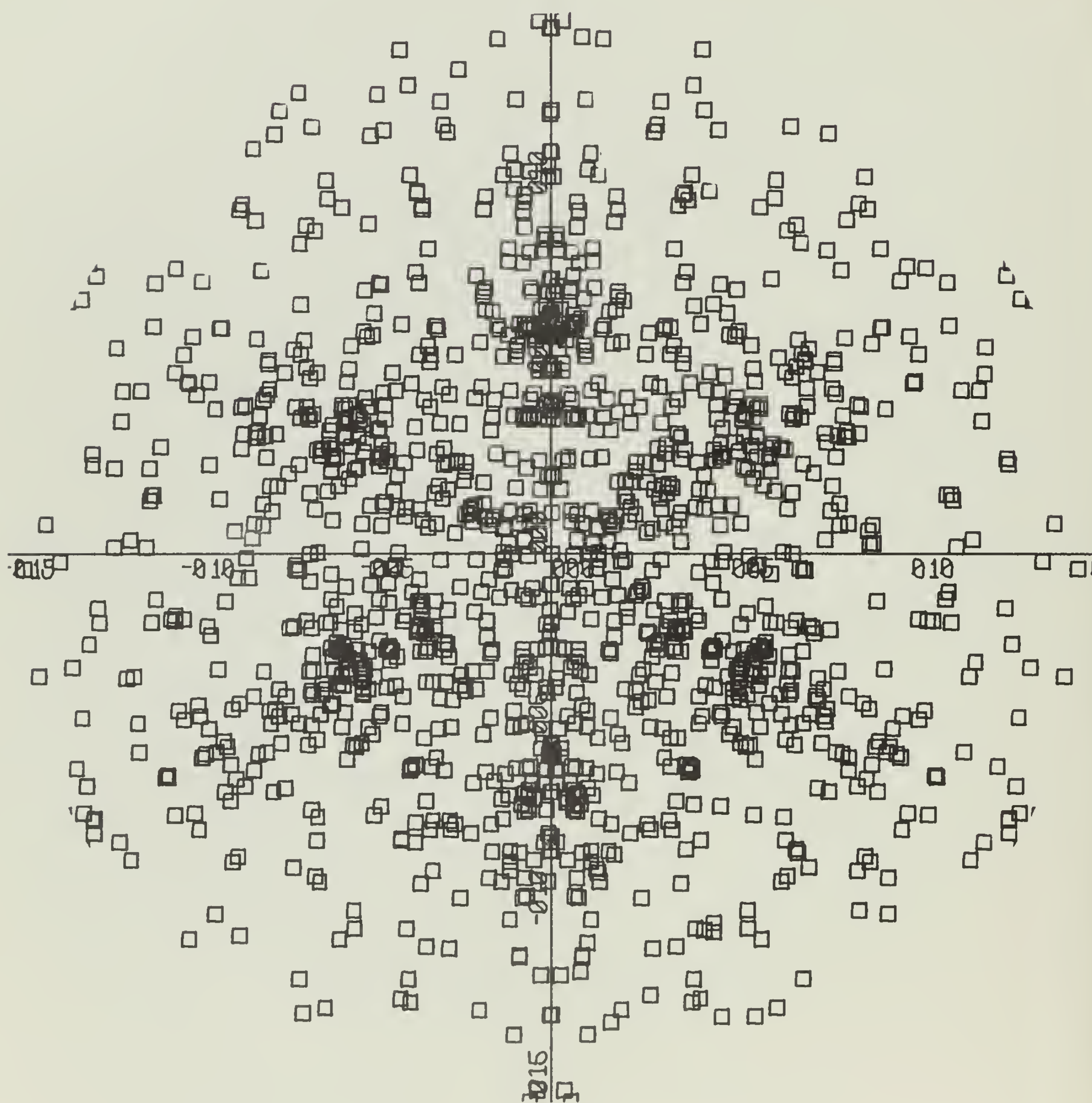

2.0 Kev Bombardment Energy

3.00 ev Binding Energy

Figure 7a

Argon Copper Sputtering
(111) Surface

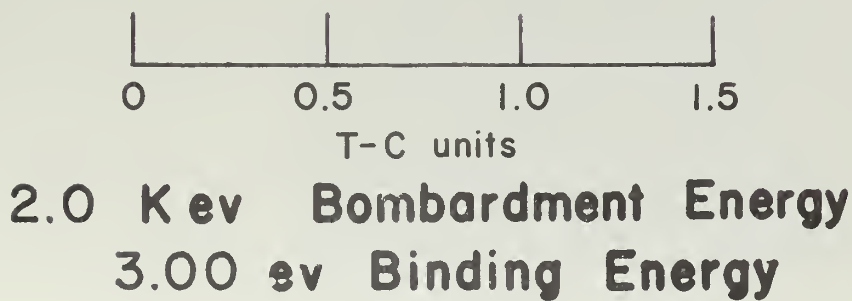

Figure 7b

Argon Copper Sputtering
(111) Surface

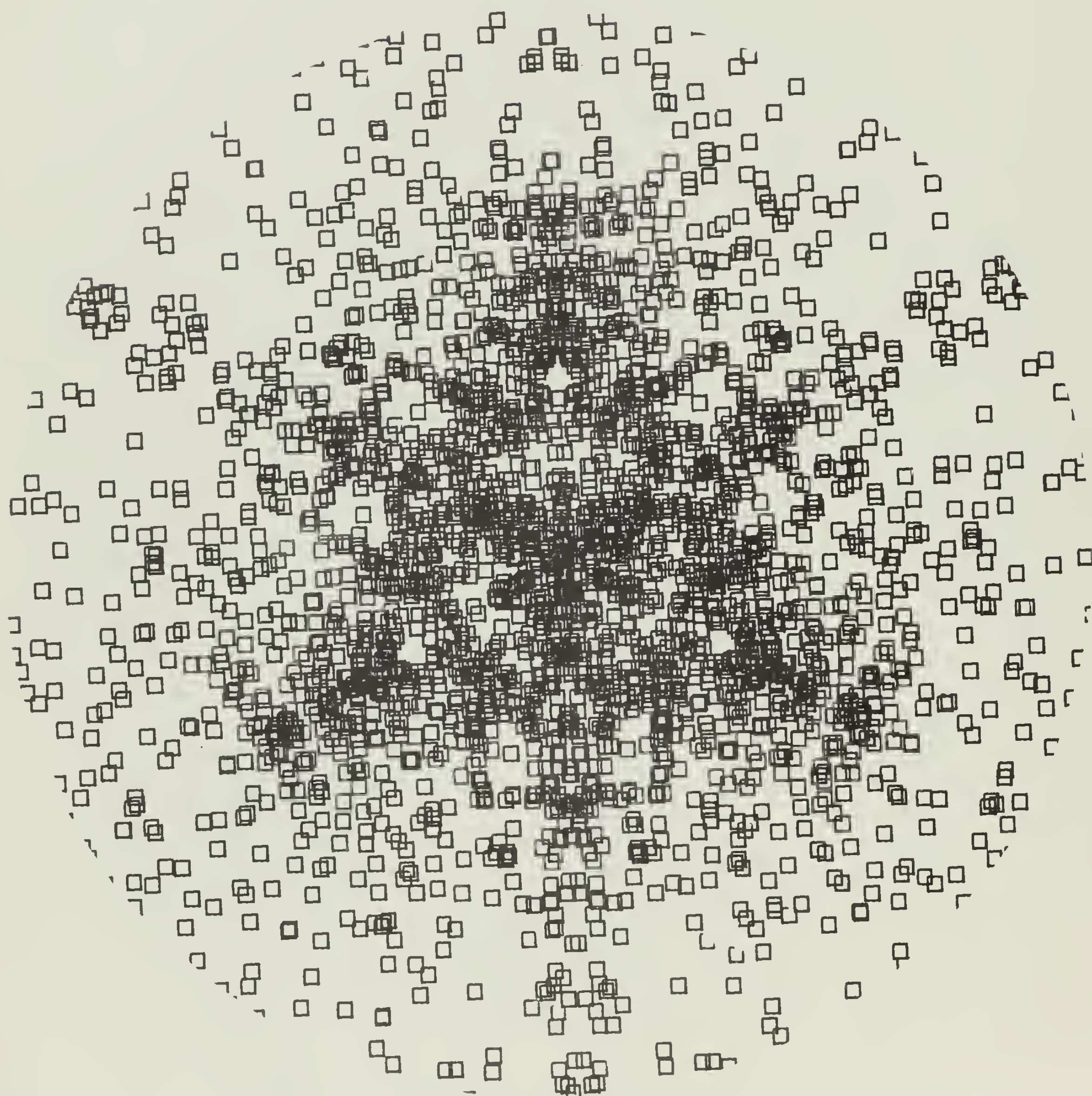

3.0 Kev Bombardment Energy
1.50 ev Binding Energy

Figure 8a

Argon Copper Sputtering
(111) Surface

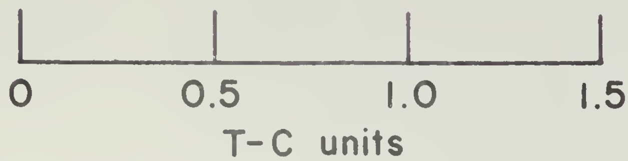

3.0 Kev Bombardment Energy
1.50 ev Binding Energy

Figure 8b

Argon Copper Sputtering
(111) Surface

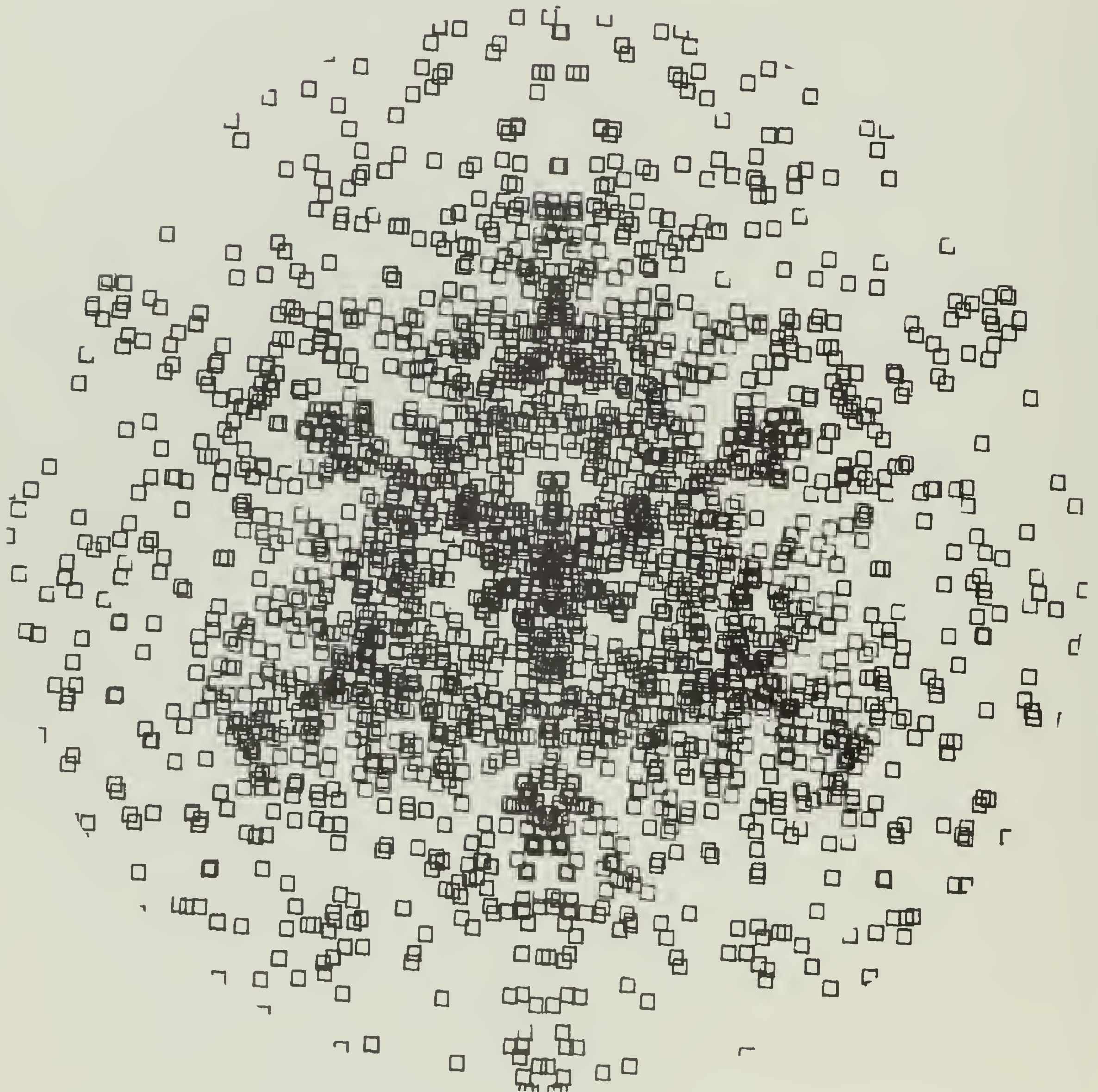

3.0 Kev Bombardment Energy
2.00 ev Binding Energy

Figure 9a

Argon Copper Sputtering
(111) Surface

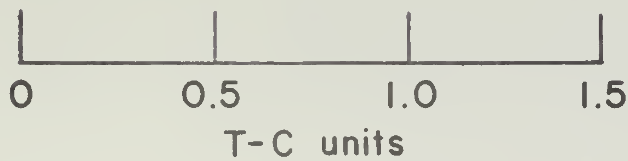

3.0 Kev Bombardment Energy
2.00 ev Binding Energy

Figure 9b

Argon Copper Sputtering
(111) Surface

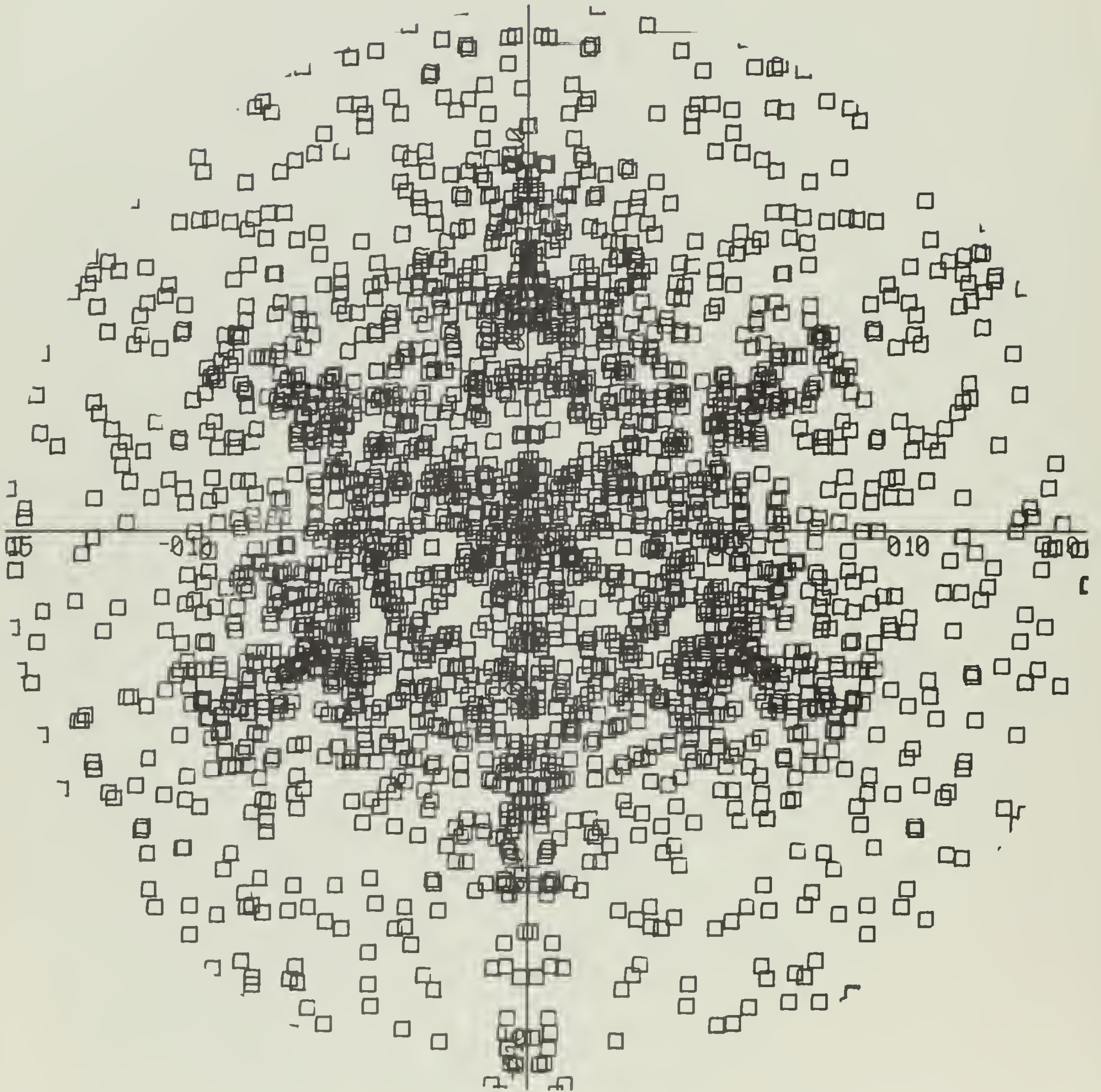

3.0 Kev Bombardment Energy
2.50 ev Binding Energy

Figure 10a

Argon Copper Sputtering
(111) Surface

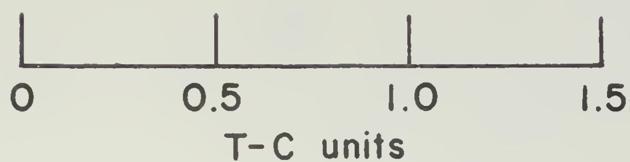

3.0 Kev Bombardment Energy
2.50 ev Binding Energy

Figure 10b

Argon Copper Sputtering

(111) Surface

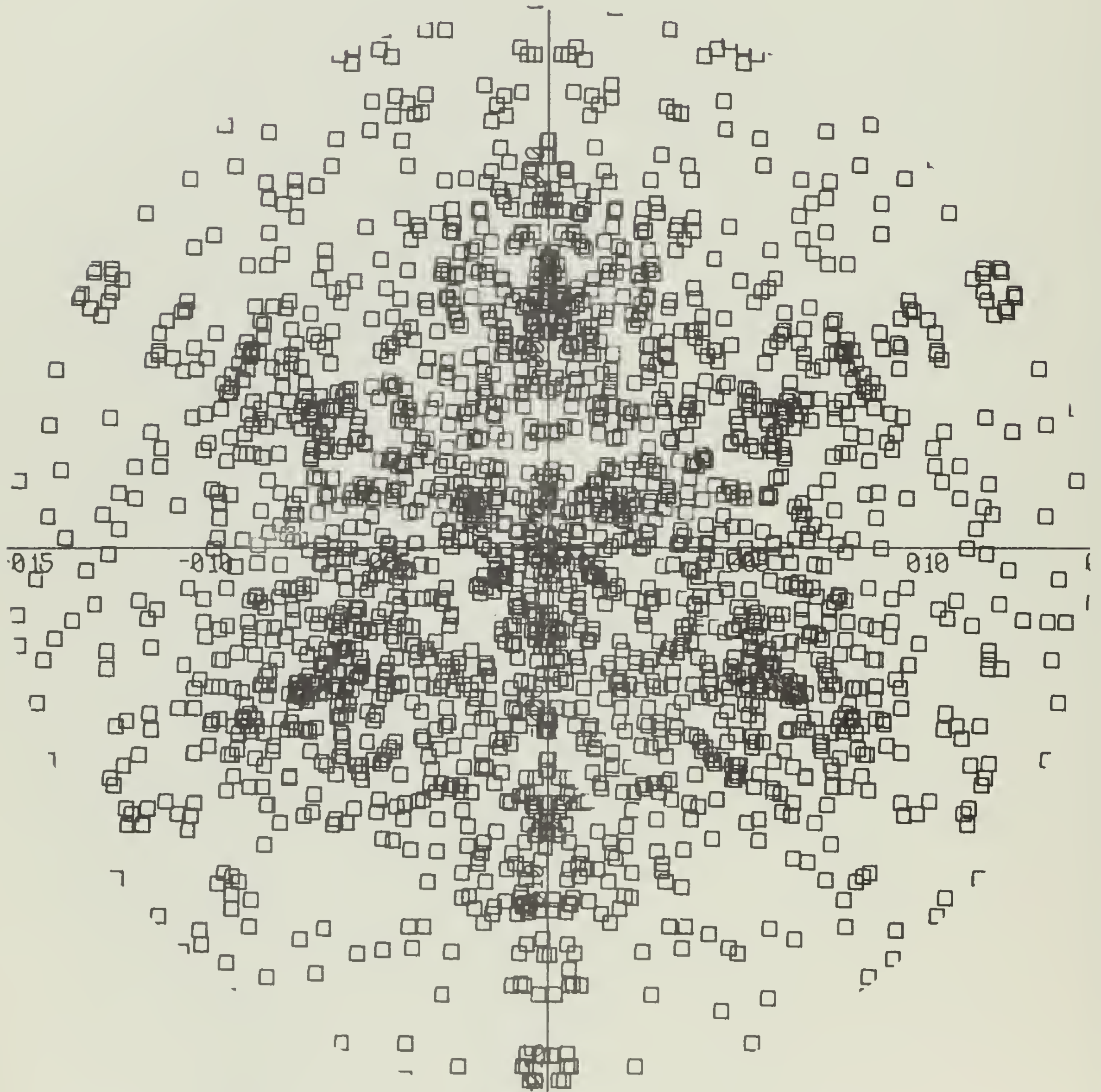

3.0 Kev Bombardment Energy

3.00 ev Binding Energy

Figure 11a

Argon Copper Sputtering
(111) Surface

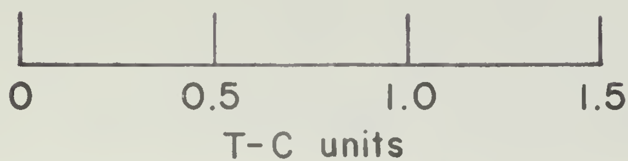

3.0 Kev Bombardment Energy
3.00 ev Binding Energy

Figure 11b

Argon Copper Sputtering

(111) Surface

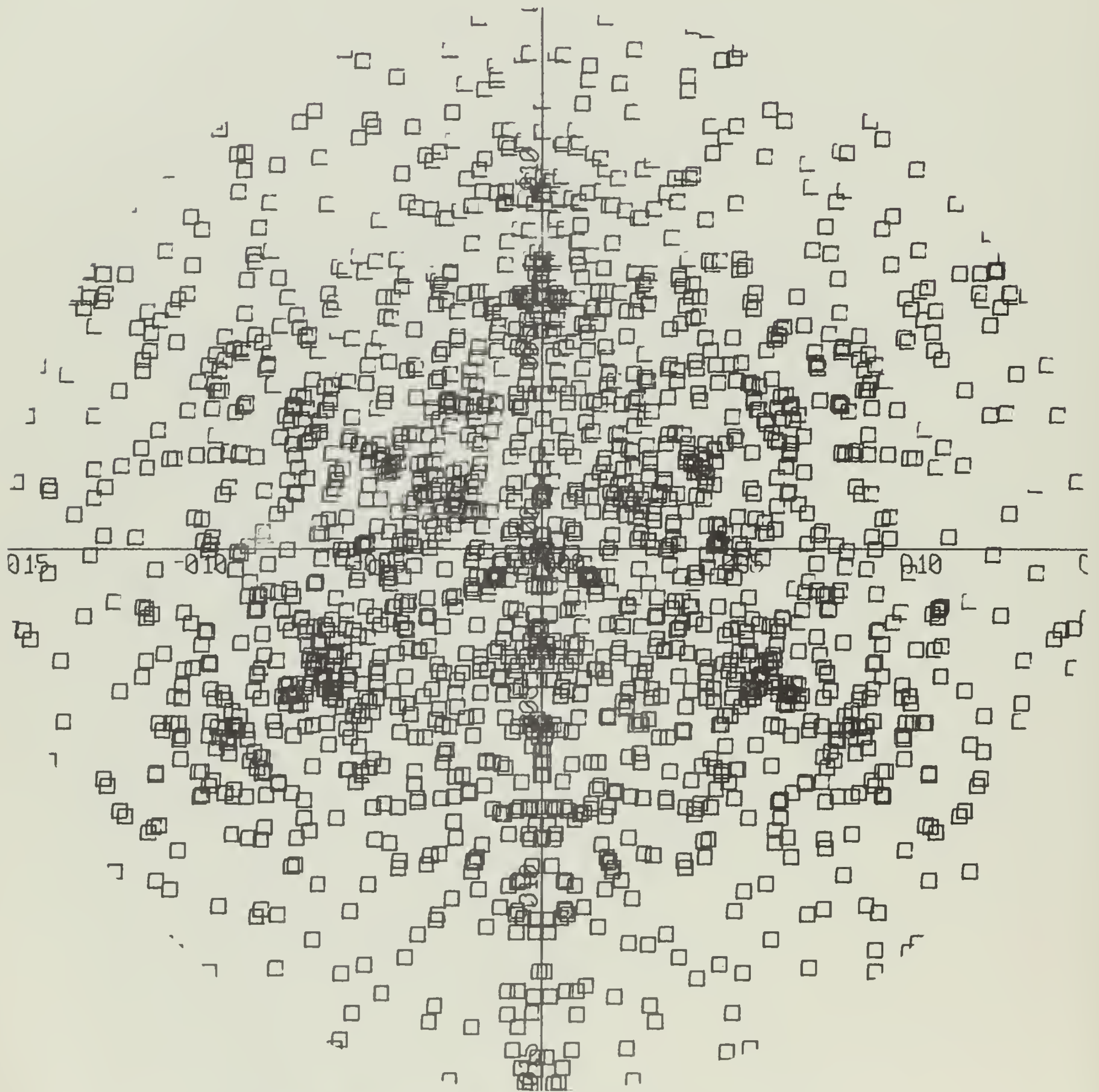

3.0 Kev Bombardment Energy

4.00 ev Binding Energy

Figure 12a

Argon Copper Sputtering
(111) Surface

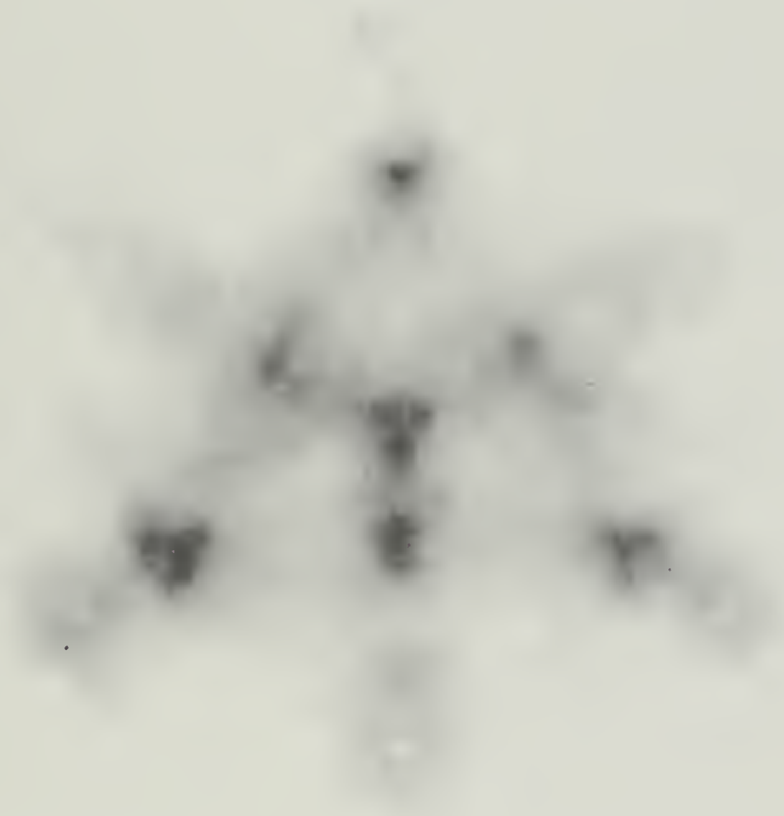

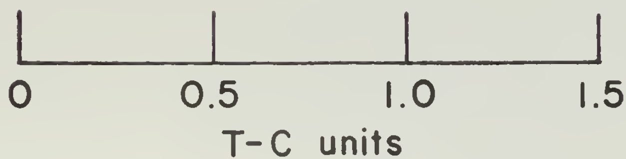

3.0 K ev Bombardment Energy
4.00 ev Binding Energy

Figure 12b

Argon Copper Sputtering
(III) Surface

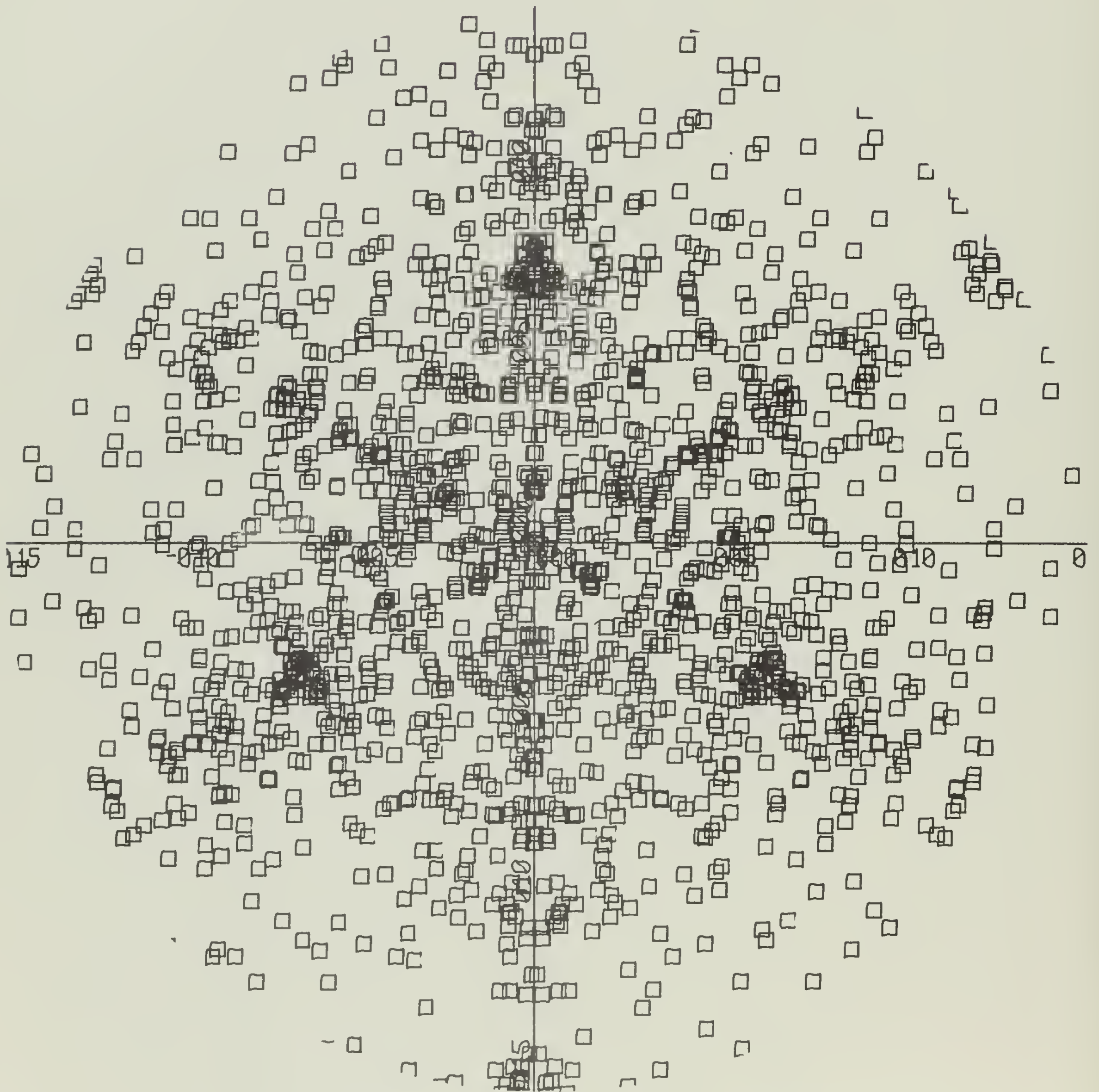

3.0 Kev Bombardment Energy
4.50 ev Binding Energy

Figure 13a

Argon Copper Sputtering
(111) Surface

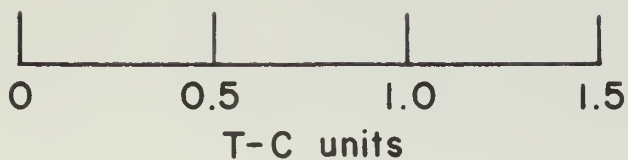

3.0 Kev Bombardment Energy
4.50 ev Binding Energy

Figure 13b

Argon Copper Sputtering

(111) Surface

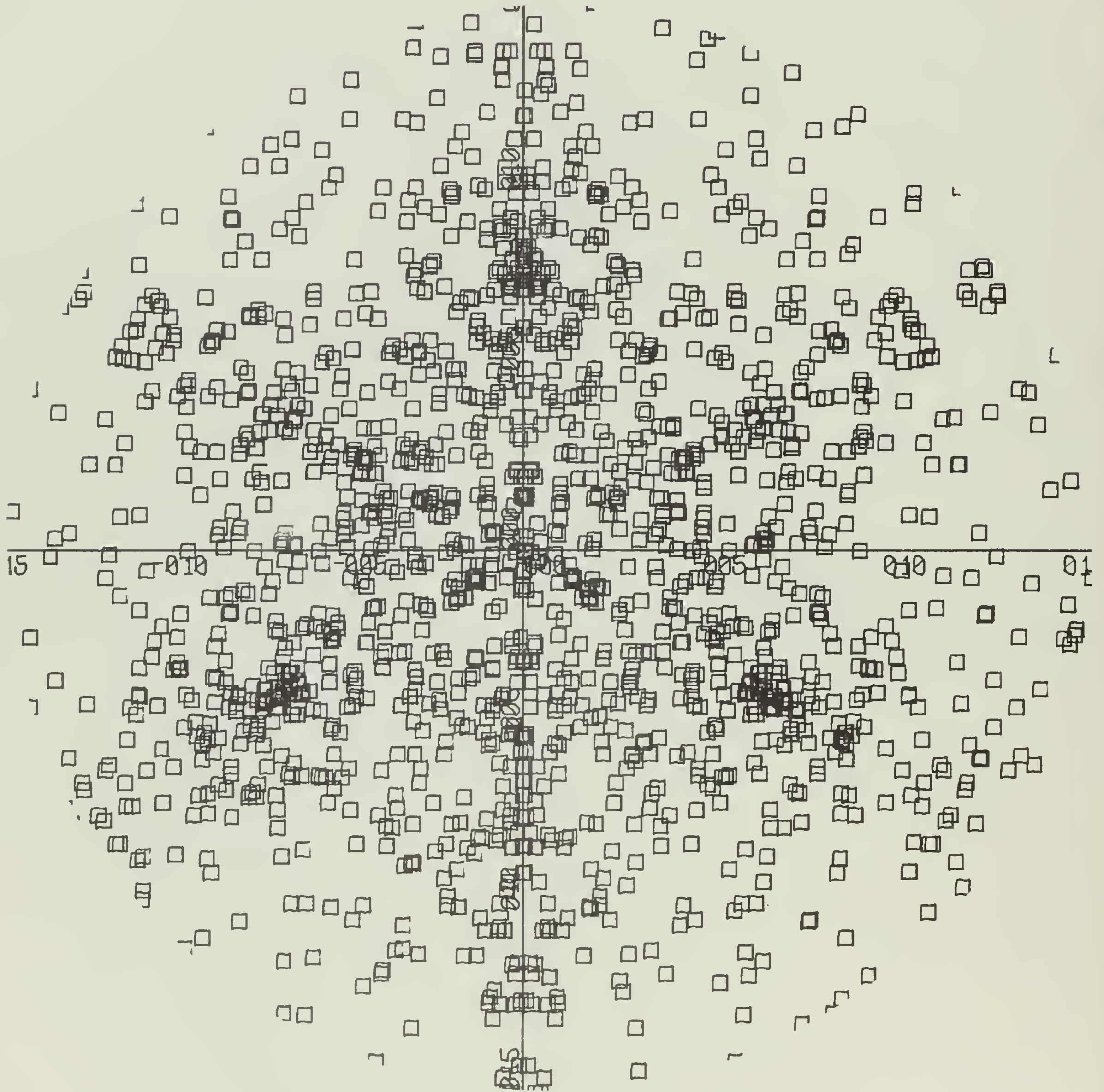

3.0 Kev Bombardment Energy

5.50 ev Binding Energy

Figure 14a

Argon Copper Sputtering
(111) Surface

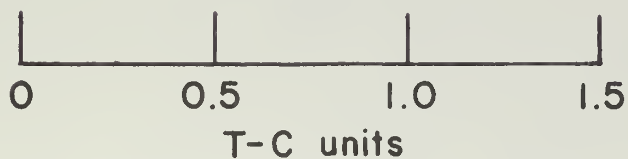

3.0 Kev Bombardment Energy
5.50 ev Binding Energy

Figure 14b

Argon Copper Sputtering

(111) Surface

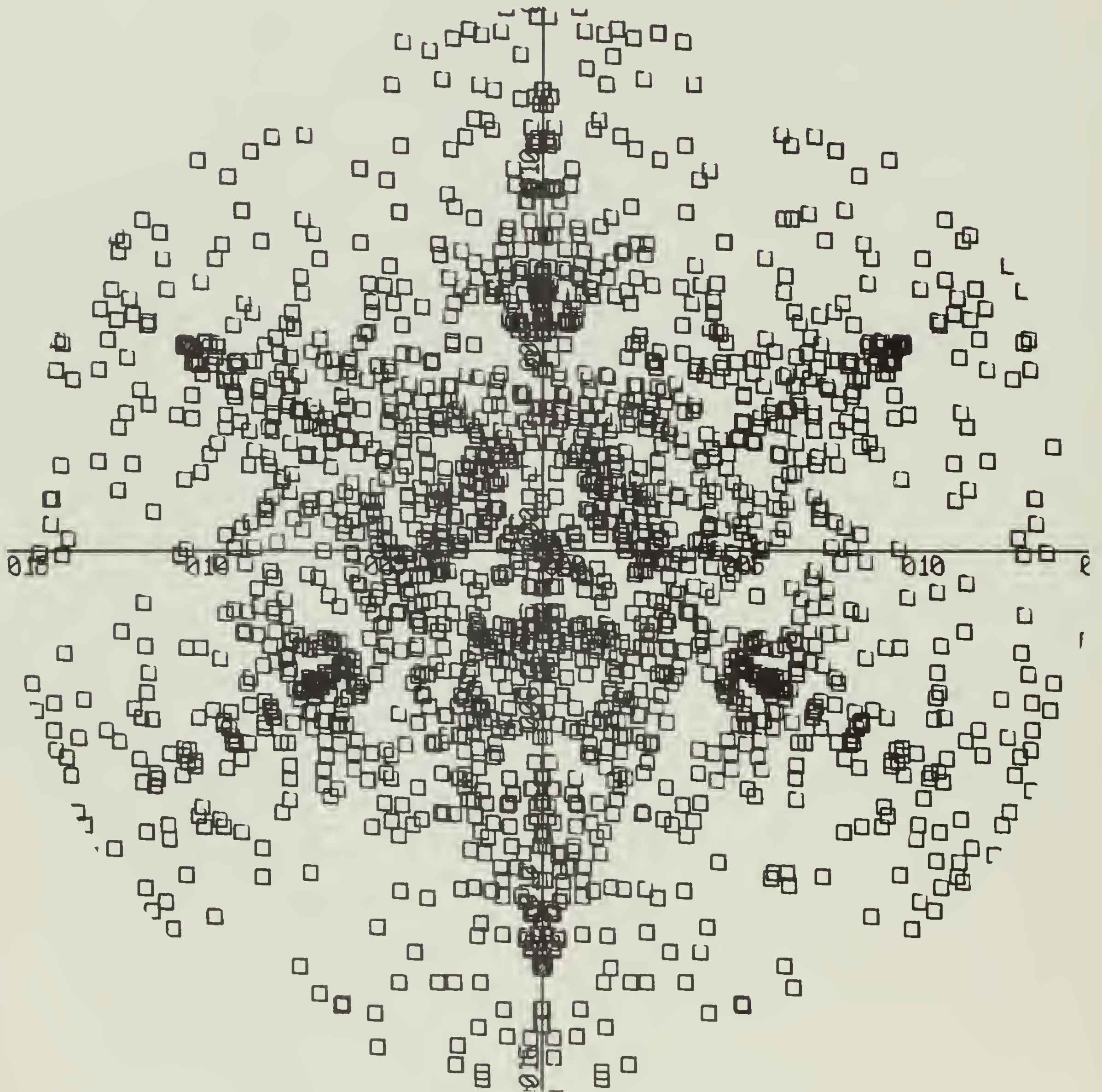

4.0 Kev Bombardment Energy

3.00 ev Binding Energy

Figure 15a

Argon Copper Sputtering
(111) Surface

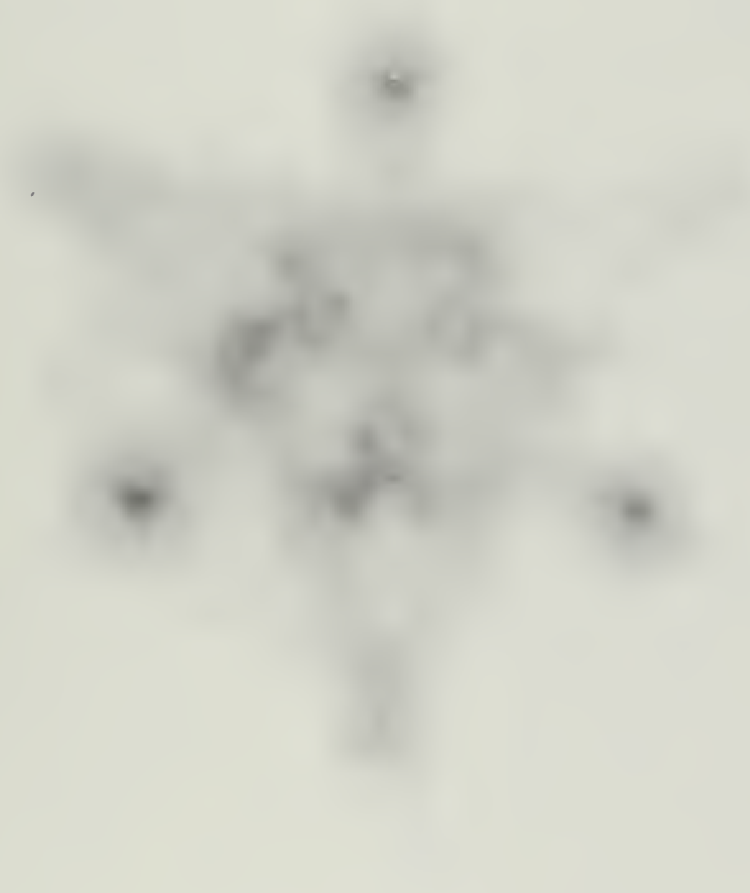

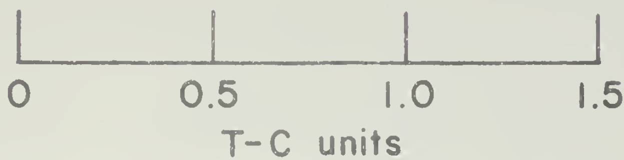

4.0 Kev Bombardment Energy
3.00 ev Binding Energy

Figure 15b

[illegible]

[illegible]

[illegible]

[illegible]

[illegible]

[illegible]

Argon Copper Sputtering

(111) Surface

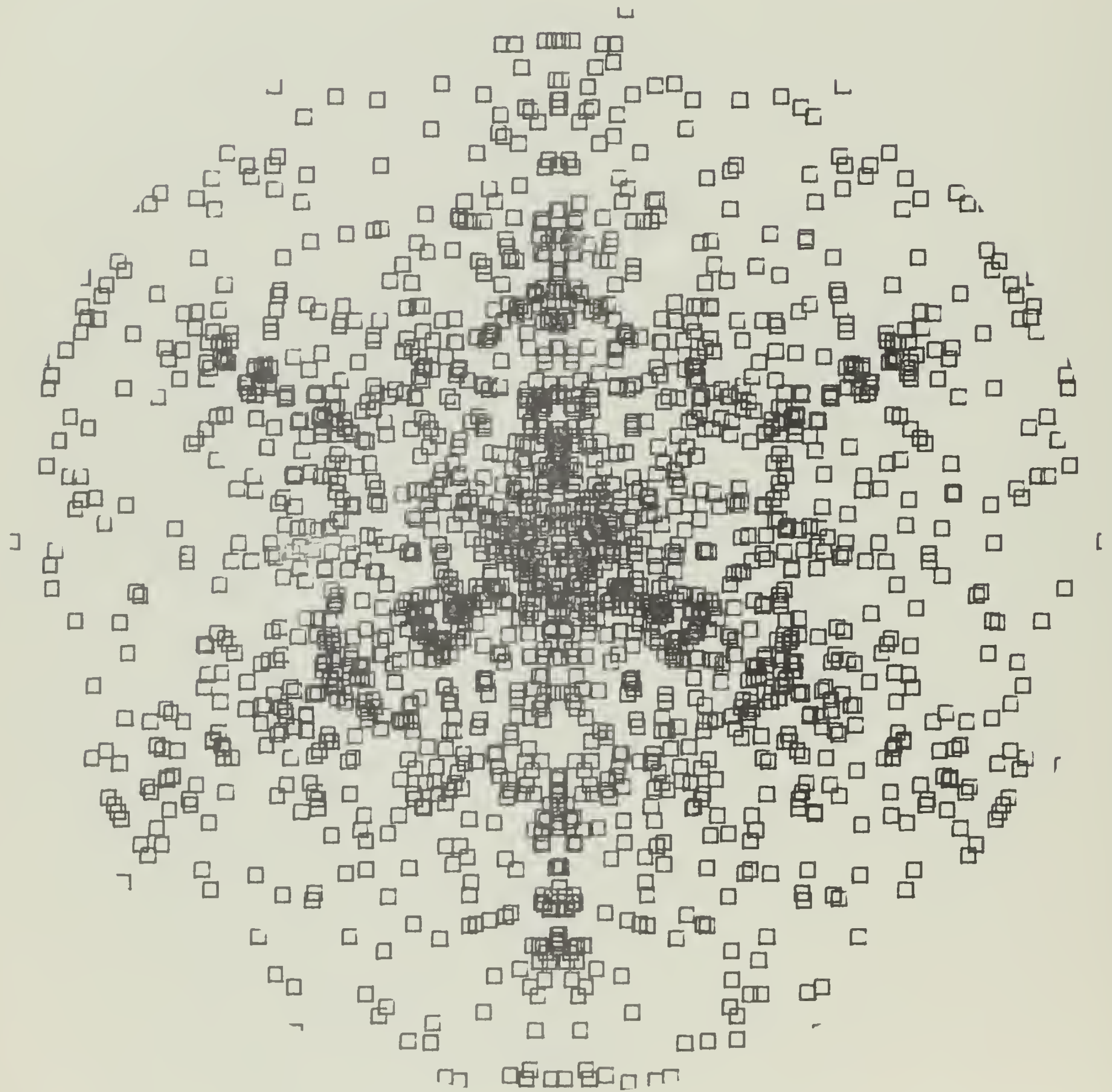

5.0 Kev Bombardment Energy

3.00 ev Binding Energy

Figure 16a

Argon Copper Sputtering
(111) Surface

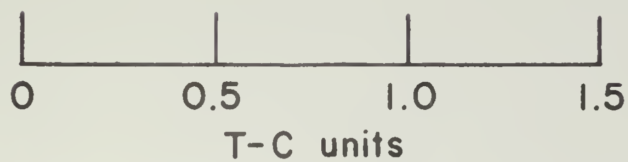

5.0 Kev Bombardment Energy
3.00 ev Binding Energy

Figure 16b

Argon Copper Sputtering

(111) Surface

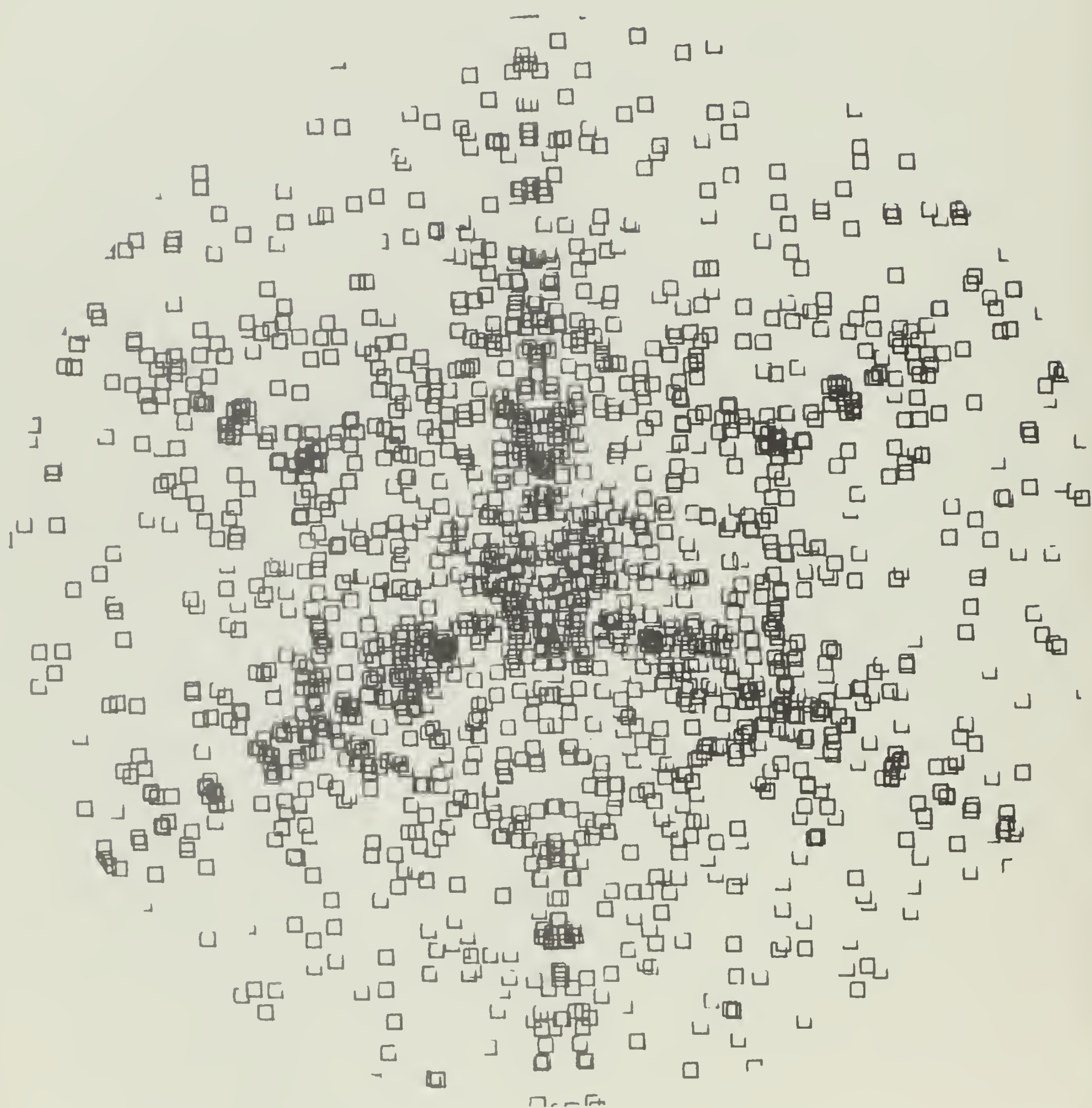

5.0 K ev Bombardment Energy

3.50 ev Binding Energy

Figure 17a

Argon Copper Sputtering
(111) Surface

5.0 K ev Bombardment Energy
3.50 ev Binding Energy

Figure 17b

Argon Copper Sputtering

(111) Surface

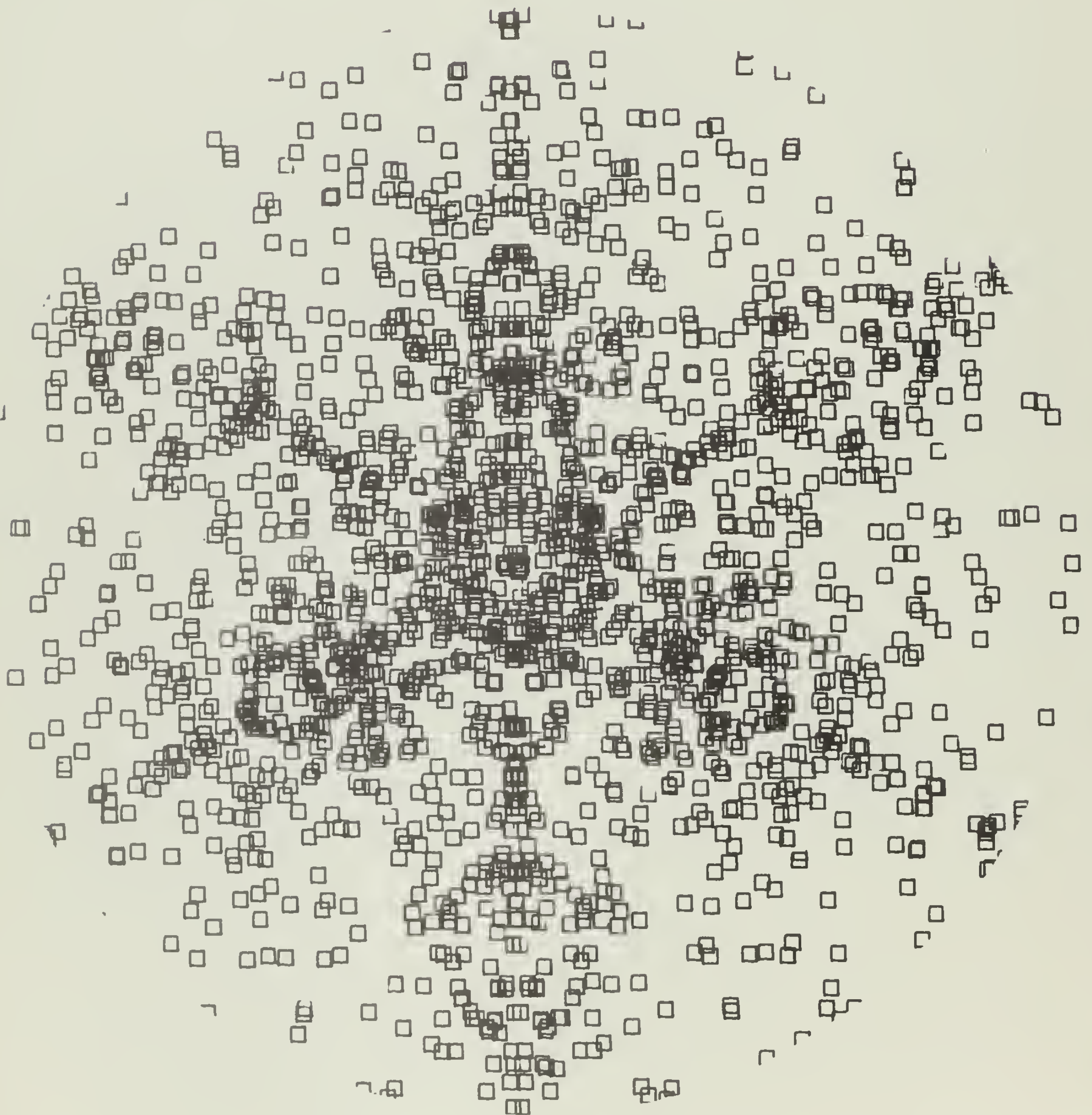

7.0 Kev Bombardment Energy

3.00 ev Binding Energy

Figure 18a

Argon Copper Sputtering
(111) Surface

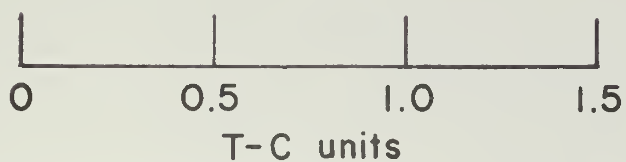

7.0 K ev Bombardment Energy
3.00 ev Binding Energy

Figure 18b

Argon Copper Sputtering

(111) Surface

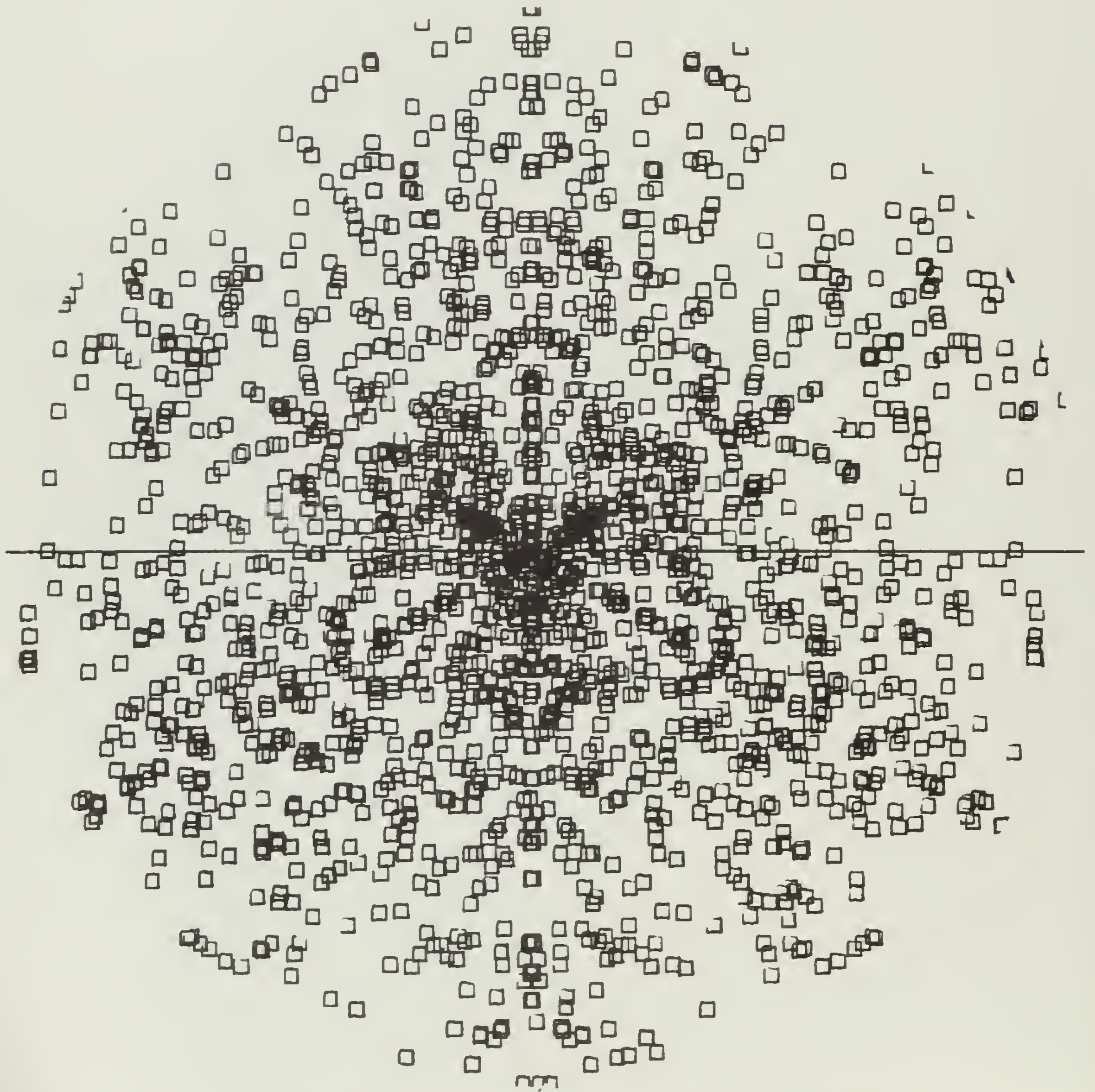

10 K ev Bombardment Energy

3.50 ev Binding Energy

Figure 19a

Argon Copper Sputtering

(111) Surface

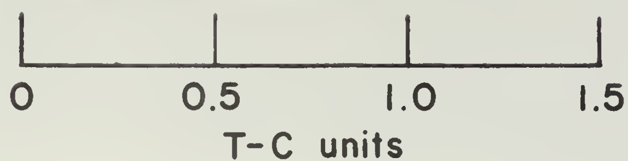

10 K ev Bombardment Energy

3.50 ev Binding Energy

Figure 19b

Argon Copper Sputtering

(111) Surface

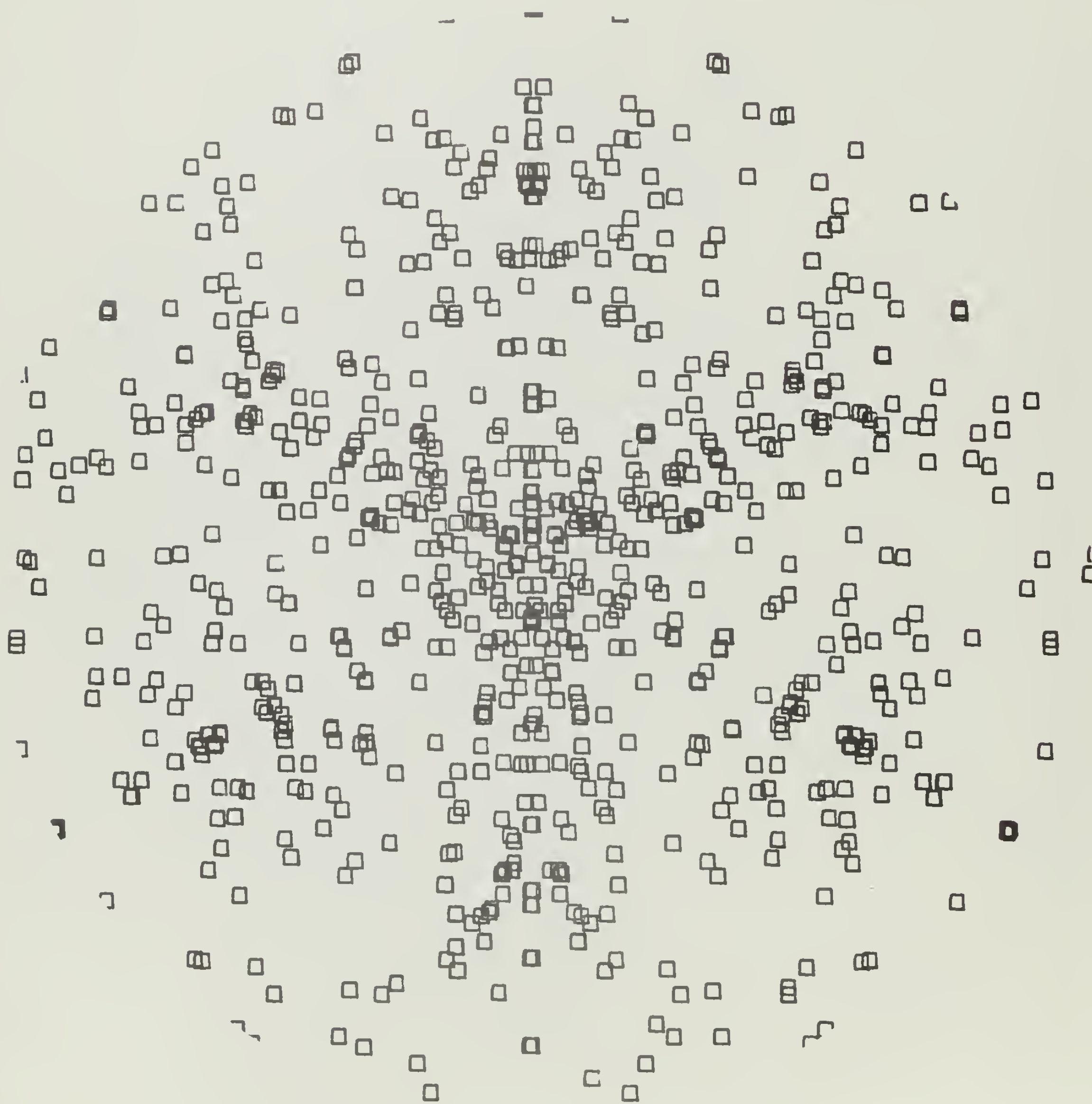

20 K ev Bombardment Energy

3.50 ev Binding Energy

Figure 20a

Argon Copper Sputtering
(111) Surface

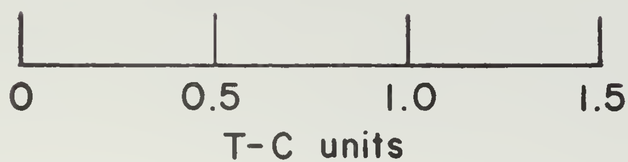

20 K ev Bombardment Energy
3.50 ev Binding Energy

Figure 20b

Argon Copper Sputtering
(111) Surface

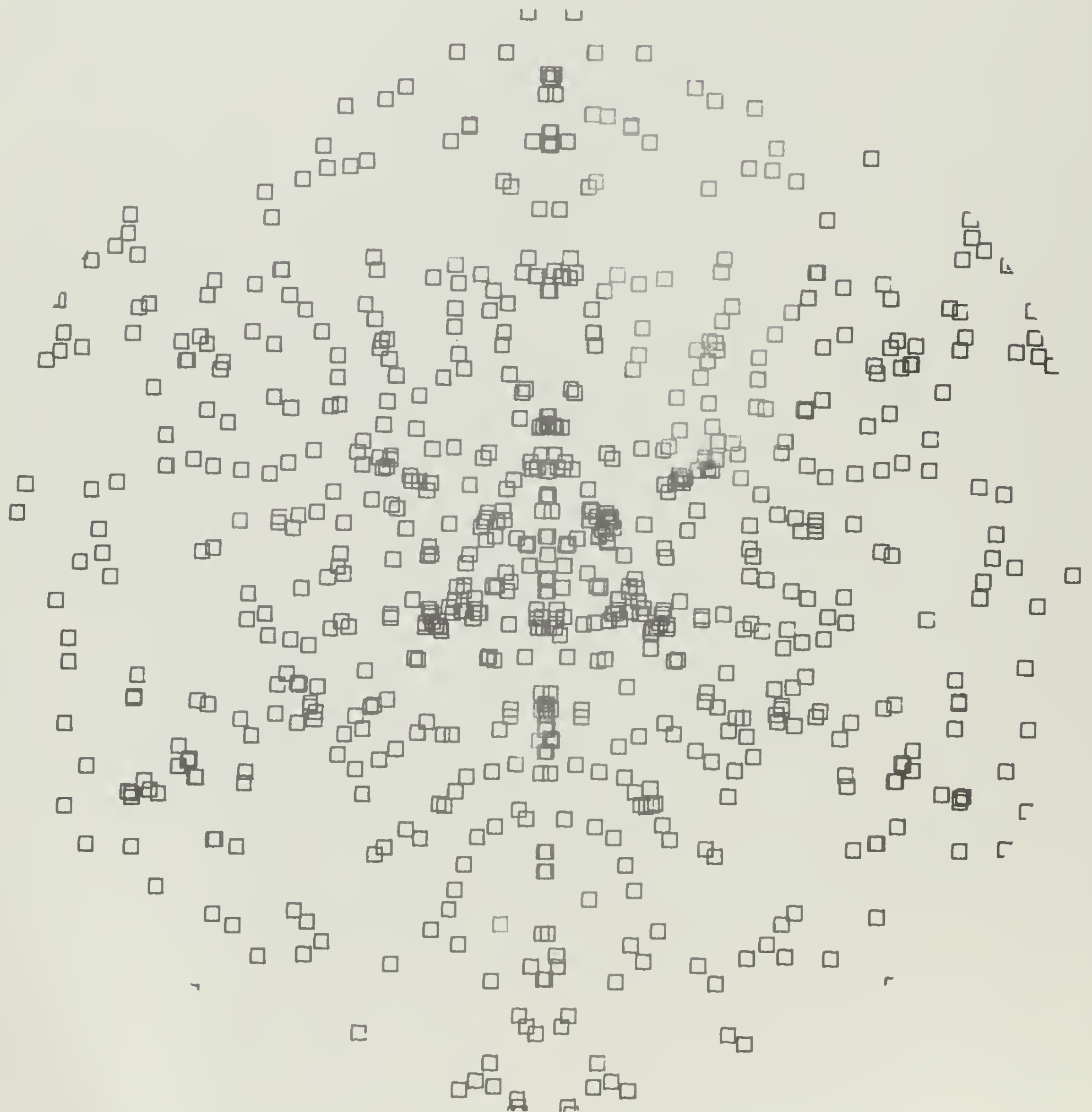

40 K ev Bombardment Energy
3.50 ev Binding Energy

Figure 21a

Argon Copper Sputtering
(111) Surface

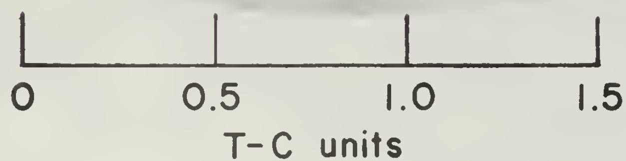

40 Kev Bombardment Energy
3.50 ev Binding Energy

Figure 21b

(111) Surface

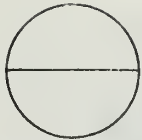

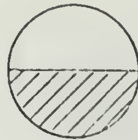

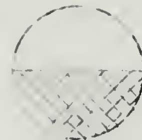

Sputtering frequency-location diagram for (111) surface.
1 keV

Figure 22

(111) Surface

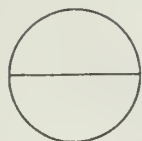

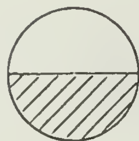

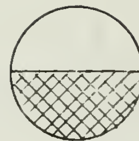

Scattering frequency-location diagram for (111) surface.
2 keV

Figure 23

(111) Surface

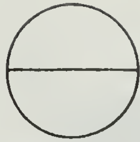

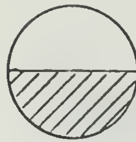

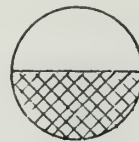

Sputtering frequency-location diagram for (111) surface.
3 keV

Figure 24

(111) Surface

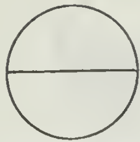

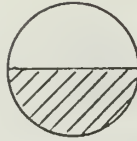

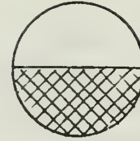

Sputtering frequency-location
diagram for (111) surface.
4 keV

Figure 25

(111) Surface

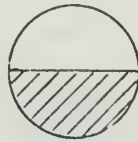

Sputtering frequency-location diagram for (111) surface.
5 keV

Figure 26

(111) Surface

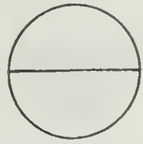

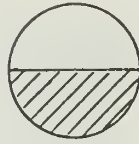

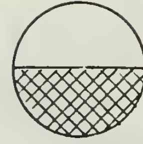

Sputtering frequency-location diagram for (111) surface.
7 keV

Figure 27

(111) Surface

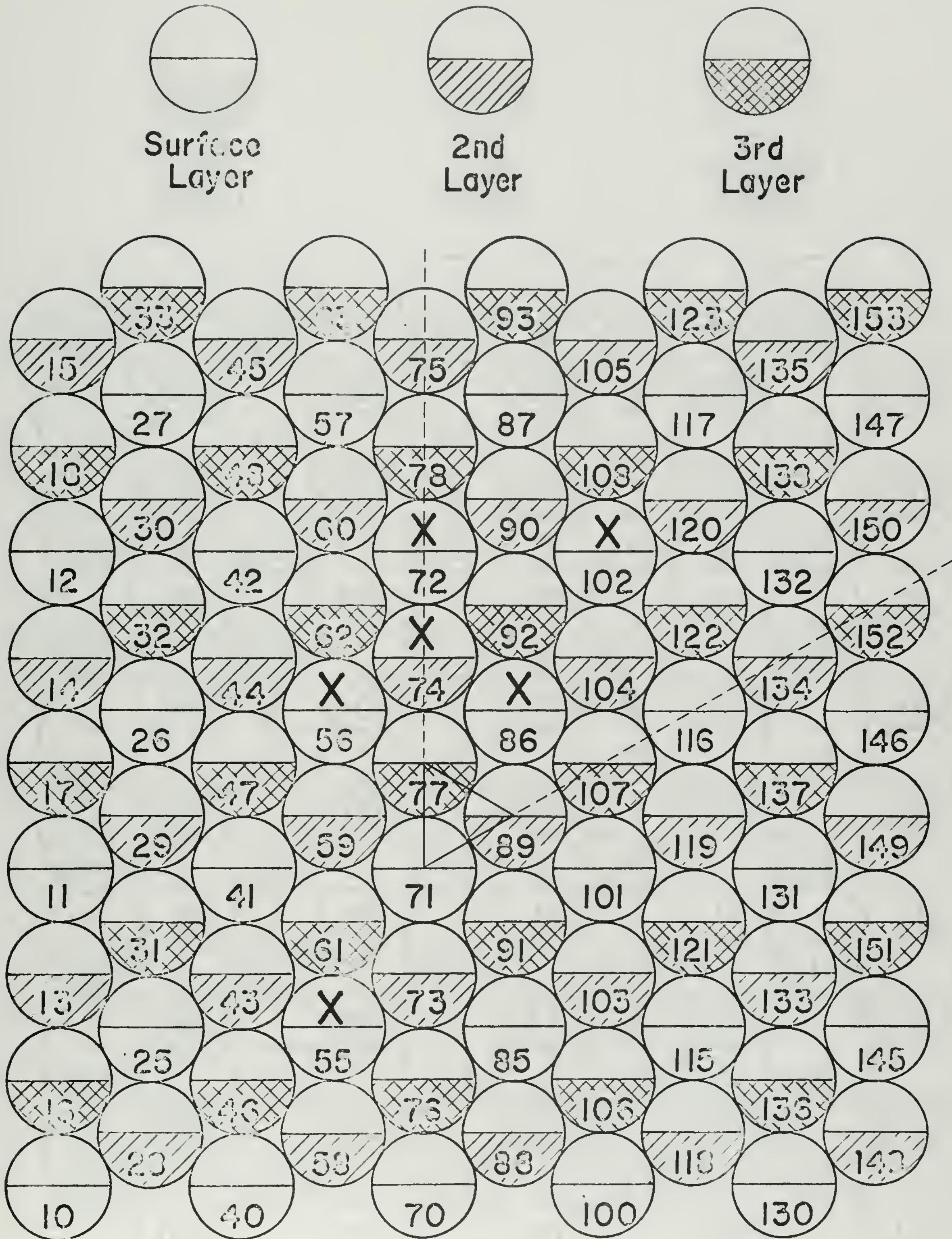

Sputtering frequency-location diagram for (111) surface.
10 keV

Figure 28

(111) Surface

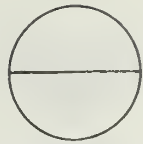

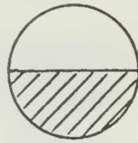

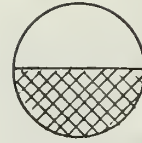

Sputtering frequency-location diagram for (111) surface.
20 keV

Figure 29

(111) Surface

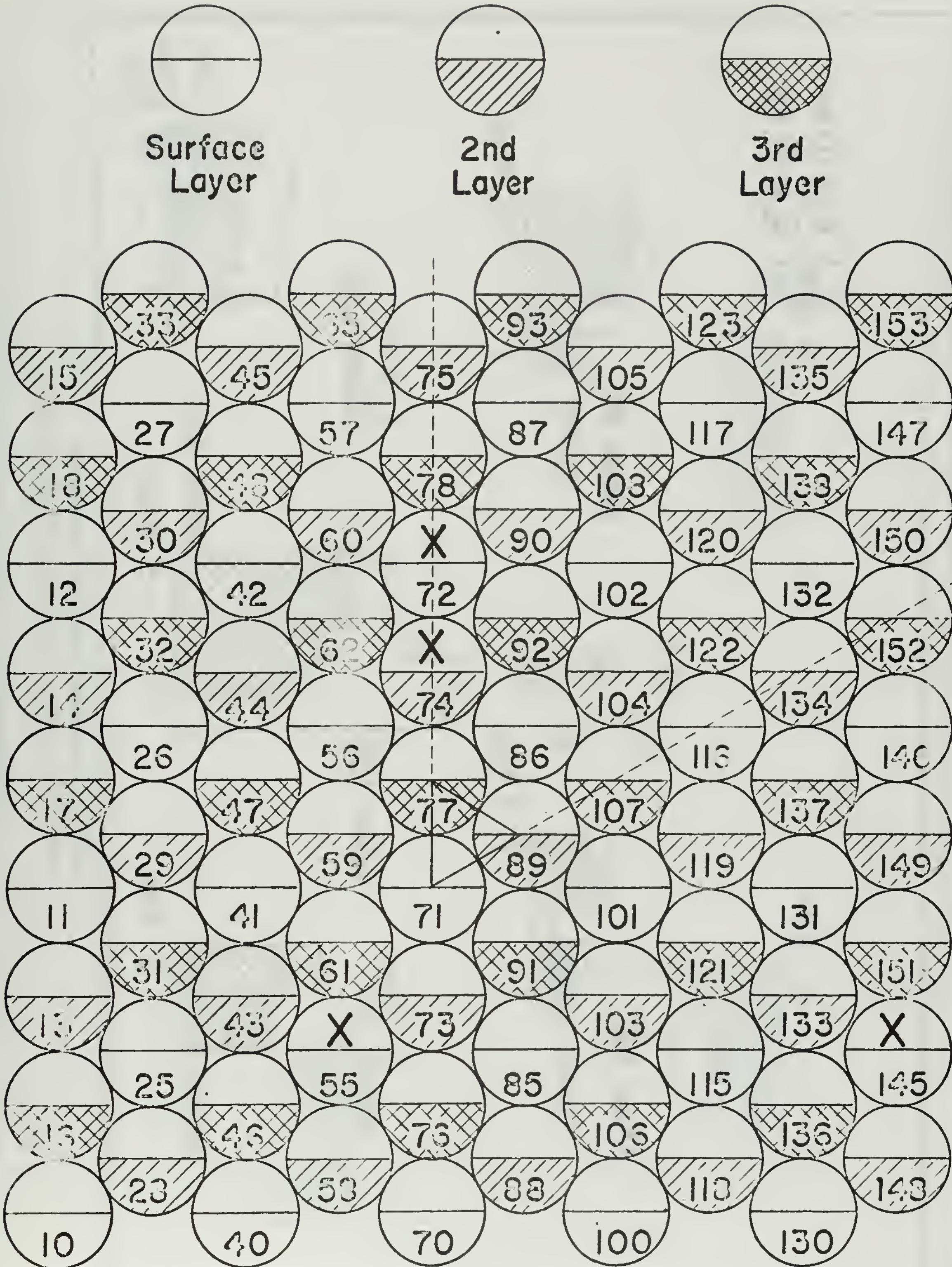

Sputtering frequency-location diagram for (111) surface.
40 keV

Figure 30

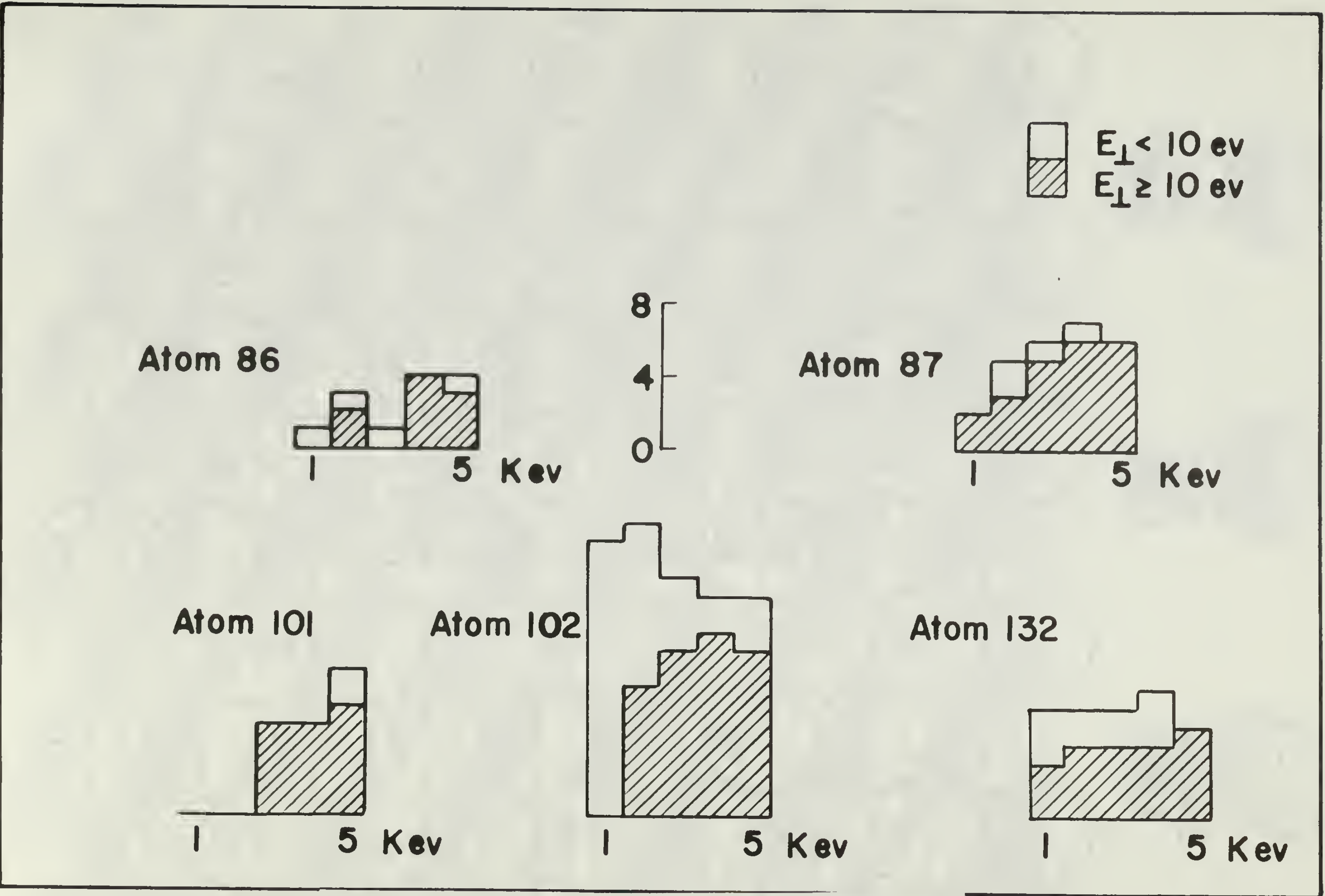

Sputtering profiles of atoms sputtered from (111) surface by Surface Mechanisms.

Figure 31

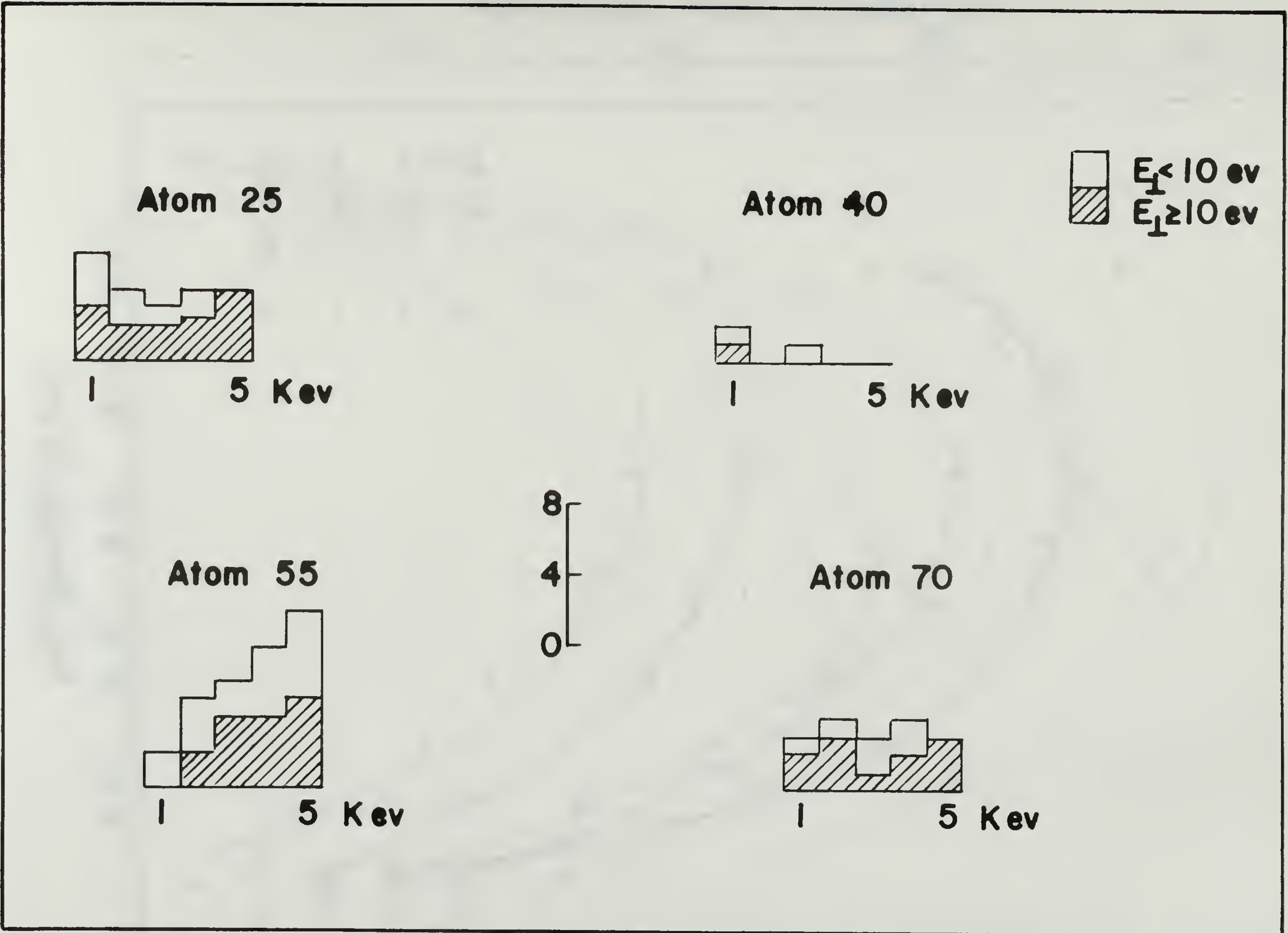

Sputtering profiles of atoms sputtered from (111) surface by Deep Mechanism.

Figure 32

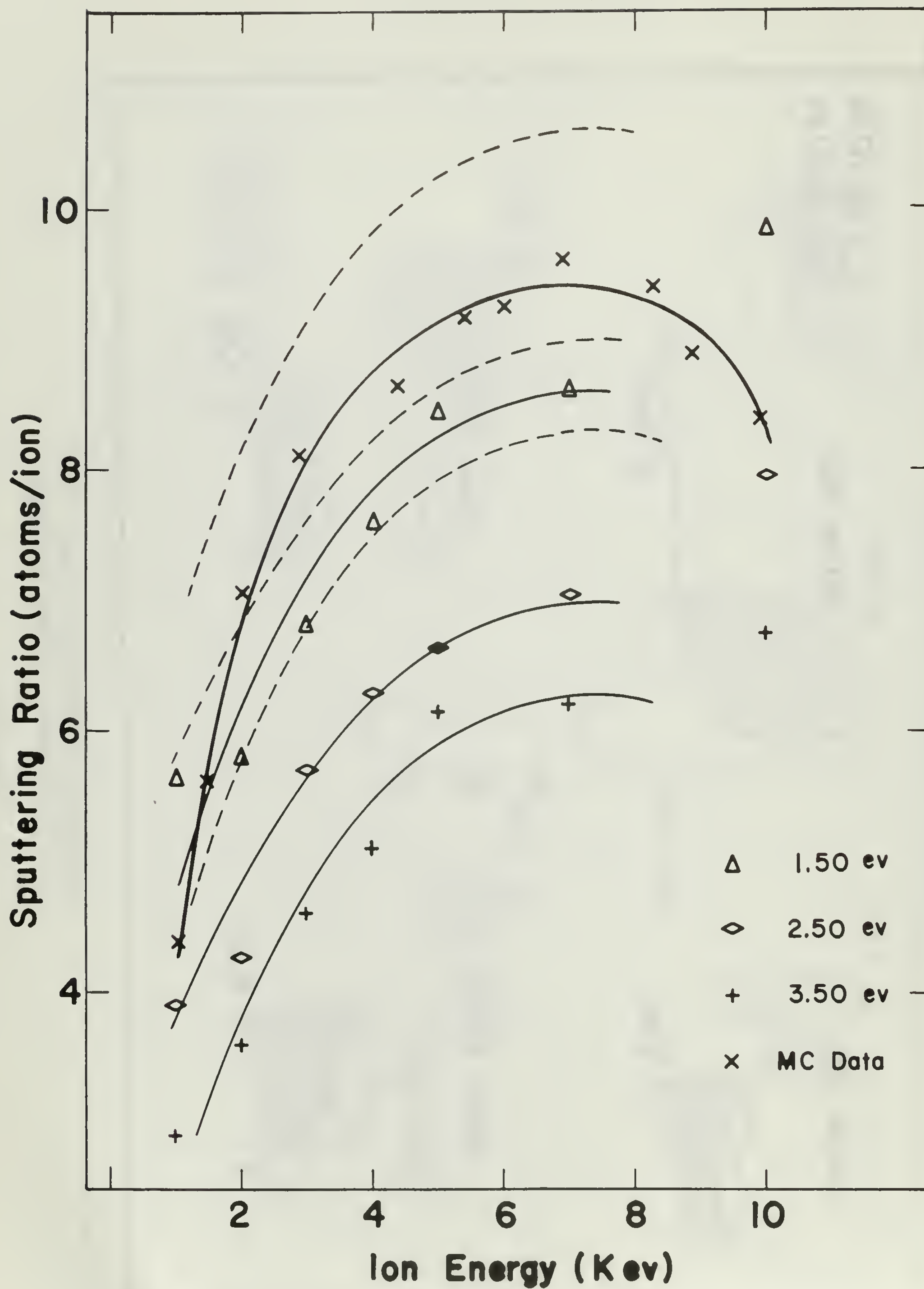

Sputtering Ratio of (111) Surface
Regular Surface

Figure 33a

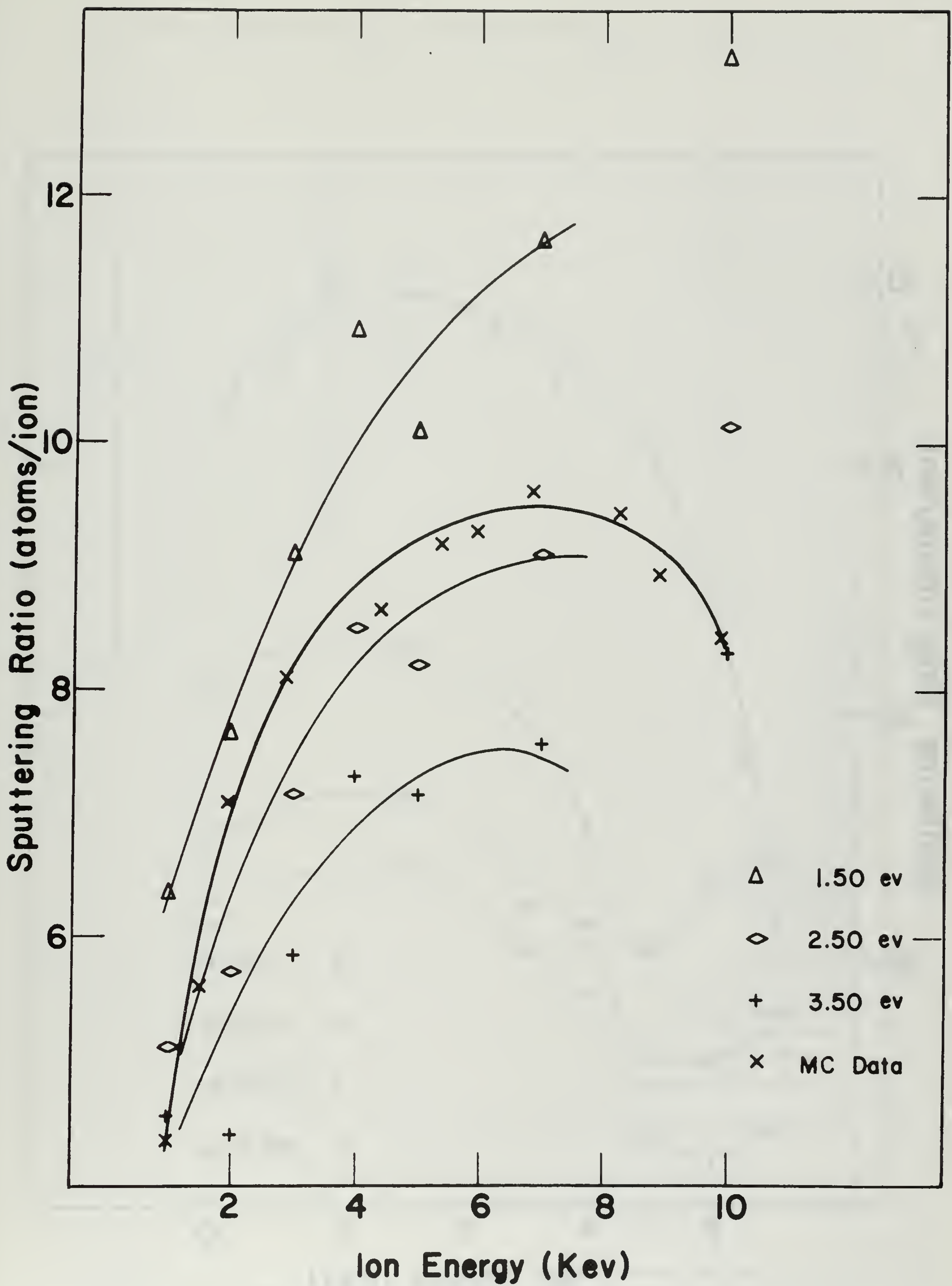

Sputtering Ratio of (111) Surface
Vacancy Surface

Figure 33b

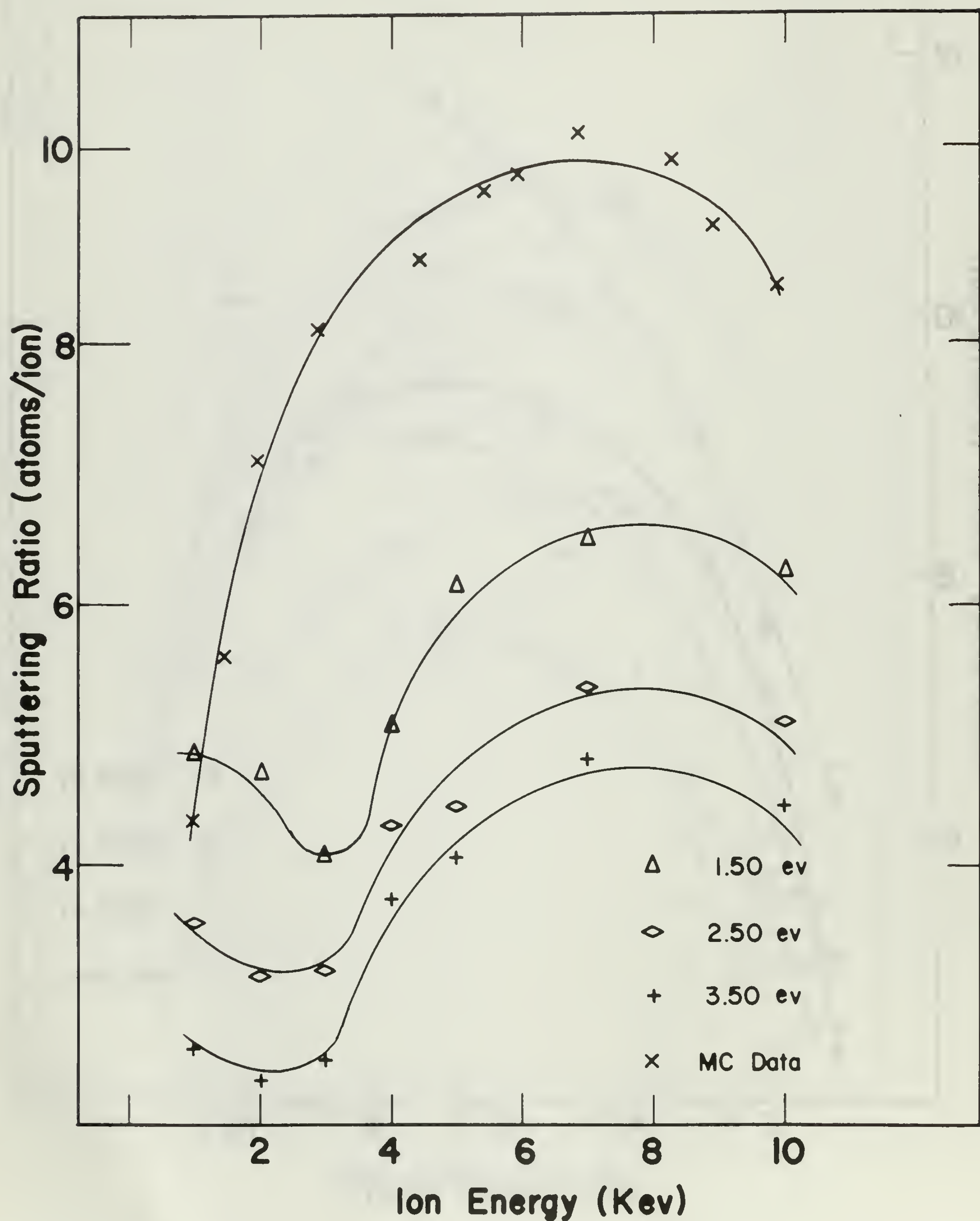

Sputtering Ratio of (111) Surface
Stub Surface

Figure 33c

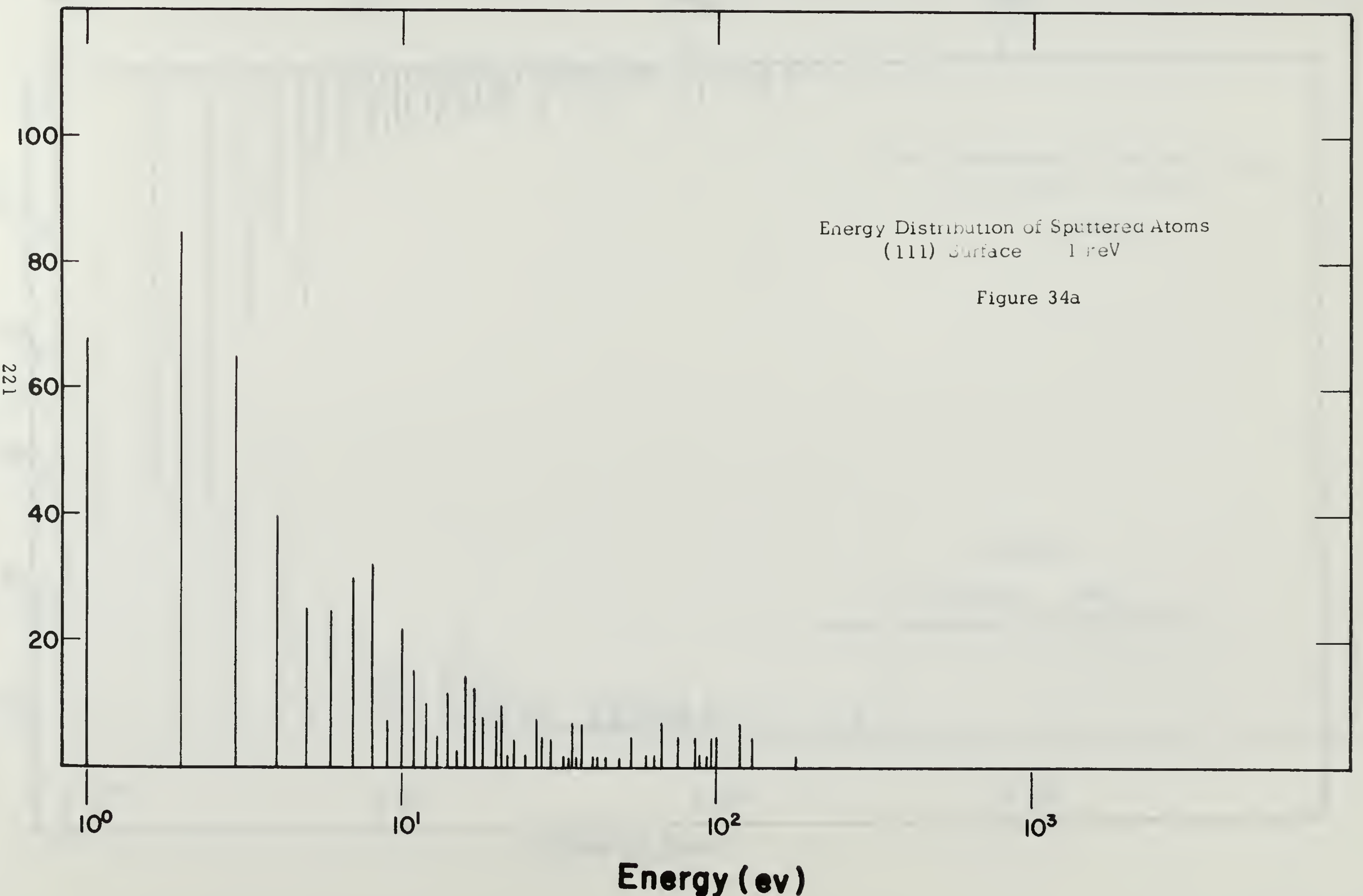

Energy Distribution of Sputtered Atoms
(111) Surface 1 keV

Figure 34a

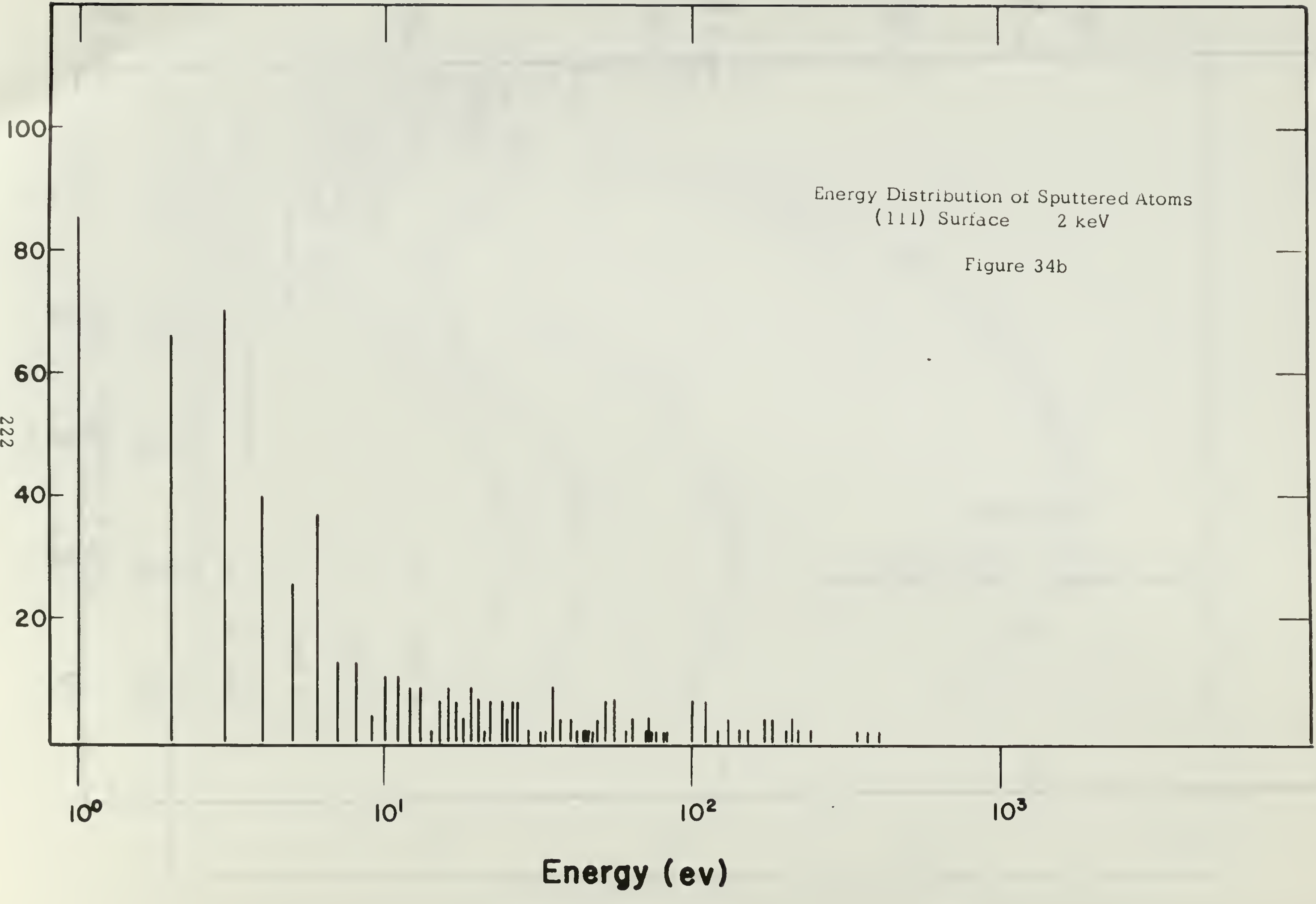

Energy Distribution of Sputtered Atoms
(111) Surface 2 keV

Figure 34b

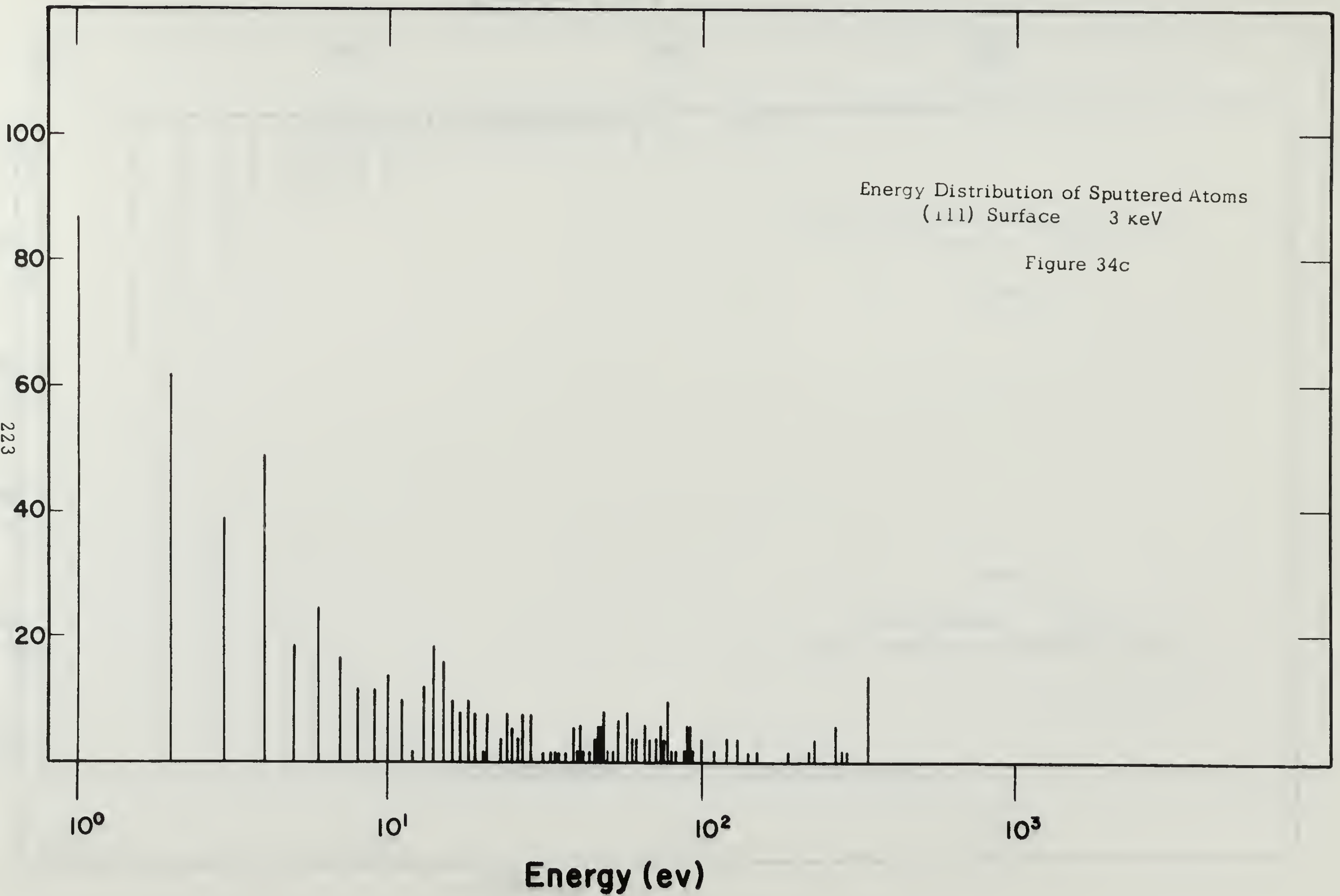

Energy Distribution of Sputtered Atoms
(111) Surface 3 keV

Figure 34c

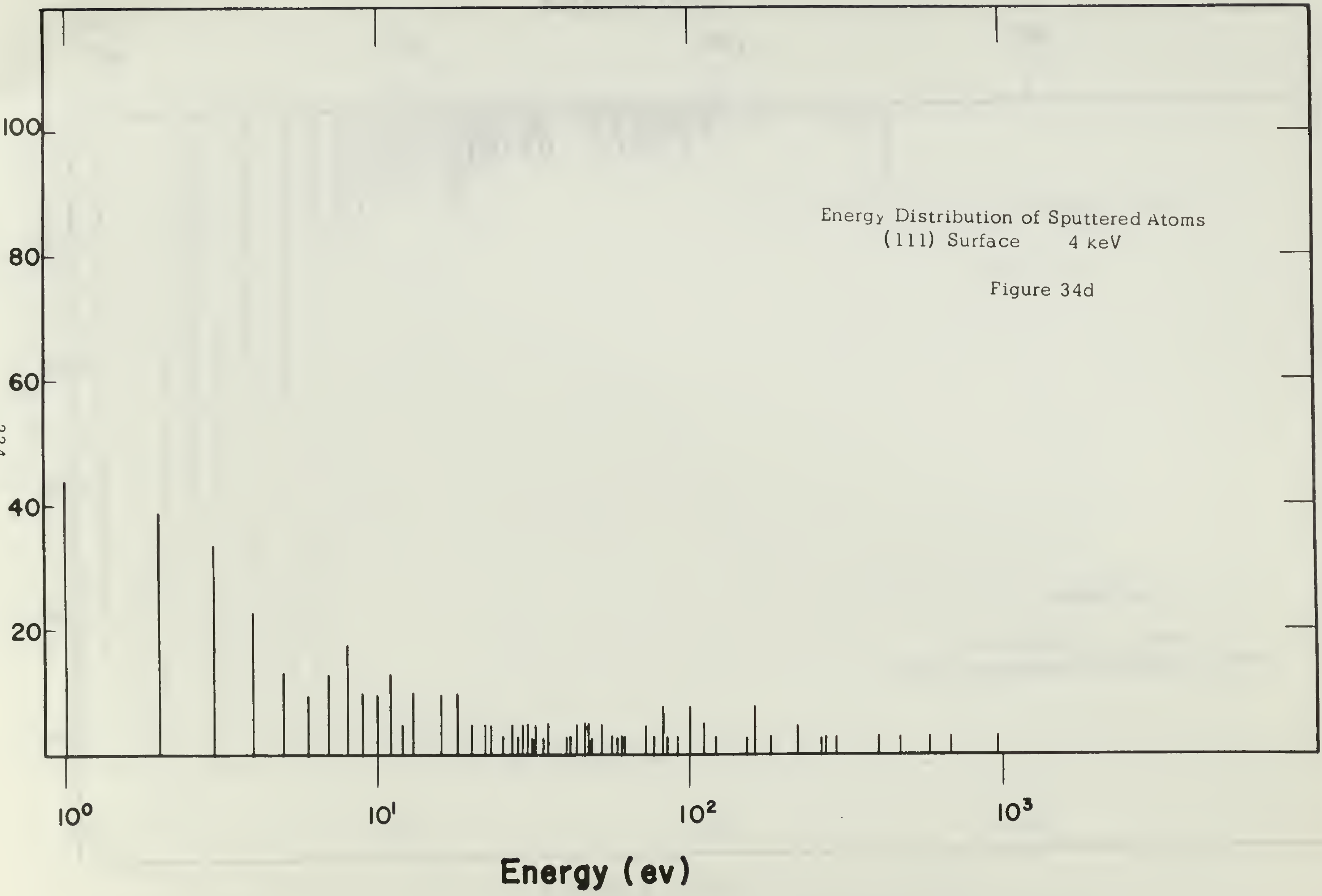
Energy Distribution of Sputtered Atoms
(111) Surface 4 keV
Figure 34d
100
80
60
40
20
10^0
10^1
10^2
10^3
Energy (ev)

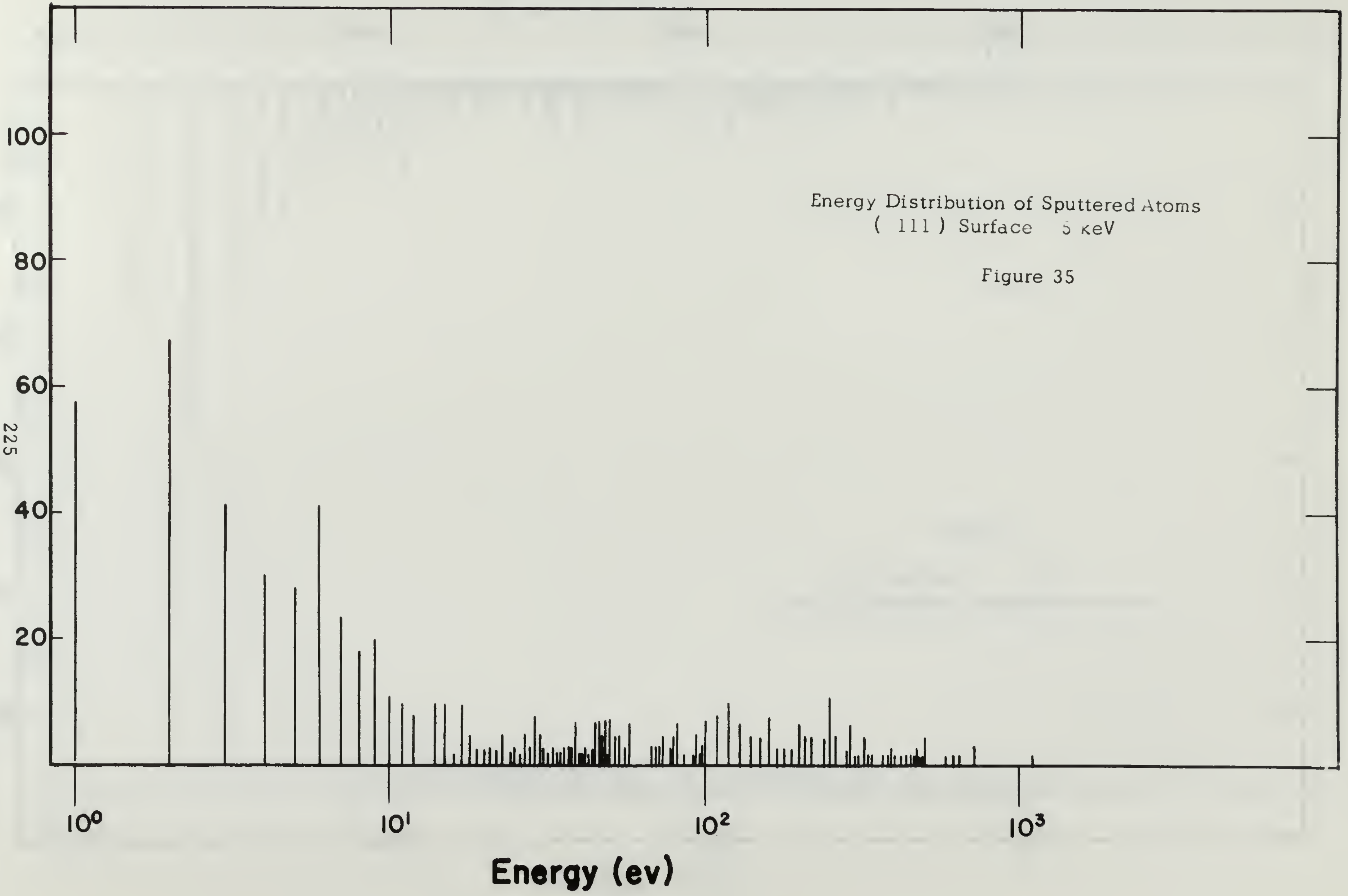

Energy Distribution of Sputtered Atoms
(111) Surface 5 keV

Figure 35

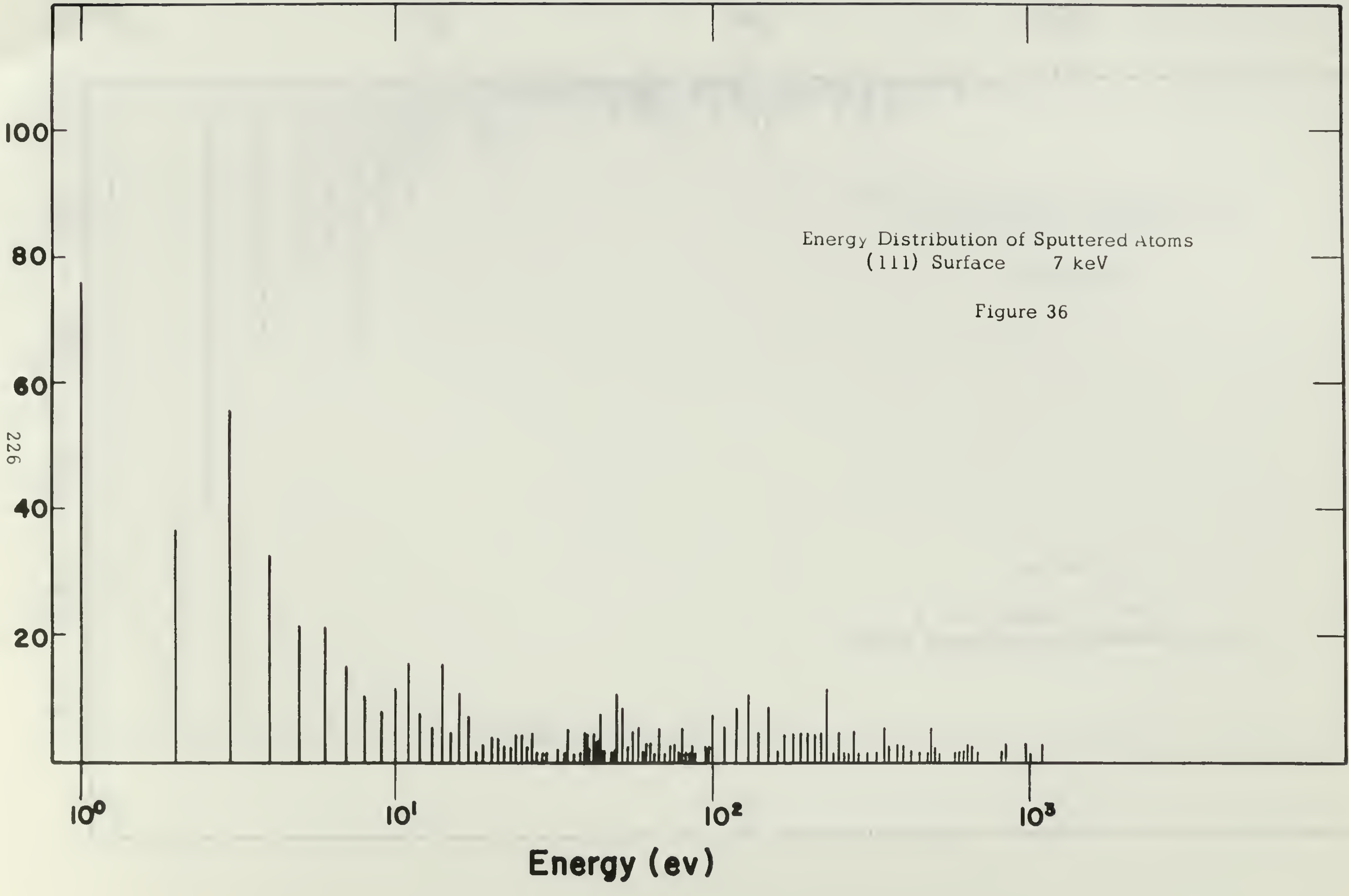

Energy Distribution of Sputtered Atoms
(111) Surface 7 keV

Figure 36

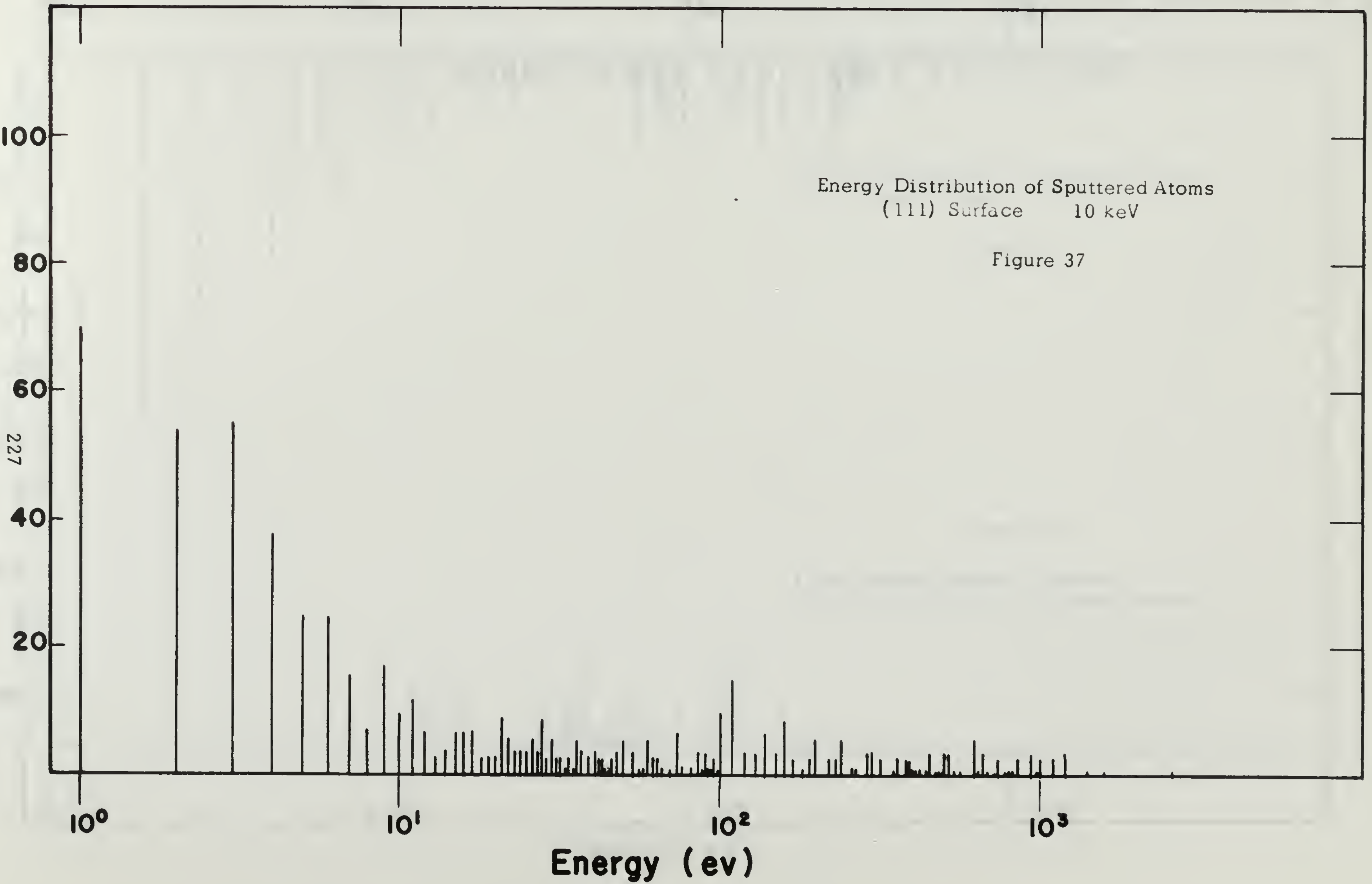

Energy Distribution of Sputtered Atoms
(111) Surface 10 keV

Figure 37

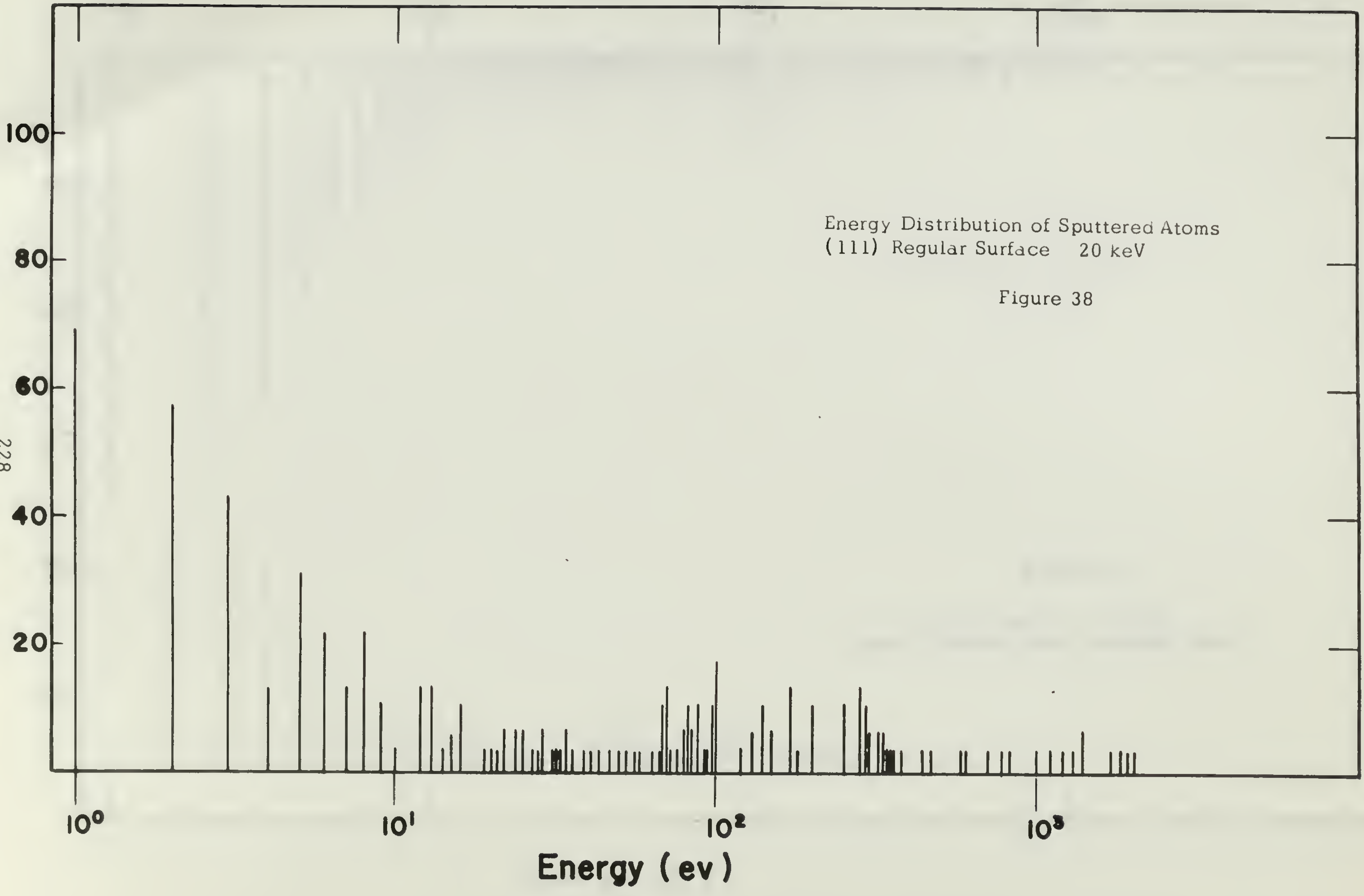

Energy Distribution of Sputtered Atoms
(111) Regular Surface 20 keV

Figure 38

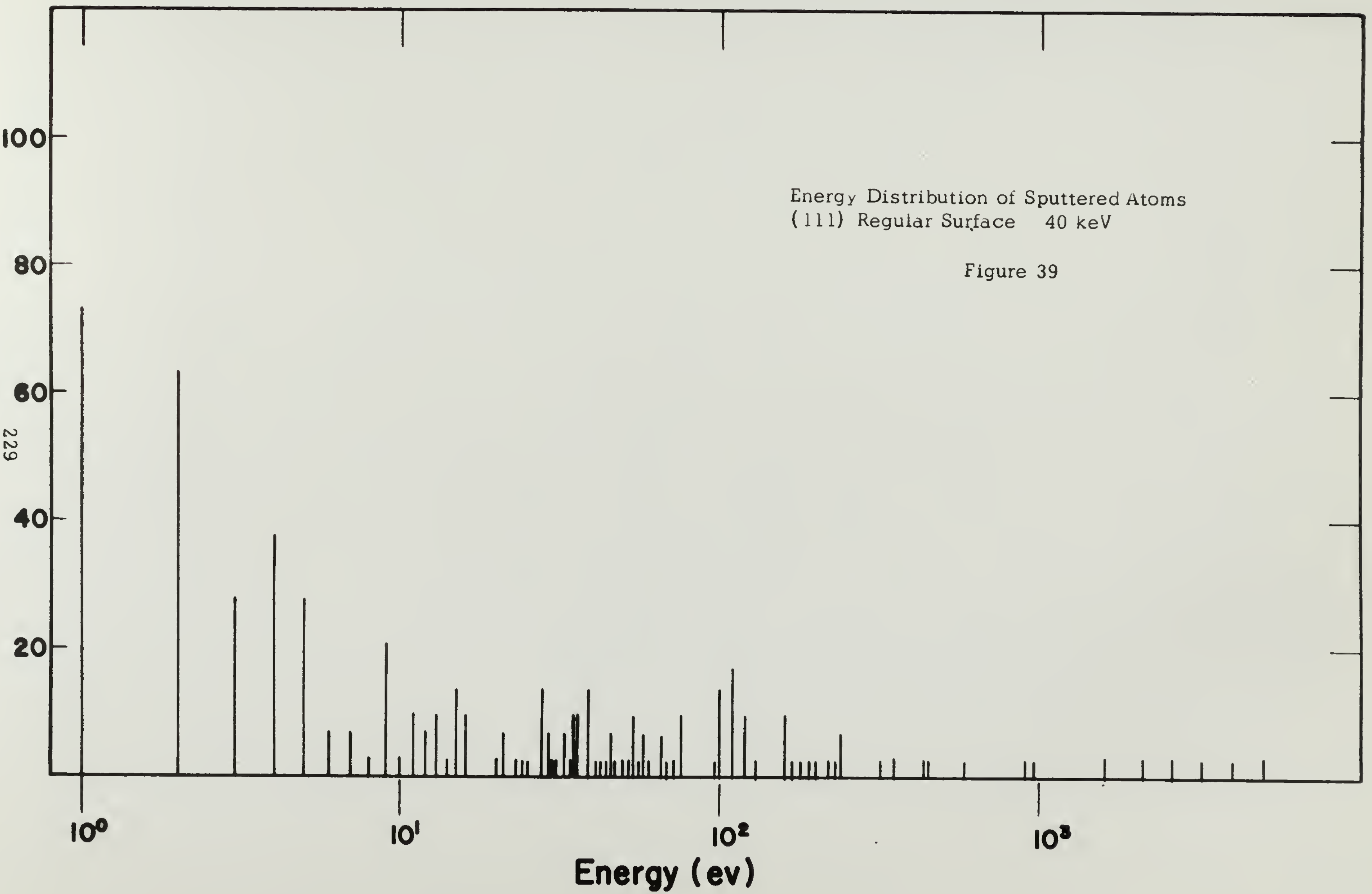

Figure 39

Argon Copper Sputtering
(100) Surface

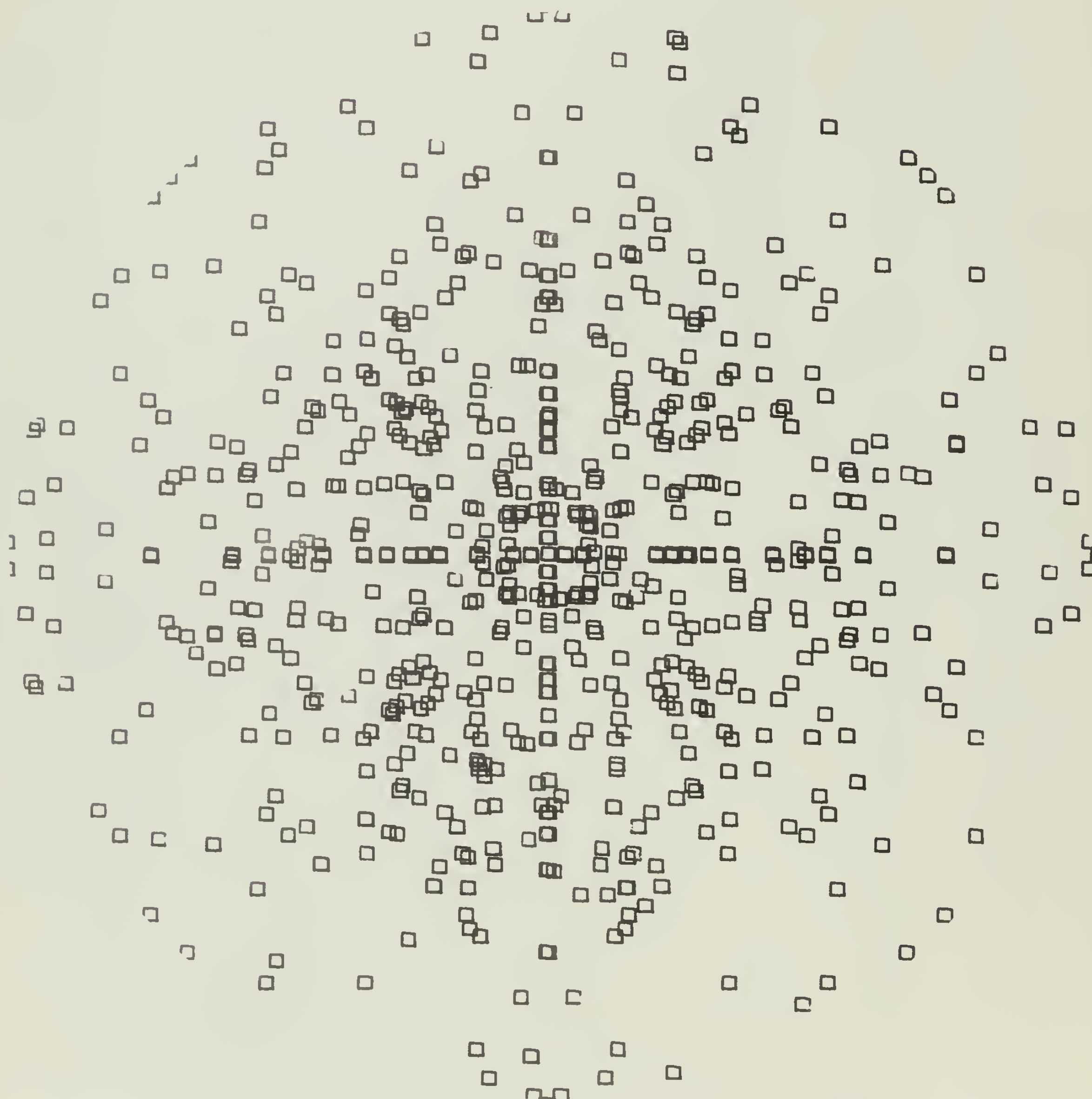

1.0 K ev Bombardment Energy
3.50 ev Binding Energy

Figure 40a

Argon Copper Sputtering
(100) Surface

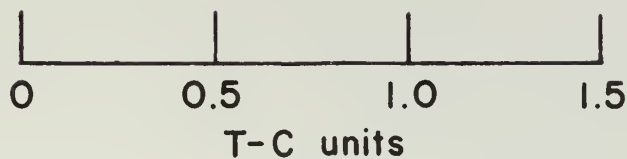

1.0 K ev Bombardment Energy
3.50 ev Binding Energy

Figure 40b

Argon Copper Sputtering
(100) Surface

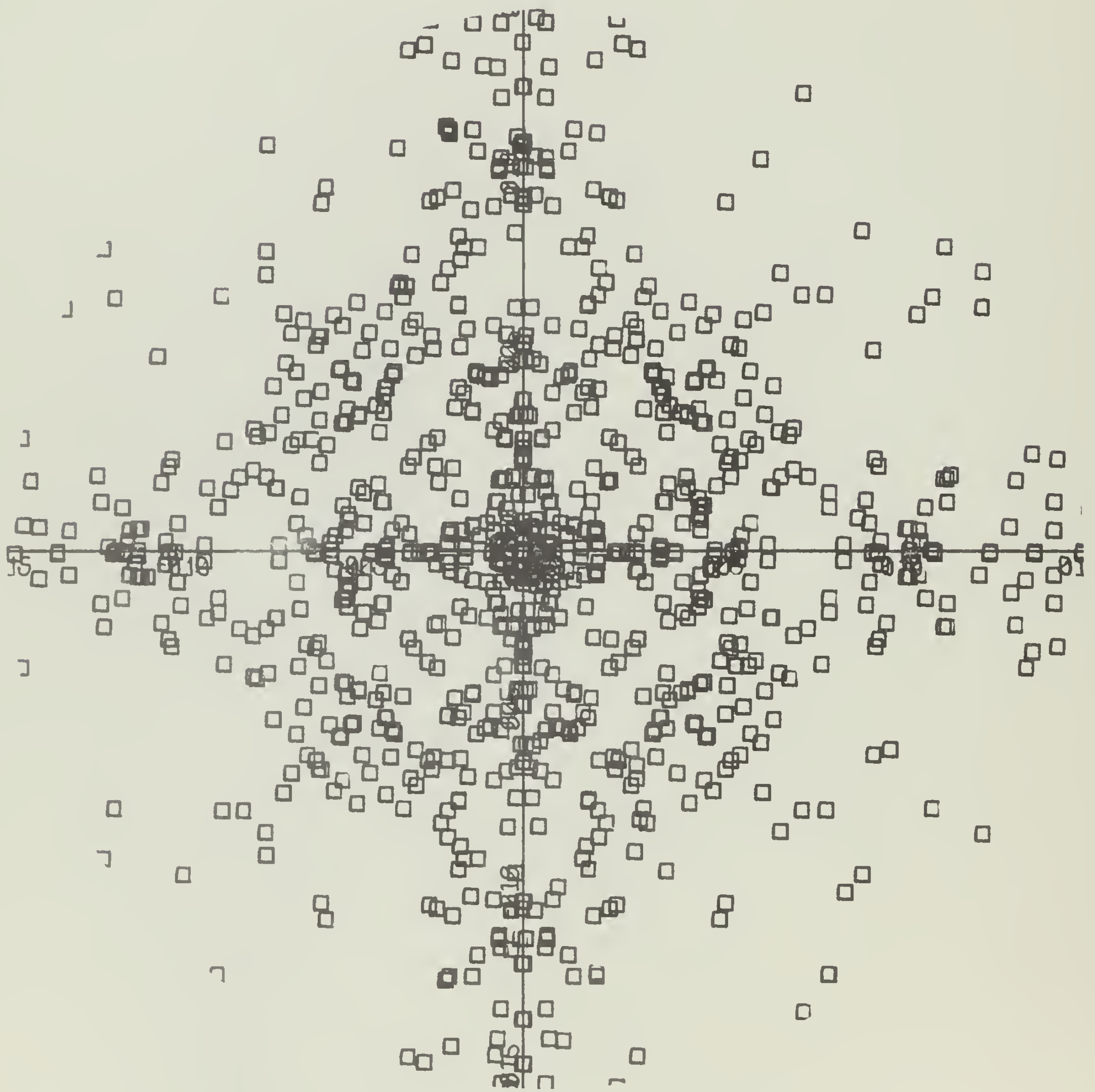

3.0 K ev Bombardment Energy
3.00 ev Binding Energy

Figure 41a

Argon Copper Sputtering
(100) Surface

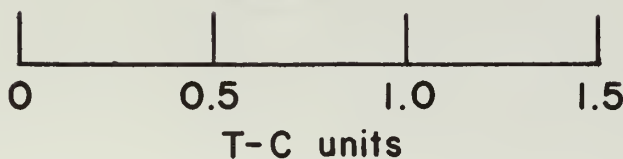

3.0 Kev Bombardment Energy
3.00 ev Binding Energy

Figure 41b

Argon Copper Sputtering
(100) Surface

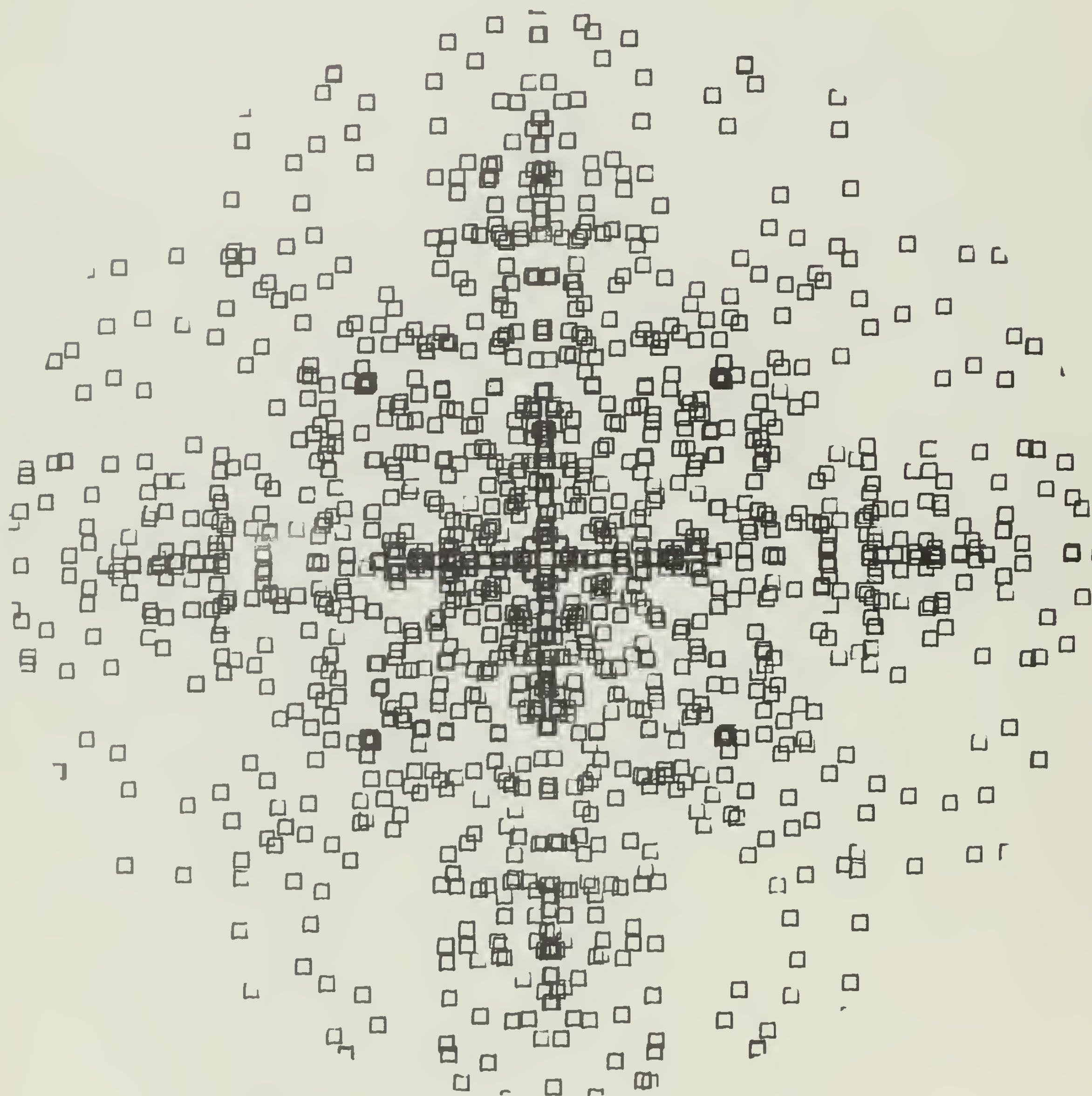

5.0 K ev Bombardment Energy
2.00 ev Binding Energy

Figure 42a

Argon Copper Sputtering

(100) Surface

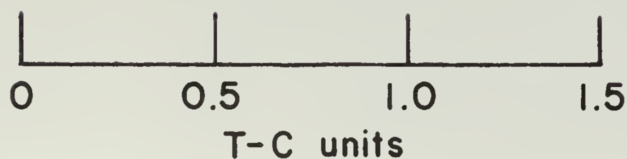

5.0 K ev Bombardment Energy

2.00 ev Binding Energy

Figure 42b

Argon Copper Sputtering
(100) Surface

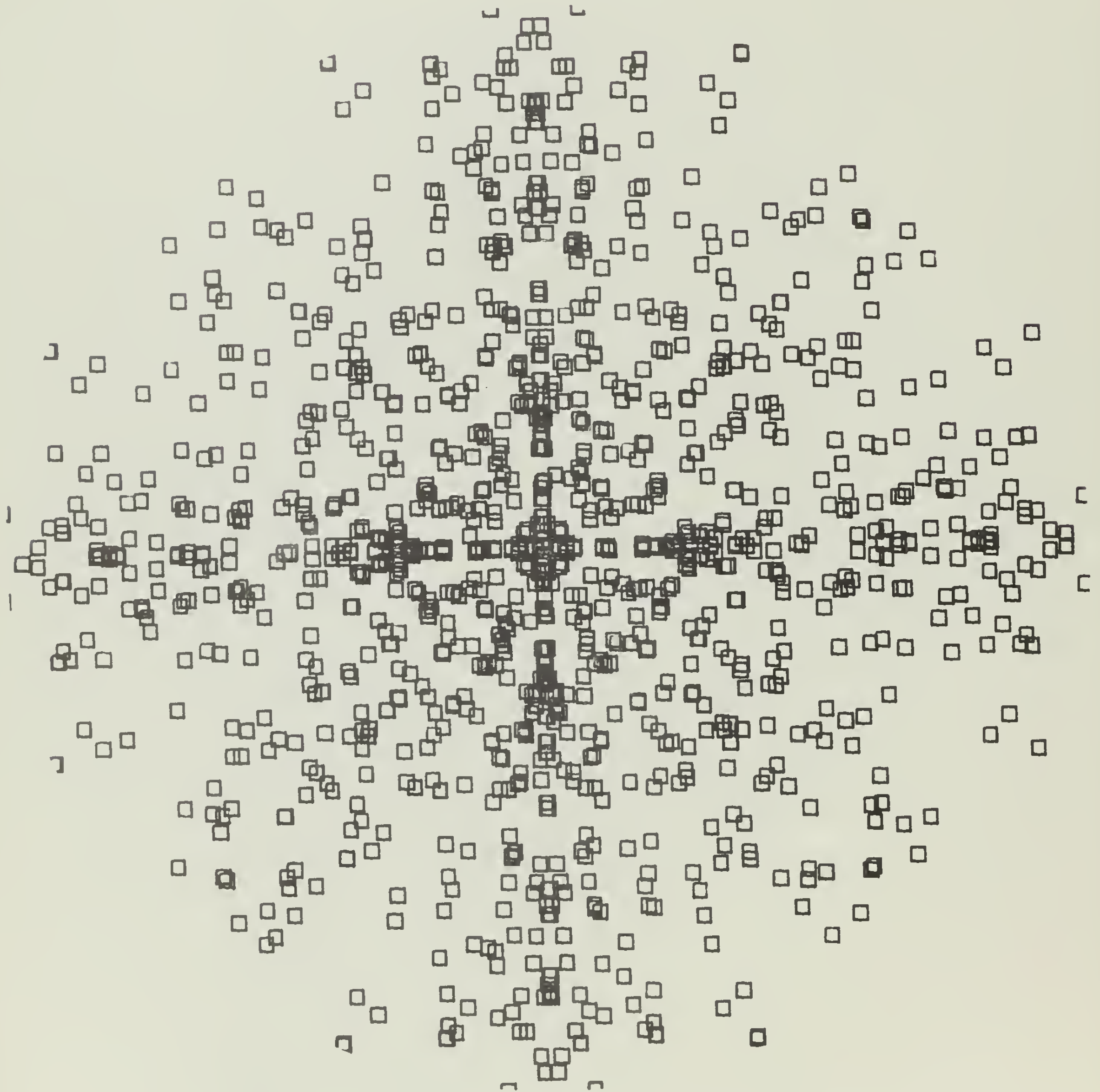

5.0 K ev Bombardment Energy
3.00 ev Binding Energy

Figure 43a

Argon Copper Sputtering

(100) Surface

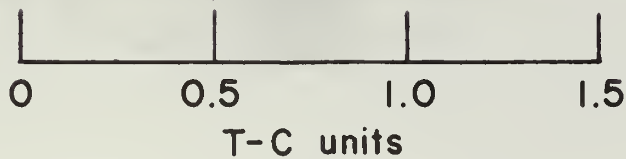

5.0 Kev Bombardment Energy

3.00 ev Binding Energy

Figure 43b

Argon Copper Sputtering
(100) Surface

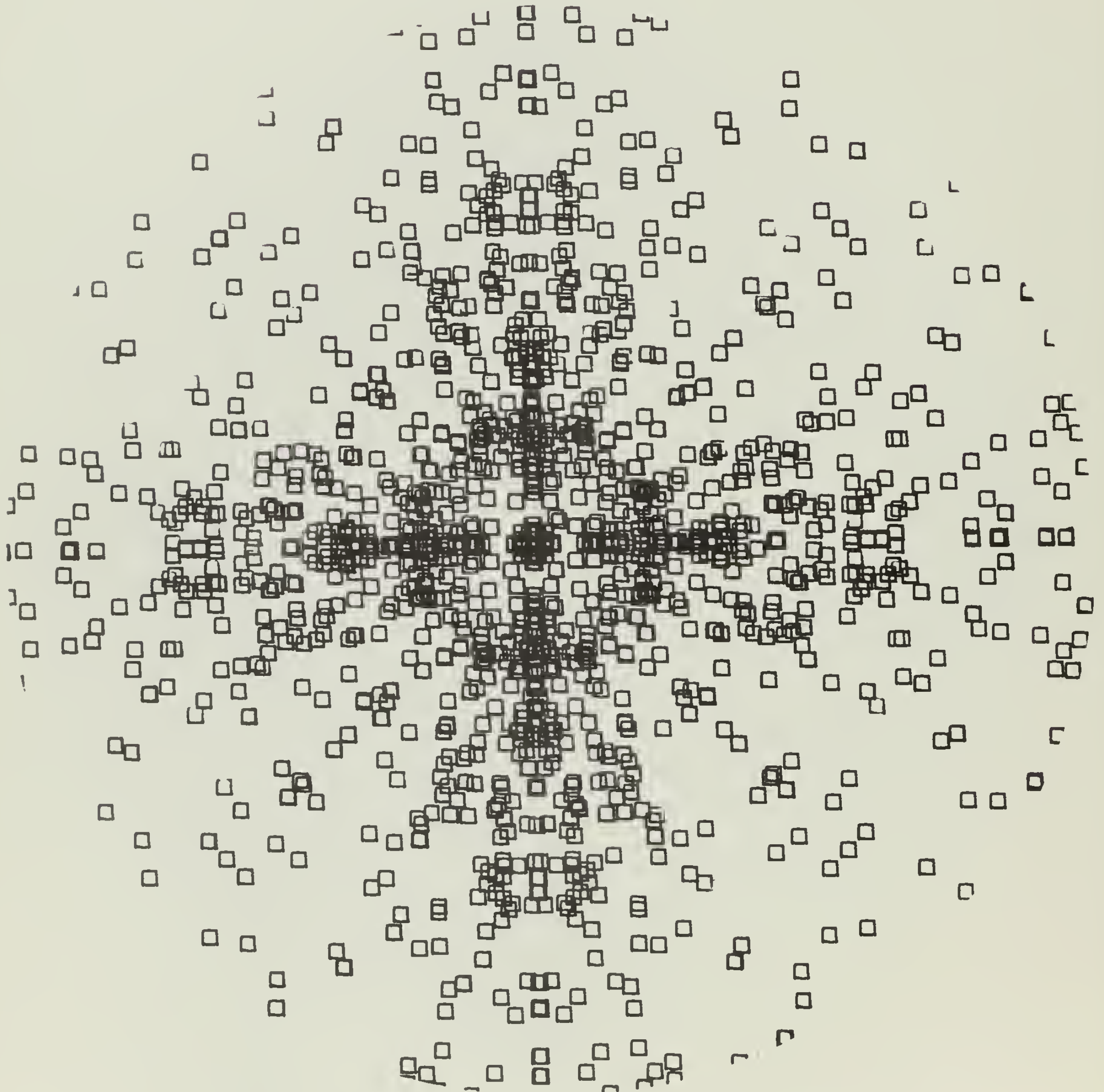

7.0 K ev Bombardment Energy
1.50 ev Binding Energy

Figure 44a

Argon Copper Sputtering
(100) Surface

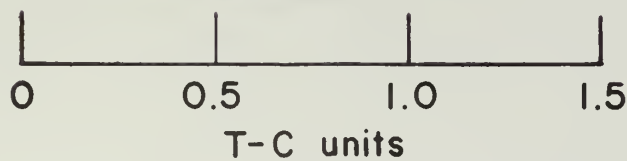

7.0 K ev Bombardment Energy
1.50 ev Binding Energy

Figure 44b

Argon Copper Sputtering
(100) Surface

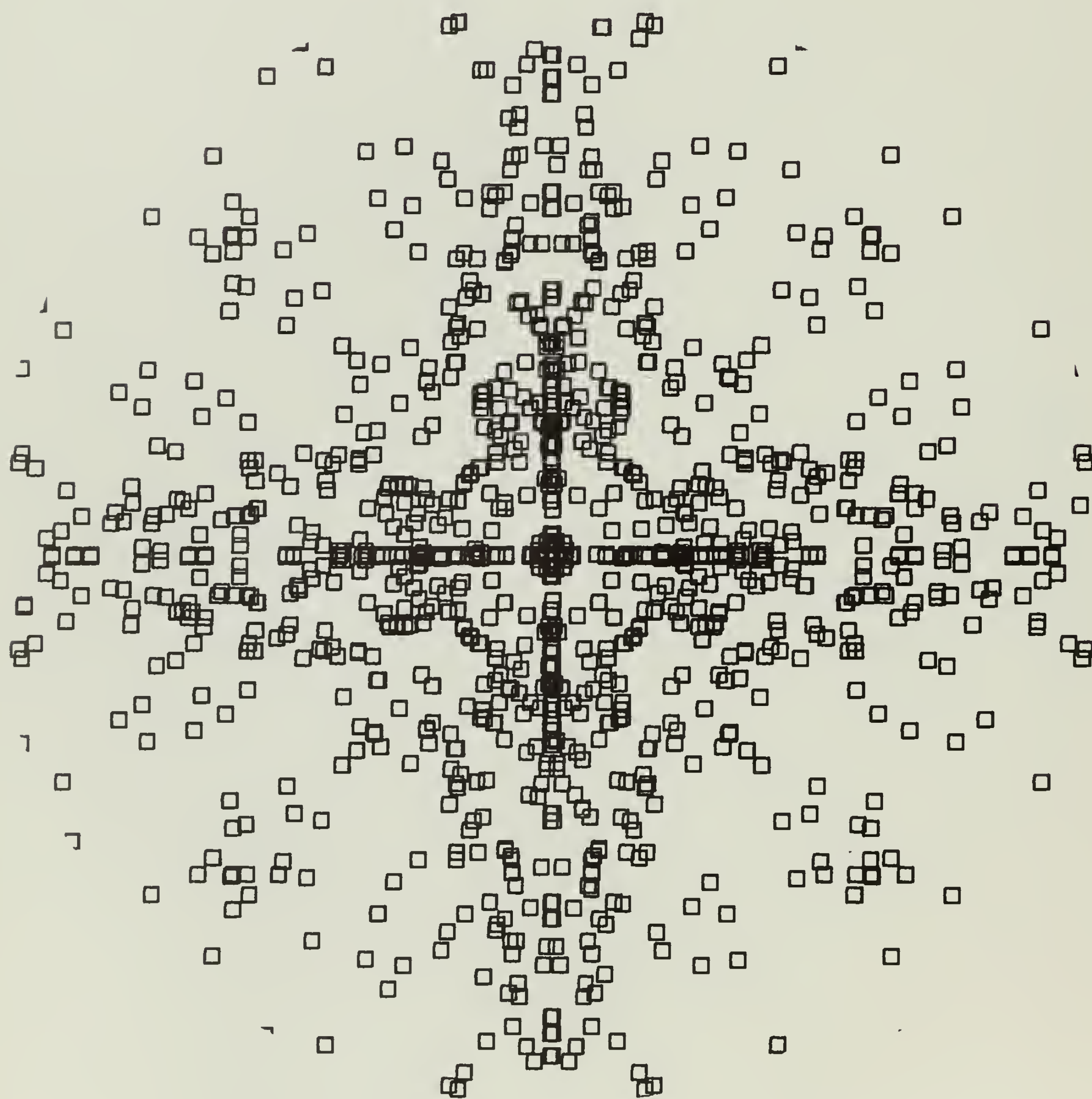

7.0 K ev Bombardment Energy
3.00 ev Binding Energy

Figure 45a

Argon Copper Sputtering
(100) Surface

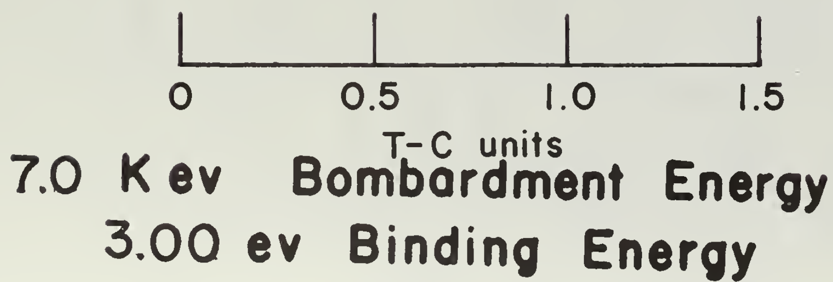

Figure 45b

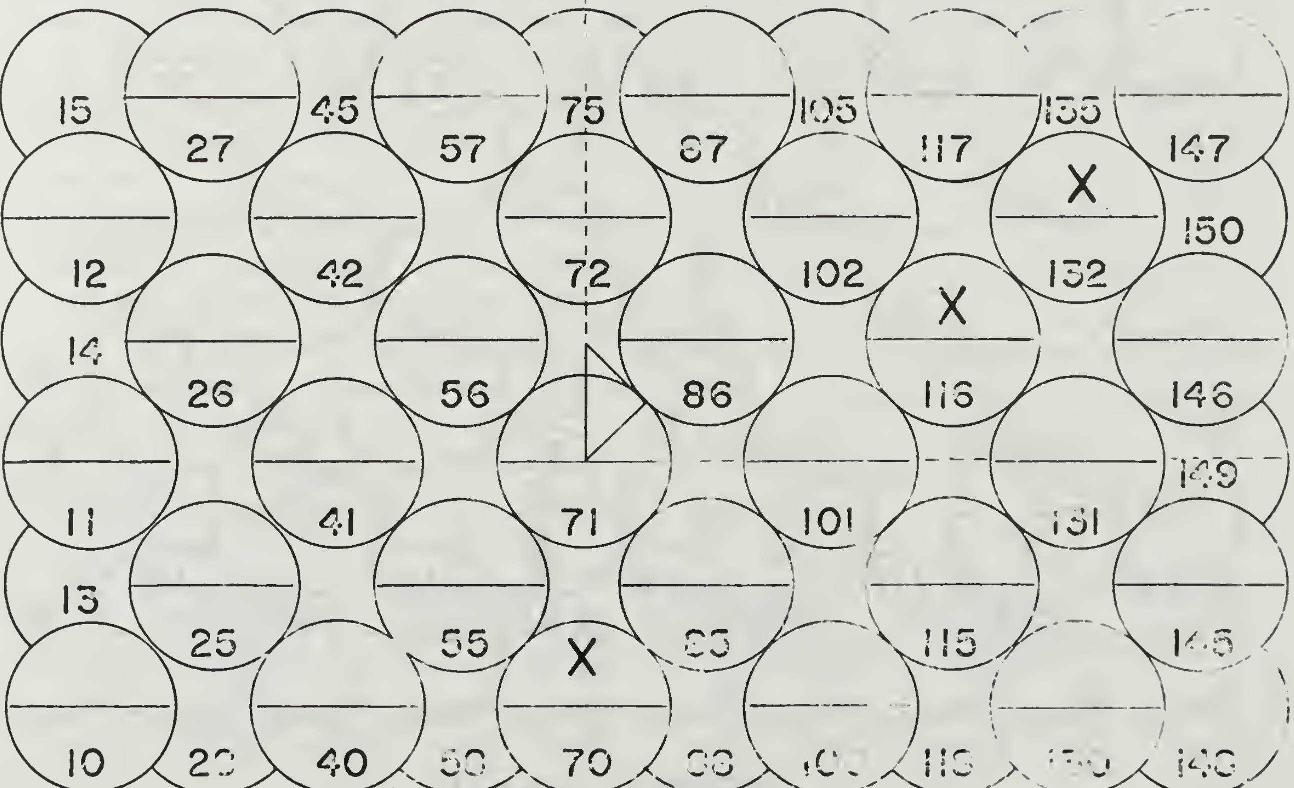

Sputte[illegible] c[illegible]cation diagra[illegible]
for (100) surface
1 keV

Figure 46

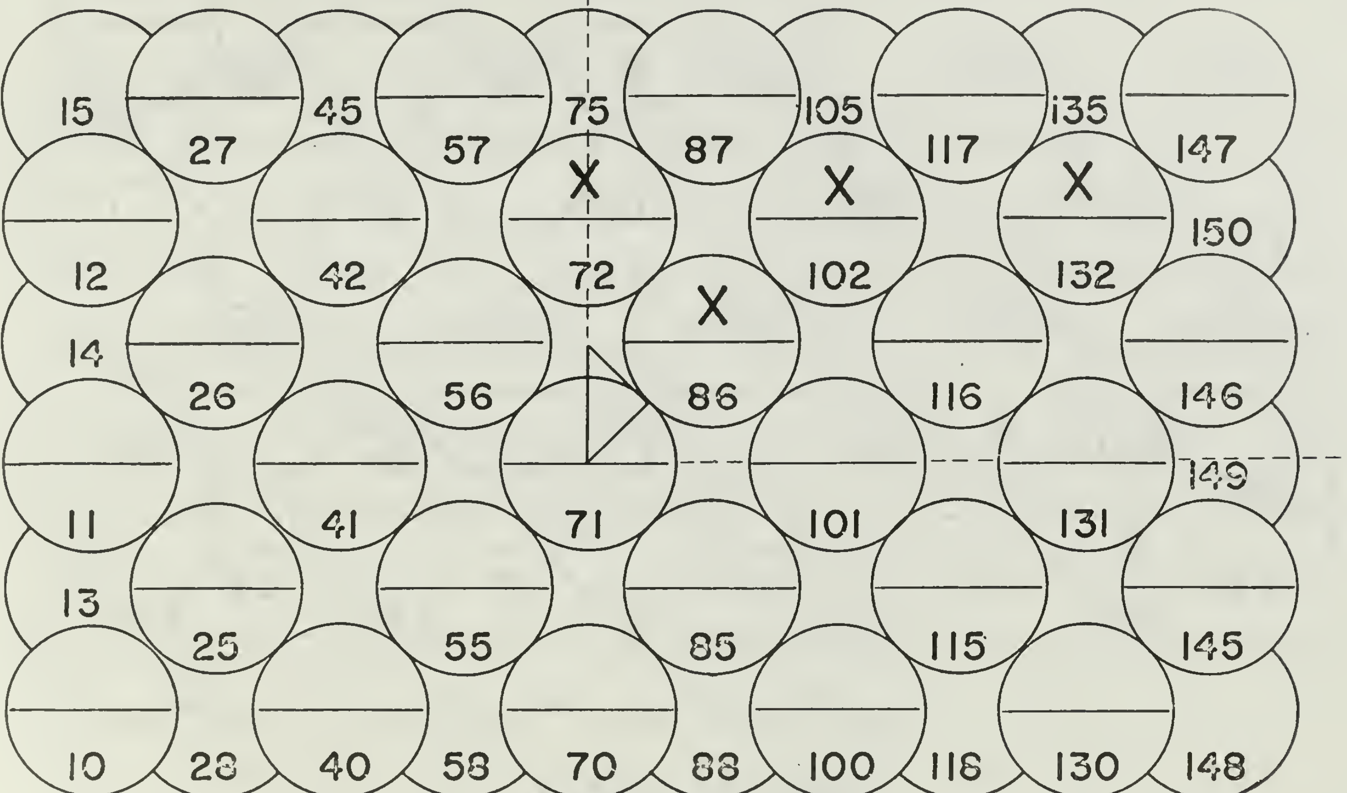

Sputtering frequency-location diagram
for (100) surface.
3 keV

Figure 47

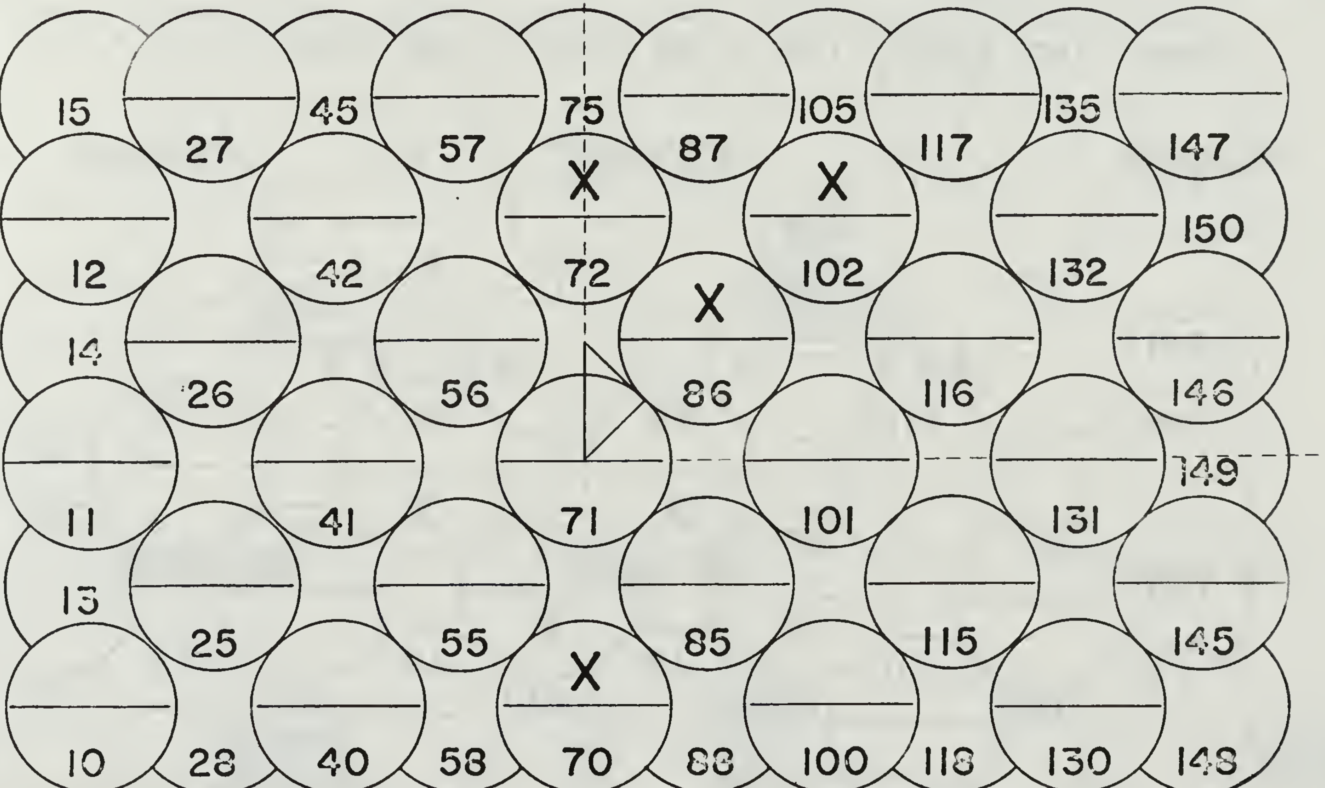

Sputtering frequency-location diagram
for (100) surface.
5 keV

Figure 48

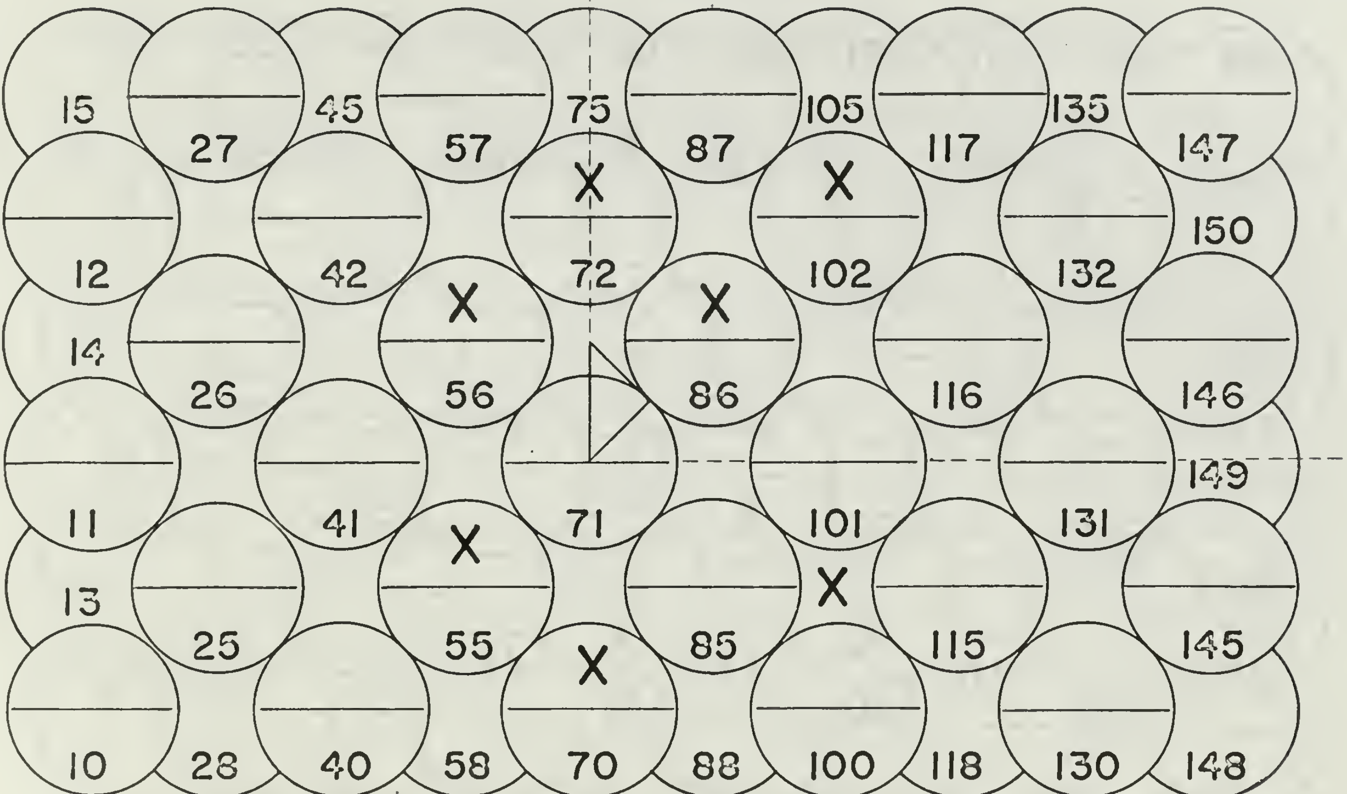

Sputtering frequency-location diagram
for (100) surface.
7 keV

Figure 49

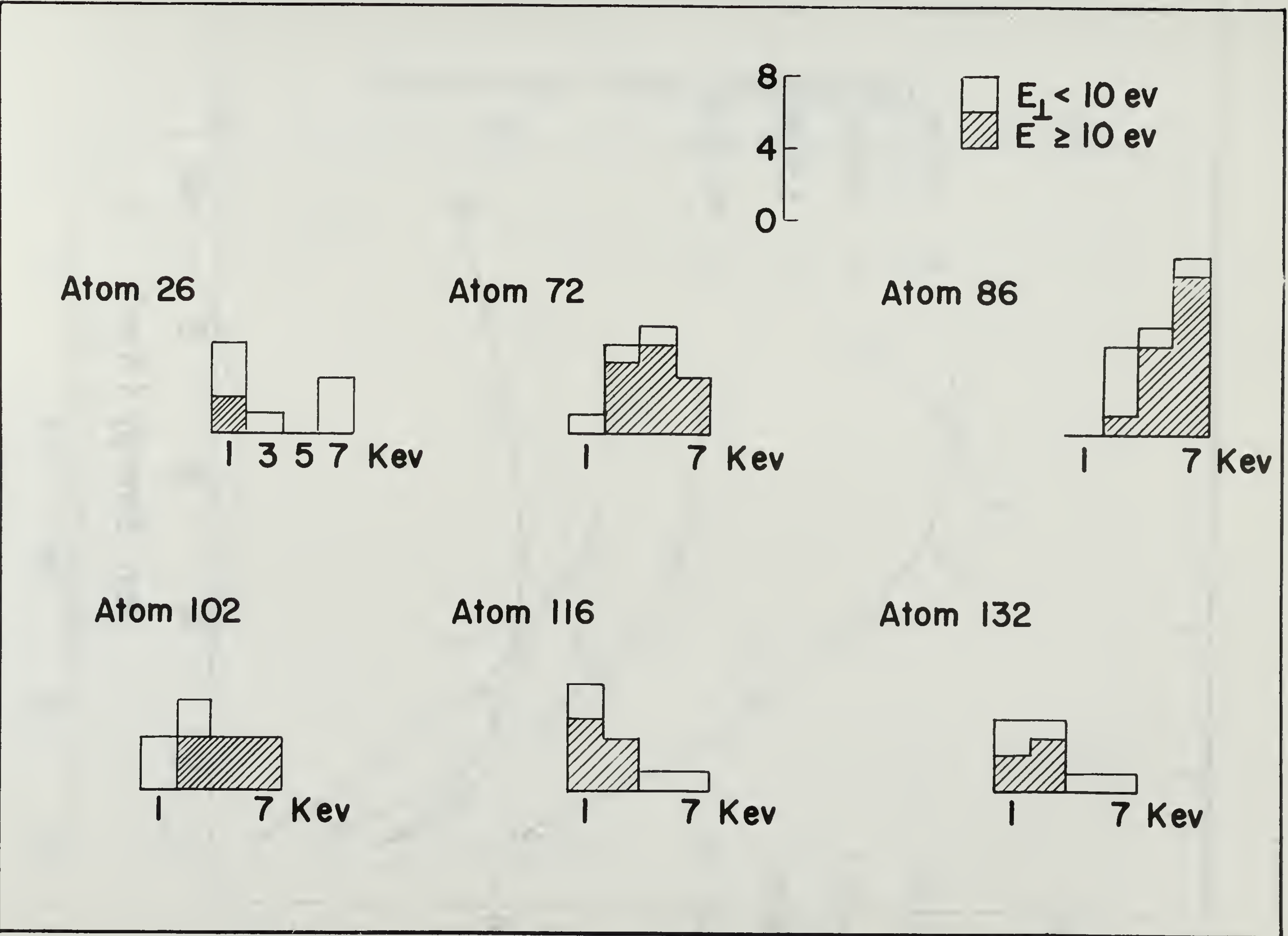

Sputtering profiles of atoms sputtered from (100) surface.

Figure 50

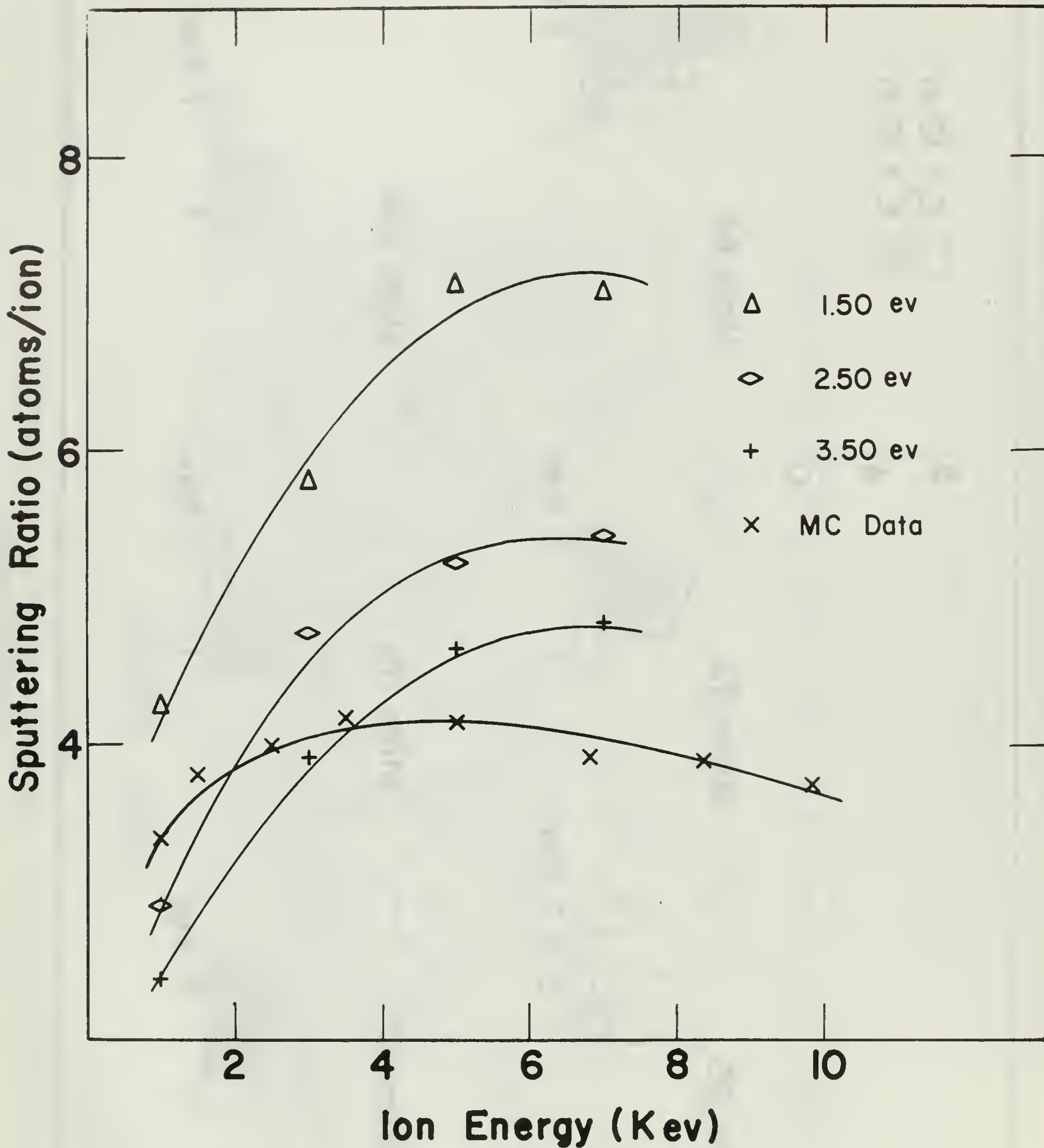

Sputtering Ratio of (100) Surface
Regular Surface

Figure 51a

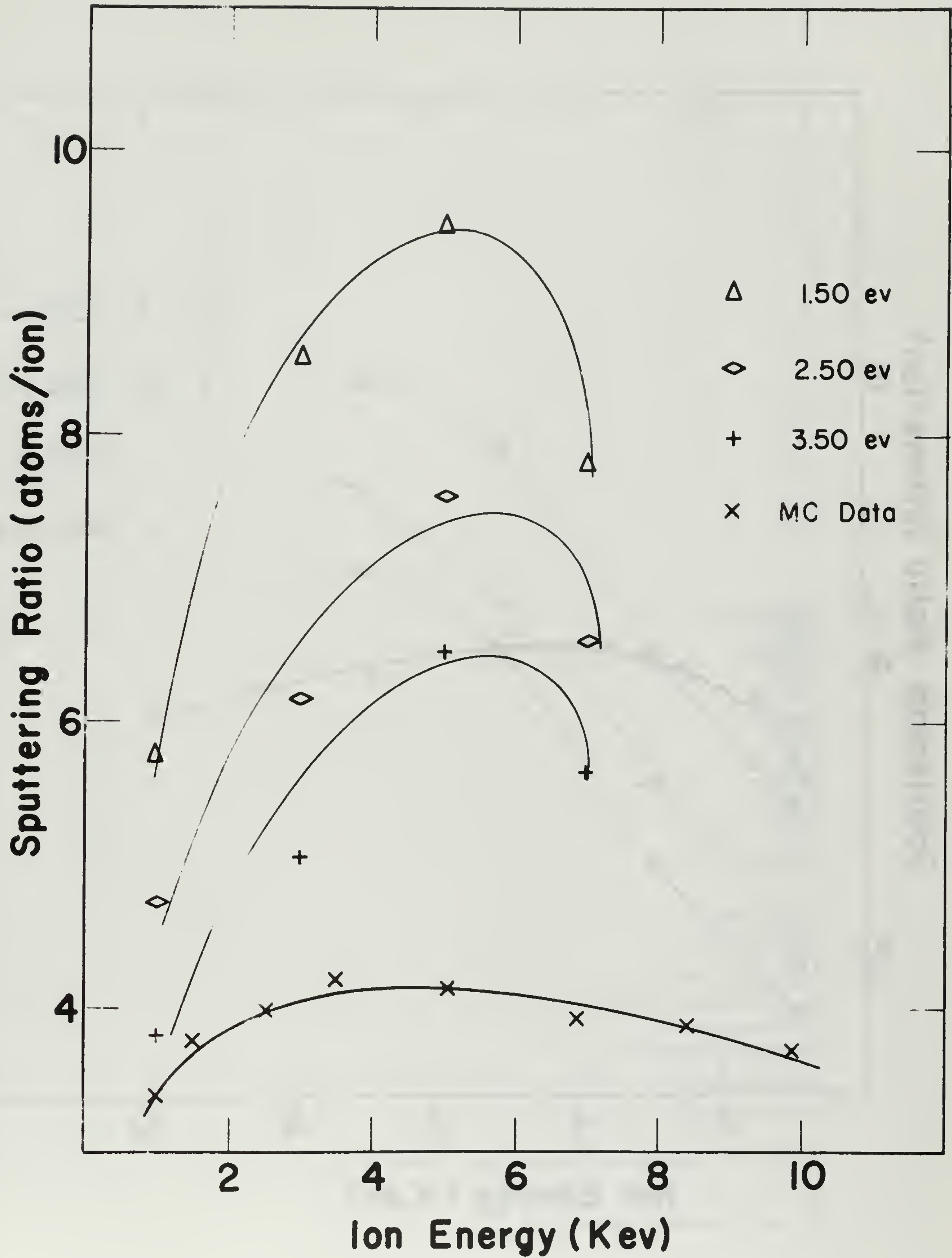

Sputtering Ratio of (100) Surface
Vacancy Surface

Figure 51b

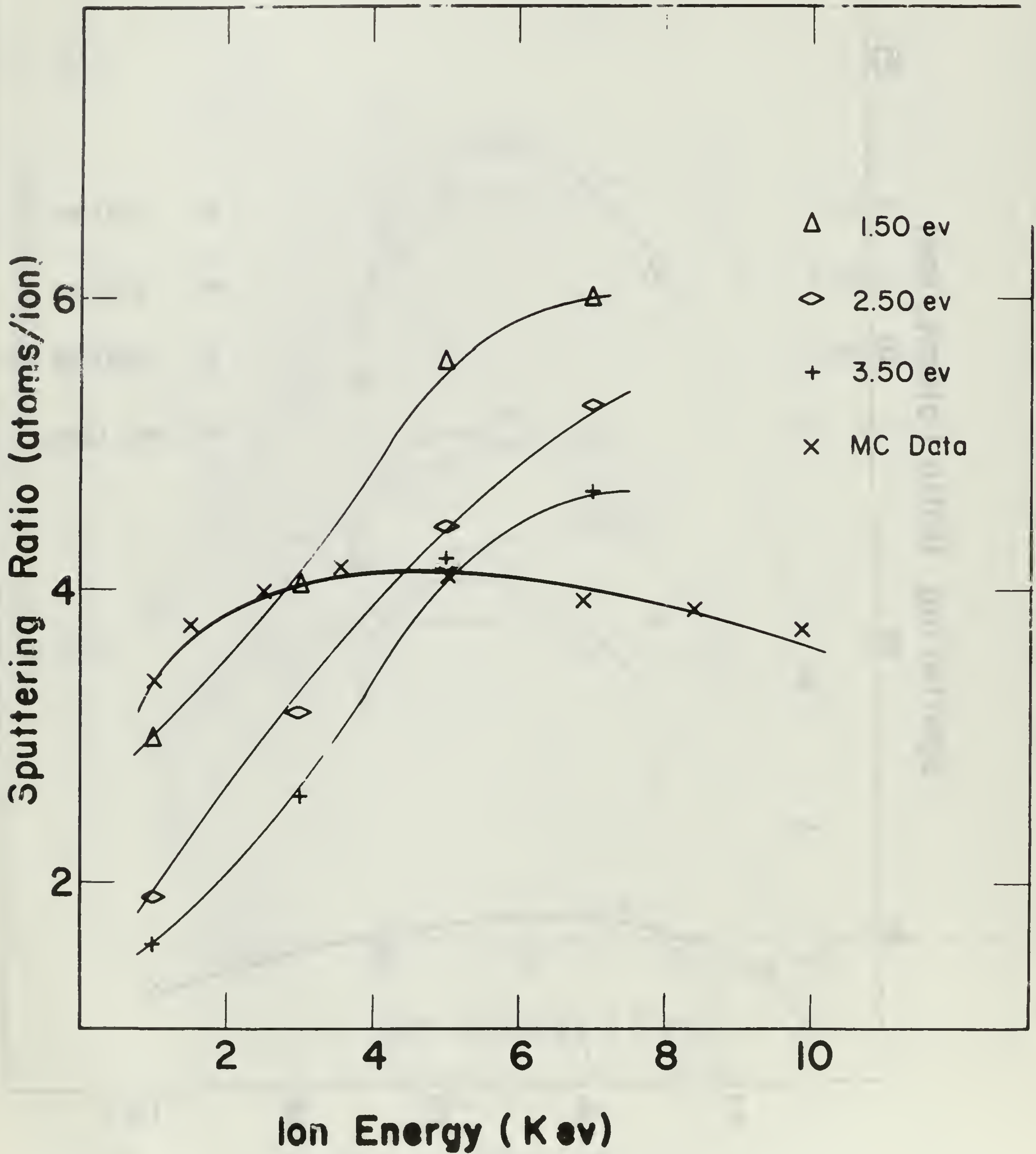

Sputtering Ratio of (100) Surface
Stub Surface

Figure 51c

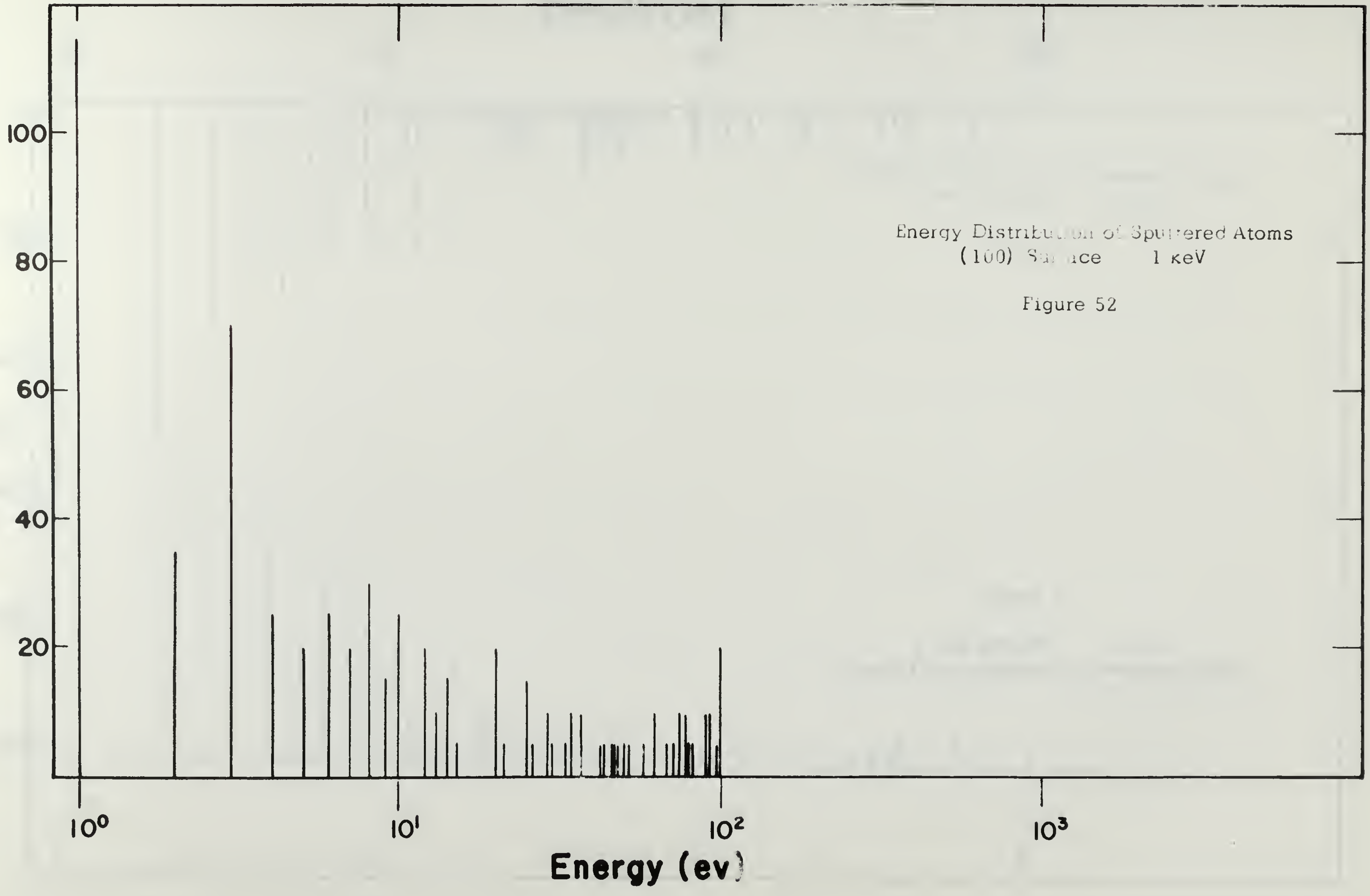

Energy Distribution of Sputtered Atoms
(100) Surface 1 keV

Figure 52

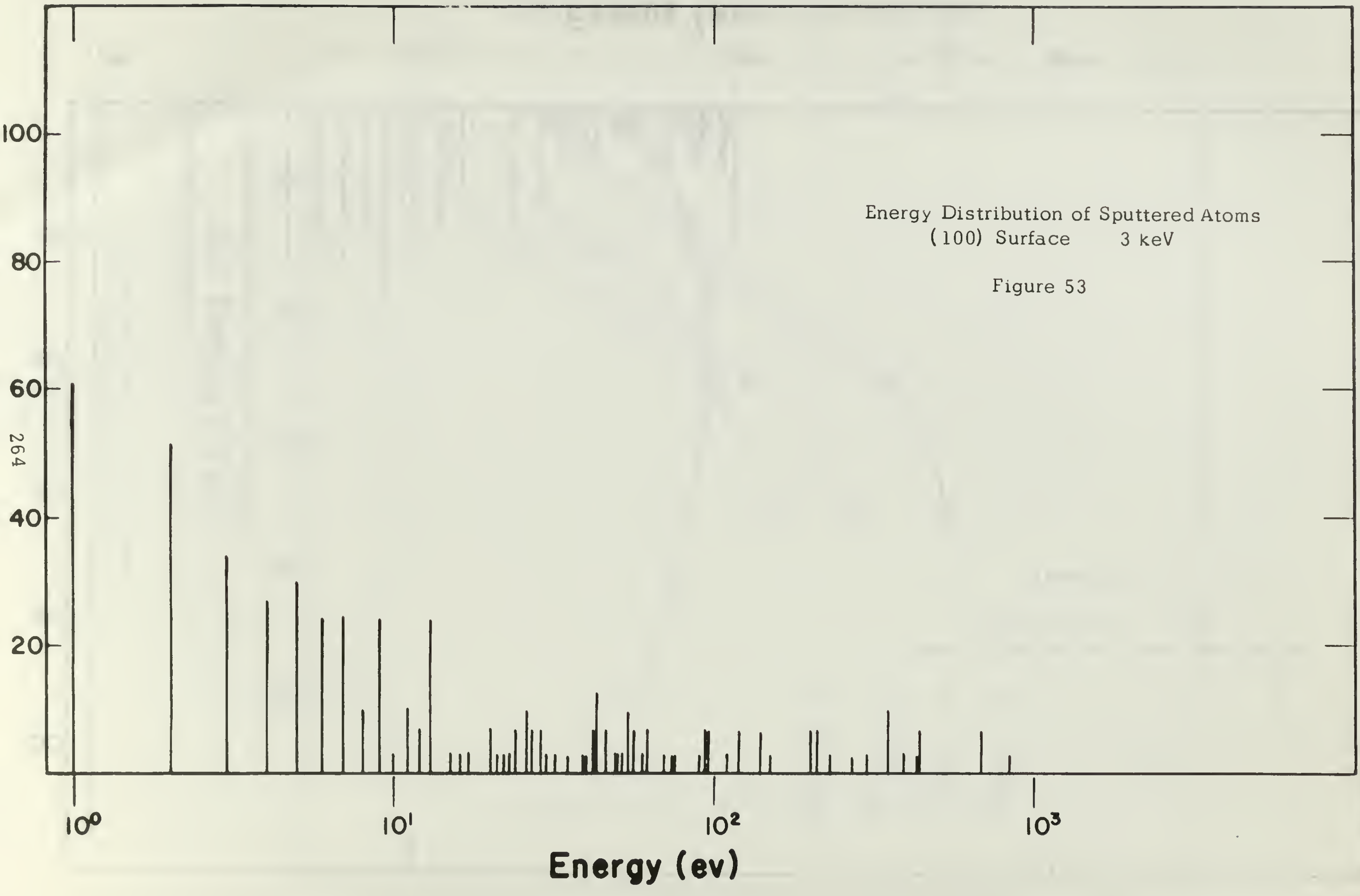

Energy Distribution of Sputtered Atoms
(100) Surface 3 keV

Figure 53

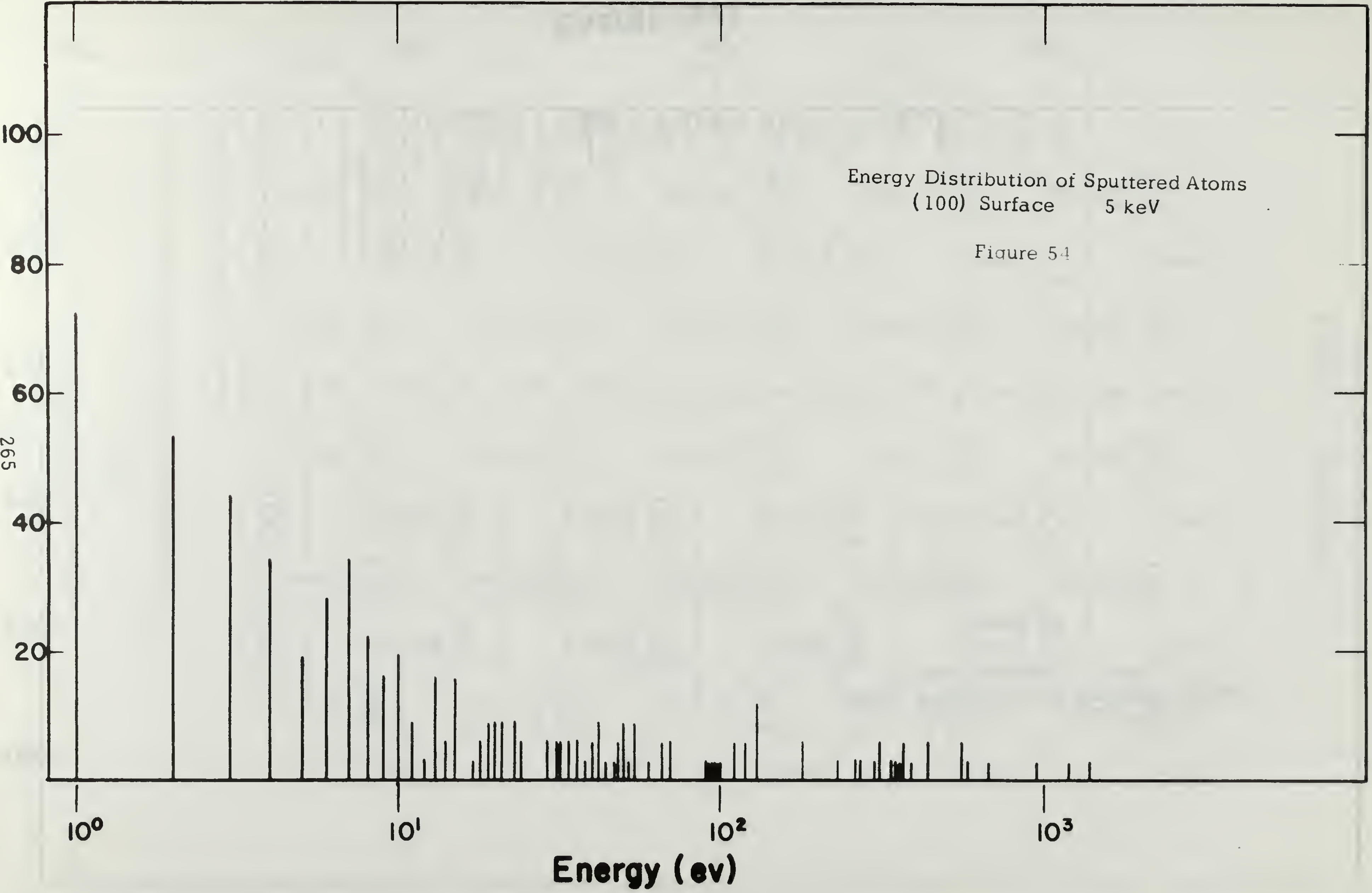

Energy Distribution of Sputtered Atoms
(100) Surface 5 keV

Figure 54

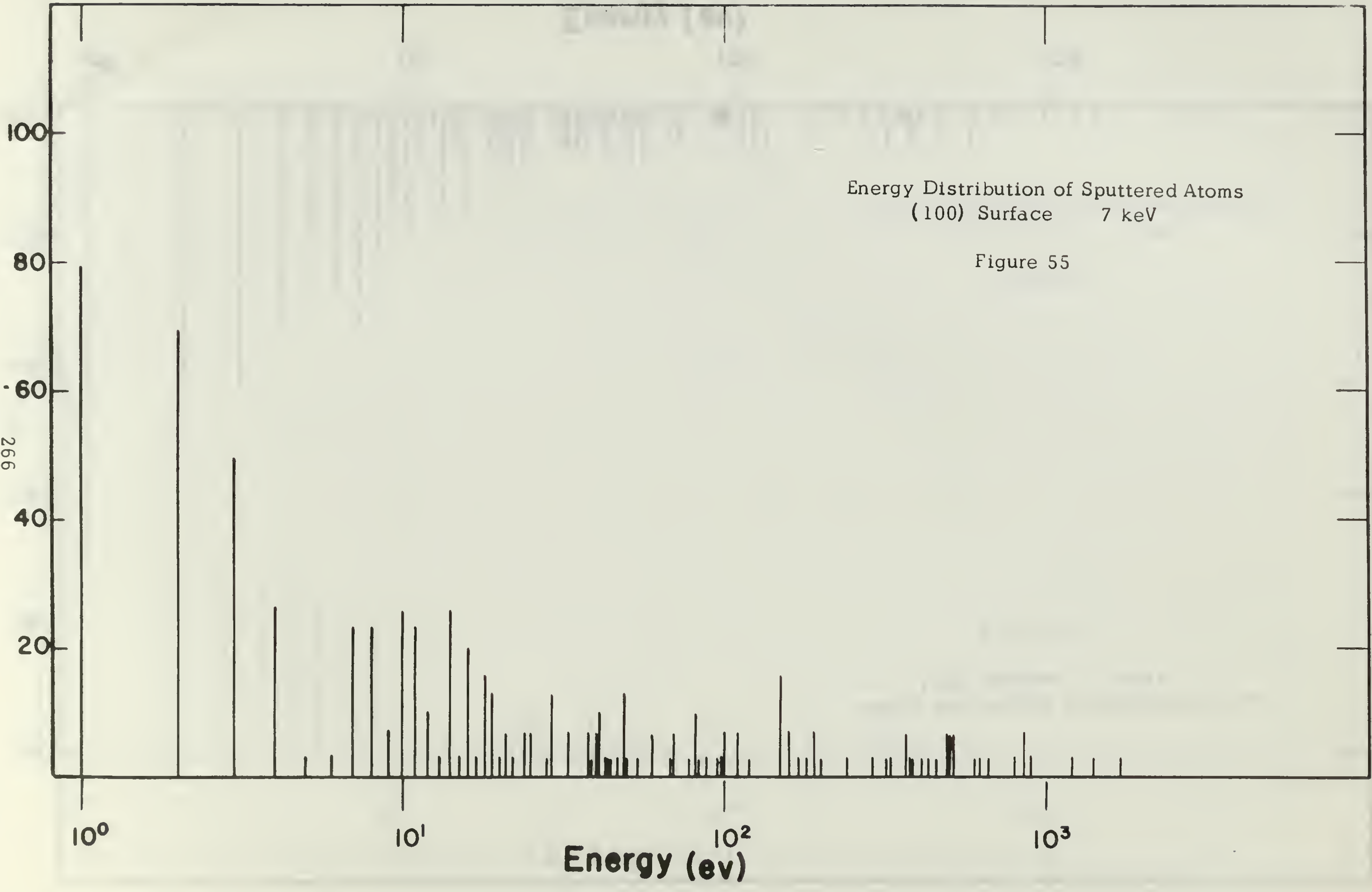
Energy Distribution of Sputtered Atoms
(100) Surface 7 keV
Figure 55
100
80
60
40
20
10^0
10^1
10^2
10^3
Energy (ev)

(110) Surface

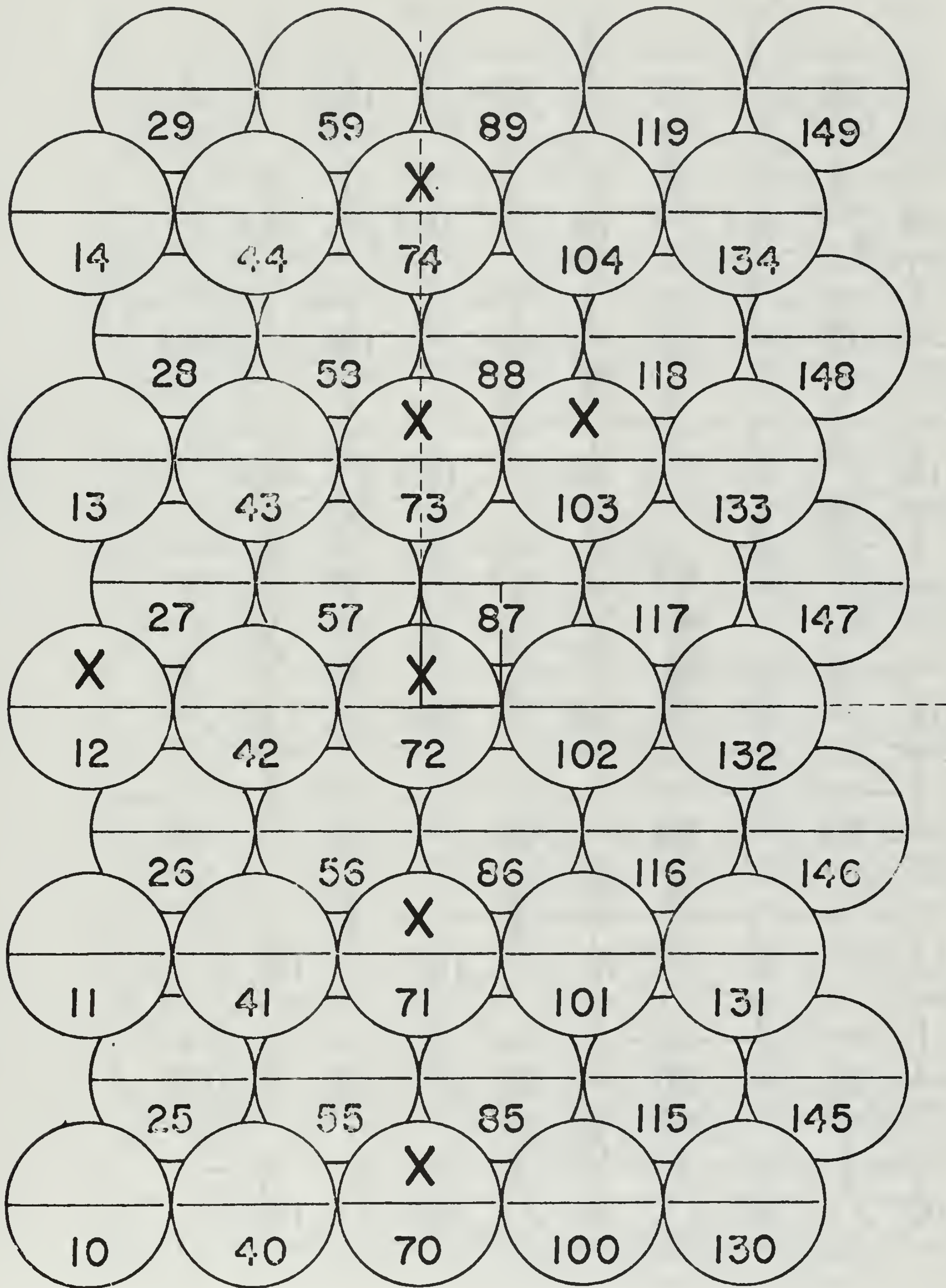

Sputtering frequency-location diagram
for (110) surface.
1 keV

Figure 56

(110) Surface

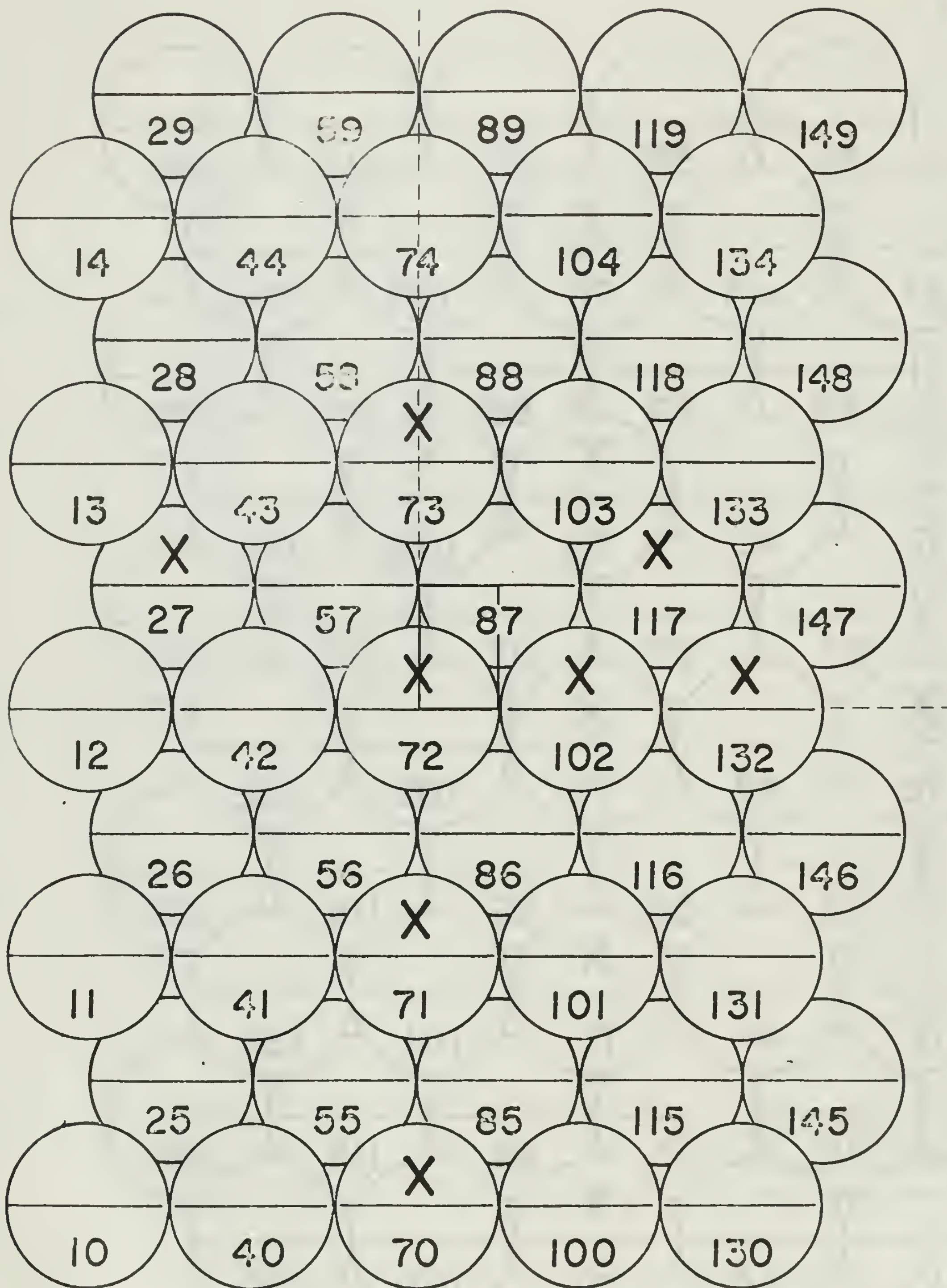

Sputtering frequency-location diagram
for (110) surface.
3 keV

Figure 57

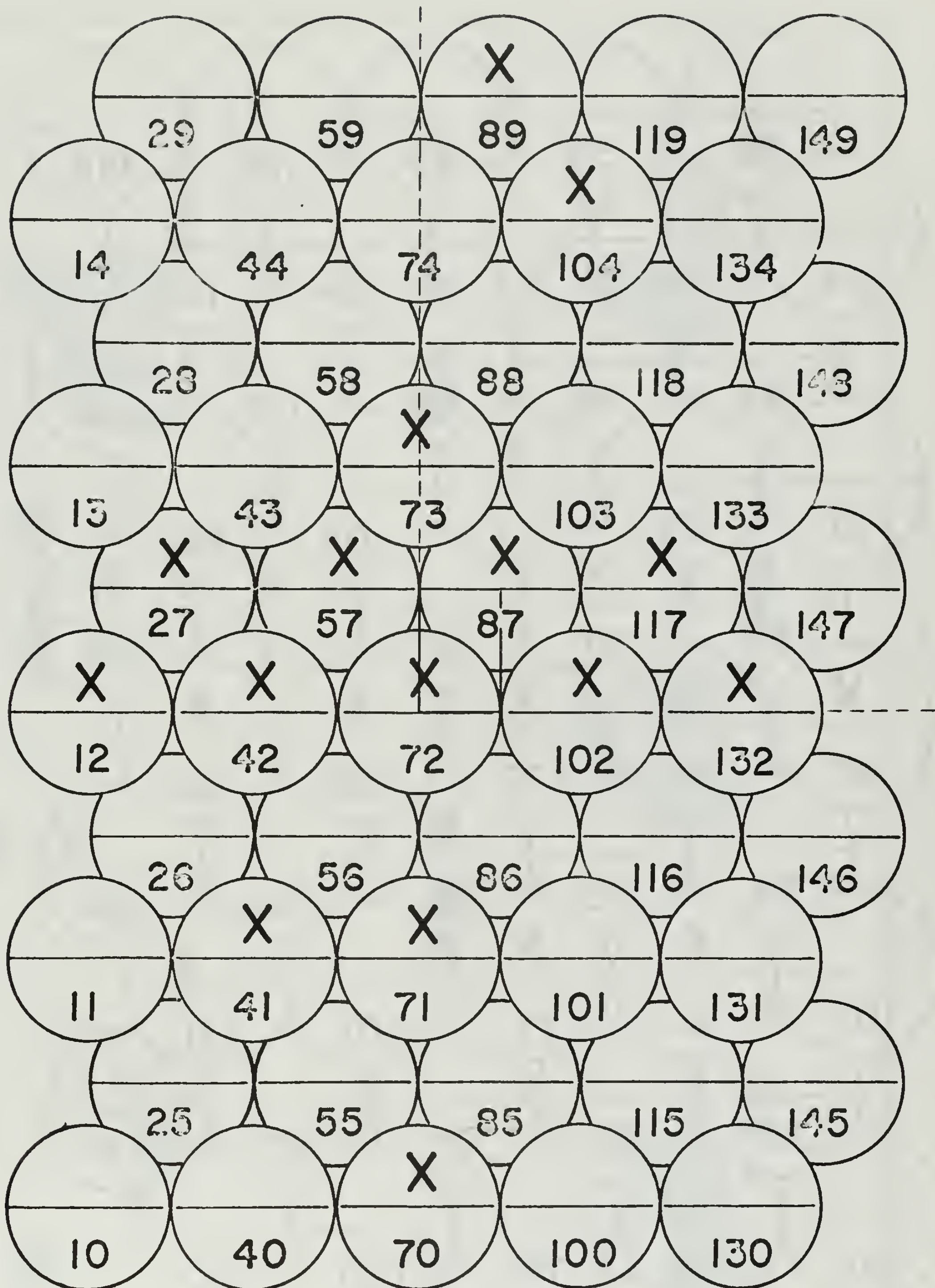

Sputtering frequency-location diagram
for (110) surface.
5 keV

Figure 58

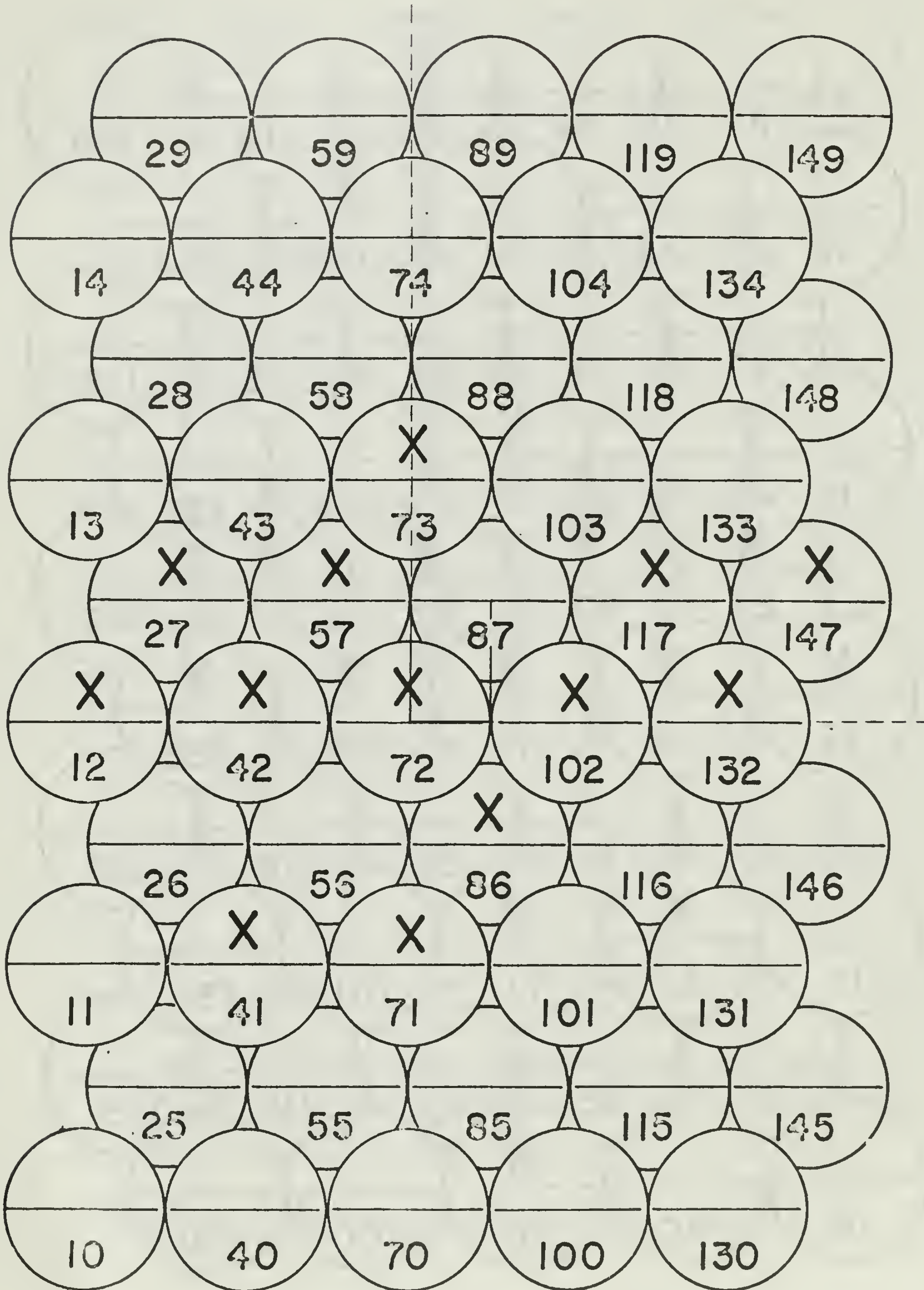

Sputtering frequency-location diagram
for (110) surface.
7 kev

Figure 59

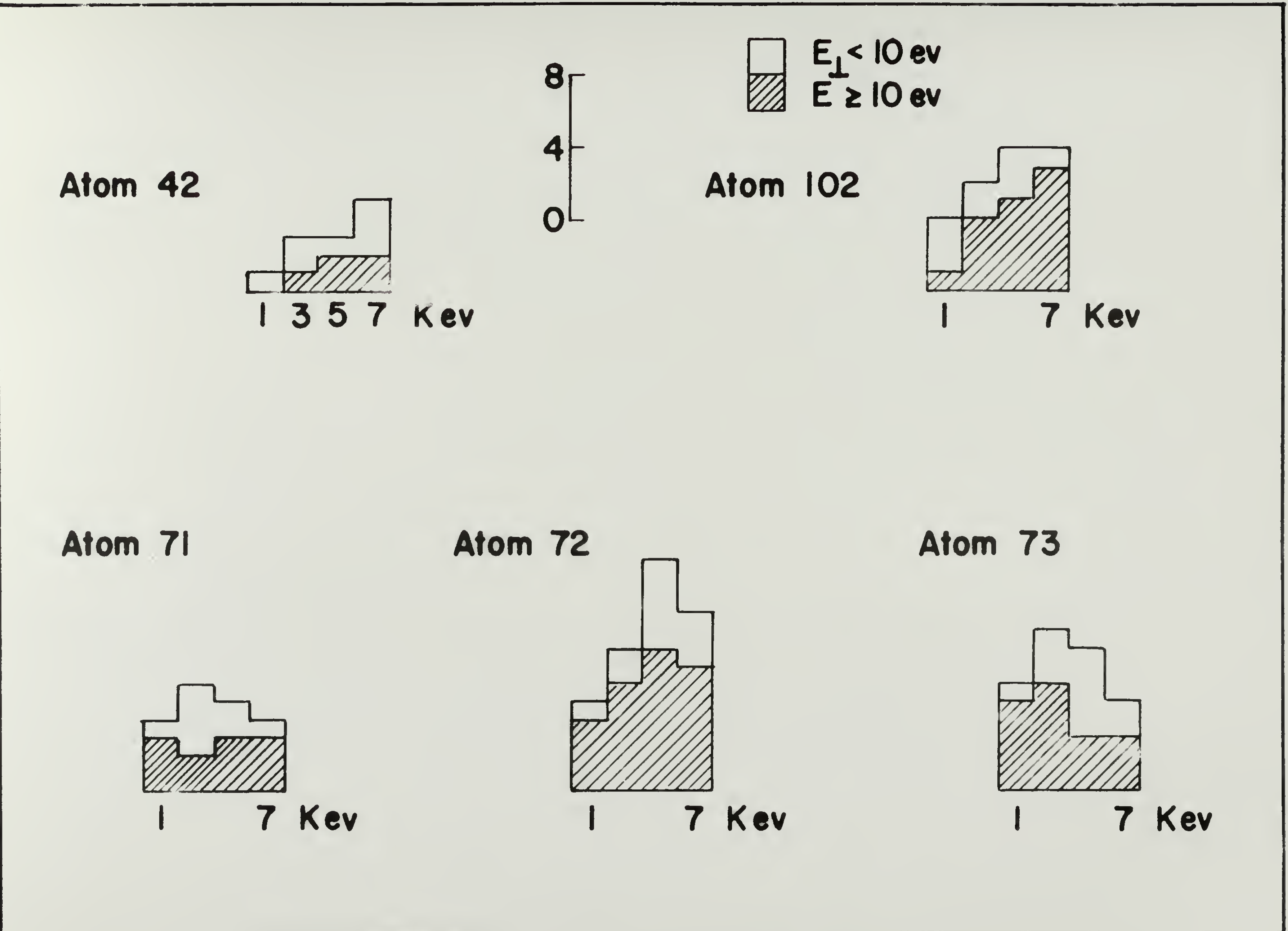

Sputtering profiles of atoms sputtered from (110) surface.

Figure 60

Argon Copper Sputtering
(110) Surface

1.0 Kev Bombardment Energy
3.50 ev Binding Energy

Figure 61a

Argon Copper Sputtering
(110) Surface

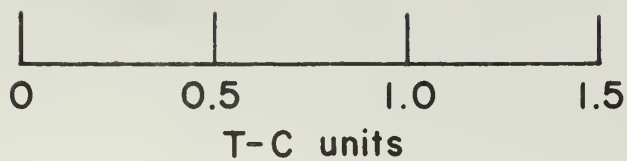

1.0 Kev Bombardment Energy
3.50 ev Binding Energy

Figure 61b

Argon Copper Sputtering
(110) Surface

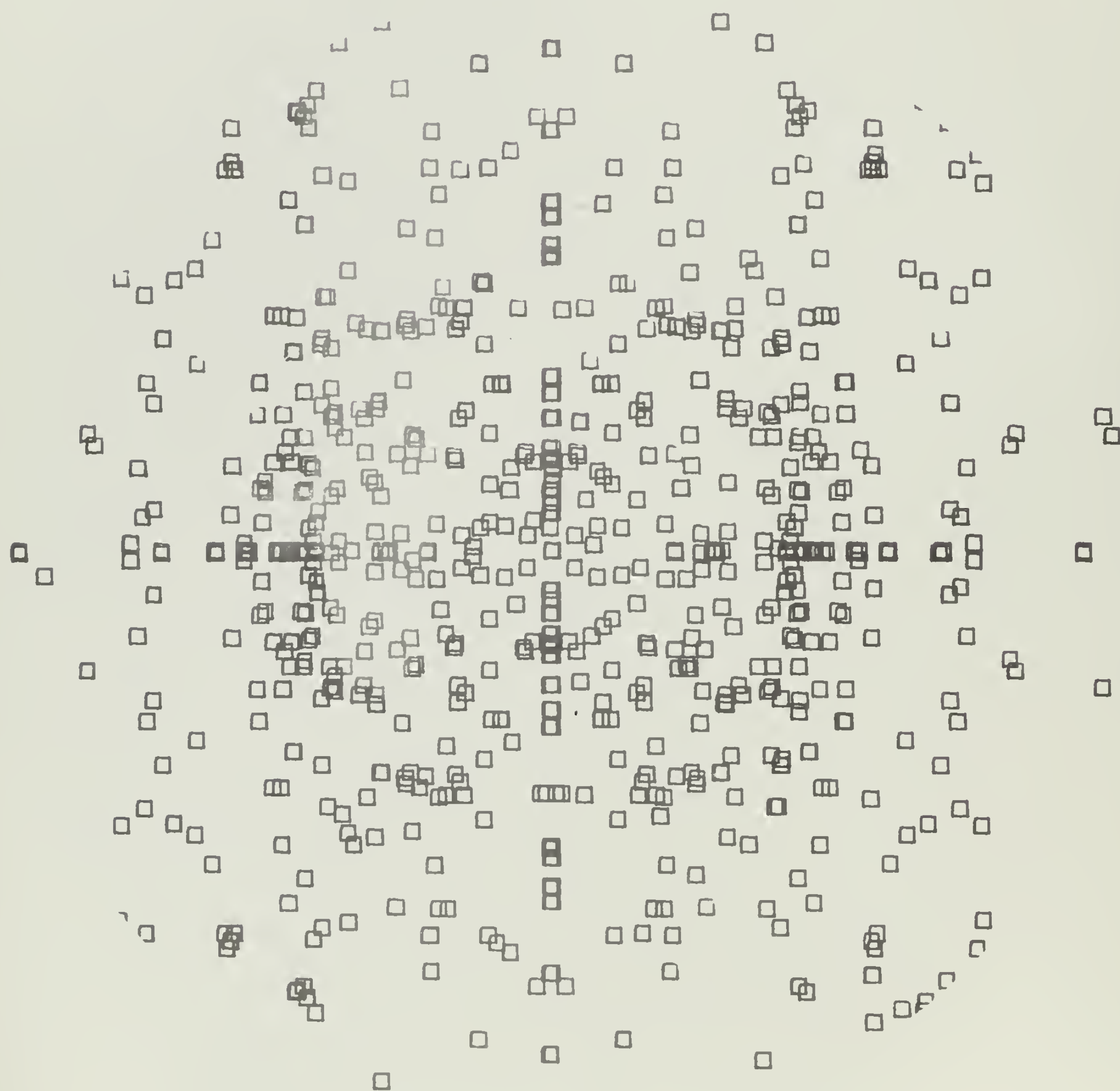

3.0 Kev Bombardment Energy
3.50 ev Binding Energy

Figure 62a

Argon Copper Sputtering

(110) Surface

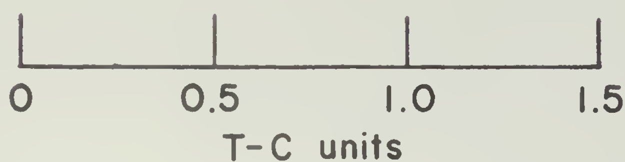

3.0 Kev Bombardment Energy

3.50 ev Binding Energy

Figure 62b

Argon Copper Sputtering

(110) Surface

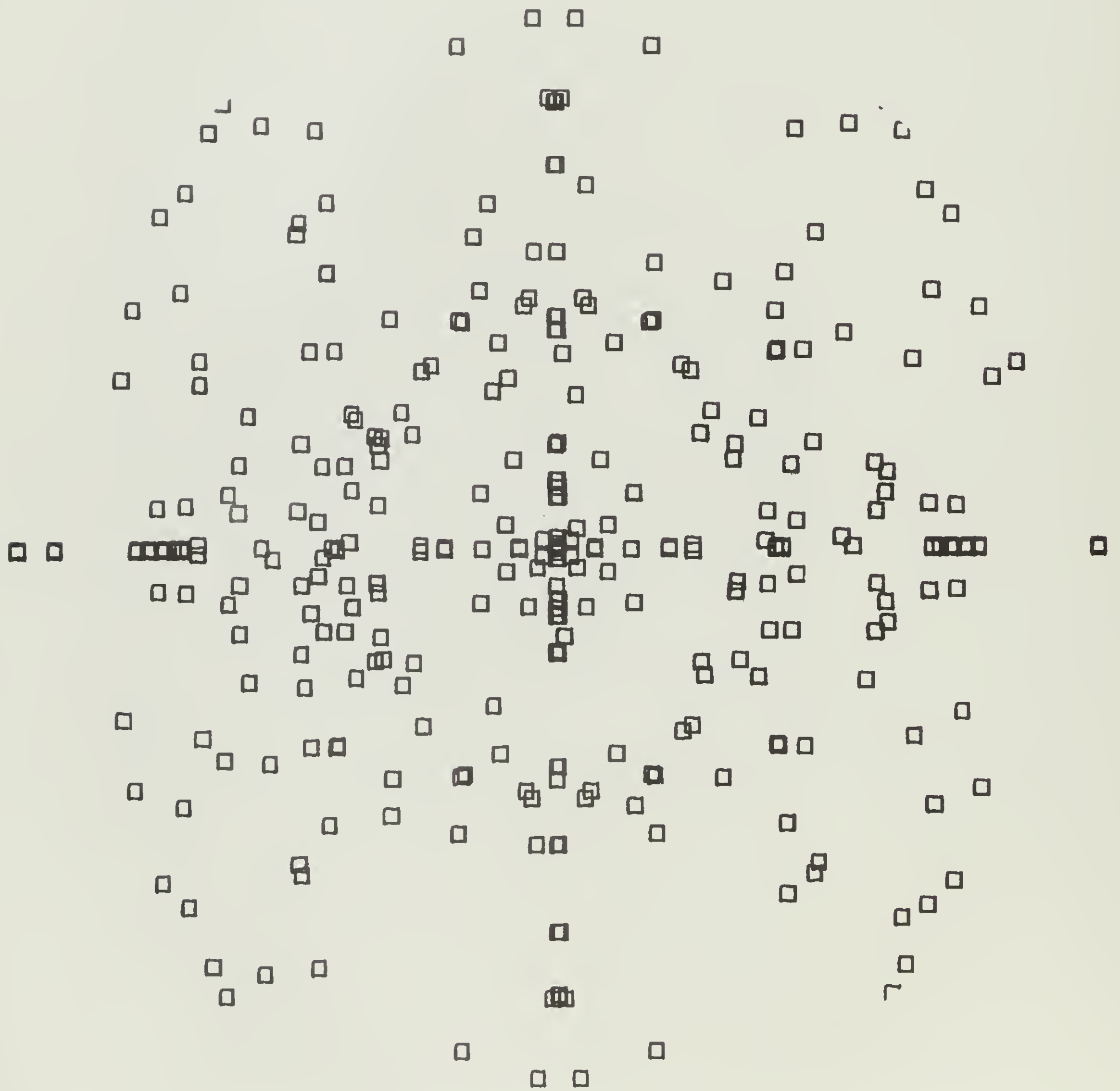

5.0 Kev Bombardment Energy

3.50 ev Binding Energy

Figure 63a

Argon Copper Sputtering
(110) Surface

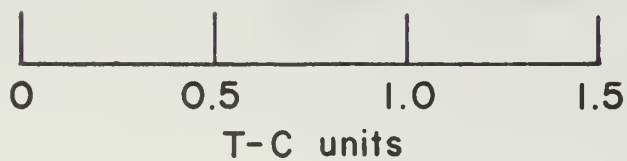

5.0 K ev Bombardment Energy
3.50 ev Binding Energy

Figure 63b

Argon Copper Sputtering
(110) Surface

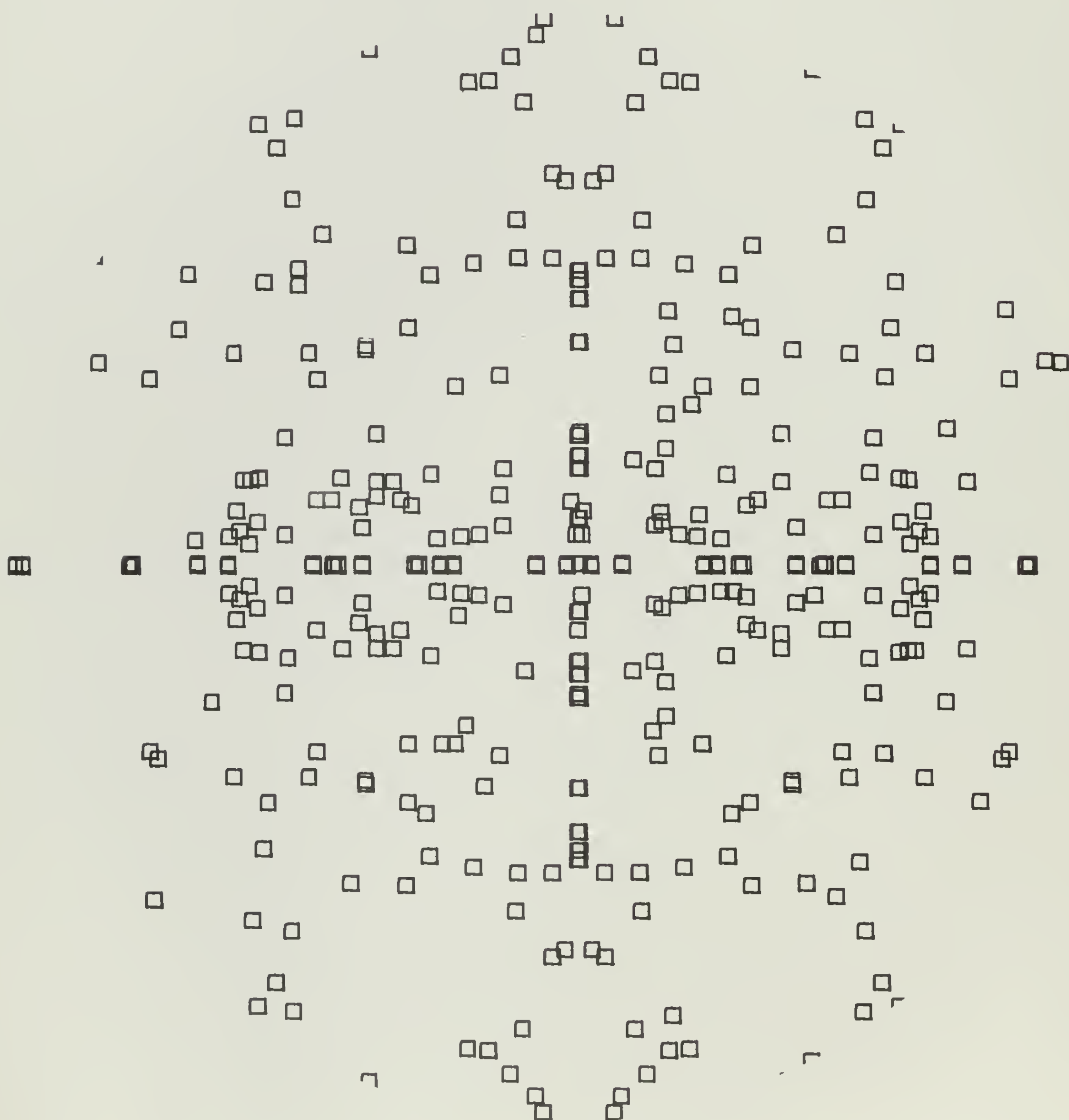

7.0 K ev Bombardment Energy
3.50 ev Binding Energy

Figure 64a

Argon Copper Sputtering
(110) Surface

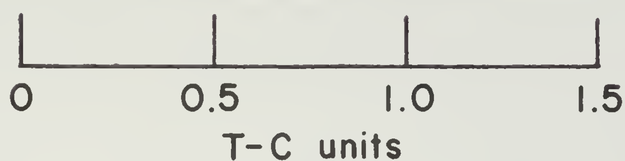

7.0 K ev Bombardment Energy
3.50 ev Binding Energy

Figure 64b

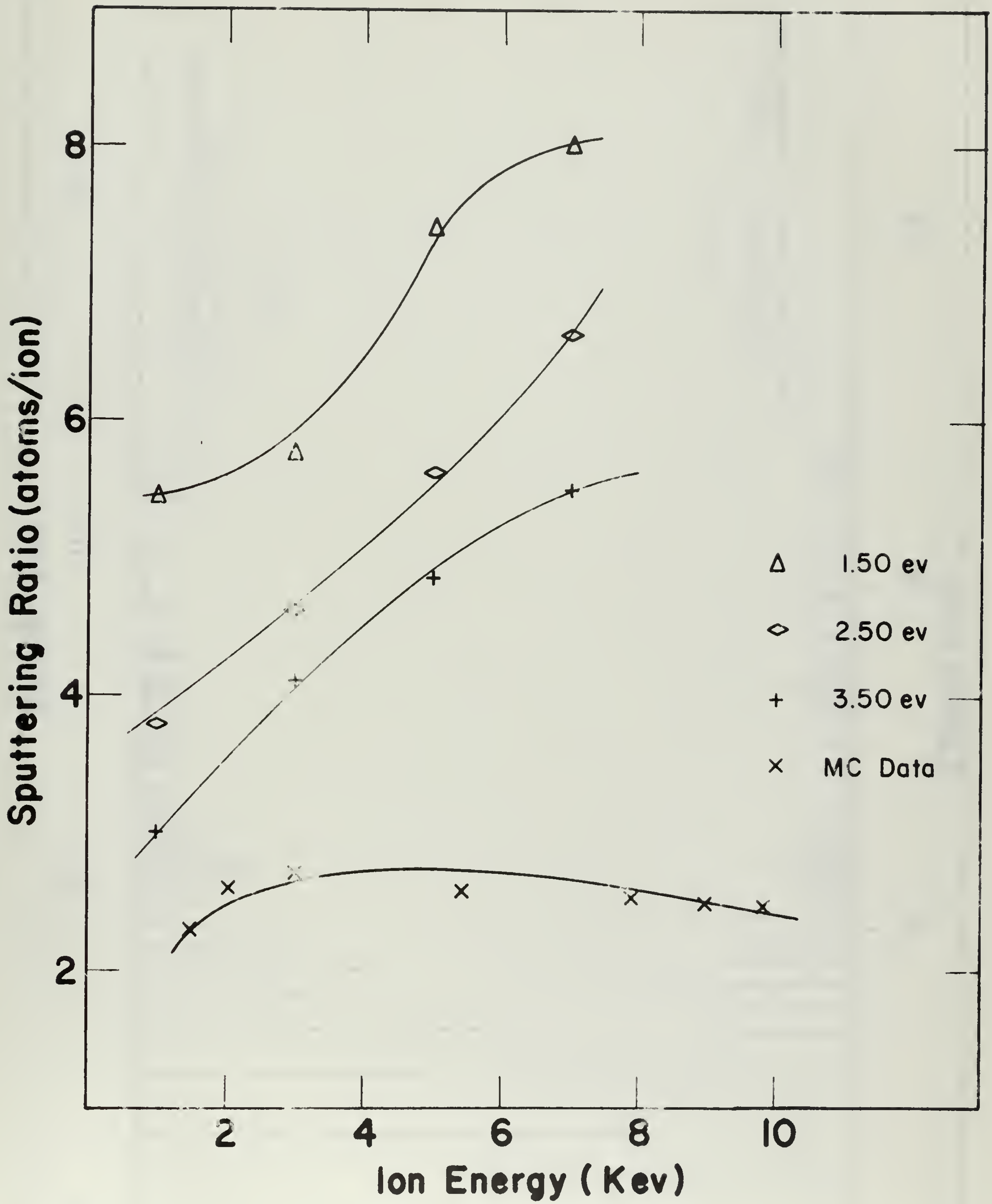

Sputtering Ratio of (110) Surface
Regular Surface

Figure 65

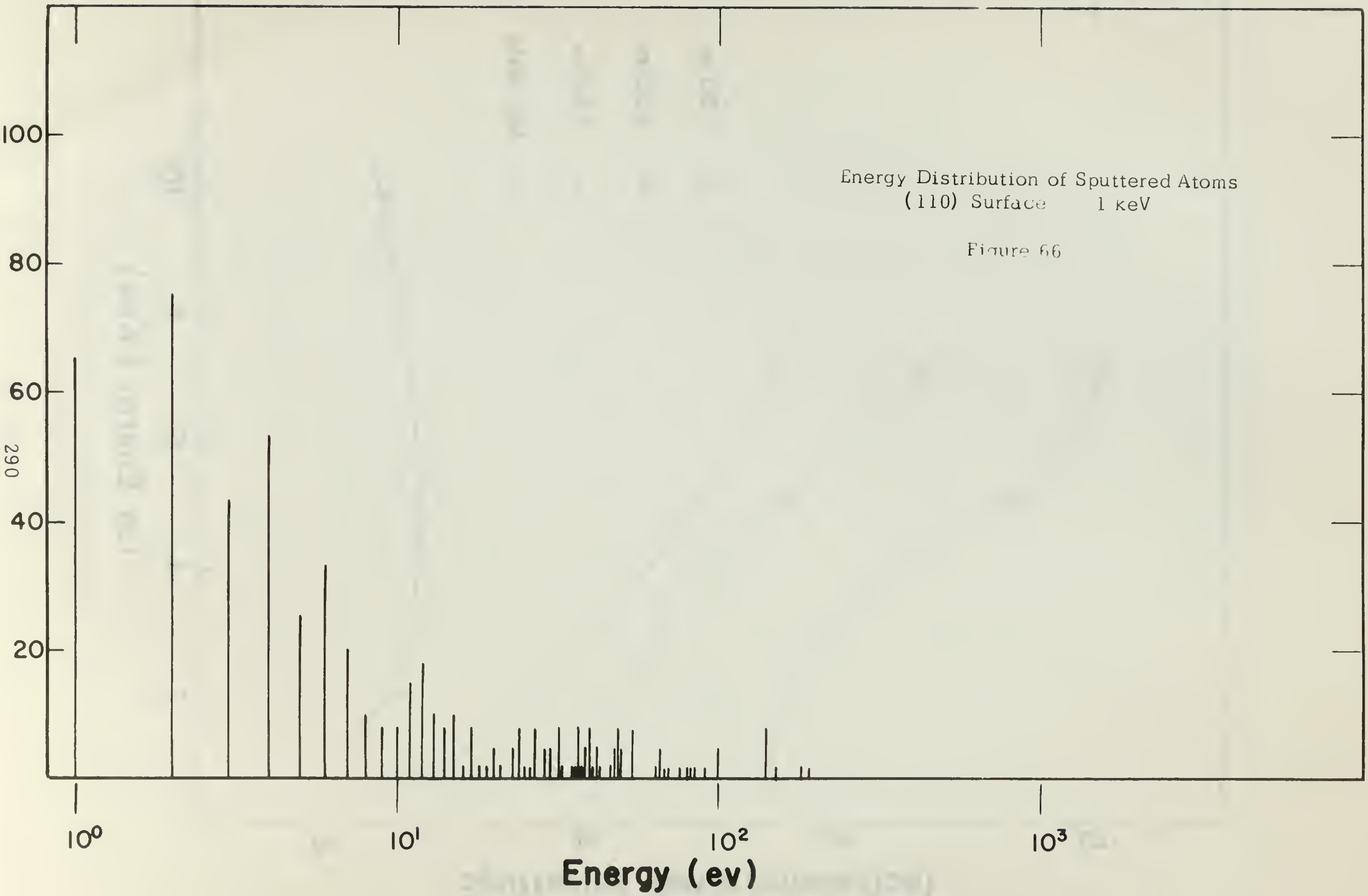

Energy Distribution of Sputtered Atoms
(110) Surface 1 keV

Figure 66

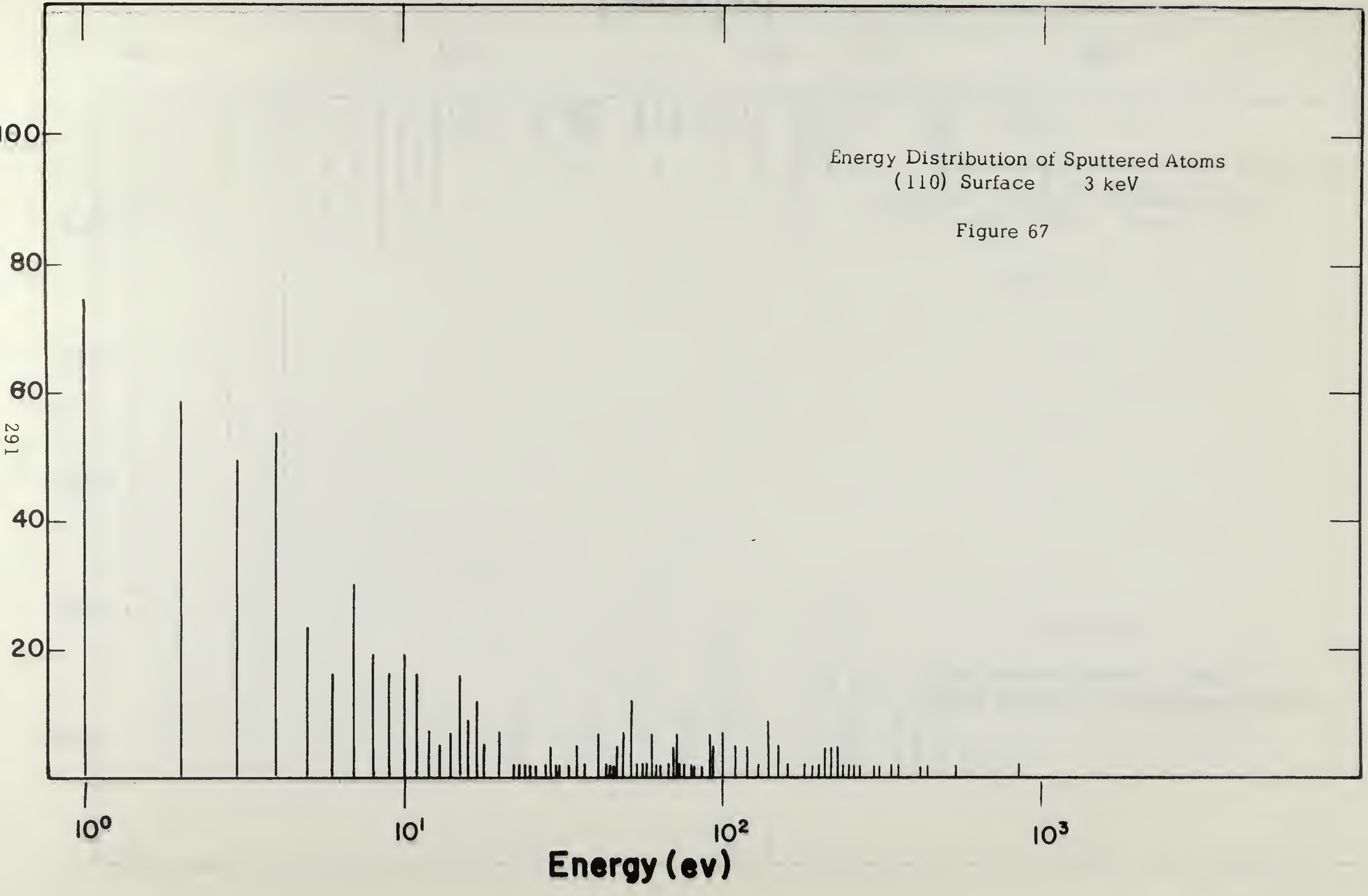

Energy Distribution of Sputtered Atoms
(110) Surface 3 keV

Figure 67

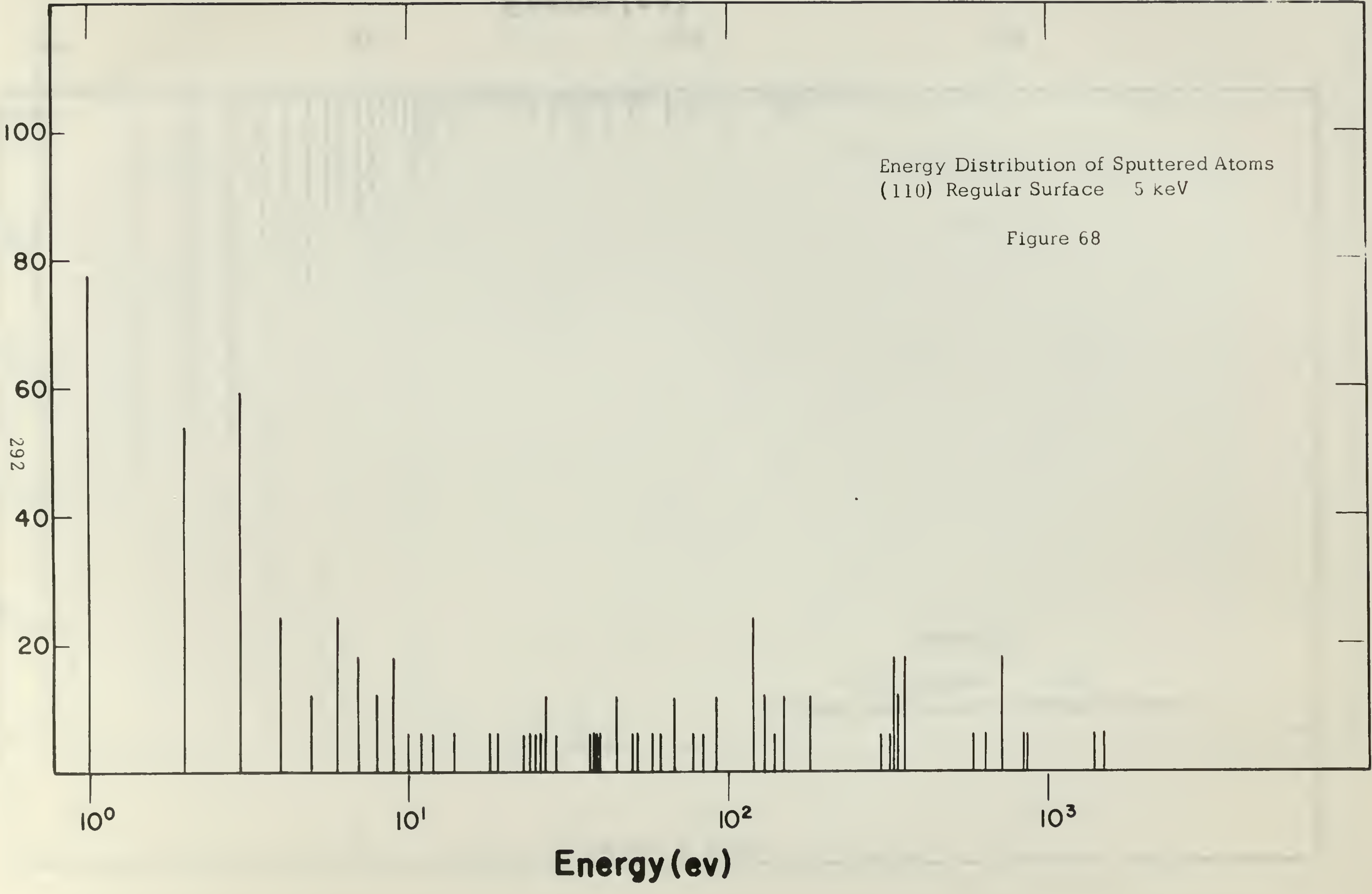

Energy Distribution of Sputtered Atoms
(110) Regular Surface 5 keV

Figure 68

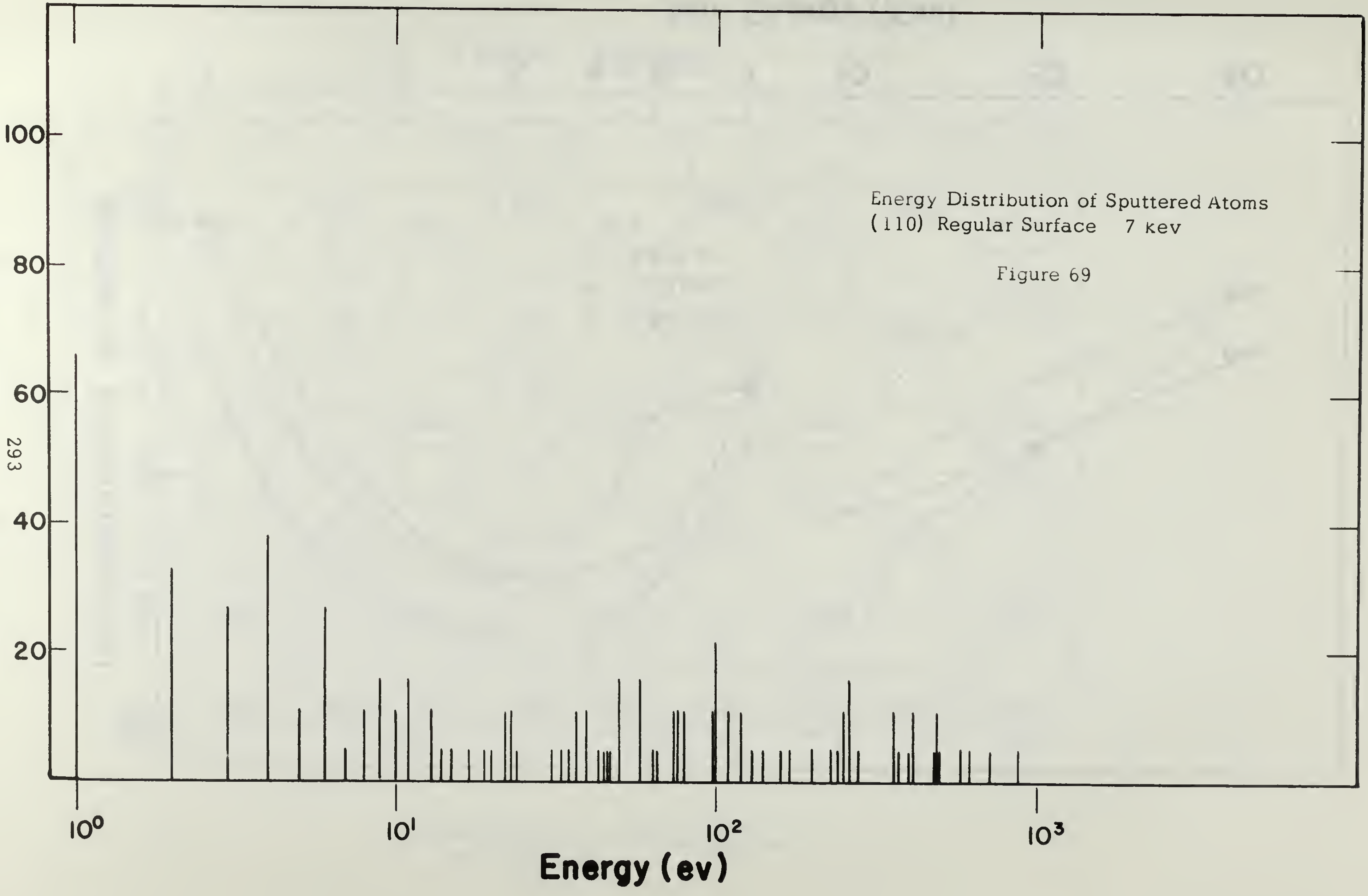

Energy Distribution of Sputtered Atoms
(110) Regular Surface 7 kev

Figure 69

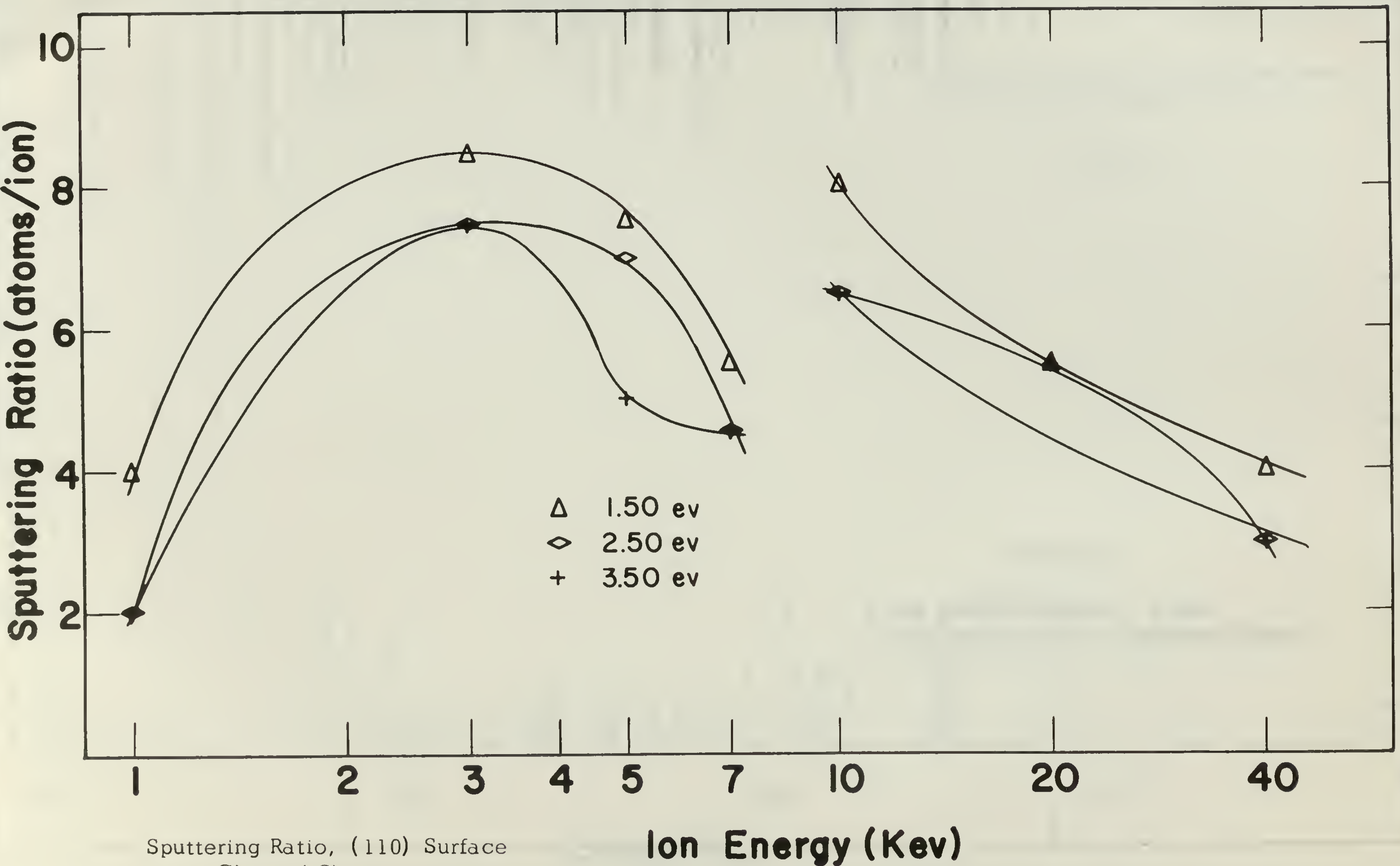

Sputtering Ratio, (110) Surface
Channel Shots

Figure 70

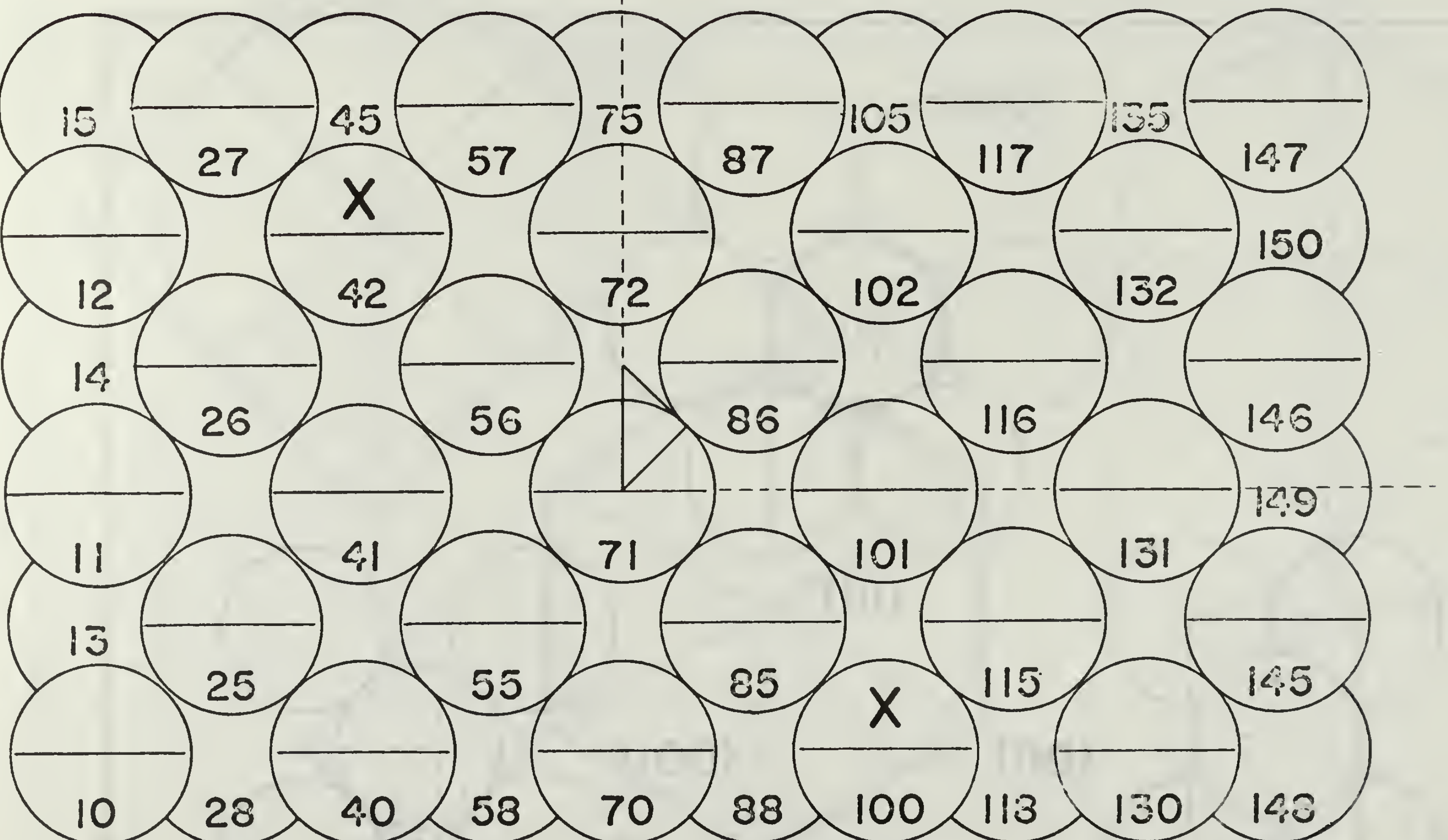

Sputtering frequency-location diagram for (100) surface.
100 ev

Figure 71

Intrinsic
Geometry

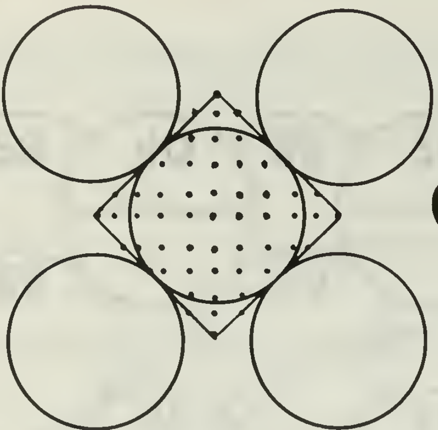

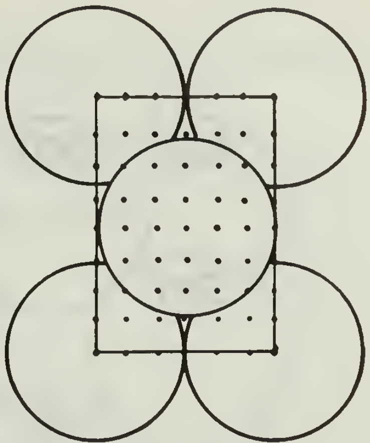

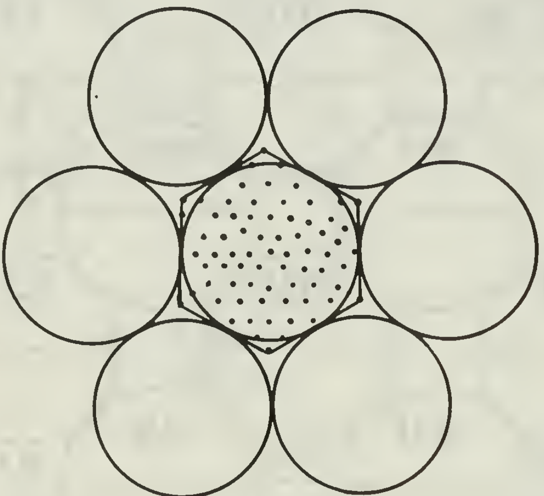

Intrinsic volumes of the crystals

Figure 72

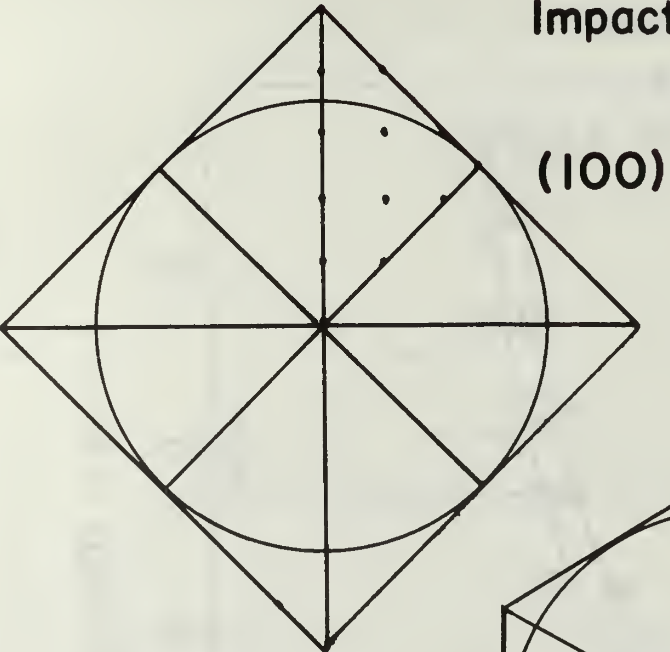

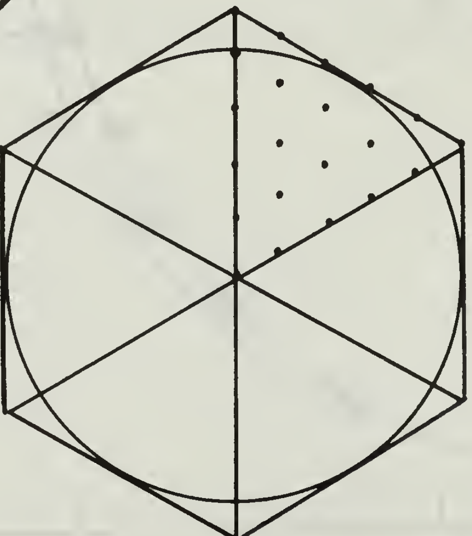

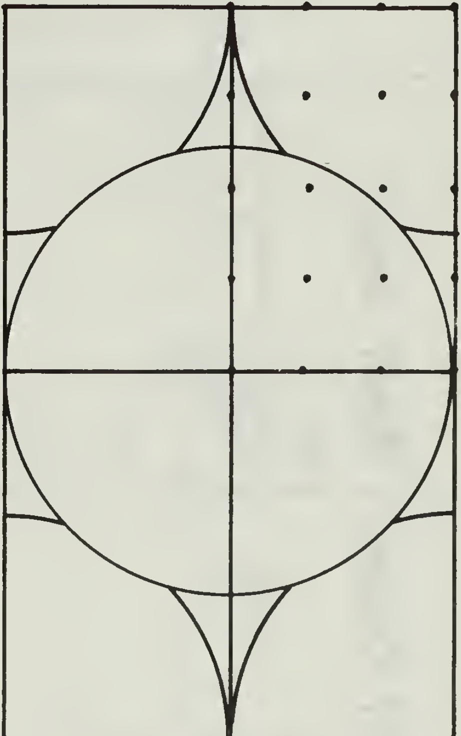

Impact Areas

Figure 73

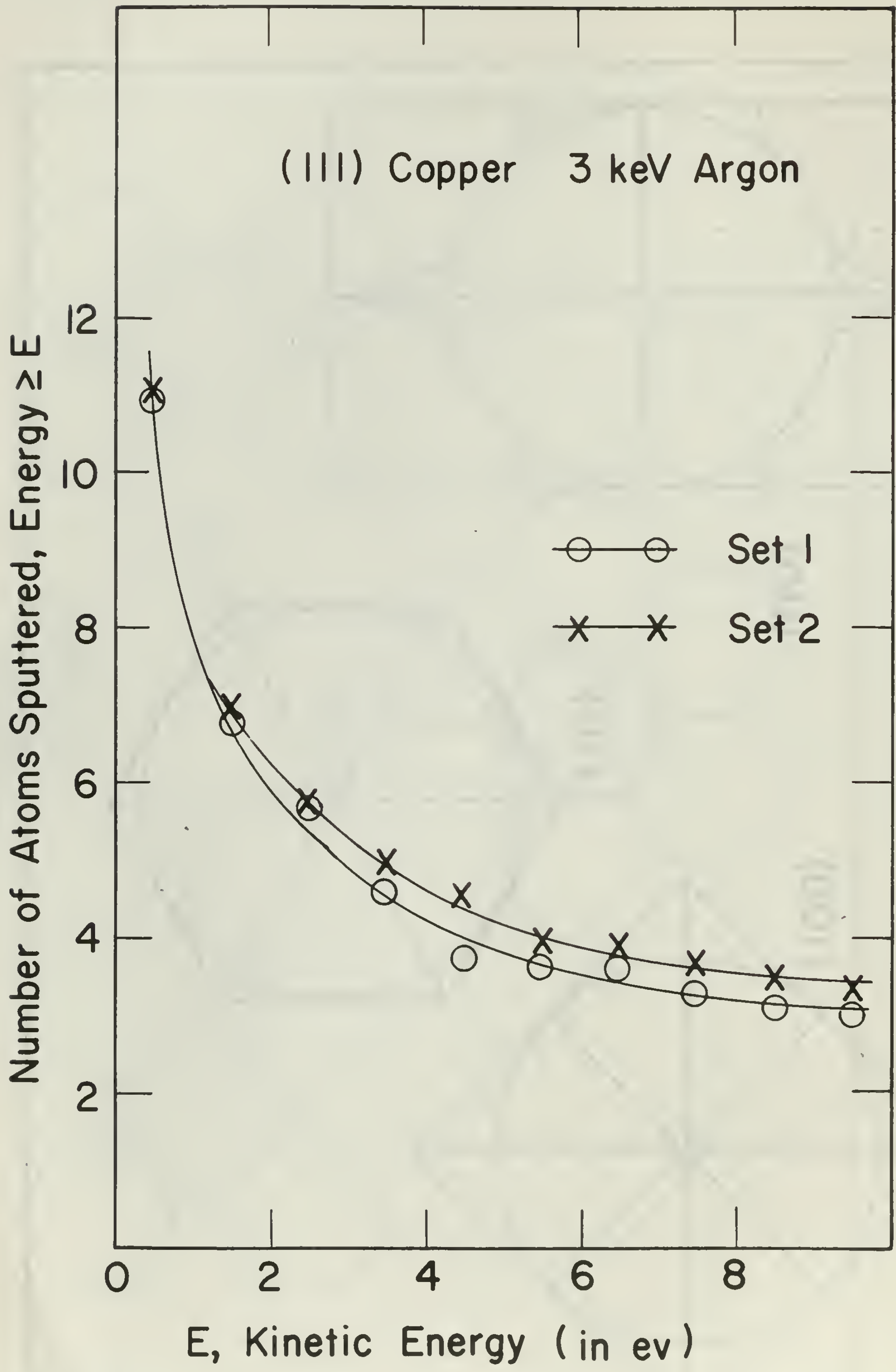

Sputtering Ratio variation with Impact Point Set

Figure 74

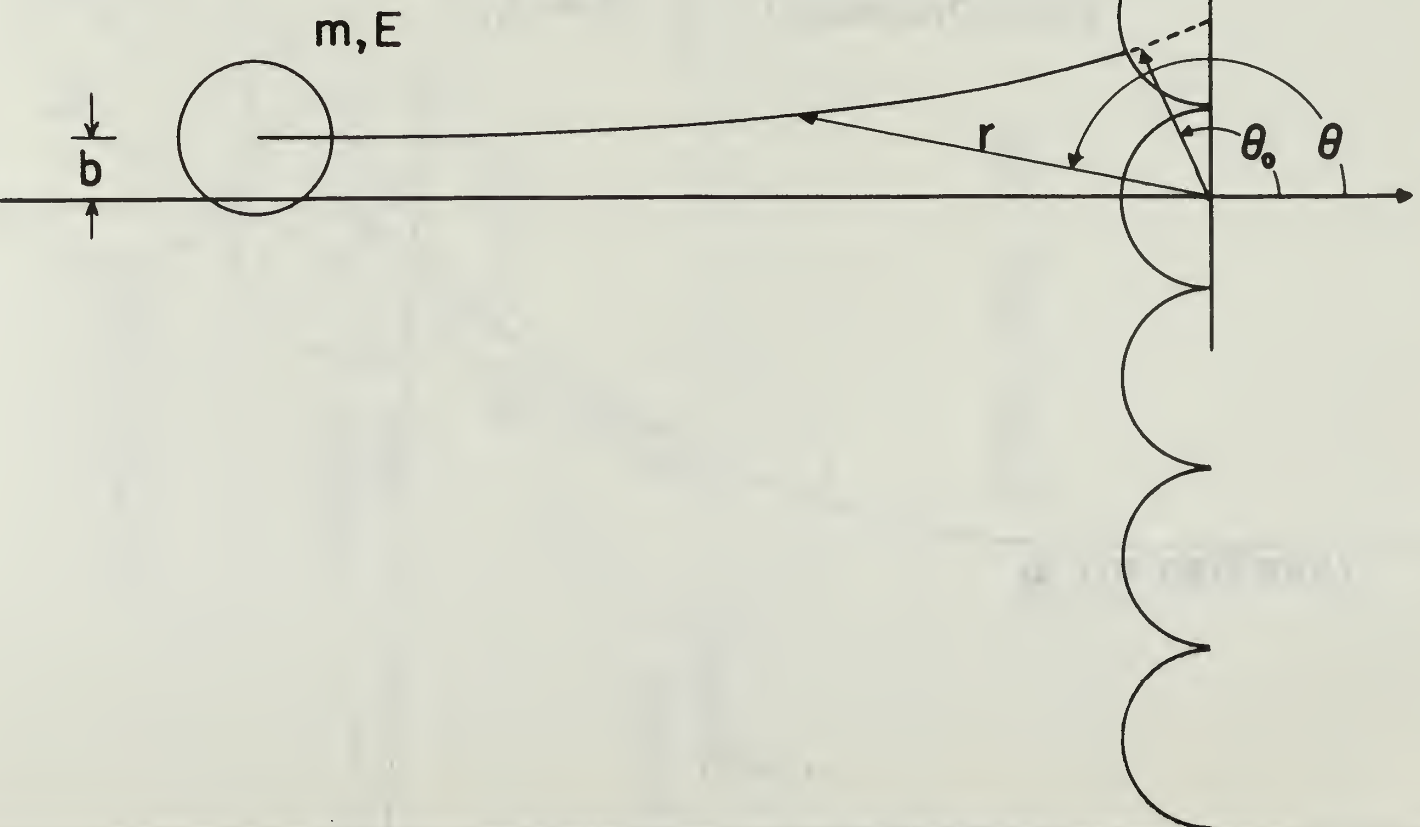

Scattering from a fixed force center

Figure 75

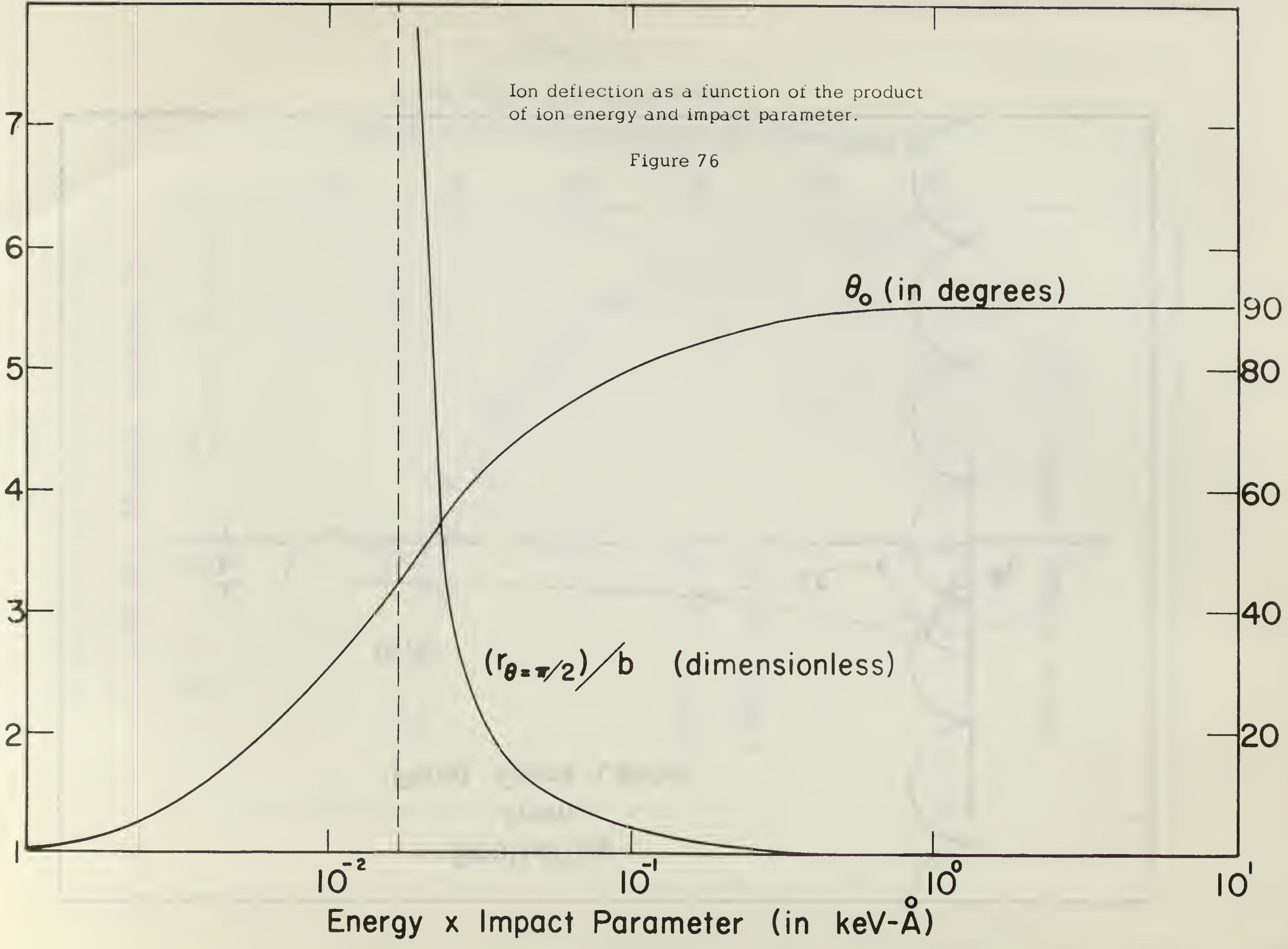

Ion deflection as a function of the product of ion energy and impact parameter.

Figure 76

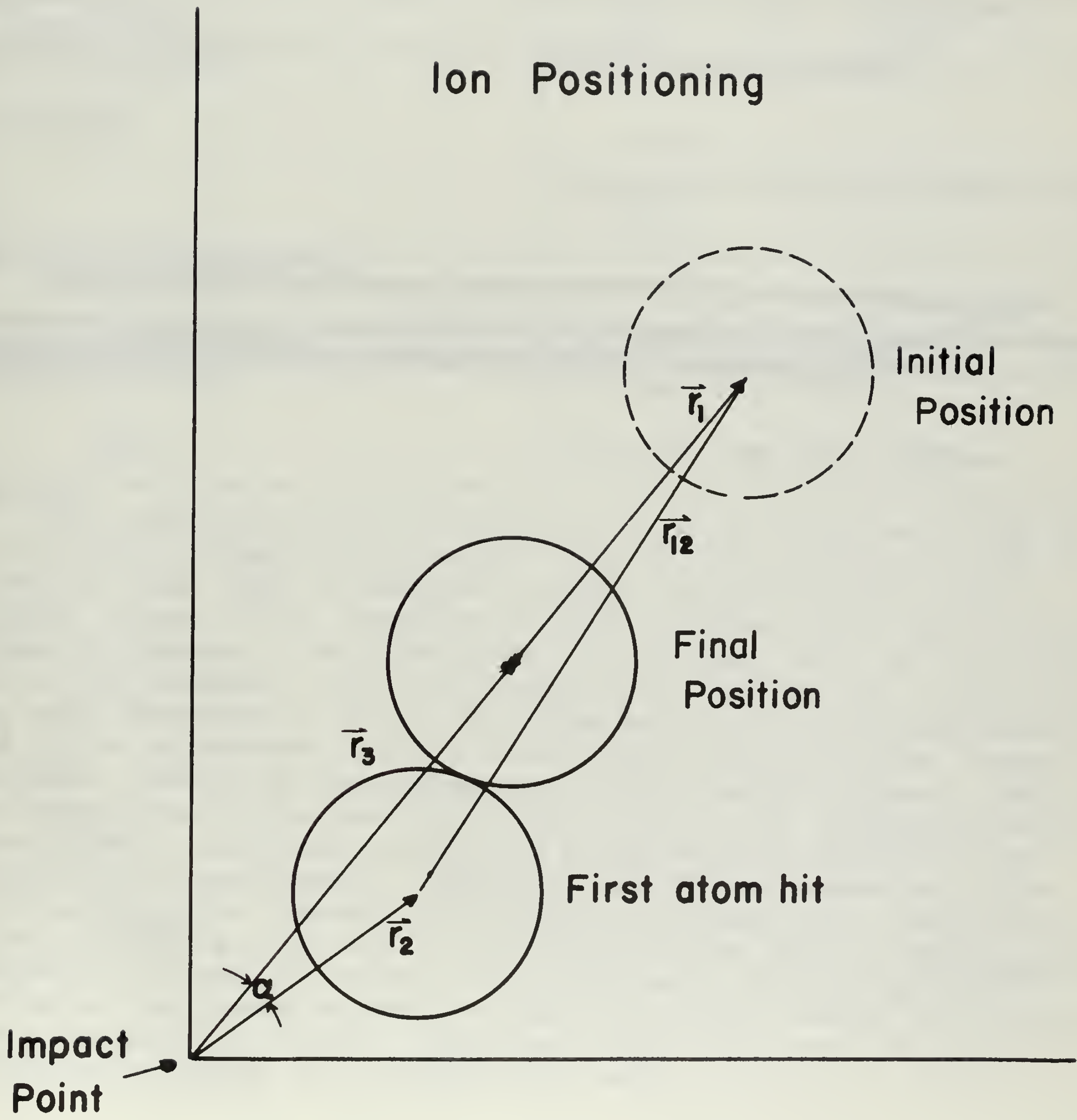

Ion positioning process

Figure 77

UNCLASSIFIED

Security Classification

DOCUMENT CONTROL DATA - R&D

(Security classification of title, body of abstract and indexing annotation must be entered when the overall report is classified)

1. ORIGINATING ACTIVITY (Corporate author)	2a. REPORT SECURITY CLASSIFICATION
Naval Postgraduate School Monterey, California 93940	Unclassified
	2b. GROUP

3. REPORT TITLE
Correlation of Argon-Copper Sputtering Mechanisms with Experimental Data Using A Digital Computer Simulation Technique

4. DESCRIPTIVE NOTES (Type of report and inclusive dates)
Thesis

5. AUTHOR(S) (Last name, first name, initial)
EFFRON, Herbert M.

6. REPORT DATE	7a. TOTAL NO. OF PAGES	7b. NO. OF REFS
1 June 1967	245	38

8a. CONTRACT OR GRANT NO.	9a. ORIGINATOR'S REPORT NUMBER(S)
b. PROJECT NO.	N.A.
c.	9b. OTHER REPORT NO(S) (Any other numbers that may be assigned this report)
d.	N.A.

10. AVAILABILITY/LIMITATION NOTICES

11. SUPPLEMENTARY NOTES	12. SPONSORING MILITARY ACTIVITY
None	Naval Postgraduate School

13. ABSTRACT

The sputtering process has been investigated by simulating the sputtering of single-crystal copper with 1-7 keV argon. A digital computer was used to build the crystal, bombard it, and move crystal atoms. Four mechanisms were observed which cause surface atoms to sputter. An atom is sputtered when (1) it is squeezed out of the surface, (2) it is scooped out when another atom strikes its inner hemisphere, (3) it is ejected when an atom passes behind it, and (4) it is knocked out by a second layer atom which is moving outward. Nearly all sputtered atoms were surface atoms. Second and third layer atoms were sputtered only for ion energies greater than 5 keV. They were sputtered by mechanisms similar to the surface atom mechanisms. "Silsbee chains" were observed to be directed into the crystal, and momentum focusing was observed to cause sputtering only when it occurred in close packed, surface rows. Outward directed chains were not observed. Sputtering deposit patterns, sputtering ratios, and sputtered atom energy distributions were obtained for (100), (110), and (111) surfaces. All data compared favorably with experimental data.

UNCLASSIFIED

Security Classification

14. KEY WORDS	LINK A		LINK B		LINK C	
	ROLE	WT	ROLE	WT	ROLE	WT
Sputtering of Copper						
Sputtering Mechanisms						
Simulation of Sputtering						

thesE258
DUDLEY KNOX LIBRARY
3 2768 00421945 1
DUDLEY KNOX LIBRARY